Volcanic Geology and Hydrothermal Alteration of the Onemana Area, Eastern Coromandel Peninsula

A thesis submitted in partial fulfilment

of the requirements for the

Degree of Master of Science in Earth Sciences

at the University of Waikato

by

Sean Mark Aldrich

University of Waikato

1995

Abstract

The Onemana Peninsula is located on the eastern side of the Coromandel Peninsula north of the township of Whangamata. This study investigates the volcanology, structure and hydrothermal alteration of the northern half of the Onemana Peninsula. The study area is dominated by rhyolite domes and lava flows, with minor andesite lavas, rhyolite pyroclastics and lake sediments. The central region is extensively hydrothermally altered, with high levels of the original system preserved including hydrothermal eruption breccias and sinters.

The Onemana area is dominated by three rhyolite dome complexes: Pohakahaka, Pokohino, and Wharekawa. The Pohakahaka Dome Complex in the south of the study area consists of pyroxene rhyolite domes, lavas and autoclastic breccias. The Pokohino Dome Complex in the central region of the study area consists of biotite rhyolite domes, lavas and autoclastic breccias. Lavas appear to have erupted as coulées and have flowed in a SE direction from a NE-trending ridge. The Wharekawa Dome Complex and Eastern Flows are dominated by biotite rhyolites. Pyroclastic and epiclastic material is overlain by rhyolite lavas in coastal sections north of Pokohino Beach, suggesting explosive activity preceded the eruption of some lavas. Some Eastern Flow lavas have flowed into water and produced a hyaloclastite in the north of the area. The deposition of the Glassy Dome Pyroclastics is thought to have resulted from the collapse of a rhyolite dome. Andesite lavas occur in the west of the study area, and their compositions suggest that they are related to the McBeths Andesite which outcrops 6 km to the NW. A hornblende-biotite ignimbrite is exposed in the north of the area, and is thought to have been erupted from outside the area. Thick lake sediments occur between the Pokohino and Wharekawa dome complexes and infill a graben structure. A hydrothermal eruption breccia resulting from over-pressuring of a geothermal system overlies the lake sediments.

The structure of the area is dominated by NW, N, and NE striking faults, and minor E-W striking faults. The local structure plays an important role in controlling the locations of volcanism and hydrothermal activity. Older N-striking structures appear to have controlled vent locations for the pyroxene rhyolites, while NE-striking structures have controlled the location the biotite rhyolites and hydrothermal alteration. Mineralised structures are controlled by NW and N striking faults between the NE-striking Whitipirorua and Pokohino Faults.

XRF analysis of selected volcanic rocks from Onemana show the area to be dominated by medium-K to high-K rhyolites (75-78 wt% SiO_2), with minor andesite (56-58 wt% SiO_2). On the basis of Zr abundance the rhyolites can be divided into high Zr (pyroxene rhyolites) and low Zr (biotite rhyolites, Glassy Dome Rhyolite). The rhyolites are thought to be closely associated with partial melting of the continental crust in a rifting environment.

Pervasive to weak alteration occurs within a NE-trending corridor bounded by the Whitipirorua and Pokohino Faults. There are two main alteration types in the area which represent different hydrothermal environments: alkaline and acid alteration. Alkaline alteration consists of an inner core of quartz silicification, surrounded by quartz + K-feldspar alteration, which grades out into epidote and weak clay alteration assemblages. Zeolites also occur as an overprinting alteration assemblage. Acid alteration consists of pervasive kaolinite alteration, with small areas of quartz + illite/smectite ± pyrophyllite alteration and opaline quartz silicification.

The Onemana area shows many volcanic and hydrothermal features that are typical of caldera settings and are comparable with the rhyolite volcanic centres in the TVZ. It is suggested that the rhyolitic volcanism at Onemana resulted from late stage volcanism along the ring fracture of a large caldera structure.

Acknowledgments

- Firstly most of my thanks must go to my supervisor Roger Briggs, who initially suggested the topic, and who provided invaluable suggestions and guidance throughout the course of this study.

- Many thanks must go to Heritage Mining for providing me with financial and logistic support, and a place to stay. Heaps of thanks to Colin, Tony, Geoff, Wera and Murray for stimulating discussions, suggestions, and proof reading.

- Thanks are given to the Earth Science Department staff: Ian for his help in solving all my computer problems; Renat for his help with thin sections and XRD analyses; Steve for supplying the right equipment at the right time; Sydney and Elaine for those numerous administrative details.

- Thanks to Ritchie Sims at the Geology Department, University of Auckland for helping with the microprobe, and his prompt reply to my queries later on. Stella Belliss at Landcare Research for supplying SAR imagery Also to Ken Palmer at Victoria University for his prompt return of XRF analyses.

- Thanks must go out to my fellow MSc students who helped make the last two years very memorable. Thanks to Wendy, Nicky, and Andy for the brain storming sessions (especially geochemistry). Thanks to all the other people who showed an interest in this study.

- Many thanks must go to my family for their support (and field assistance from Heath) during the last six years. A special thank you to Naomi for all her help during this study, and for just being there.

Table of Contents

List of Figures and Tables

Figures

Tables

Chapter One

Introduction

1.1 Introduction

The study area occurs along the north-south trending Onemana Peninsula located on the eastern side of the Coromandel Peninsula. The area is dominated by rhyolite domes, lava flows and associated breccias of the Whitianga Group, minor andesites, layered lake deposits, and late stage hydrothermal eruption breccias. The area is being actively prospected for deeper mineralisation because of the occurrence of hydrothermal alteration, and features associated with the upper levels of a geothermal system. Hydrothermal alteration occurs in a zone that is structurally controlled by a complex fault system.

This study will discuss the geological features of the Onemana area, and will attempt to determine the relationships between the geology, structure and hydrothermal alteration that is evident within the area.

1.2 Study Objectives

The aims of this study are the following:

- To construct a map of the Onemana Peninsula.
- To study the volcanology and petrology of the rocks in the Onemana area.
- To determine the controls on mineralisation
- To study the geochemistry and mineralogy of the volcanic rocks using petrological techniques, XRF and microprobe.
- Delineate alteration mineralogy and patterns, and geochemical changes in the host rock due to increased intensity of alteration.

1.3 Regional Setting

1.3.1 Location/Physiography

The study area occurs over the northern and central parts of the Onemana Peninsula (Fig. 1.1). The area is bounded by the coastline to the east, Wharekawa Harbour to the north, Rangipo Road to the west, and latitude 6443000 to the south. The study area consists of approximately 14km^2 of exotic forests, pasture, and the Onemana village. Elevation in the area varies from sealevel to a maximum height of 210m, with topography ranging from undulating hill country to steep ridges. The coastal area is steep with cliffs up to 60m high. The topography is related to the nature of volcanism, structure and hydrothermal alteration.

The area is dominated by three main rhyolite massifs: Pohakahaka, Pokohino and Wharekawa dome complexes. The Pohakahaka Dome Complex occurs in the south of the study area. This highly eroded dome complex has a maximum height of 128m, and appears to have a north south alignment. The Pokohino Dome Complex dominates the central region of the study area. This dome complex has a maximum height of 180m, and has a distinctive NE alignment. Numerous lava flows are evident on the southeastern side of the Pokohino Dome Complex. The Wharekawa Dome Complex in the north of the study area consists of three main domes: Ridge, Main and Peak domes. Ridge dome reaches a maximum height of 210m.

Between the Pohakahaka and Pokohino dome complexes, the topography is subdued due to the erosion of hydrothermal altered lake sediments and rhyolite lavas. Areas of silicification are typically represented by hills and ridges inland , bluffs along the coast and on the western flanks of The Knob.

1.3.2 Regional Geology

The Coromandel Volcanic Zone (CVZ) occurs from Great Barrier Island in the north to the Kaimai Ranges in the south, and is part of the larger Hauraki Volcanic Zone (HVR) (Skinner 1986) (Fig. 1.2). The HVR is an extensive region of late Cenozoic volcanism created by oblique westward dipping subduction along the Australian and Pacific Plate boundaries (Clarke et al. 1990).

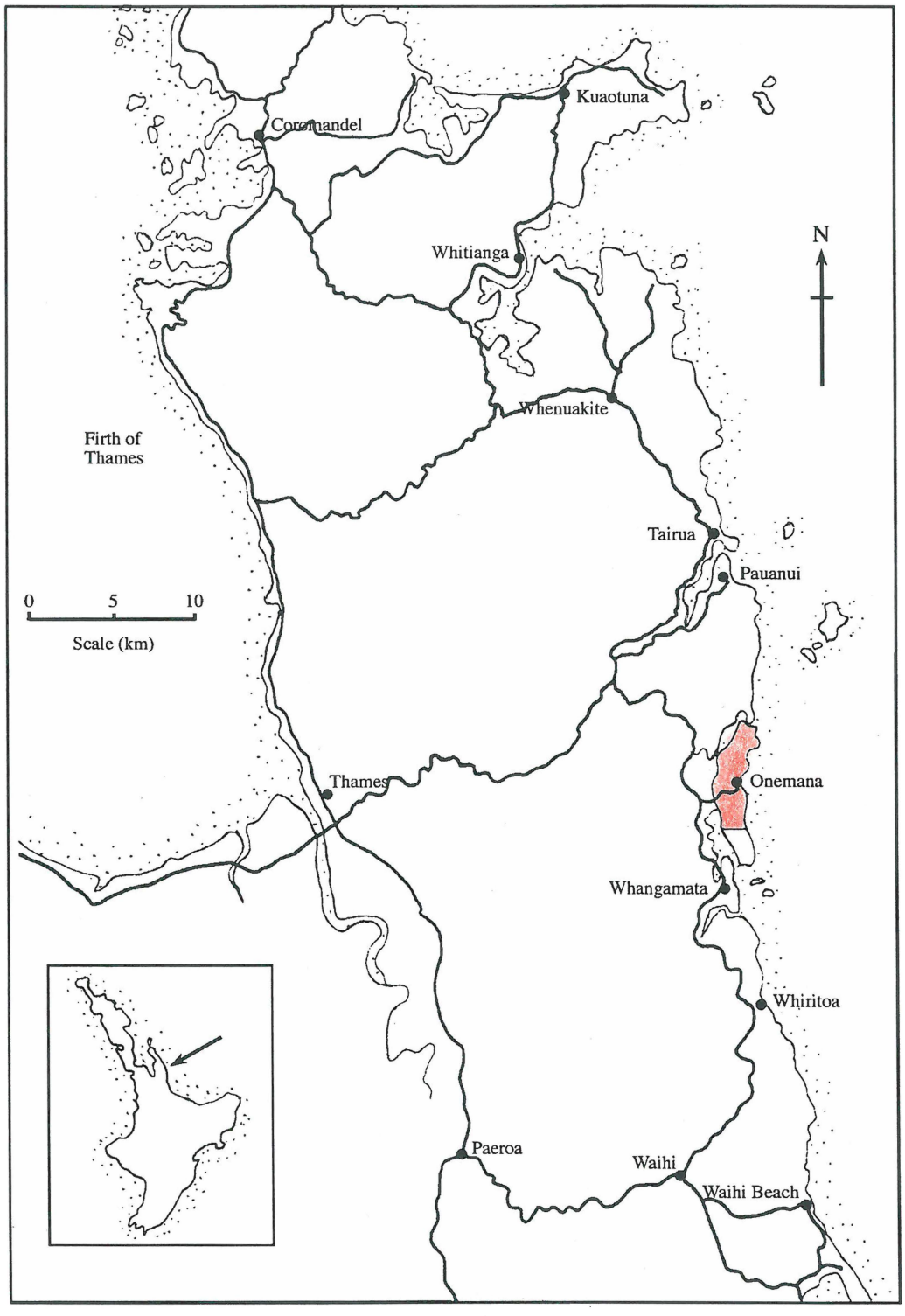

Figure 1.1. Location map of study area.

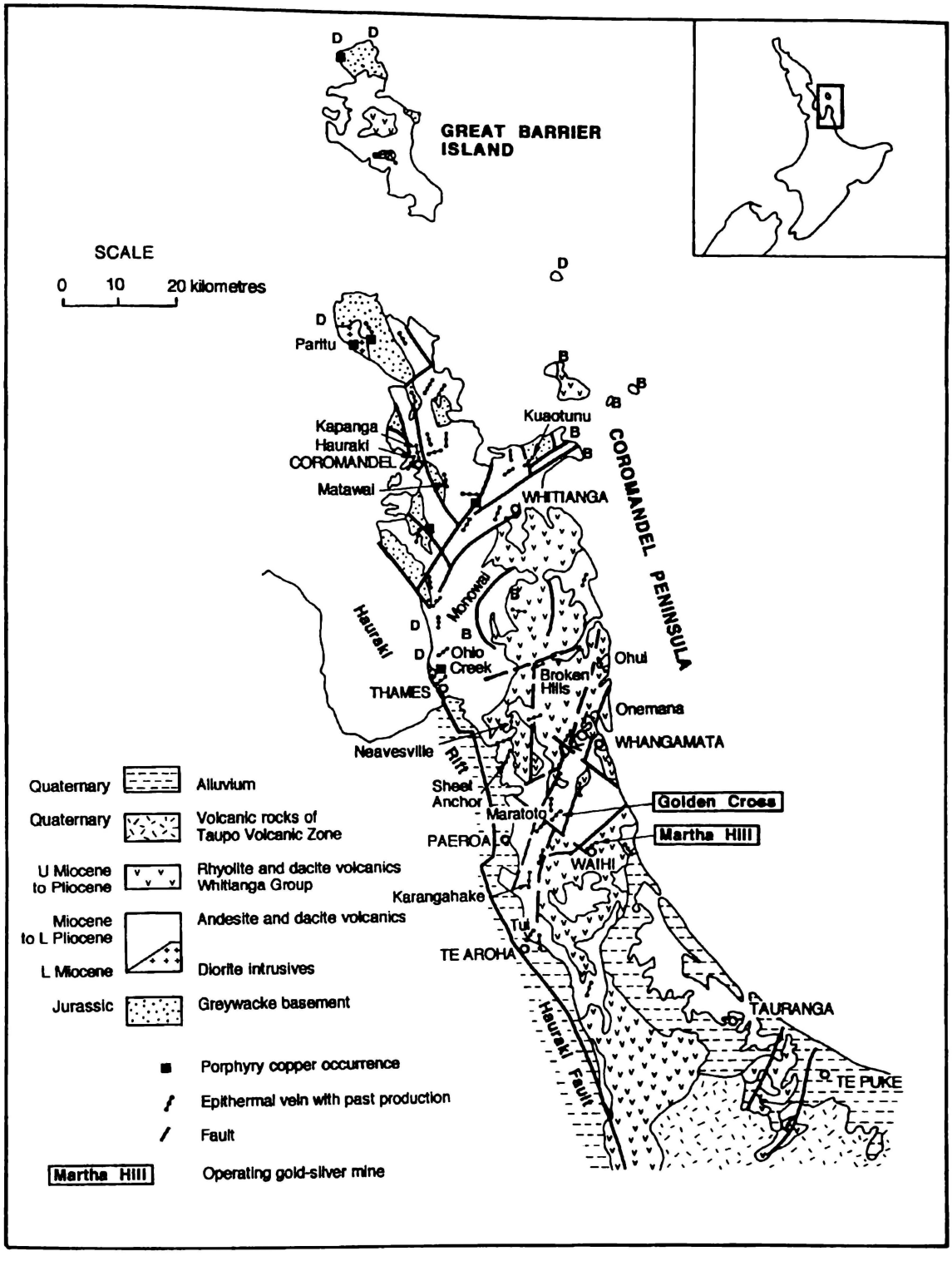

Figure 1.2. Coromandel Peninsula showing geology (after Skinner 1986), and distribution of epithermal gold-silver veins and porphyry copper occurrences. B=Mercury Basalts (Miocene to Pliocene), D=diorite intrusions (Miocene), KOST=Karangahake-Ohui Structural Trend (after Brathwaite et al. 1989; Merchant et al. 1988; Barker 1991).

The CVZ has a basement consisting of horst and graben blocks of Jurassic greywacke (Manaia Hill Group), which are locally overlain by non-volcanogenic marine sediments (Te Kuiti Group), and minor volcanogenic marine sediments (Waitemata Group) of early Miocene age (Skinner 1986). The volcanic history is predominantly one of alternating pyroxene andesite and hornblende-hypersthene andesite to dacite, followed by significant volumes of rhyolite (Skinner 1986; 1993). New K-Ar age data determined by Adams et al. (1994) showed that volcanism was continuous on the Coromandel Peninsula from c. 18 to 4 Ma (early Miocene to early Pliocene).

Early mapping of the volcanic sequence on the Coromandel Peninsula by Fraser and Adams (1907) subdivided the volcanic rocks based on hydrothermal alteration and mineralisation. Healy et al. (1964) and Schofield (1967) used lithology and composition to compile the New Zealand Geological Survey 1:250 000 maps. A summary of the regional stratigraphy is given by Skinner (1986, 1993) in Table 1.1.

Table 1.1. Summary of regional stratigraphy of the Hauraki Volcanic Region, after Skinner (1986).

Group	Sub Group	Formations	Age
Whakamarama		Waiteariki Ignimbrite Aongatete Ignimbrite	mid Pleistocene
	`Waitawheta Dacite'	informal	Plio-Pleistocene
Kerikeri Volcanics	Mercury Basalts	several centres	late Upper Miocene
Whitianga	Minden Rhyolite	5 formal units + many informal centres	Late Miocene to Pliocene
	Coroglen	several flow sheets +7 formal units	Late Miocene to Early Pleistocene
Coromandel	Omahine	1 formal + few informal units	Late Miocene-Pliocene
	Kaimai	3 formal units	Late Miocene-Pliocene
	Kiwitahi	several centres	Mid to Late Miocene
	Waiwawa	3 formal units	Early late Miocene
	Kuaotunu	16 formal units	Early to mid Miocene
		Paritu and Cuvier Plutonics	Late early Miocene
Waitemata	Kawau and Warkworth	Colville	Early lower Miocene
Te Kuiti		Torehina	Mid to upper Oligocene
Manaia Hill		several formal units	Late Jurassic

Overlying the sediments of the Manaia Hill Group are andesites and dacites of the Coromandel Group. Rocks of the Coromandel Group were emplaced from the late Miocene to Pliocene and are generally older than the

Whitianga Group. The exception to the rule is the Omahine Andesite which post-dates the rhyolitic volcanics of the Whitianga Group.

Plutonic members of the Coromandel Group intrude older Coromandel Group units in the north of the Coromandel Peninsula, and are associated with andesite-dacite dyke swarms (Skinner 1986). The Paritu quartz diorite pluton gives a K-Ar age of 16.0 to 17.1 Ma (Richards et al. 1966).

The Whitianga Group consists of ignimbrites, dome forming rhyolites, rhyolite flows and tuffs, and sediments (Christie and Brathwaite 1986). These rocks are mainly confined to explosive centres on the eastern part of the peninsula. Near Whangamata there are two known explosive centres: the Wharekawa Caldera, based on landsat photo lineations (Skinner 1986); and the Tunaiti Caldera (Briggs and Fulton 1990). A larger centre (Kapowai Caldera) is also identified 20km NW of Onemana by Skinner (1986). Mapping of rhyolite centres suggest that many sequences begin with pyroclastic eruptions followed by the extrusion of rhyolite domes and flows (Christie and Brathwaite 1986). This is evident from mapping of the Kapowai Caldera (Skinner 1986) and the Tunaiti Caldera (Briggs and Fulton 1990). The Whitianga Group has been subdivided into subgroups based on the two main phases of activity (Table 1.2).

Table 1.2. Subdivisions of the Whitianga Group, after Skinner (1986).

Subgroup	Formation	Composition
Minden Rhyolite	Ohena Rhyolite	bi-plag±hn
	Ahu Ahu Rhyolite	bi-hn-san-qu-olig
	Rangihau	hy-plag±aug
	Ruahine	bi-qu-plag±hn
	informal	bi-qu-plag
		hn-hy-plag
		bi-hn-plag
		hn-plag
		bi-san-qu-plag
	Te Weraiti	hn-bi-plag-qu
Coroglen Ignimbrite	Coralie Breccia	plag±san±qu±hn±aug±bi
	Te Koru Ingnimbrite	qu-olig±bi
	Whakapenui Ignimbrite	plag-hy-hn±aug±qu±bi
	Hot Water Beach Ignimbrite	plag
	Wharepapa Ignimbrite	plag-hy-lithic±aug±bi
	'Owharoite'	plag-qu-hy-bi
	'Tridymite rhyolite'	plag-hy±qu±bi

Minor basaltic volcanism occurred in scattered localities in the northeast of the Coromandel Peninsula. The eruption of basalts is thought to have a bimodal association with some Whitianga Group rhyolites (Skinner 1986).

1.3.4 Structure

The regional structure in the Onemana area is dominated by the NNW trend of the Coromandel Peninsula and NNE to ENE trending normal faults (Figs. 1.2, 1.3). Most of the NNE to ENE faults are downthrown to the south and some appear to have a strike-slip component (Brathwaite et al. 1989). These trends are thought to be controlled by pre-existing horst and graben faults in the basement rocks (Skinner 1986; Clarke et al. 1990). The regional structure is influenced mainly by the Hauraki Rift in the west, and the NE-trending Colville Ridge to the east (Clarke et al. 1990).

A major NNE structural corridor extends from Karangahake in the south to Onemana and Ohui in the north, and is defined by Merchant et al. (1988) as the Karangahake-Ohui Structural Trend (KOST) (Fig. 1.2). The 5km wide corridor appears to be an extensional rift-type feature. A number of important epithermal deposits are associated with this structural feature, e.g. Karangahake, Waitekauri, Golden Cross, Maratoto, Wharekirauponga, and Ohui.

Preliminary analysis of SAR imagery over the eastern Coromandel by Belliss and Christie (1994) and Christie et al. (1994), show the eastern Coromandel to be dominated by NNE-NE trending structures.

1.3.5 Hydrothermal Alteration and Mineralisation

The Coromandel Peninsula is noted for its epithermal gold-silver mineralisation, with more than a 1000 workings in nearly 50 separate deposits (Brathwaite et al. 1989). Epithermal mineralisation predominantly occurs associated with steeply dipping normal faults with a strike-slip component. The dominant strike of the veins is NE with minor N-S and E-W trends (Christie and Brathwaite 1986; Clarke et al. 1990; Gadsby et al. 1990; Brathwaite et al. 1994).

Most of the epithermal gold-silver mineralisation appears to be related to the late Miocene to Pliocene rhyolitic volcanism (Christie and Brathwaite 1986), while Miocene andesite is the dominant host rock. Rhyolitic rocks are the main host rocks of some smaller deposits, e.g., Broken Hills, Wharekirauponga, and Neavesville (Brathwaite et al. 1989).

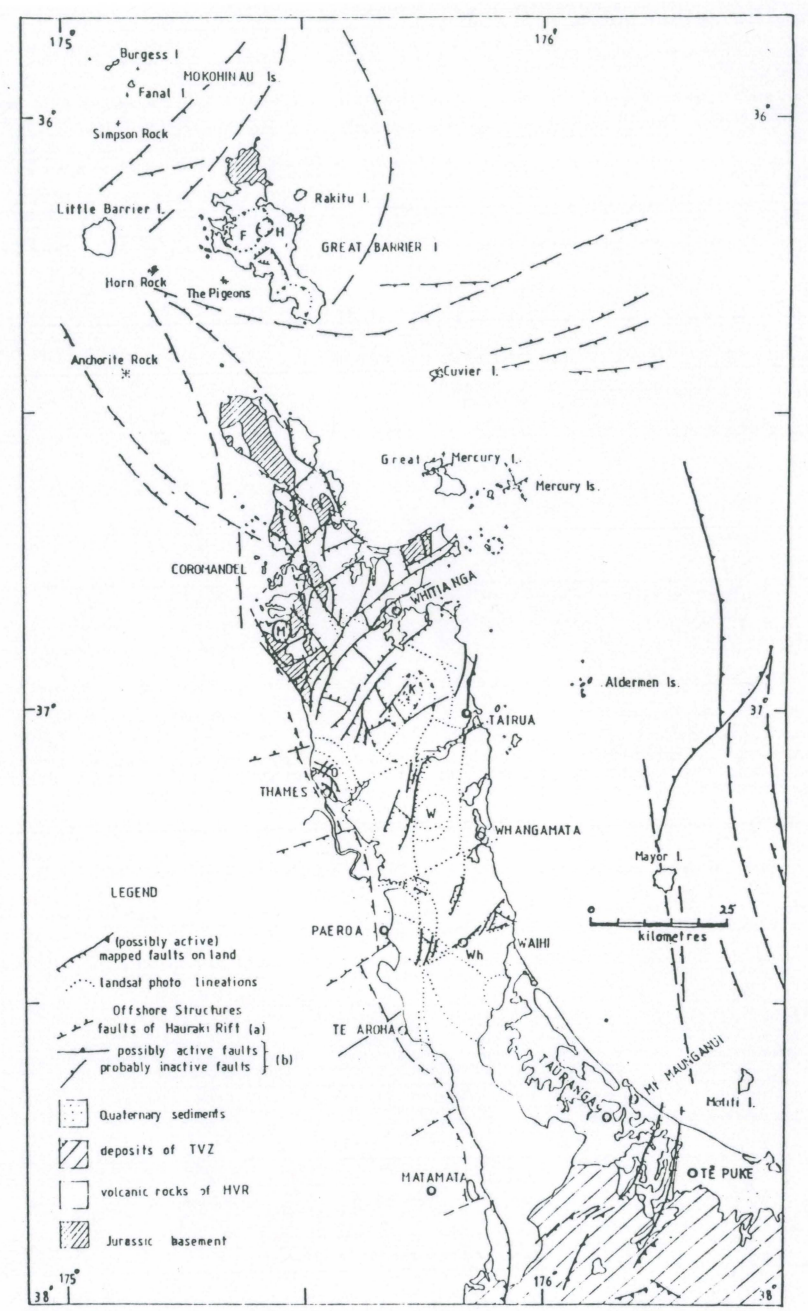

Figure 1.3. Structural and tectonic map of the Coromandel Volcanic Zone. K=Kapowai Caldera, W=Wharekawa Caldera (after Hochstein and Nixon 1979; Skinner 1986).

Hydrothermal alteration is generally zoned parallel to the strike of the quartz veins. Alteration adjacent to veining is characterised by quartz - illite - adularia ± pyrite. Argillic alteration (kaolinite - smectite - illite-smectite ± pyrite) commonly occurs as a late stage overprint alteration. An outer zone of weaker alteration is characterised by chlorite - calcite alteration of primary pyroxenes and biotites, and replacement of groundmass glass by smectites (Brathwaite et al. 1989).

Hydrothermal alteration of epithermal deposits in the NNE structural zone typically has an inner adularia - sericite zone, surrounded by a sericite - argillic intermediate zone, which grades outwards into a zone of propylitic alteration.

1.4 Previous literature

No historical work has been published on the geology of the Onemana region. All previous regional maps have mapped the Onemana region as Minden Rhyolites of the Whitianga Group or its older equivalent classification (Fraser 1910; Bell and Fraser 1912; Thompson 1966; Schofield 1967; Skinner 1986). Early detailed mapping was restricted to prospective areas for silver and gold mining (Downey 1935). Many unpublished theses by University of Waikato and Auckland students have provided detailed studies on small areas. Previous studies on areas south of Onemana have been done by Fulton (1988), Hunt (1991), and Haworth (1993). The study by Fulton (1988) on an area south of Whangamata led to the development of a facies model for the Tunaiti Caldera by Briggs and Fulton (1990). This is the first detailed description of a caldera on the Coromandel Peninsula. Rhyolite volcanics in the Whenuakite and Cooks Beach areas have been discussed in detail By Adams (1992) and Rogers (1994). Adams (1992) has also attempted to apply a caldera model for the evolution of the Whenuakite area.

The northern Onemana Peninsula is presently being actively prospected by Heritage Mining. A number of unpublished company reports document results of preliminary exploration activity. Published reports include the identification of a hydrothermal eruption breccia (Robson and Stevens 1991), and interpretation of an aerial magnetic survey over the Onemana area (Vidanovich 1991).

Chapter Two

Stratigraphy

2.1 Introduction

Description and mapping of lithostratigraphic units[1] is based on field work done during the summer of 1993/94 (Fig. 2.1; Map pocket). Field work consisted of mapping coastal exposures and inland outcrops. Unweathered outcrops were provided by coastal cliffs. Inland outcrops were moderately to highly weathered except where silicified. A lack of exposed contacts and restricted extent of volcanic units has limited the determination of the stratigraphic sequence. Interpretive cross-sections of the area in Figure 2.2 show contact relationships between various units.

Lithostratigraphy

The Onemana Peninsula is dominated by rhyolite domes and flows. Three dome complexes occur in the study area: Pohakahaka Dome Complex; Pokohino Dome Complex; and Wharekawa Dome Complex.

Domes and flows of the Pohakahaka Dome Complex in the south of the study area appear to be the oldest unit. This unit has been dated previously using fission track methods by Seward and Moore (1987) at 7.21±0.84 Ma (T12 662456).

The Pokohino Dome Complex is dominated by biotite rhyolites that appeared to have flowed in a SE direction from a NE trending ridge (presumed to be a fissure). Flows are less evident in the Wharekawa Dome Complex and the area may be dominated by rhyolite intrusives and dome lavas. From coastal exposures it is evident that pyroclastic material was deposited prior to the eruption of Peak Dome rhyolite lavas.

From flow structures exposed in lavas east of the Wharekawa Dome Complex, it is evident that some flows were erupted east of the present shoreline. These

[1] All lithostratigraphic names are informal

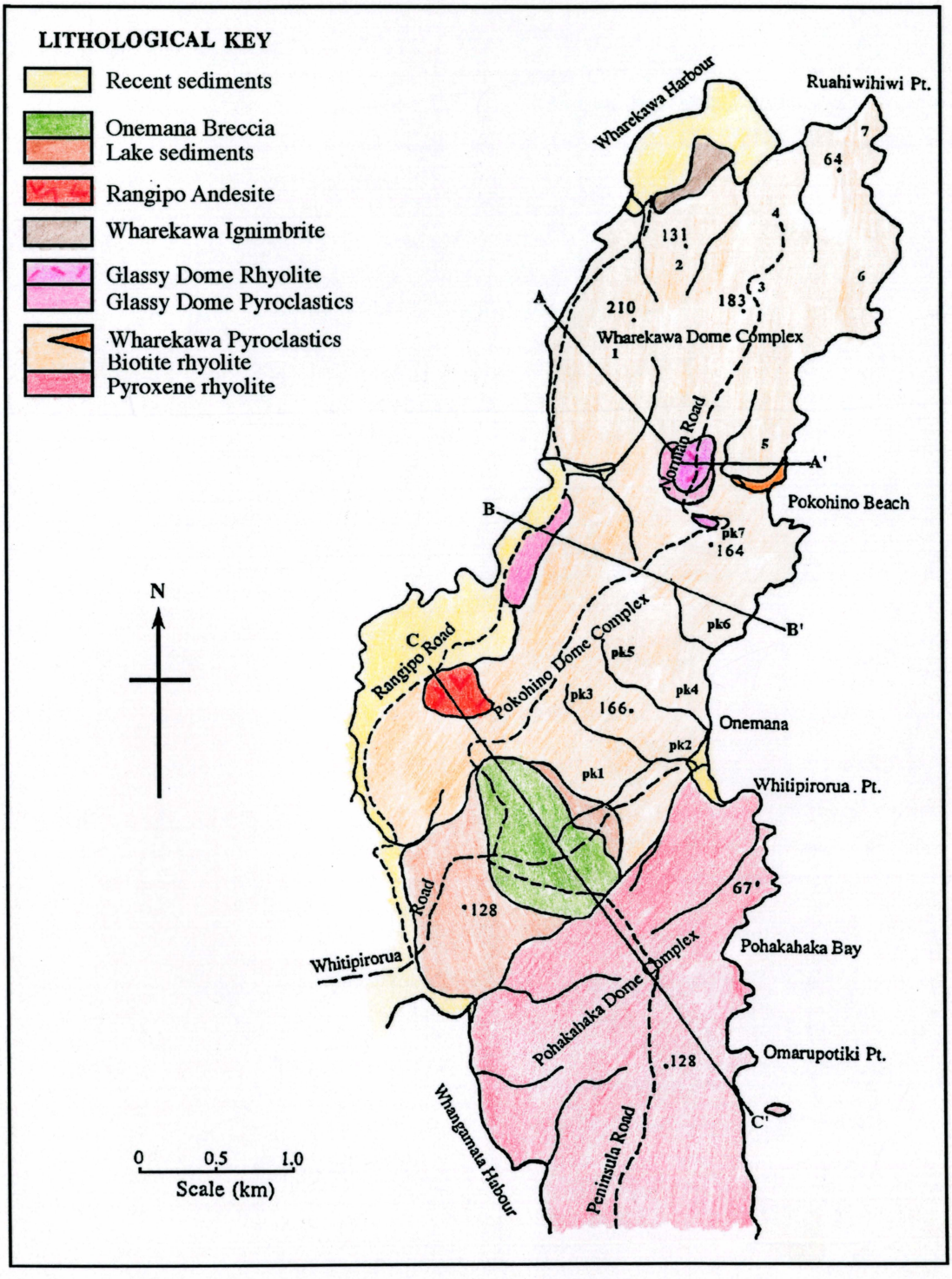

Figure 2.1. Simplified geology of the Onemana area, and cross-section locations for Fig. 2.2. Key : pk1-7: flows from Pokohino Dome, 1: Ridge Dome, 2: Ridge Dome Flow, 3: Main Dome, 4: Main Dome Flow, 5: Peak Dome, 6: Eastern Flows, 7: Subaqueous block lavas.

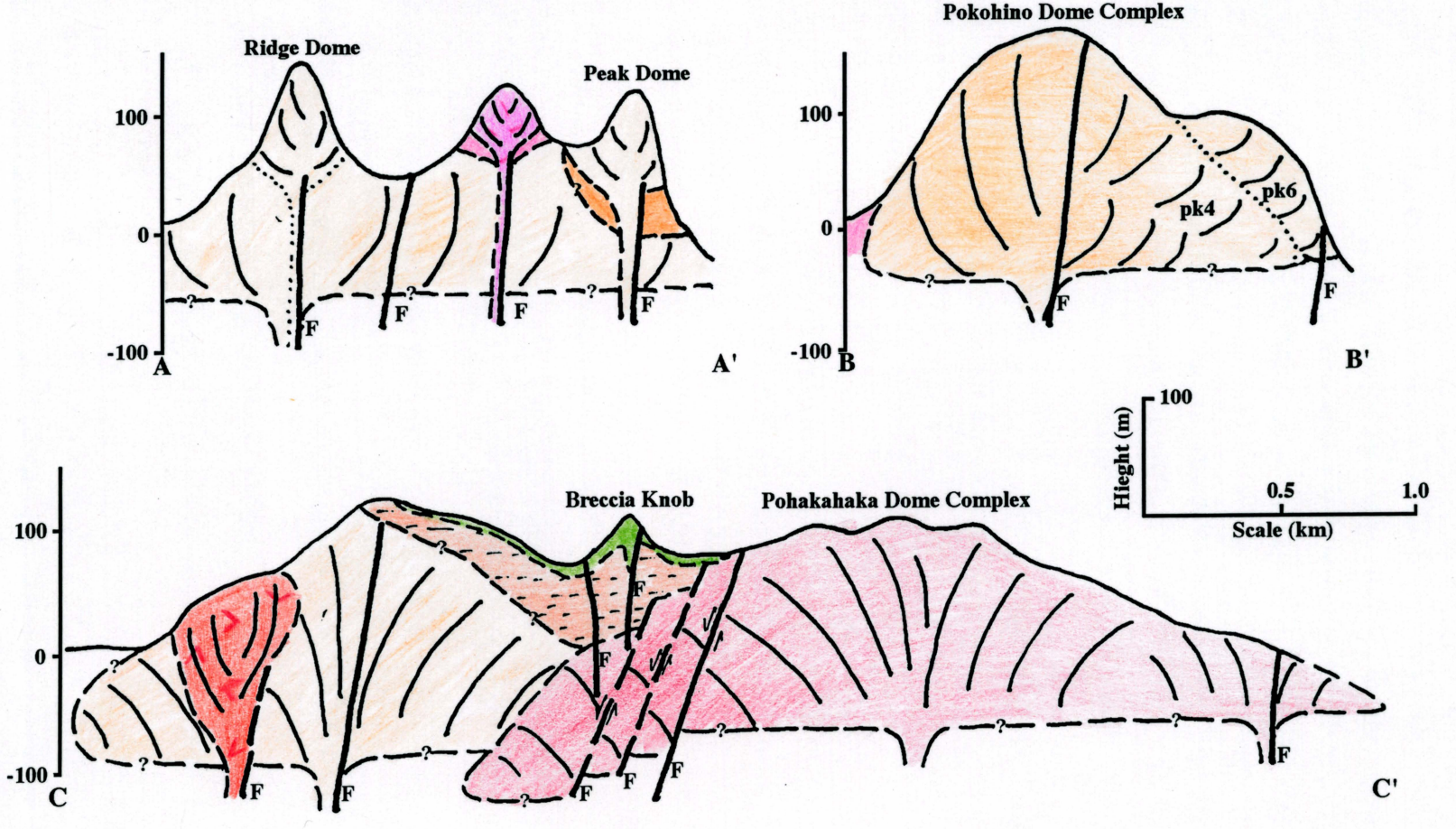

Figure 2.2. Interpretive cross sections through the northern and central areas of the Onemana Peninsula, showing geology and major structures.

flows become brecciated to the north, forming thick and extensive volcanic breccias.

Age correlation of the younger deposits (Glassy Dome Rhyolite and pyroclastics, Wharekawa Ignimbrite, and Rangipo Andesite) is difficult due to their limited spatial extent. The Wharekawa Ignimbrite outcrops to the north of the Wharekawa Dome Complex and appears to lap onto it. The source of this unit is presumed to be outside the study area. The Glassy Dome Rhyolite has intruded into both the Wharekawa and Pokohino dome complexes (Fig. 2.2a). Emplacement of this unit is thought to have occurred after the eruption of lithic-rich breccias that outcrop near the glassy biotite rhyolite and to the west of the Pokohino Dome Complex.

To the west of the study area (T12 450650) the Rangipo Andesite appears to have intruded the biotite rhyolites of the Pokohino Dome Complex (Fig. 2.2c). The andesite is unaltered and there is no significant increase in alteration in the surrounding country rocks.

Between the Pokohino and Pohakahaka dome complexes occurs a thick sequence of lake sediments. This unit is partially covered by a hydrothermal eruption breccia which appears to be erupted from a vent near Breccia Knob, where it appears thickest (>15m) (Fig. 2.2c) (Robson and Stevens 1991).

An airfall lapilli (Tuhua Tephra) deposit erupted from Mayor Island 20km SE of Onemana drapes over all of the units discussed above. This tephra is typically no more than 30cm thick, but can occur up to 6m deep.

2.2 Rhyolite Volcanism: a review

Emplacement Mechanisms

Silicic domes and flows commonly occur in rifts, grabens, and caldera settings. Extrusion of viscous magma generally occurs in groups of vents or along structural boundaries.

Fink (1983) developed a model for silicic flow emplacement based on a low volume (<1km^3) rhyolite obsidian flow (Fig. 2.3). Initial activity is marked by explosive eruptions due to the release of gas from the volatile-rich cap (Fig. 2.3b). The remaining volatile cap is erupted as a highly inflated pumiceous lava (Fig. 2.3c).

As the eruption continues, the less volatile magma reaches the surface and is erupted as an obsidian flow with low viscosity (Fig. 2.3d). As the obsidian flows over the pre-erupted pumice layer, volatiles escape the cooling upper surface forming a thin finely vesicular carapace (Fig 2.3e). In thicker flows, a stony rhyolite core can occur, with obsidian occurring as the chilled glassy carapace.

This model developed by Fink (1983) implies that the flow stratigraphy should consist of a basal layer or layers of tephra, overlain by coarsely vesicular pumice, obsidian, and finally poorly vesicular pumice. Towards the end of the eruption cycle crystalline rhyolite forms a summit dome.

The emplacement history and physical properties of a low viscosity, fountain-fed pantelleritic flow has been described by Stevenson et al. (1993) on Mayor Island. The flow stratigraphy comprises from top to base: a finely vesicular pumiceous carapace; an obsidian layer; central crystalline rhyolite; a lower obsidian layer incorporating a crumble breccia; above a fall lapilli layer (Stevenson et al. 1993).

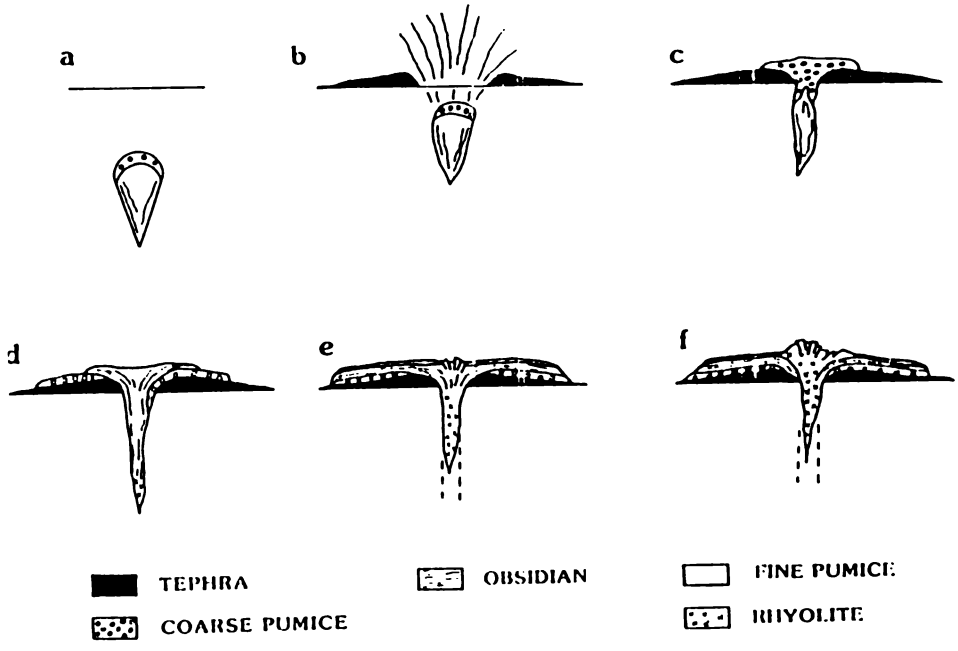

Figure 2.3. Diagram showing emplacement of a small rhyolite lava flow with concurrent development of flow stratigraphy. Geometry of rising magma in a and b is highly schematic (from Fink 1983).

Spherulites are a common devitrification feature in rhyolite flows. They occur as radiating aggregates of alkali feldspars, with or without cristobalite and tridymite (Cas and Wright 1987). Spherulites are commonly between 0.1-2.0 cm, but have been found up to a meter in diameter (Snake River Plain, Bonnichsen and Kauffman 1987). The morphology of the individual spherulites varies distinctly with temperature at which they form (Lofgren 1970; 1971a,b). Below 400°C spherulites are generally circular, between 400-600°C bow tie shapes occur, and above 700°C spherulites are lath like or circular with widely spaced large diameter fibres. Spherulites within the peralkaline 8ka flow at Mayor Island are thought to have begun growing above the brittle glass transition temperature (Stevenson et al. 1992), which is considered for calc-alkaline rhyolite glasses to be ~670°C by Westrich et al. (1988). High water contents in layers could promote growth rates of spherulites locally, producing lenses or layers of spherulites.

Common with spherulitic textures is poikilitic textures which form between 400-600°C at pressures less than 3kb. Granophyric textures are more common in older devitrified glassy rocks.

The devitrification textures are superimposed on flow structures showing their formation occurs when the flow has ceased.

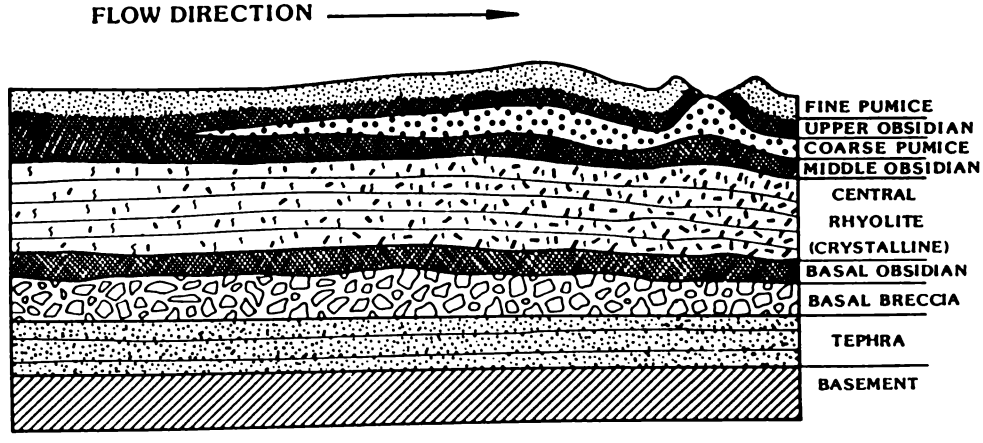

Figure 2.4. Schematic diagram showing formation of the coarsely vesicular pumice layer. Increasing downstream crystallisation accompanied by the release of gases and formation of micro-cracks leads to the rise of the gases to the base of the brittle surface crust, where the resultant bubbles can expand and coalesce. Thickness of this layer increases downstream, and eventually allows the rise of diapirs to the flow surface (from Fink and Manley 1987).

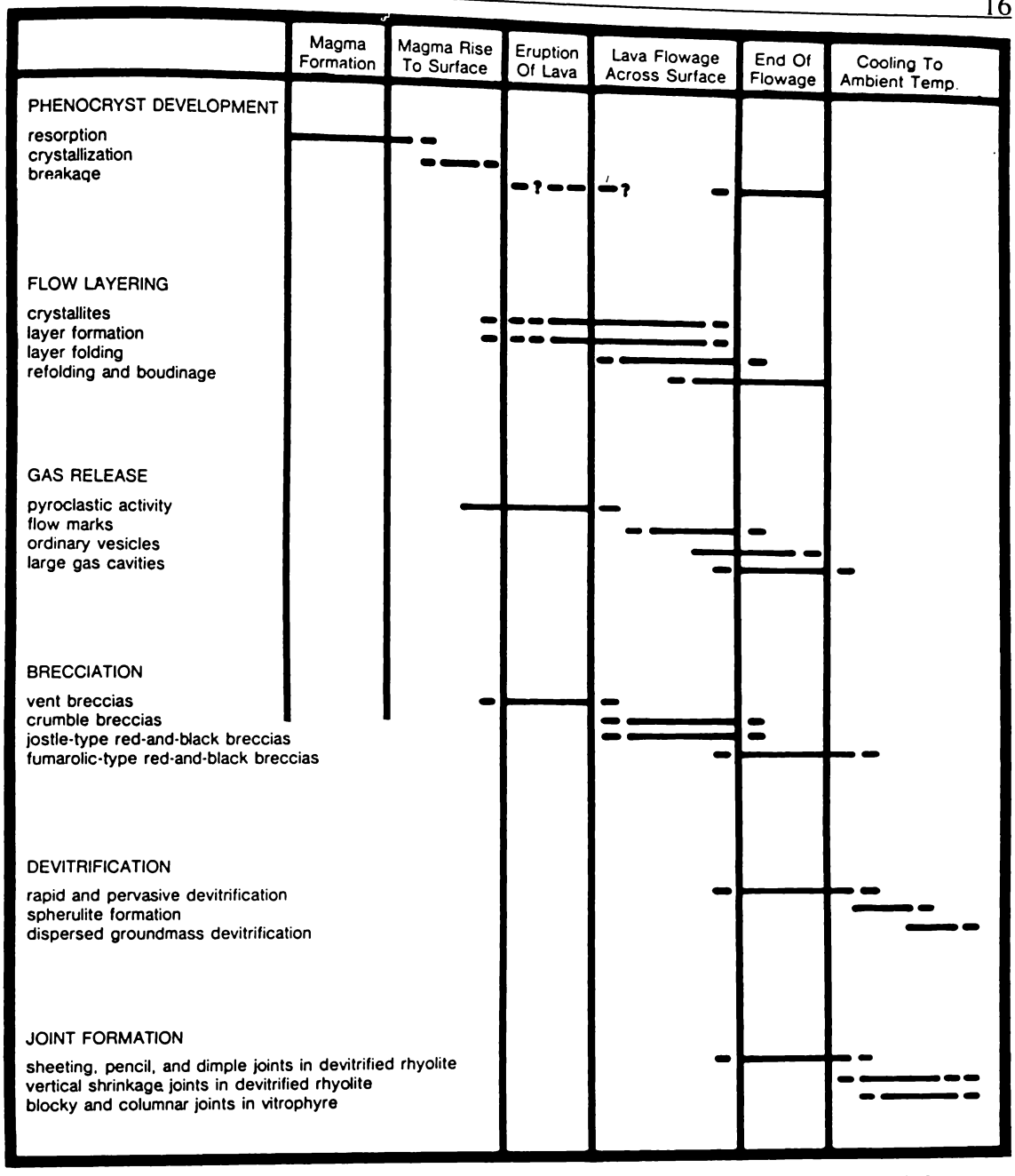

Figure 2.5. The approximate time sequence for the development of textural features within rhyolite lava flows that formed during the magma rising to the surface, and as the lava flowed along the surface and cooled to ambient temperatures (after Bonnichsen and Kauffman 1987).

Fink and Manley (1987) discuss three principal steps in the development of textures in silicic lavas and domes:

1) crystallisation within the flow releases dissolved magmatic volatiles

2) advance of lava forms microcracks through which these gases can move upwards

3) cooling of the upper surface increases the yield strength creating a non-deforming crust through which gases cannot migrate.

This gas rich low density layer can then rise buoyantly to the surface (Fig 2.4). From Bonnichsen and Kauffman (1987) a summary for the development of rhyolite flow textures is shown in Figure 2.5.

Tephra deposits associated with silicic domes

Heiken and Wohletz (1987) have discussed four general types of explosive volcanic activity accompanying the emplacement of silicic domes:

1) initial plinian and pheatomagmatic eruptions preceding dome emplacement

2) vulcanian explosions during episodic dome growth

3) peléean and merapian activity associated with dome destruction

4) phreatic explosions preceding magmatic activity or accompanying energetic hydrothermal activity at older domes.

The characteristics of each deposit is shown in Table 2.1.

Table 2.1. Dome tephra characteristics (from Heiken and Wohletz 1987).

Eruption type	Deposit	Size	Tephra Composition	Texture
Magmatic	Plinian pumice fall and flow	Coarse (near vent) fall (0 to -3ϕ)	magma composition	vesicular, angular
Pheatomagmatic	Dry surge	Fine ash (0 to 3ϕ)	slight to moderate surface alteration	non-vesicular, slablike and abraded
Vulcanian	Wet and dry surges, coarse and fine fallout	Medium to fine ash (1 to 4ϕ)	Fresh and altered juvenile, altered lithic clasts	Blocky and equant, non-vesicular to poorly vesicular, rounded
Peléean and Merapian	Poorly bedded avalanche and flow bedded ash cloud surge	Blocks and ash (-5 to 1ϕ)	Fresh magma and lithic clasts	Poorly vesicular and blocky
Phreatic	Poorly bedded thin ash and	Fine ash and minor lapilli (-1 to 3ϕ)	Altered lithic clasts	Aggregated, complex shapes, 'muddy'

2.3 Pohakahaka Dome Complex

Distribution

The Pohakahaka Dome Complex is a >3km long, 1.5km wide belt of rhyolite domes and flows which trend in a N-S direction south of Onemana. The Pohakahaka Dome Complex has multiple vents, with three vent sites suggested based on structures evident along the coastline. There are possibly more vents inland, but these are not exposed. The area has a maximum topographical height of 128m suggesting that this is the minimum thickness for the rhyolite lavas. Exposures inland are limited to road cuttings and streams due to the highly weathered nature of the rhyolites, and lapilli cover.

A fission track age of 7.21±0.84Ma (Seward and Moore 1987) was obtained from obsidian in the Whitipirorua Point area (T12 662456). This method has now been superseded by more reliable methods with less error (e.g. K-Ar). Comparison of dates from other Minden Rhyolites dated by Seward and Moore (1987) with corresponding K-Ar dates obtained by Adams et al. (1994) show little variation, but do appear to show slightly lower ages than those obtained by the K-Ar method.

Lithology

The rhyolites of the Pohakahaka Dome Complex are typically pinkish-brown, flow banded, spherulitic, porphyritic rhyolites with phenocrysts of plagioclase, quartz, relict pyroxenes, and opaques. The flow morphology suggests that these lavas can be highly variable within a single flow unit. This was most distinctive in flow folds at Whitipirorua Point. Nelson (1981) suggested that lithological differences in rhyolite flow banding could result from thermal feedback in layers, due to shear stresses in the moving lava.

At Whitipirorua Point the rhyolite shows well developed flow banding with layers of pink crystal-rich layers and dark-grey/black vesicular spherulitic layers within large overturned flow folds. The distinct layering is most noticeable closer to the fold axis. Further away the spherulitic layers become discontinuous and lensoidal. The centre of these folds are assumed to be brecciated, and through weathering some are found to be hollow.

A lava flow exposed along the coastal section (Fig. 2.6) at +0.6km (T12 663455) shows poorly developed columnar jointing. There is no major change in

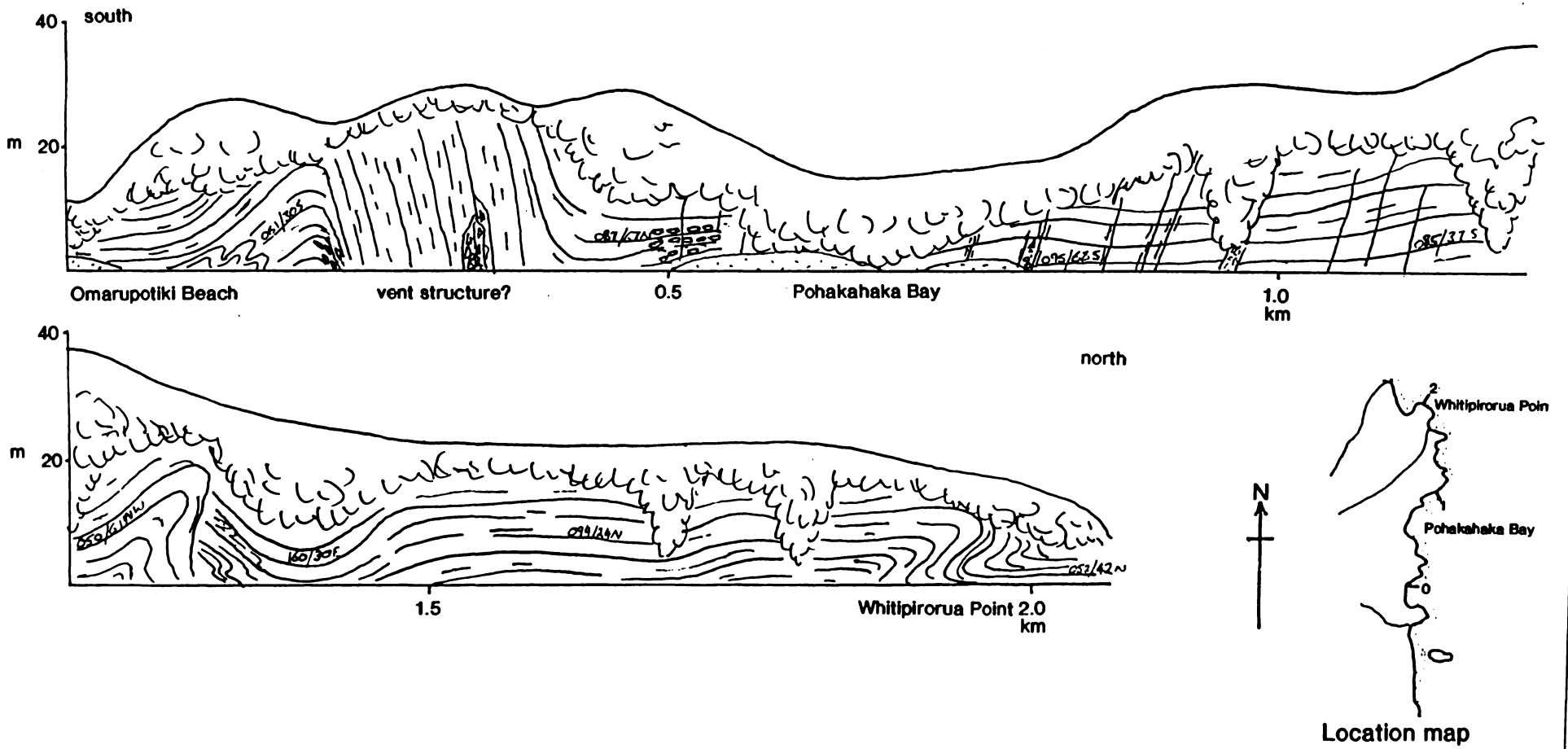

Figure 2.6. Sketch of coastal section from Omarupotiki Beach to Whitipirorua Point.

lithology but samples taken from this lava show rare (<1%) dark grey subrounded inclusions up to 5 mm in diameter.

In the Pohakahaka Bay area the rhyolites are dominantly pinkish orange, flow banded, and have abundant spherulites up to 2cm in diameter. North of Pohakahaka Beach numerous cracks up to 10cm thick are infilled by a fine grained pink clay. The areas of clay are thought to have formed where there has been extensive devitrification of glass along large scale perlitic fractures.

The only exposure of autoclastic breccia found in the Pohakahaka Dome Complex is in limited exposures to the south of Pohakahaka Bay. Exposed at the southern end of Pohakahaka Beach there is a 10 m exposure of autoclastic breccia that occurs adjacent to a subvertically flow banded rhyolite (Fig. 2.7). The coarse welded breccia is composed of flow banded pink and orange spherulitic clasts in a grey, fine grained ash weathered to clay matrix. Clasts are aligned in a subparallel manner in the upper part of the breccia. Near the contact with the coherent flow there is interlayered breccia with the pink flow banded rhyolite. Near the base of the exposed breccia the clasts become increasingly angular and increasingly tightly packed, and there is a distinct lack of the ash matrix.

Figure 2.7. Autoclastic breccia exposed at the southern end of Pohakahaka Bay (T12 662447) showing elongated clasts of rhyolite within a weathered ash matrix.

Dadd (1992) has described elongated fragments within rhyolite flows which are of a similar nature to those exposed at Pohakahaka Bay. Figure 2.8 shows the

model used by Dadd (1992) to illustrate the formation of lenticulite breccias. The development of lenticulitic breccia or shear zones within a rhyolitic mass may be due to an increase in water content or water movement in these zones (Dadd 1992).

Structure

Coastal exposures south of Onemana show the exposed lava flows to be planar to undulating, with dips to the NNW and SSE, which are parallel to the present day coastline (Fig. 2.6). A small area of eastward dipping flows occur between Whitipirorua Point and Pohakahaka Bay (T12 663456). It is difficult to determine the source of this flow, as there is no obvious vent site to the west. A cross-section through this flow shows distinct layering within a single flow unit (Fig. 2.9).

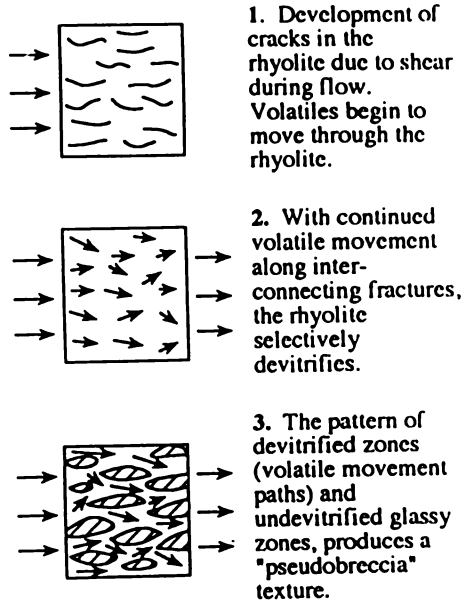

Figure 2.8. The development of lenticulite breccia though the formation of a "pseudobreccia" by a process of a process of aqueous diffusion and selective devitrification (after Dadd 1992).

Large scale folding occurs in the southern side of Whitipirorua Point. Small scale (<10cm) fold structures are evident within each layer that occurs in the large fold.

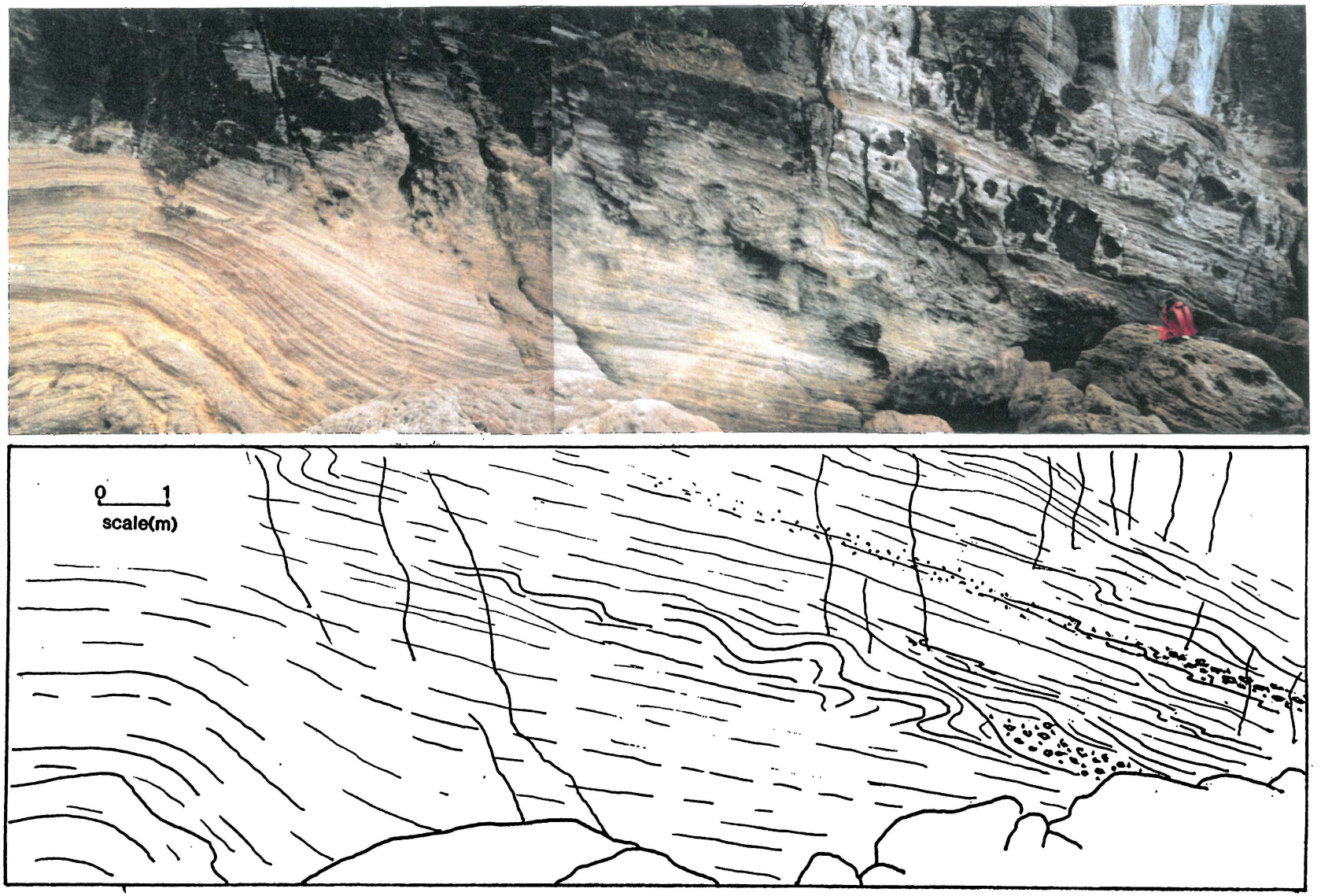

Figure 2.9. Photograph and schematic interpretation of variation within a single rhyolite flow (T12 663453). Direction of flow is left to right as determined from the nature of the flow folds.

Two areas are proposed as possible vent sites for the flows exposed in the coastal sections: Whitipirorua Point area, and Pohakahaka Bay area (Fig. 2.10).

The fold axis and occurrence of overturned folds at Whitipirorua Point suggests that the source is close and to the SE of the folds, which suggests a vent in the small bay south of Whitipirorua Point. The strike and dip on flow banding exposed in the south side of this bay also points to a vent site within the bay.

Two vents are thought to occur in the Pohakahaka Bay area based on flow direction and topographical expression. Flow direction north of Pohakahaka Bay may have originated from a position near Trig ITB (T12 663452). Direction of flows in the south suggest a vent within the headland south of Pohakahaka Bay. The southern headland of Pohakahaka Bay shows dominantly vertical flow banding which may be inferred as an extrusion point for the lavas to the south. The flow banding does not appear to be funnel shaped like those described in the Hot Water Beach Rhyolite Dome by Adams (1992), but does show the development of caves at the base of the exposure. The autoclastic breccias described above occur on the flanks of this structure. In the centre of this structure there is a small area of angular, insitu breccia, in a fine weathered ash matrix.

The suggested vent positions for the Pohakahaka Dome Complex coastal section are all aligned along N-S faults and shear zones (Chapter 3).

Inland domes and flows are best determined through topographical expression. Evidence for lava flows is best seen to the west of the Pohakahaka Dome Complex. Lava flow morphology interpreted from aerial photos suggest lavas flowed in a west to southwest direction from a possible vent at T12 651444.

A NE trending ridge near the northern boundary of the Pohakahaka Dome Complex is thought to be an intrusive feature. The exposure is intensely spherulitic with subvertical to vertical flow banding.

Nature of contact

There have been no observed surface contacts of the Pohakahaka Dome Complex with any other unit. Holes drilled into Breccia Knob have intersected altered rhyolite flows at 60 masl below lake sediments and pyroclastics. The northern boundary of the Pohakahaka Dome Complex appears to be fault bounded by the NE-striking Whitipirorua Fault. Contact with the Pokohino

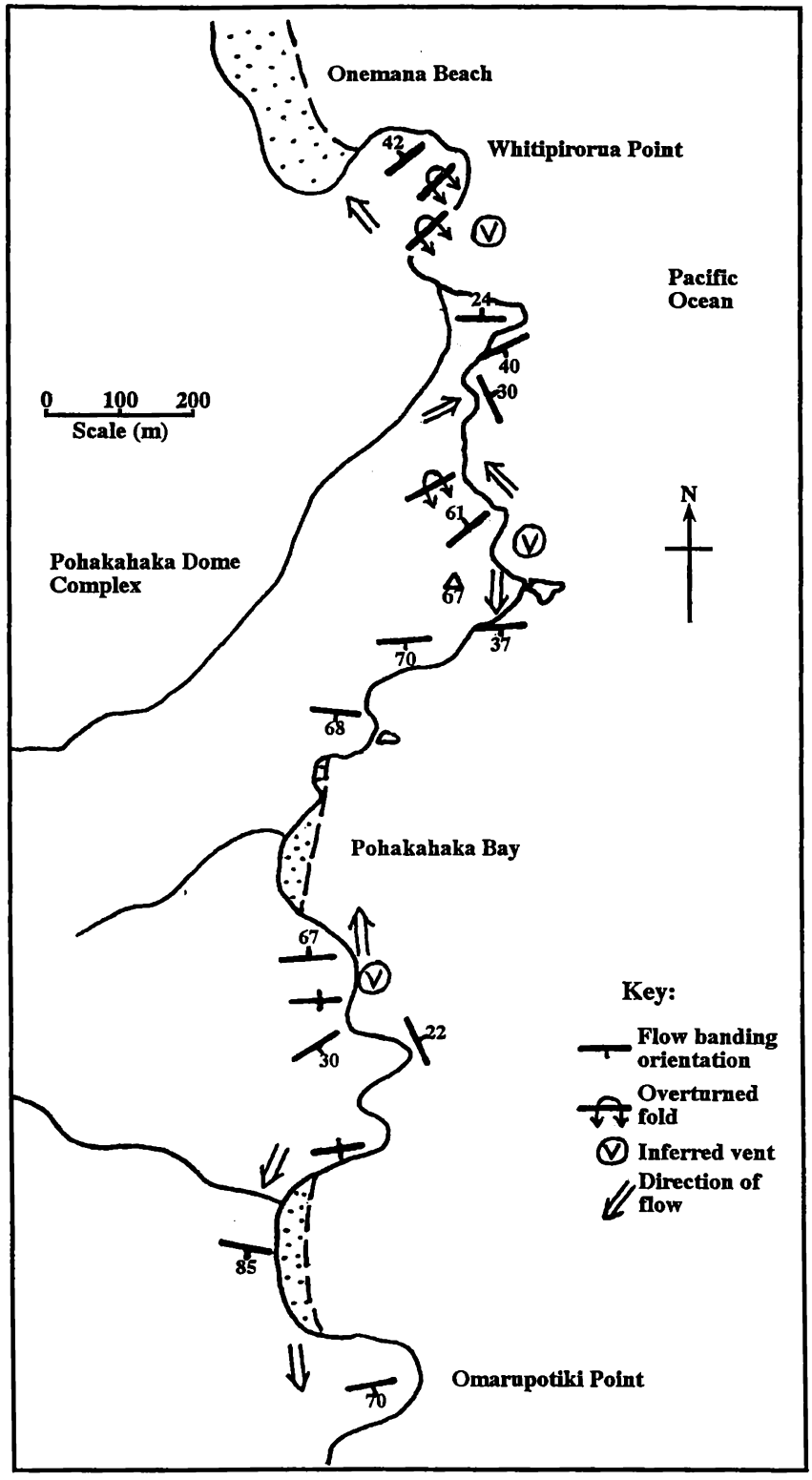

Figure 2.10. Flow directions and inferred vent locations for pyroxene rhyolite lavas from the Pohakahaka Dome Complex exposed in coastal section south of Onemana.

Dome Complex is unclear, but is thought to occur along either the Whitipirorua or Onemana faults. Ground magnetic surveys show a strongly undulating boundary approximately parallel with the Whitipirorua Fault. However, this may be due to alteration north of the fault.

2.4 Pokohino Dome Complex

Distribution

The Pokohino Dome Complex is a 3.5km long 1.5km wide belt of rhyolite domes and flows stretching from The Knob to Pokohino Beach. The Pokohino Dome Complex has multiple vents which appear to occur along a NE structural lineation. All flows are thought to be erupted from vents aligned along this structure except those east of Pokohino Beach.

Based on topographic highs the minimum thickness of the rhyolite is presumed to be 180m in the north and 156m at The Knob.

Lithology

The rhyolites of the Pokohino Dome Complex are dominantly pink, flow banded and spherulitic with phenocrysts of plagioclase, quartz and biotite. Original textures and phenocryst assemblages have been altered in the east along the coastline and around The Knob by hydrothermal alteration (Chapter 7).

From coastal exposures three lava flows from the Pokohino Dome Complex are exposed north of Onemana; pk2, pk4, pk6 (Fig. 2.11). No contacts were seen due to non-exposure and hydrothermal alteration masking primary textures and mineralogy.

Altered flows exposed north of Onemana in coastal section are a pale orange white, highly porphyritic (10%) with large quartz phenocrysts up to 2mm. The flows are slightly vesicular due to the removal of plagioclase and biotite.

The pk2 flow shows distinct thick flow banding and undulating flow structures. The exposed section of the flow is altered and in outcrop is whitish orange vesicular rhyolite with thin (<10mm) bands of crystal-rich spherulites. The dip direction of the flow bands is SE to S.

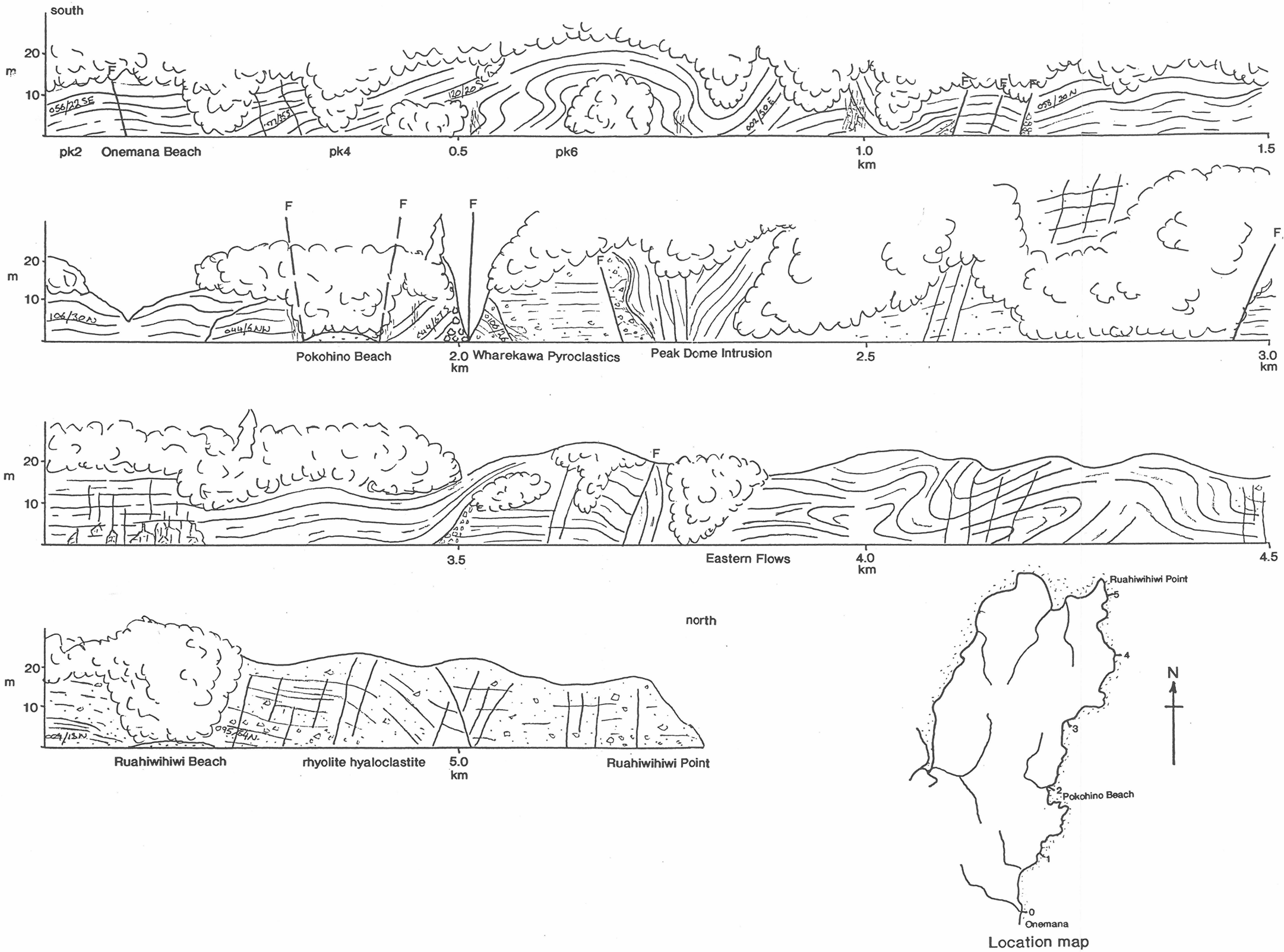

Figure 2.11. Sketch of coastal section from Onemana to Ruahiwihiwi Point.

The pk4 flow exposed to the north of pk2 is distinctly more spherulitic in outcrop. Alteration has masked the original textures, but the well developed spherulitic texture is still evident, with individual spherulites up to 20mm. The flow is vesicular and some lithophysae are present. Lenses of well developed spherulitic textures with lithophysae occur up to 10cm wide and 2m long. A small amount of autobrecciation is evident within these lenses. Flow banding commonly dips to the south indicating the vent for the flow is further north than the vent for pk2.

In outcrop pk6 is similar to pk2, but from petrographic investigation the pk6 flow is highly vesicular with numerous small elongated vesicles up to 1.0mm long and 0.5mm wide. Vesicles make up 20% of sample W941300. Vesicles have been infilled by hydrothermally derived quartz.

Samples collected from the top of the dome and its western flanks have distinctly well developed spherulitic textures, crystal-rich (up to 16 modal %), weakly developed perlitic fractures, with minor flow banding evident. Sample W941336 (T12 651467) shows a spherulitic glassy texture. Its lack of flow banding suggests it is part of the dome carapace.

Figure 2.12. Autoclastic breccia 100m north of Pokohino Beach within the biotite rhyolites of the Pokohino Dome Complex (T12 662476), with large pink unaltered rhyolite blocks in a coarse grained silicified matrix.

The only area of autobrecciation occurs north of Pokohino Beach (T12 664476). The breccia is silicified, very poorly sorted, matrix supported, and monolithic (Fig. 2.12). Though the clasts are monolithic there are two clast sizes and alteration types. Most noticeable are the large (>10cm) unaltered, subrounded, pink, spherulitic biotite rhyolite clasts that make up 7-10% of the breccia. Some clasts are altered around their rims. Much of the breccia is made up of small (<2cm) angular, pale yellow, spherulitic, biotite rhyolite clasts (40-50%). The matrix is made up of fine grained quartz with numerous quartz fragments and rare plagioclase.

Structure

From the morphology of the Pokohino Dome Complex it appears that the lava was erupted from a NE-trending structural lineation presumed to be a rift. This zone extends for 3km, and probably represents a deep seated basement fracture that acts as a conduit for rising magma. Wilson et al. (1984) and Nairn (1989) have recognised similar structures in the Okataina Volcanic Centre which have controlled the location and activity of linear vent zones.

From aerial photos it appears that the eastern lavas of the Pokohino Dome Complex were erupted as coulées. Cas and Wright (1987) describe coulées as lavas which form when the flow is asymmetrical and concentric to one side of the vent producing an extrusion which is elongated in plan. Ramp structures which are common in rhyolite coulées were not seen here, but have been observed in other domes in the Coromandel Peninsula (eg. Rogers 1994).

Lava flows are evident around The Knob and to the east of the Pokohino Dome Complex. The flows at the southern extent of the Pokohino Dome Complex appeared to have flowed in a radial pattern to the west, suggesting that this is the southern-most vent along the Pokohino Linear Vent Zone. Flows east of the Pokohino Dome Complex flow to the SSE to SE from several different vents aligned NE along the rift. From aerial photo interpretation and collection of structural data, seven flows were identified (pk1-7), though no flow contacts were observed in coastal section. It appears that activity along the vent zone moved to the north, as flows to the north flowed over southern flows. Also the volume of each individual flow appears to decrease to the north.

The flow pk6 at the north end of Onemana Beach shows chaotic flow structures possibly due to flowing over the edge of the preceding flow. Flow orientation to the east suggests a similar vent as pk4.

Further north intense alteration in the Pokohino Beach area has destroyed any flow morphology. Measurements from the flow banding indicate that lava has flowed from the south to south-east. These flows are included in the Pokohino Dome Complex as they are similar in lithology, geochemistry and mineralogy.

To the west of the Pokohino Dome Complex exposure is poor and there is no evidence for significant flows. The steep sided nature of the western side is suggested as an exposed side of a dome.

2.5 Wharekawa Dome Complex

2.5.1 Wharekawa Pyroclastics: pre-dome pyroclastics

Pyroclastic and associated epiclastic material is exposed in a coastal section north of Pokohino Beach (T12 664475). The exposed volcanogenic material represents erupted material prior to the eruption of the Peak Dome rhyolites. A stratigraphic column of the exposure is shown in Fig. 2.13. These deposits have been collectively named the Wharekawa Pyroclastics in relation to the Wharekawa Dome Complex. The Wharekawa Pyroclastics consist of rhyolitic pyroclastic flows, ash falls, breccia and laharic deposits.

Lithology

Unit 1 consists of very poorly sorted, matrix supported, multilithological breccia. Clasts are dominated by red lithoidal rhyolites, pink spherulitic rhyolites, and rare grey altered porphyritic andesite. Clasts are generally subrounded to subangular with an average size of 150mm, but occur up to 2.5m. Other smaller clasts to occur are white pumice and rare quartz fragments. Layers of coarse ash and lapilli in beds up to 10cm thick occur between breccia layers. Accretionary lapilli are evident in one ash and lapilli layer indicating water was associated with the eruption. Bomb sags are evident in some ash layers.

An unconformity occurs at 15m. Above the unconformity the bedding is approximately horizontal.

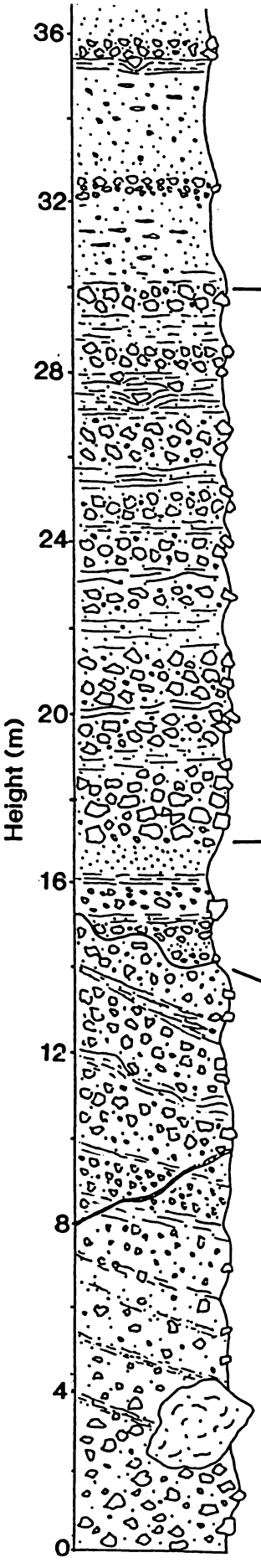

Unit 4: Sequence of laterally extensive well bedded lapilli tuffs and pyroclastic breccias, alternating with partially welded, proximal pyroclastic flows and airfall units. Lithics are dominated by red rhyolite and minor grey rhyolite. Pyroclastic flows are lithic poor (5%) with a fine grained pale green matrix. White altered pumice up to 20mm occur in pyroclastic flow deposits (20%).

Unit 3: Crudely stratified, poorly sorted block-and-ash flow deposits alternating with fine grained ashfall deposits. Lithic clasts consist of subangular red and grey rhyolite (max size 140mm), minor andesite (max size 60mm), and rare quartz vein fragments (<10mm).

Unit 2: Coarse white ash and lapilli deposits. Abundant (30%) lithic blocks of red rhyolite up to 100mm are embedded in the ash layers. Small white subrounded pumice up to 5mm occur in the ash layers (10%). Deposits are flat lying but occur over an erosion surface at 080/32N.

Unit 1: Multi-lithological, poorly sorted, laharic deposits, with intermittent layers of coarse white ash and lapilli up to 5cm thick. Breccias are matrix supported but lithic-rich (50%). Lithics consist of red rhyolite up to 2.5m (30%), grey spherulitic rhyolite up to 90mm (20%), and grey andesite up to 70mm (5%). Deposits are dipping 100/28N.

Figure 2.13. Stratified sequence of Wharekawa Pyroclastics exposed in coastal section (T12 664476).

Unit 2 is dominated by flat lying, crudely bedded ash fall deposits. Layers vary from 10-20cm thick and appear to fine upwards. Included in these layers are small white fibrous pumice clasts (30%), and pink rhyolite lithics up to 10cm.

Unit 3 is made up of 12m of breccia and coarse ash. The breccias are weakly indurated, stratified, poorly sorted, and include angular rhyolite clasts up to 150mm. The laterally continuous ash layers show finely bedded wavy structures.

Unit 4 is dominated by proximal ignimbrites, airfall deposits and breccias. The ignimbrites are white with green discolouration due to vapour phase alteration. White powdery pumice up to 16mm make up 20% of the deposit. Similar lithic types occur as below but are very small (<5mm) and of low abundance (5%). The matrix is crystal-rich with numerous quartz and plagioclase. Occurring above each ignimbrite is a white ash layer up to 8cm. Bomb sags are common in these layers.

Mode of deposition/eruption type

Almost all dome-building eruptions are accompanied by some form of explosive activity (Heiken and Wohletz 1987; Brooker et al. 1993).The Wharekawa Pyroclastics are made up of cumulative block and ash flows and their reworked equivalents (lahars) with proximal ignimbrites as the final phase of explosive activity. The occurrence of large lithics and moderate dips on bedding sequences suggest these deposits are proximal to source.

The deposition of the block-and-ash flows occurs as a pyroclastic flow that separated into two parts, with the block-and-ash flow overlain by ash and lapilli which may or may not include a secondary surge deposit.

Block-and-ash flows have been well documented by Fisher et al. (1980), and Fisher and Heiken (1982) from the 1902 eruption of Mt Pelée. The 1902 ash-cloud surges consisted of a basal breccia overlain by a poorly sorted to well developed ash-cloud deposit. Fisher and Heiken (1982) define the 1902 eruption as vulcanian. Vulcanian eruptions are typically associated with intermediate compositions (Cas and Wright 1987). Proximal block-and-ash flows have been documented by Brooker et al. (1993) in the 14ka Puketarata eruption of Maroa Caldera in the Taupo Volcanic Zone. The breccia occurs only as a minor constituent of the erupted sequence which was dominated by alternating pyroclastic falls and surges.

2.5.2 Wharekawa Dome rhyolites

Distribution

The Wharekawa Dome rhyolites consist of domes, lava flows and vent intrusives. Three domes are evident from aerial photographic interpretation, coastal exposure, and inland outcrops: 1) Ridge Dome; 2) Main Dome; 3) Peak Dome (Fig. 2.1).

Ridge Dome

Ridge Dome occurs in the west of the Wharekawa Dome Complex as a linear NNE trending ridge. At the base of the dome, exposures are limited to road cuttings. Here the rhyolite is weathered, pink, spherulitic with phenocrysts of plagioclase, quartz and relict biotite. Weak flow banding is evident.

Upper slopes of the dome are dominated by extensive cliffs on the western side and southern end of the dome. Here the biotite rhyolite is light grey/pink, lithoidal to intensely spherulitic with phenocrysts of plagioclase, quartz, biotite and minor opaques.

From petrographic interpretation and difference in weathering, it is assumed the rhyolites near the base of the dome were erupted prior to those exposed further upslope. The dome is elongated in a NNE direction, suggesting it is related to a similar trending structure.

A lava flow extends for 1km N to NNE from the northern end of the dome. In outcrop the lava shows well developed flow bands (1-2mm thick) which are planar to slightly undulating, but turbulent in thin section, and rarely planar. Geochemistry (Chapter Six) suggests that this lava is chemically distinct from other biotite rhyolites in the area.

Main Dome

The biotite rhyolite of the Main Dome has a minimum distribution of $1km^2$ and is the largest dome in the Wharekawa Dome Complex. The dome has a maximum height of 183m, though from topographical expression the present day morphology represents a once much larger dome. The dome is typified by pink, flow banded, slightly spherulitic biotite rhyolite. A distinctive feature of

rhyolites from the Main Dome is the occurrence of amygdules infilled with tridymite.

From aerial photo interpretation the morphology of the dome is related to two NE-trending lineations. This trend is similar to the NE structural trend in the Pokohino Dome Complex.

A north flowing lava is evident north of the Main Dome. An exposure at T12 665493 shows the flow to have well developed planar flow banding (Fig. 2.14). An exposure at T12 666501 shows well developed flow banding and flow folds. Mineralogy is similar to the Main Dome flow, but is not thought to be part of the same flow. Dip on the flow banding suggests the Main Dome as the most likely area for a possible vent.

Peak Dome

Peak dome consists of the post-eruptive rhyolites after the eruption of the Wharekawa Pyroclastics (Fig. 2.15). A vent zone is exposed in coastal section 200m north of Pokohino Beach (T12 665479). The intrusive rhyolite is typically massive with well developed vertical joints, but flow laminations are evident up to 4m from the contact with the pyroclastics. The contact between the rhyolite and pyroclastics is sub-vertical, wavy with a 1m thick baked zone. The waviness of the contact suggests that this is not fault related. Up to 30m of brecciation of the pyroclastics occur adjacent to the rhyolite.

The intrusive rhyolite appears to be a pale yellow, spherulitic, biotite rhyolite. Rhyolite clasts in the underlying pyroclastic deposits are thought to represent the intrusive rhyolite.

It is unknown if the large cliffs north of Peak Dome are lavas from the same vent or represent another dome.

2.6 Eastern Flows

The Eastern Flows are a group of biotite rhyolite lavas that appear to have flowed from the SSW and lapped on to the Main Dome. The lavas are exposed in coastal section (Fig. 2.11). Much of the section shows the lava flows to have well developed flow banding which is planar to undulating. Sample W941263

Figure 2.14. Main Dome lava flow exposed on a forestry road (T12 665492) showing well developed planar flow banding(112/24S).

Figure 2.15. Peak Dome rhyolite intruding through Wharekawa Pyroclastics 200m north of Pokohino Beach (T12 665479). The boundary of the intrusion is denoted by a wavy baked boundary and 30m of disrupted pyroclastics. Undisturbed pyroclastics are evident in the far left of the picture.

(T12 670492) shows that the flows have well developed spherulitic textures up to 8mm, and well developed perlitic fractures (Fig. 2.16).

There is evidence for more than one flow occurring at T12 672487 (+3.5km along section) where a whitish pink rhyolite has flowed over an older flow banded lava (Fig. 2.11). The contact between the flows is brecciated.

Flow structures become increasingly more contorted further north and show large isoclinal folds (+4.0km) (Fig. 2.17). Inferred direction of dip of flow banding is NW, suggesting that these flows were sourced offshore.

At +4.5km there is a transitional contact from the coherent flow banded lava to a brecciated blocky flow, which extends north to Ruahiwihiwi Point. The lava is thought to have brecciated due to the subaerial flow entering a subaqueous environment.

2.7 Subaqueous rhyolite block lavas

Subaerial silicic volcanism has been summarised in this chapter based on work by Fink (1983), Bonnichsen and Hauffman (1987), and Heiken and Wohletz (1987). Subaqueous silicic lava flows are similar but intense cooling by water produces important quench fragmentation. Work on subaqueous silicic lavas and domes is well documented by Cas (1978), Kano et al. (1991), and Yamagishi and Dimroth (1985). Much of the work done on silicic volcanism has been done on lavas erupted subaqueously. In this case it is suggested that the lavas erupted subaerially but flowed into water. Work done on subaerial lavas that have flowed into a subaqueous environment are restricted to basaltic examples (e.g. Jones 1970; Jones and Nelson 1970; Moore et al. 1973). It is thought that the lavas may have flowed into a lake, as lake sediments are well exposed to the south, and lakes are common in rhyolitic centres, e.g. volcanic centres in the TVZ. Though silicic magmas are more viscous and have higher thermal conductivities than mafic magmas, subaqueous lavas described by Kano et al. (1991) bifurcate in a similar manner to pillow lava.

Characteristic of subaqueous effusive eruptions is the generation of voluminous hyaloclastic breccia. Hyaloclastic breccia is fragmentation in response to thermal stress built up during rapid cooling, and stress imposed on the chilled outer parts of the lava flow by movement of a ductile interior (Pichler 1965; Kokelaar 1986). Internal flow banding is commonly subparallel to the base and top contacts, and at the side oblique to the bedding (Mc Phie 1993).

Figure 2.16. Well developed spherulitic textures within the biotite rhyolites of the Eastern Flows (sample W941263; T12 670492). Magnifying lens is 7cm long.

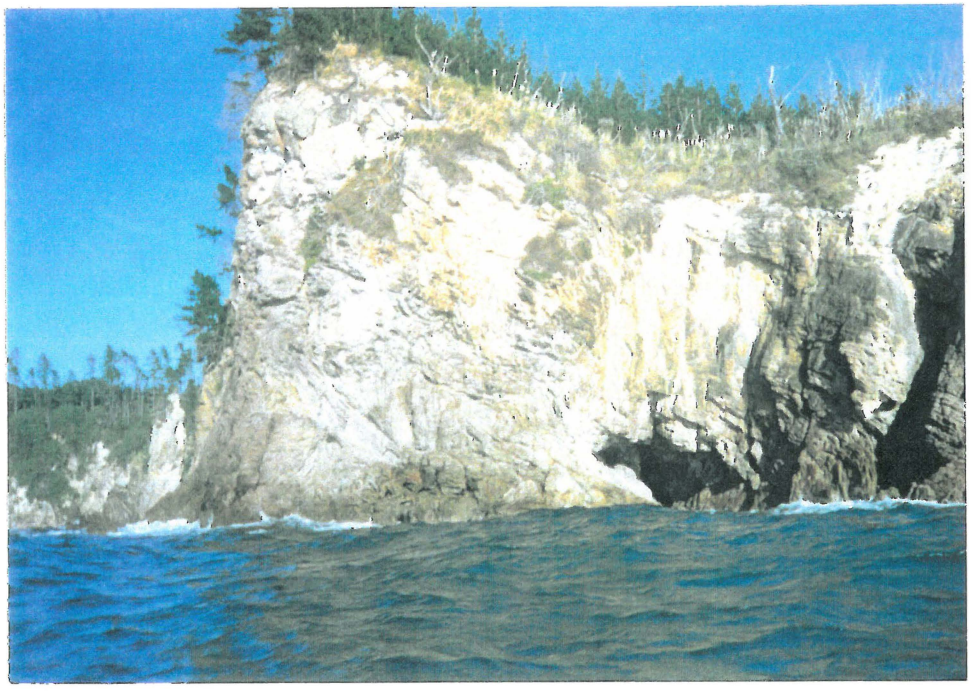

Figure 2.17. Contorted overturned flow folds in Eastern Flow lavas exposed in coastal section. Cliff is approximately 20m high.

Where a lava flows into a subaqueous environment mixing at the base with the lava and the wet sediment produces a texturally complex lava sediment breccia (peperite) (Mc Phie 1993). At the front of the lava some hyaloclastics are remobilised due to the steep flow front and form reworked hyaloclastites. The above features were seen to be well developed in rhyolite lavas in the Miocene Ushikiri Formation, SW Japan (Kano et al. 1991), where three units made up a pile 600m thick. Kano et al. (1991) found each unit included four lithofacies (Fig. 2.18): 1) flow banded coherent lava; 2) insitu volcanic breccia; 3) poorly sorted non-stratified volcanic breccia; 4) stratified volcanic breccia (remobilised hyaloclastite).

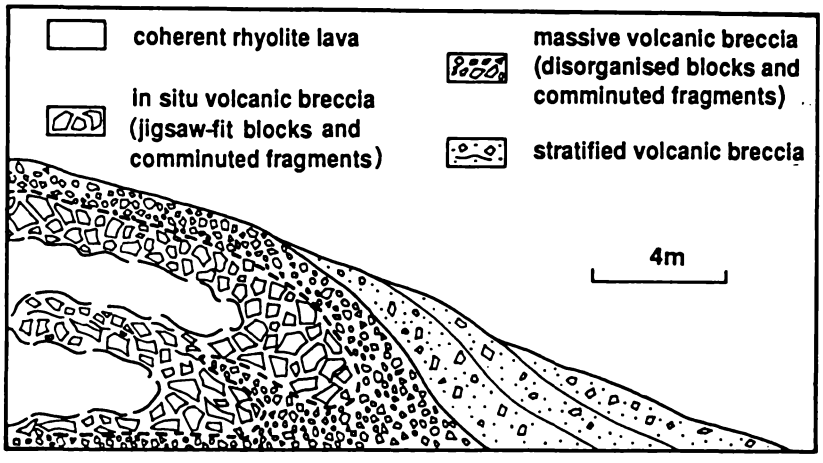

Figure 2.18. Schematic volcanic facies associated with subaqueous emplacement of rhyolite lava; Miocene, Ushikiri Formation, Japan (after Kano et al. 1991).

Generally, subaqueous silicic lavas do not flow far from source (Mc Phie 1993), but Cas (1978) described subaqueous silicic lavas that were fluid enough to form extensive sheet flows (1800km^2). Cas (1978) suggested that flows erupted in very deep water environments would have lower viscosity and greater mobility due to the retention of volatiles due to high confining pressures of water.

As with subaerial lava which comes in contact with small water bodies or wet sediment, small explosive hydrovolcanic eruptions can occur, leaving shallow pits in the lava surface. Sigvaldson (1992) recorded hundreds of small (2-5m diameter) hydrothermal explosion craters across the upper surface of a hyaloclastite ridge in central Iceland. Any evidence for the existence for these craters within the hyaloclastite at Onemana would have been removed by erosion.

Lithology

The subaqueous rhyolite lavas exposed at the northern extent of the Onemana Peninsula do show similar variations in the nature of the deposit to those described by Kano et al. (1991). The hyaloclastite has a minimum thickness of 30-50m, and appears to thicken to the south. The topography represented by the top of the hyaloclastite has a distinct planar surface that dips 20° to the NW. In outcrop the dip angle on individual bedding is variable, ranging from 30-70°, dipping N to NW.

It is thought that the breccia is made up of numerous individual lava flows. However, it is unknown whether these flows bifurcated from a single subaerial flow or a series of flows.

The hyaloclastite is monolithic with clasts of well developed spherulitic biotite rhyolite. Some spherulites occur up to 30cm , and are commonly associated with lithophysae. Based on the Kano et al. (1991) classification the hyaloclastic breccia is divided into four subunits: stratified volcanic breccia, massive breccia, insitu breccia, and coherent lava. Best exposures were seen at Ruahiwihiwi Beach (informal name) (Fig. 2.19, 2.20).

The coherent flow banded lavas exposed are thinner than the other subunits (30-60cm). Spherulites in this layer are abundant, but are no larger than 2cm. Vertical jointing is common throughout the coherent lava. A clayey layer is evident around the lava. This may represent the remnants of a chilled glassy margin. The boundary with the outer insitu breccia appears to be transitional.

The insitu breccia shows an increase in frequency of vertical jointing, with some pink clay infill. Brecciation is thought to occur due to quenching after the flow had stopped, as there is little evidence for rotation or movement of the blocky clasts. Clasts in the insitu breccia are subangular, blocky, up to 40cm, and moderately to well sorted.

The massive breccia is made up of large disorganised blocks of poorly vesicular, spherulitic rhyolite 0.2 -1.5m in the long diameter. Many of these blocks consist of a single spherulite with associated lithophysae. Clasts are subrounded, moderately to poorly sorted, and clast supported. Massive breccia appears to be the most abundant subunit, with some massive bodies over 10m thick and laterally extensive (>50m).

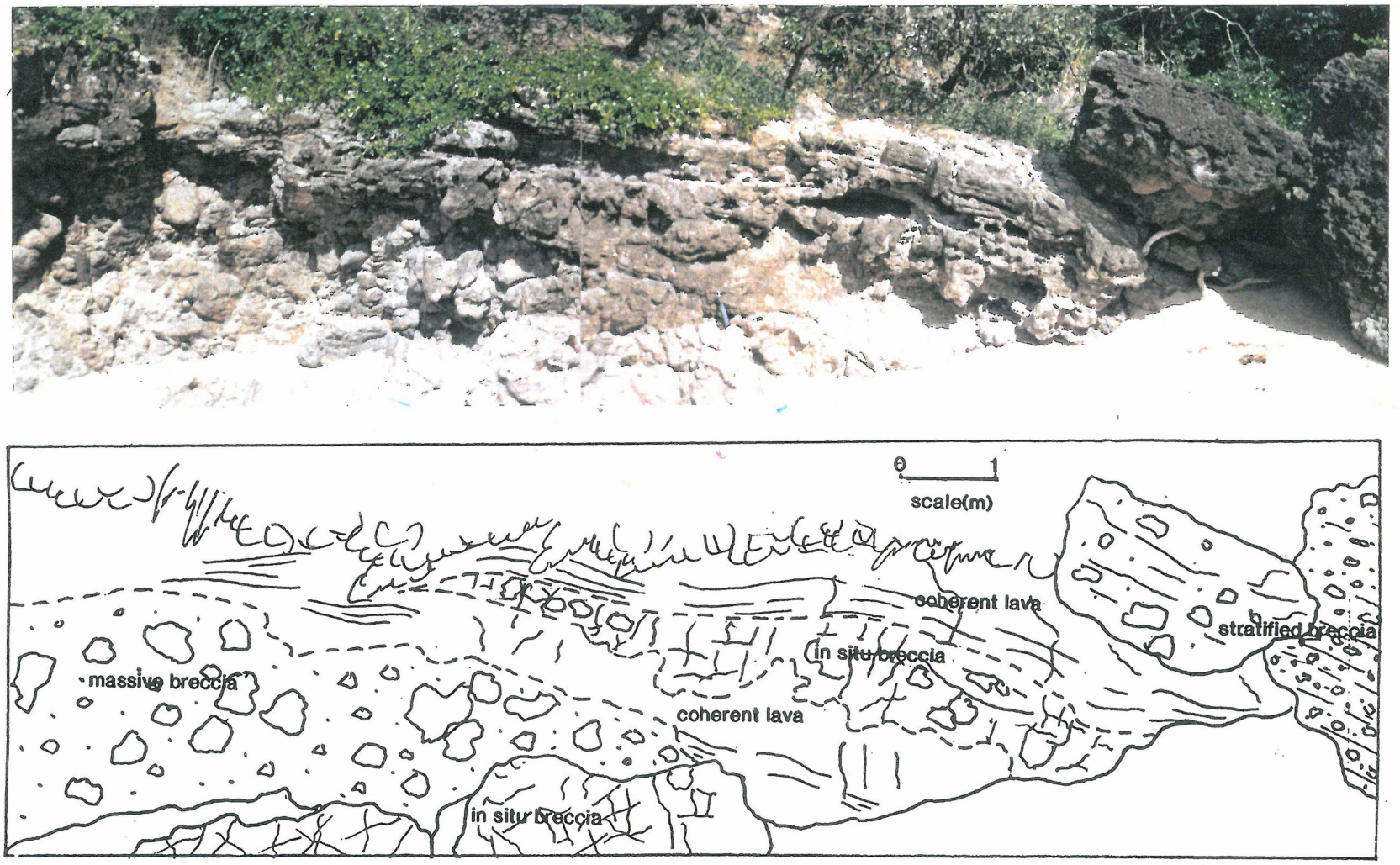

Figure 2.19. A) two bifurcating lava lobes with associated hyaloclastite (T12670497). B) schematic interpretation of the hyaloclastite facies, with the coherent lava flow surrounded by insitu breccia. Massive breccia appears to be overrun by the flow.

The stratified volcanic breccia has layers of breccia ranging from 10 to 50cm thick. The spherulitic rhyolite breccia beds are massive, and are overlain by a thin layer (1 - 5cm) of coarse sand. Each layer is thought to have formed by a blocky avalanche cascading off the brecciated flow lobe, with the lighter sand sized fragments settling on top of the deposit. Individual beds appear to be laterally extensive, and have a gradational upper boundary with overlying breccia.

Figure 2.20. Stratified hyaloclastite breccia exposed at the southern end Ruahiwihiwi Beach (T12 670497).

2.8 Glassy Dome Rhyolite and associated pyroclastics

2.8.1 Glassy Dome Pyroclastics

Occurrence

The Glassy Dome Pyroclastics are a sequence of pyroclastic deposits relating to the growth of the Glassy Dome Rhyolite. The pyroclastics are exposed in distinct fluted bluffs on the west side of the Pokohino Dome complex (Fig. 2.21) and adjacent to the Glassy Dome Rhyolite. An exposure on Rangipo Road (T12 649475) shows the pyroclastics to consist of approximately 10-20m of rhyolitic pyroclastic flows, overlain by approximately 20m of block-and-ash flow (Fig. 2.22) material thought to be associated with dome instability (Fig. 2.23).

Lithology

Unit 1 at the base of the pyroclastic section in Figure 2.22 is made up of moderately welded block-and-ash flows, shower bedded coarse ash deposits, and surge deposits showing undulating cross bedded structures dipping 108/25W. The lithics are dominated by grey/green glassy biotite rhyolite some of which are slightly vesicular. There is a small amount of andesite lithics (<2%). Size of the lithics is generally up to 10mm but blocks of grey rhyolite occur up to 60cm, indicating proximity to source.

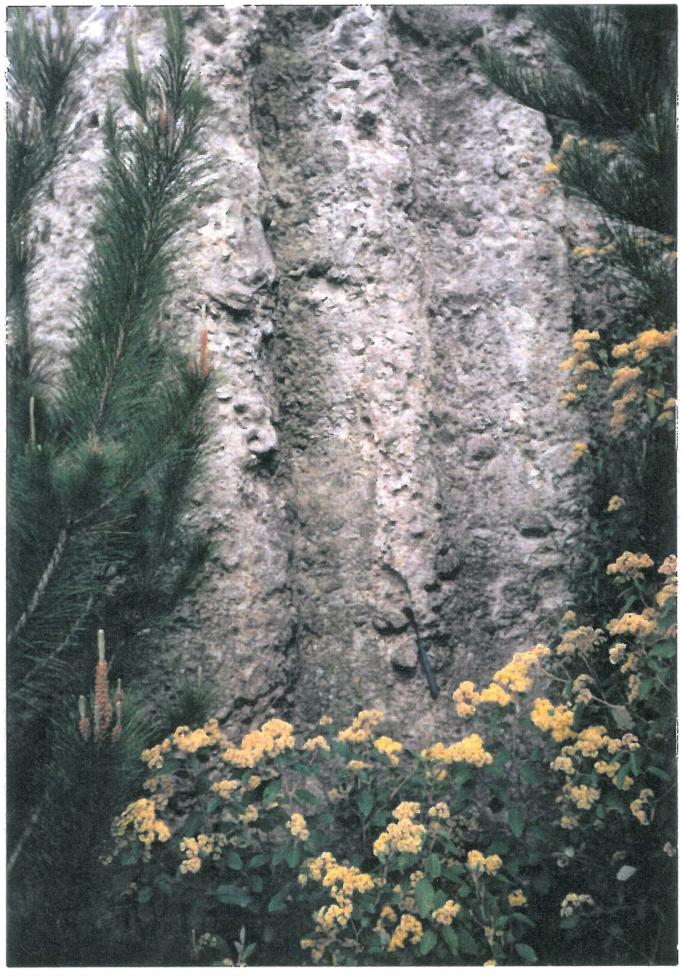

Figure 2.21. Mass emplaced block and ash deposit resulting from instability of the Glassy Dome Rhyolite (unit 2b) exposed in fluted bluffs adjacent to Rangipo Road (T12 649475). Hammer is 33cm long.

Overlying the lower pyroclastic section is a thick densely welded blocky unit. Between these units is an unconformity representing an erosion surface. The unconformity strikes at 024/36E and is thought to represent an erosional gully that has cut into Unit 1.

Unit 2 is separated into two parts. Unit 2a is 2.5-3.0m of crudely bedded, poorly sorted ash and lapilli. Individual beds vary from 4-15cm thick. Lithics

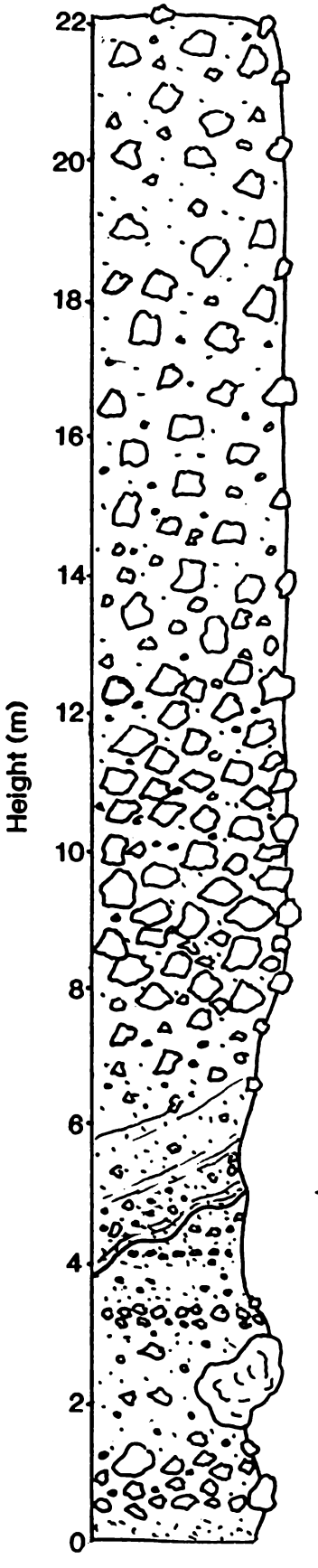

Unit 2b: Avalanche breccia. Block-and-ash flow deposit dominated by glassy green rhyolite lithics up to 300mm in diameter, in a coarse grained moderately welded matrix. Unit is clast supported near base (60% lithics, but becomes matrix supported above 13m (20% lithics).

Unit 2a: Coarse bedded ash and lapilli layers, and minor surge deposits up to 10cm thick. Lithics are dominated (80%) by green glassy rhyolite (max size 180mm) and minor red/brown spherulitic rhyolite and andesite. Upper boundary appears to be transitional. Layers overlie an erosion surface (024/36E).

Unit 1: Coarse ashfall layers, surges, and poorly sorted block-and-ash flow deposits. Abundant (50%) green glassy rhyolite up to 300mm diameter. Anomalous blocks up to 600mm. Rare (2%) andesite lithics up to 50mm diameter. Bedding dipping at 108/25S.

Figure 2.22. Stratigraphic section through Glassy Dome Pyroclastics (T12 649475).

are dominated by grey/green glassy rhyolite up to 18cm diameter, with minor red/brown rhyolite and grey andesite. Some small slightly vesiculated rhyolite lithics are also evident. The ash sized component appears to contain only glassy rhyolite fragments.

Unit 2b is a thick blocky layer which is thought to be emplaced in a single event. The blocky layer is poorly sorted and clast supported, though clast abundances decrease upwards (60 to 20%), making the unit appear matrix supported near the top. Lithic clasts are dominated by subangular, poorly vesiculated, grey/green glassy rhyolite, up to 30cm diameter. Smaller abundances (3%) of red/brown rhyolite clasts up to 20cm diameter also occur. The matrix appears to be pale green, coarse grained and glassy.

An ignimbrite is exposed in a road cutting along Rangipo Road. Due to its limited exposure it is difficult to determine its stratigraphic relationship to the other units described above. The ignimbrite has a distinctive green colour in outcrop and is lithic-rich (50%), with green, subangular, moderately sorted, biotite rhyolite up to 2cm in long diameter. Little matrix material is evident, which gives the ignimbrite a slightly vesicular appearance. Large (up to 70mm), white, powdery, vapour phase altered pumice with quartz phenocrysts make up 10% of the ignimbrite. Some small rare andesite lithics are also evident.

Eruptive mechanisms

Heiken and Wohletz (1987) have studied pyroclastic deposits associated with silicic domes and have proposed types of explosive activity accompanying dome building based on field characteristics (Table 2.1).

The material exposed in the stratigraphic column can be loosely related to the model proposed by Heiken and Wohletz (1987). Initial activity is thought to be plinian or sub plinian preceding dome emplacement.

With the formation of domes, vulcanian eruptions occurred producing layers of ash and lapilli, and surges. The occurrence of larger lithics can be attributed to the remobilisation of the deposit as lahars or as a individual boulders.

The occurrence of a thick block-and-ash flow overlying the above units is thought to be due to collapse of a rhyolite dome or flow. The emplacement of this unit is thought to be similar to the 1902 eruption of Mt Pelée (Fisher et al.

1980; Fisher and Heiken 1982), 1991 eruption of Unzen Volcano (Sato et al. 1992), Mt St Helens 1981-86 (Swanson et al. 1987; Mellors et al. 1988), and Redoubt Volcano 1989-90 (Miller 1994) where the destruction of the dome produced a small volume of highly destructive block-and-ash flows.

Observations from the 1991 eruption of Unzen Volcano (Sato et al. 1992) suggests that instantaneous explosive fragmentation of a fallen block caused a Merapian-type pyroclastic flow. Heiken and Wohletz (1987) define Merapian activity as dome destruction some time after dome emplacement. Peléean activity is only different in time. Peléean activity occurs during or immediately after dome emplacement. The cause of the Peléean and Merapian-type eruptions at Unzen Volcano can be attributed to the relationship between tensile strength and excess pore pressures of lava (Sato et al. 1992).

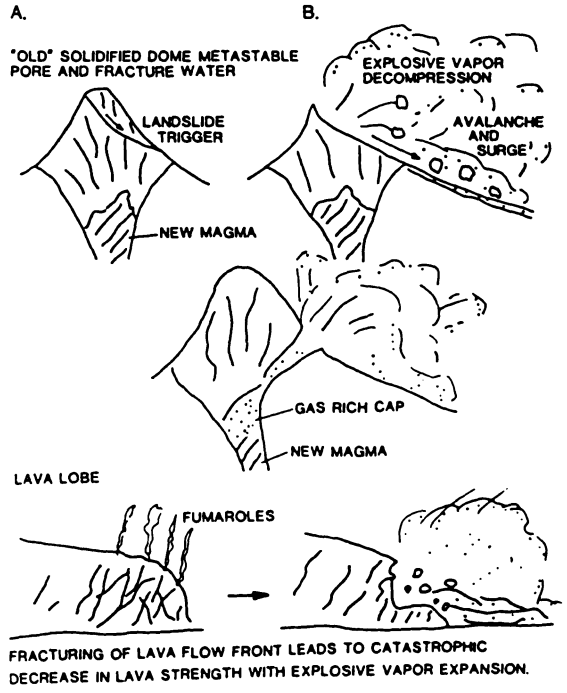

Figure 2.23. Schematic illustration of Peléean and Merapian dome destruction, showing initial landslide (A) followed by avalanching and dome explosion (B) caused by explosive release of new gas-rich magma (centre), and explosion of lava flow front (bottom) (from Heiken and Wohletz 1987).

Heiken and Wohletz (1987) note that the common feature of Peléean and Merapian eruptions is that the deposit consists of mostly lithic pyroclastics formed by the fragmentation of the dome lavas (Fig. 2.23). Pressure from magmatic gases and vaporisation of groundwater is thought to have caused the explosive fragmentation of the dome at Mt Pelée (Fisher and Heiken 1982).

Dome growth at Mount St Helens has been accompanied by the generation of pyroclastic flows and rock avalanches (Swanson et al. 1987; Mellors et al. 1988; Fink et al. 1990). The 1986 hot-rock-avalanche from the crater dome produced a fan shaped deposit 0.5km long and up to 30m thick. As in the Glassy Dome block-and-ash flow deposit the 1986 Mount St Helens avalanche deposit is clast supported and dominated by juvenile material. Rose et al. (1977) inferred that an explosion had occurred when a dacite lava flow became oversteepened and fragmented exposing the molten dacite. For the 1986 Mount St Helens deposits Mellors et al. (1988) argue against an explosion, believing gravity was the only driving force.

2.8.2 Glassy Dome Rhyolite

A green/grey glassy biotite rhyolite with well developed perlitic fractures outcrops on a N-S trending saddle between the Wharekawa and Pokohino dome complexes (Fig. 2.24). It is essentially unweathered and is considered to be very young compared with the surrounding rhyolite volcanics. The samples show well developed phenocrysts of plagioclase, quartz, biotite and opaques (Fig. 2.25).

No flow morphology is evident and it is presumed the Glassy Dome Rhyolite is an intrusive/resurgent dome that formed after the eruptions of the Glassy Dome Pyroclastics. An upstanding part of the dome (T12 659478) is distinctly elongated in an E-W direction, which corresponds to an E-W linear structure observed in aerial photos. From geophysical data the Glassy Dome Rhyolite shows up as a large magnetic low, which is elongated in an E-W direction (Fig. 2.26). The dome appears to occur in a large semicircular depression. This may be a crater that formed due to the eruptions of the Glassy Dome Pyroclastics and subsidence of the vent area, into which the Glassy Dome intruded as a small resurgent dome.

Where sufficiently exposed (T12 659478) the Glassy Dome Rhyolite shows well developed, continuous open joints which appear to follow the curvature of the outcrop, suggesting that these are cooling joints that have formed around the dome (Fig. 2.24). Thin quartz stringers and veinlets up to 3cm wide are common throughout the dome. Strike on these veins is similar to that of the barren cooling joints (NE and NW). Mineralisation of domes after emplacement is common. Veining typically occupies a structure that has in part the spatial relation to cooling fractures (Cunningham et al. 1991). A 10cm thick breccia zone is evident in a roadcutting. The breccia is poorly sorted,

Figure 2.24. Glassy Dome Rhyolite looking to the south adjacent to Normans Access Road (T12 659478) showing well developed jointing. Person for scale.

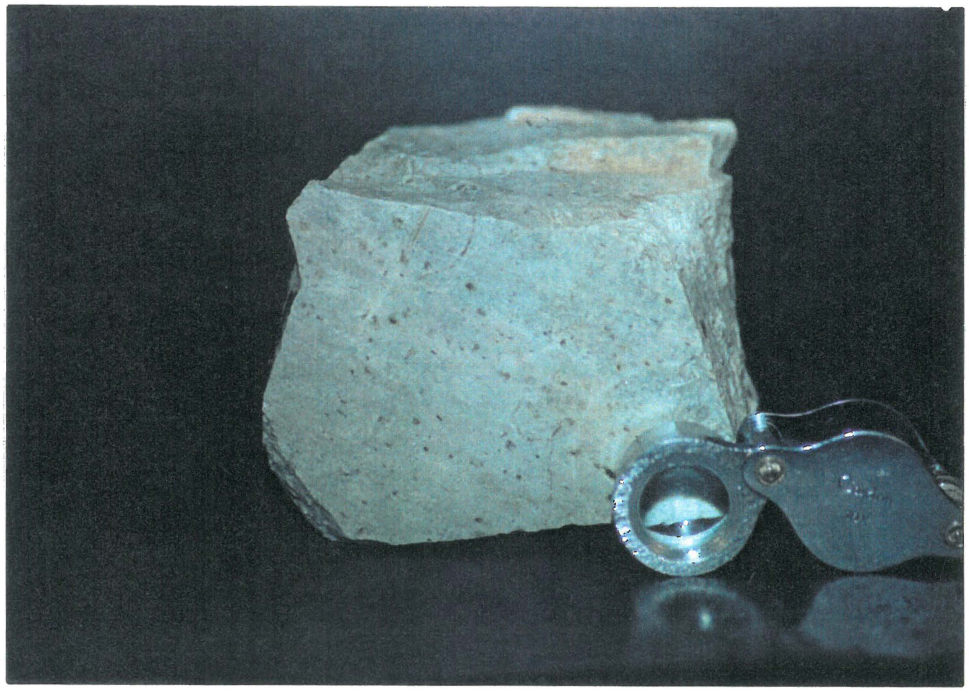

Figure 2.25. Sample W941279 from the Glassy Dome Rhyolite (T12 659479), shows its distinctive green colour and numerous subparallel biotite phenocrysts. Magnifying lens is 7cm long.

partly clast supported with subangular, monolithic clasts. This breccia is thought to be the lower section of a degassing pipe, as the upper sections tend to be flared.

Post-eruptive doming is well documented at various volcanoes that have erupted this century, e.g. Mount St. Helens (Swanson et al. 1987; Fink et al. 1990), Unzen volcano (Nakada and Kobayashi 1991; Sato et al. 1992), Redoubt Volcano (Miller 1994), Santa Maria volcano (Rose et al. 1987), and Katmai volcano (Hildreth 1983; 1987).

It is possible that the present dome was the last of a series of domes that formed and were subsequently destroyed. It is assumed a similar dome existed prior to the deposition of the above pyroclastics. In the 1989-1990 eruption of Redoubt Volcano 14 domes were formed and 13 subsequently destroyed (Miller 1994). The domes were destroyed by collapse of oversteepening flow fronts, which produced small Merapi-type pyroclastic flows (Miller 1994). Dome emplacement at Mount St. Helens from 1980-86 occurred during more than 15 eruptive phases, with each episode beginning with a period of endogenous growth followed by extrusion of an exogenous lobe (Fink et al. 1990).

2.9 Wharekawa Ignimbrite

The Wharekawa Ignimbrite is a pinkish-grey, partially welded, lithic-rich, massive unit that outcrops on a small hill on farmland in the far NW of the study area. This unit also appears to lap onto the rhyolites of the Wharekawa Dome Complex. A maximum exposed height of 20m is presumed to be the unit's minimum thickness. The area of exposure coincides with a broad magnetic anomaly, which was previously interpreted as an area of hydrothermal alteration (Vidanovich 1991) (Fig. 2.26; 2.27). This zone appears to be where the ignimbrite is thickest.

Grey fibrous pumice with large plagioclase and quartz phenocrysts are abundant throughout the unit (30%), but are generally small with few exceeding 10mm. From petrographic investigation the grey pumice is a major constituent of the fine grained matrix. Including the fibrous pumice, the matrix also contains devitrified glass and abundant broken anhedral plagioclase - quartz ± biotite ± hornblende. The unit consists of a variety of lithic types, which together constitute 20% of the unit: rhyolite obsidian, spherulitic rhyolite, rhyolitic breccia, hornblende dacite, and pyroxene andesite. The lithics are

moderately to poorly sorted, subrounded to subangular, and commonly no larger than 20mm, but do occur up to 40cm in diameter.

The source of the Wharekawa Ignimbrite is unknown, but is not thought to have erupted from within the Onemana area. The lack of bedding within the unit makes it difficult to determine the direction of flow.

2.10 Rangipo Andesite

The Rangipo Andesite is dark grey with phenocrysts of plagioclase, hypersthene and augite in a fine grained intersertal groundmass with feldspar laths. Petrographic analysis shows that the feldspar laths in the groundmass are subparallel indicating flow. The Rangipo Andesite is exposed in a small knoll 400m north of The Knob in a valley on the western side of the Pokohino Dome Complex. Surface exposure is small ($<0.2km^2$), but is of similar size to the positive magnetic anomaly that coincides with the location of the andesite (Fig. 2.26; 2.27). A maximum exposure height of approximately 35m is the minimum thickness of the andesite.

The exposure of Rangipo Andesite is thought to represent the remnents of an eroded vent plug. The lack of horizontal jointing and low phenocryst abundance suggests the exposed unit is not an intrusive feature. In outcrop the andesite shows no evidence of flow features, but does show well developed jointing. The jointing is closely spaced and in outcrop gives the andesite a blocky appearance (Fig. 2.28). In highly weathered outcrops weathering along joints has produced distinctive spheroidal corestones.

It is assumed the andesite intruded the biotite rhyolites of the Pokohino Dome Complex, although no contact was observed.

Late stage andesites (Omahine Andesite) after dominantly silicic volcanism is a common feature in the eastern Coromandel Peninsula (eg. Skinner 1986; Rabone et al. 1987; Brathwaite 1987; Haworth 1993).

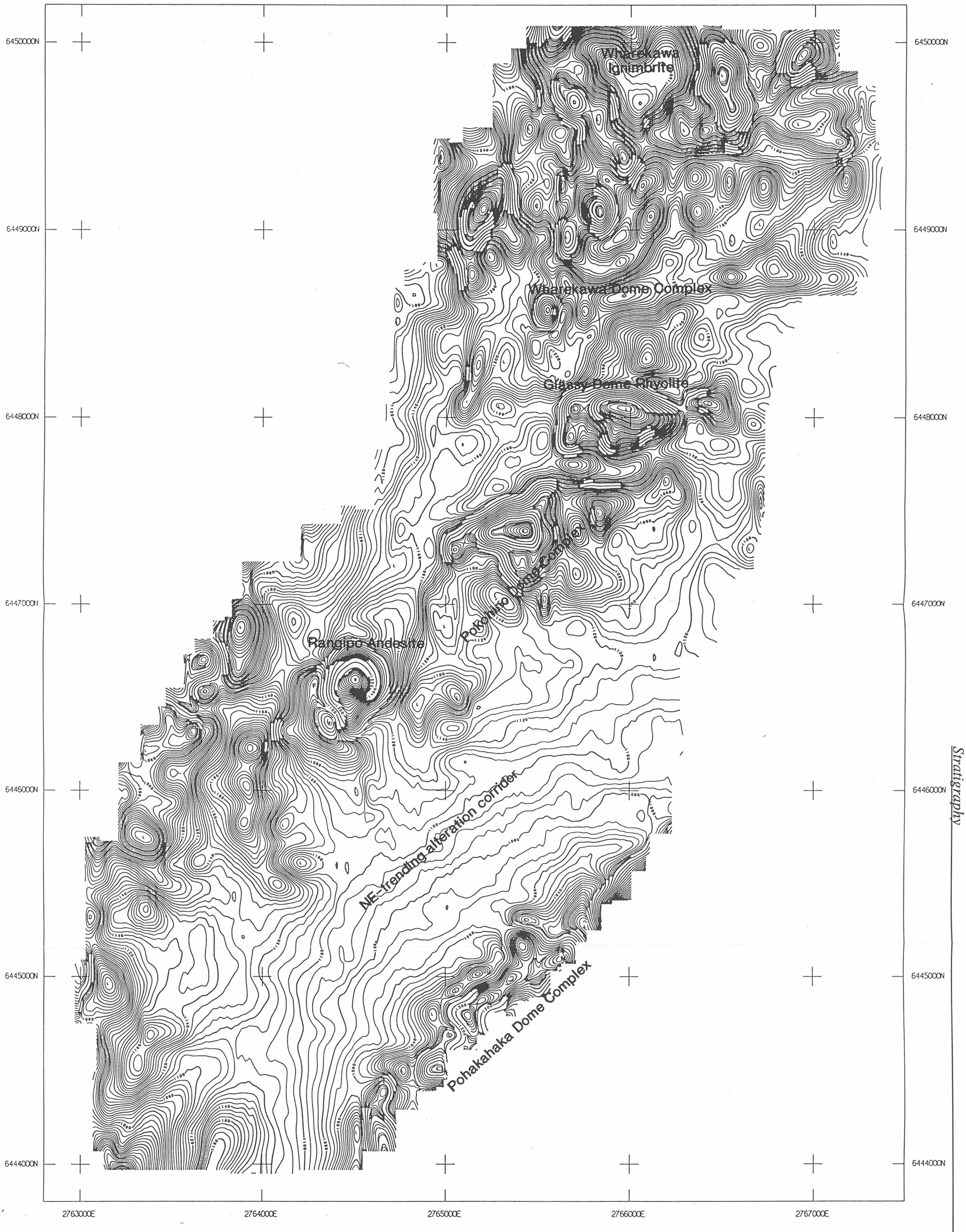

Figure 2.26. Magnetic anomaly map of the northern Onemana Peninsula (after Vidanovich 1991).

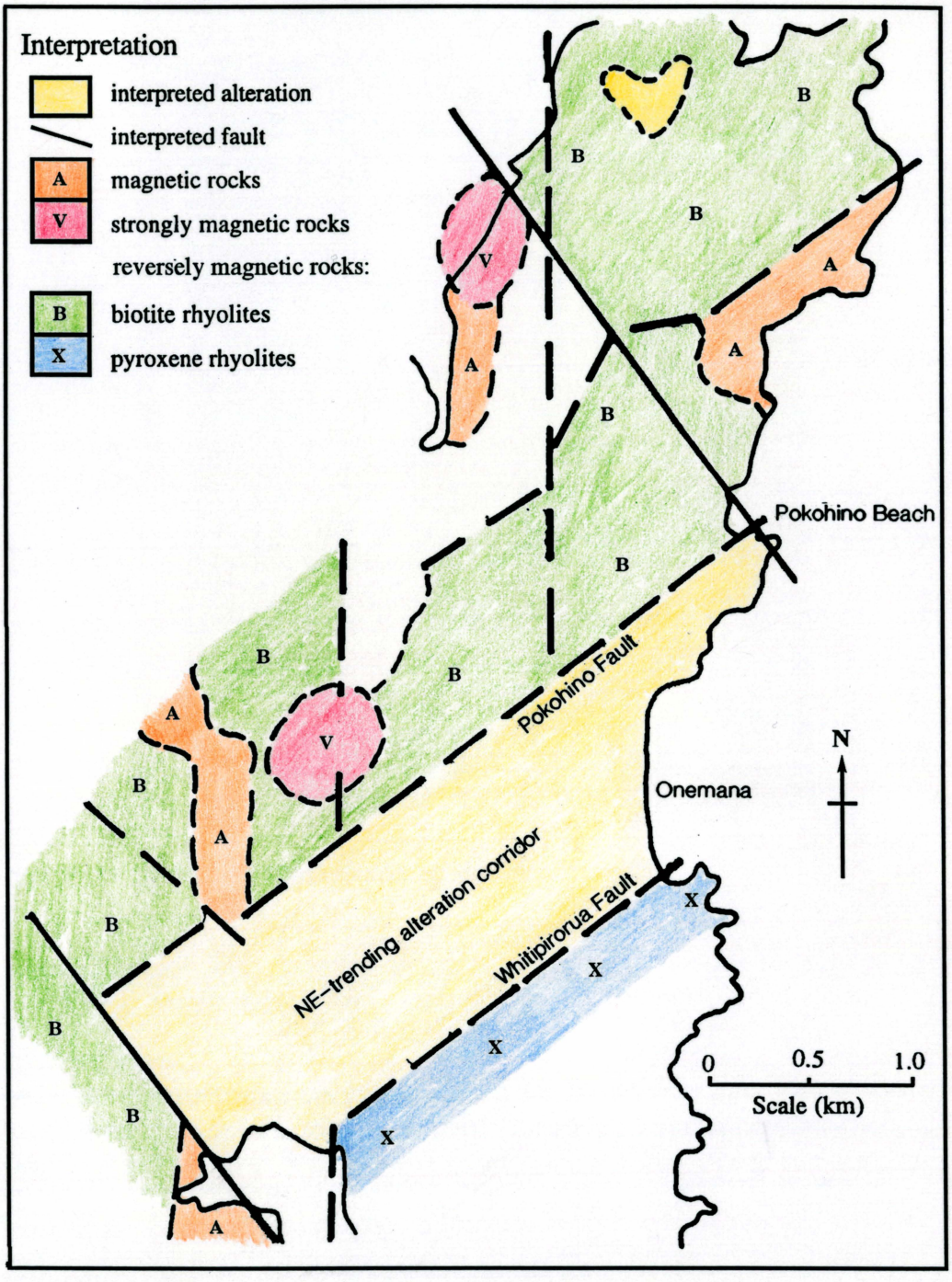

Figure 2.27. Simplified interpretation of aerial magnetic data over the Onemana area (after Vidanovich 1991).

Figure 2.28. Rangipo Andesite outcrop (T12 643466), showing the closely spaced jointing giving the andesite a blocky appearance.

2.11 Lake Sediments

Lacustrine sediments outcrop between the Pokohino and Pohakahaka dome complexes. Extent of outcrop is over 2km^2, elongated in a NE direction. The sediments are dominated by sand and silt sized fragments of quartz, variably altered rhyolite and sediment, and minor fragments of wood. Evidence from drill holes show the sediments to be stratified with layers of mudstone/siltstones, sandstones, carbonaceous sediment, and volcaniclastics (Coote 1994).

The sedimentary succession shown in drill data gives evidence for a deepening subaqueous environment, with volcaniclastic material indicating a near-shore environment, where volcaniclastics are likely to occur as talus from the NE-striking fault scarp (Whitipirorua Fault). Pebbly sandstone and lithic quartz sandstone which may indicate a shallow water beach environment occur above the volcaniclastic material. Offshore environments are indicated by

mudstone/siltstone and carbonaceous sediments, with carbonaceous sediments occurring in shallow parts of the lake. Faint bedding can be seen in some outcrops as thin (<5mm) sandstone and siltstone laminae. A low knoll besides Pokohino Beach Road (T12 648457) showed thin wavy bedding that had been truncated by slump structures.

All samples of sediment had been altered to some degree (Chapter 6). Where silicified the sediment has been locally brecciated then sealed by microcrystalline quartz.

The characteristics of the lake sediments and associated hydrothermal processes appear to be similar to other lakes in strike-slip basins and rift settings, e.g. Lake Tanganyika, East Africa (Tiercelin et al. 1993); Walker Lake, Nevada (Link et al. 1985).

Contact relationships

To the south the sediments lap onto and are faulted against the rhyolites of the Pohakahaka Dome Complex. From geophysical data and aerial photo interpretation a NE fault has been delineated as the southern boundary of the sediments. This fault is not well defined within the lake sediments, which may be due to the lake sediments not extending as far south as the fault. Other contacts are difficult to interpret as they are not fault-bounded or observed in outcrop. It is assumed that the sediments lap onto the rhyolite of the Pokohino Dome Complex.

2.12 Onemana Breccia

The Onemana Breccia has previously been identified as a hydrothermal eruption breccia (HEB) and named by Robson and Stevens (1991). The Onemana Breccia lies directly on and intrudes the lake sediments and outcrops over an area of 1km^2. The recognition of this lithotype is the first confirmed discovery of an eruption breccia within ancient hydrothermal systems of the Coromandel Volcanic Zone (Robson and Stevens 1991). Moore (1976; 1979) identified funnel shaped multi-lithological breccia pipes within the Broken Hills Mine. The occurrence of flow banded rhyolite clasts within the pipe adjacent to younger pyroclastic host rocks suggests that the material has travelled up the pipe. Though the breccia pipes do not appear to have a corresponding surface deposit, it is thought a breccia pipe of a similar nature exists below Breccia Knob. HEB's have been described from many active and fossil geothermal

fields in New Zealand, USA, and Greece (eg. Lloyd 1959; Nairn and Wiradiradja 1980; Scott and Cody 1982; Hedenquist and Henley 1985; Krupp and Seward 1987; Marini et al. 1993).

Lithology

Outcrops of the HEB are dominantly poorly sorted, matrix supported clasts varying in shape from angular to subrounded. The abundance and maximum size of the fragments decrease with increasing distance from source. Based on fragment size and apparent thickness (>15m) the source of the eruption is near Breccia Knob (T12 652452). Around Breccia Knob the HEB is poorly sorted, massive, polymict, dominantly matrix supported in a highly altered to silicified fine grained matrix. The clast types are dominated by subangular altered sediments and rhyolite with minor sinter and vein quartz. Clasts are typically no larger than 50cm but occur up to 1m. Clast abundances are generally 10-20%. Small vent structures are evident in the northern bluffs of Breccia Knob. These vents are funnel shaped, Mn oxide stained, and fines depleted. These structures appear to have developed in the initially unconsolidated HEB as gas release structures during the cooling phase (Fig. 2.29).

North of Breccia Knob the HEB thins out and the clast size reduces to <20mm. Anomalously large clasts occur in an outcrop on Pokohino Beach Road (T12 647458) up to 20cm. The range of clast types is similar to those found around Breccia Knob. This suggests the possibility for another source vent. Clasts are dominated by variably altered rhyolite and rhyolite sediment. The matrix consists of fine clays and quartz with larger quartz fragments and rare pyrite.

There are seldom any internal structures (bedding , grading) evident in the HEB, though sectional exposures are rare. An exception is in a forestry road cutting (T12651457 and 652458) 500m north of Breccia Knob, where normally graded breccia is lying on sandy lake deposits (Robson and Stevens 1991). Evidence that this deposit was associated with water at the time of eruption is shown by the display of crude size grading (T12 650458)which Robson and Stevens (1991) suggests is indicative of waterlain (lacustrine) deposition. The fact that the deposits were laid down underwater may explain the lack of impact craters as seen in other deposits (eg. Kawerau, Nairn and Wiradiradja 1980; Waiotapu, Hedenquist and Henley 1985; Rotokawa, Krupp and Seward 1987).

Figure 2.29. Vent structure in silicified hydrothermal eruption breccia on Breccia Knob (T12 651 453). Hammer is 33cm long.

Post-eruptive alteration played an important role in the lithification and preservation of the HEB. Local brecciation and sealing of vughs has occurred where the breccia has overlain fluid upflow zones (further discussion in Chapters 3 and 7).

Eruption mechanisms

Eruption mechanisms for HEB's are summarised by Nelson and Giles (1985). Hydrothermal eruptions are thought to occur due to over-pressurisation of the geothermal environment. Debate exists over the extent to which silica sealing occurs. Nelson and Giles (1985) question whether silica sealing can contain convecting geothermal fluids near the surface. Hedenquist and Henley (1985) suggest that there is only local sealing of flow paths.

Where sealing occurs, insoluble gases can accumulate which have separated from the underlying boiling fluids. As gas exsolution proceeds, the depth of the gas column increases, and with it the pressure on the seal point moves toward lithostatic (Hedenquist and Henley 1985).

Triggering of an eruption can then be due to hydraulic fracturing from pressure at the seal exceeding lithostatic pressure, or seismic activity. Hedenquist and Henley (1985) suggest that when these conditions are met jigsaw puzzle textures develop.

The fracture depth for the Onemana Breccia cannot be accurately constrained, but the occurrence of hydrothermally altered rhyolite within surface deposits suggest the fracture depth is greater than 60m. Estimated depths of eruption in the Taupo Volcanic Zone are typically deeper (eg Opal eruption 100-140m, Waiotapu, Hedenquist and Henley 1985; Lower Explosion Breccia <200m, Kawerau, Nairn and Wiradiradja 1980).

Triggering of the Onemana Breccia may be related to movement along a nearby fault, and it is evident that faults were active prior to the eruption and after the eruption, as the deposit is truncated to the south. The hydrothermal eruption of Nisyros, Greece, in 1873 was thought to be triggered by a violent earthquake which fractured a brittle aquifer allowing the sudden influx of fluid, triggering the eruption (Marini et al. 1993).

The occurrence of fumarole vent structures suggest that the present surface on Breccia Knob is close to the original surface. The fumaroles are presumed to have formed in unconsolidated to weakly consolidated breccia, because of fines depletion and little brecciation. The fumaroles would initially appear to be rootless but would develop conduits along fractures as the breccia was silicified.

After the eruption a crater would probably have developed over the vent area. Silicification and later erosion have produced an inverse topographical expression, where the core of Breccia Knob is thought to represent the silicified remnants of the vent.

Chapter Three

Structure

3.1 Introduction

The structural regime of the Onemana Peninsula is dominated by NW, N, and NE striking faulting. Minor E-W striking faults are also evident in the study area. From structural interpretation of aerial photos, geophysics and coastal exposures it is thought that local structure controlled the location of vents for explosive and effusive volcanism, and the loci for late stage hydrothermal activity.

The Onemana region lies within a major NNE trending structural corridor 50km long, 5km wide extending from Karangahake in the south to Ohui and Onemana in the north (Fig. 1.2). This structural corridor has been named the Karangahake Ohui Structural Trend (KOST) (Merchant et al. 1988) (Fig. 3.1). Included in this zone are a number of important epithermal deposits, e.g. Karangahake, Golden Cross, Maratoto, and Wharekirauponga. This corridor was shown to be an area of persistent magnetic lows by Rabone (1991). The KOST is dominated by NNE-striking faults with NW-striking crosscutting faults, and is inferred to be an extensional rift-type feature (Merchant et al. 1988). This structural corridor is thought to represent a major focus of dextral transcurrent and rifting movements (Rabone et al. 1987), and is thought to be the principal controlling mechanism for the structure found in the Onemana region.

In March 1990 a detailed aerial magnetic survey was carried out over the central Onemana Peninsula (Vidanovich 1991). Results of the survey showed that alteration was confined to a NE trending corridor 3.5km long and 1.5km wide (Fig. 2.26, 2.27) between the Pokohino and Pohakahaka dome complexes. The southern boundary of this zone shows a well defined NE trend. NW-striking lineations occur at either end of the alteration zone and appear to truncate the zone to the west. Vidanovich (1991) assumed that the zone is also truncated in the east by another NW-striking lineation, but this feature is less conclusive.

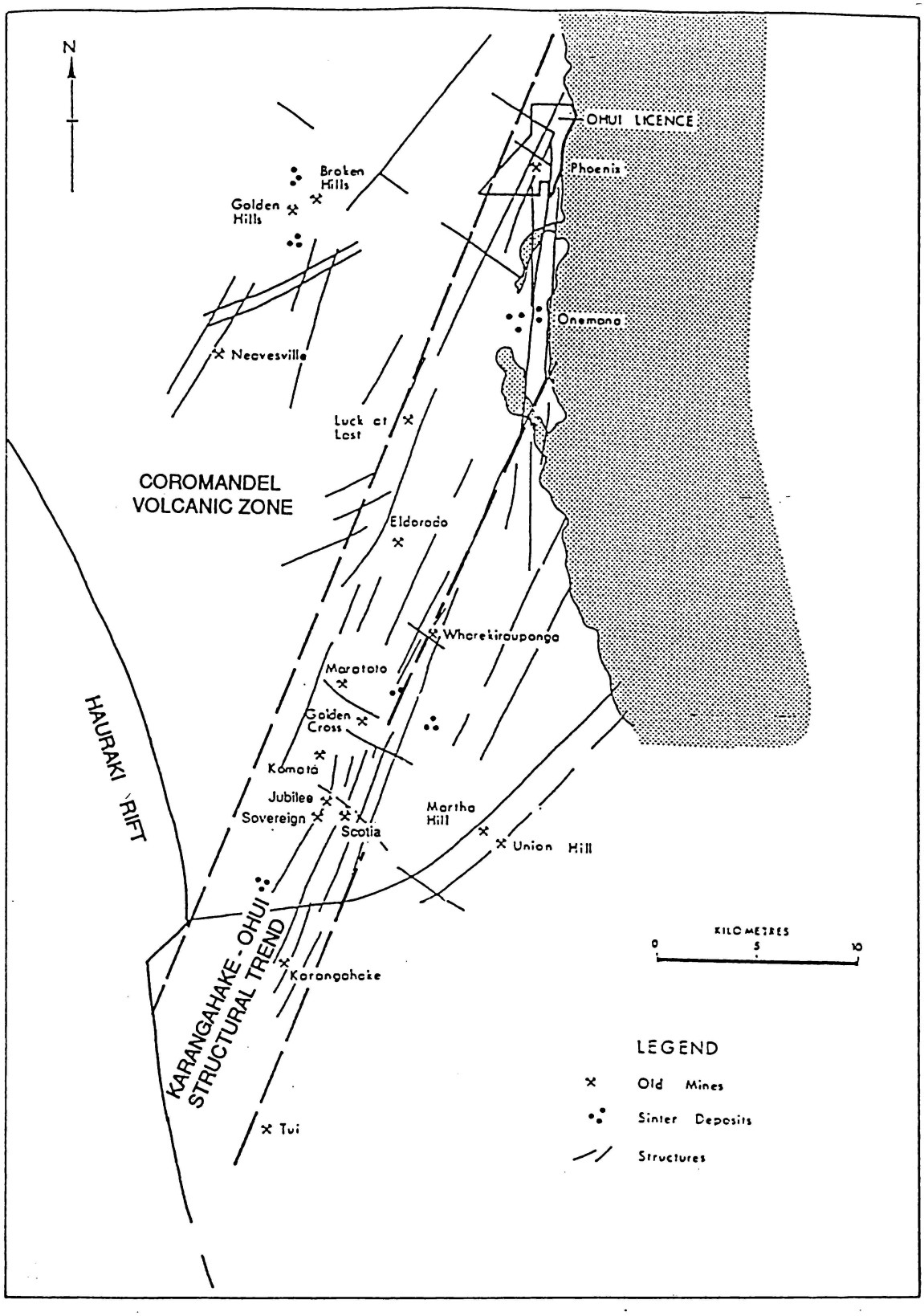

Figure 3.1. The NNE-trending Karangahake-Ohui Structural Trend (KOST) which hosts a number of epithermal deposits including Onemana (after Merchant et al. 1988).

3.2 Regional structure

At present the Coromandel Peninsula occupies a behind-arc tectonic position dominated by extensional faulting along the N-S trending Hauraki Rift (Clarke et al. 1990; Fig. 1.3). Studies by Hochstein and Nixon (1979), Hochstein and Rogan (1980), and Hochstein et al. (1986) define the Hauraki Rift as a young continental rift which has dextral strike-slip movement. Hodder (1984) found that the Cenozoic volcanics on the western shoulder show some geochemical affinity to rift volcanism. Pliocene rifting has been postulated by O'Leary (1978) as a possible control on volcanism along the eastern side of the Coromandel Peninsula. Outcrop patterns are strongly controlled by block faulting mainly along NE, NW and N-S directions (Gadsby et al. 1990; Clarke et al. 1990).

Regional vein orientations are dominated by NE trends (Brathwaite et al. 1987; Gadsby et al. 1990). Studies by Walcott (1984) suggest this trend indicates a regional strike-slip component. Rabone (1987) also suggests that the KOST has a dextral strike-slip component.

Circular features were first identified by Skinner (1986) using satellite imagery. The largest of these is the Kapowai Caldera, which occurs 20km north of Onemana. Another less well defined circular structure is the Wharekawa Caldera 10km to the west (Skinner 1986). The closest caldera to the Onemana area is the Tunaiti Caldera south of Whangamata, which was identified by Briggs and Fulton (1990) through facies interpretation.

Recent work done by Belliss and Christie (1994) on SAR imagery over the eastern Coromandel Peninsula show the region to be dominated by NNE-NE trending structures (Fig. 3.2). Few E-W and NW striking faults were identified. Volcano-tectonic depressions were identified at Kapowai and Whenuakite by Belliss and Christie (1994). Further investigation showed circular structures evident in the Wharekawa and Tunaiti areas.

3.3 Local Structure

The local structure in the Onemana Region (Fig. 3.3) consists of four main fault sets (Fig. 3.4). The dominant direction of faulting is to the N, NE, and NW with minor E-W striking faults, though N-striking faults may be over-represented due to the high number of N-striking faults in coastline surveys. This fault pattern is similar to regional trends identified by Gadsby et al. (1990), and

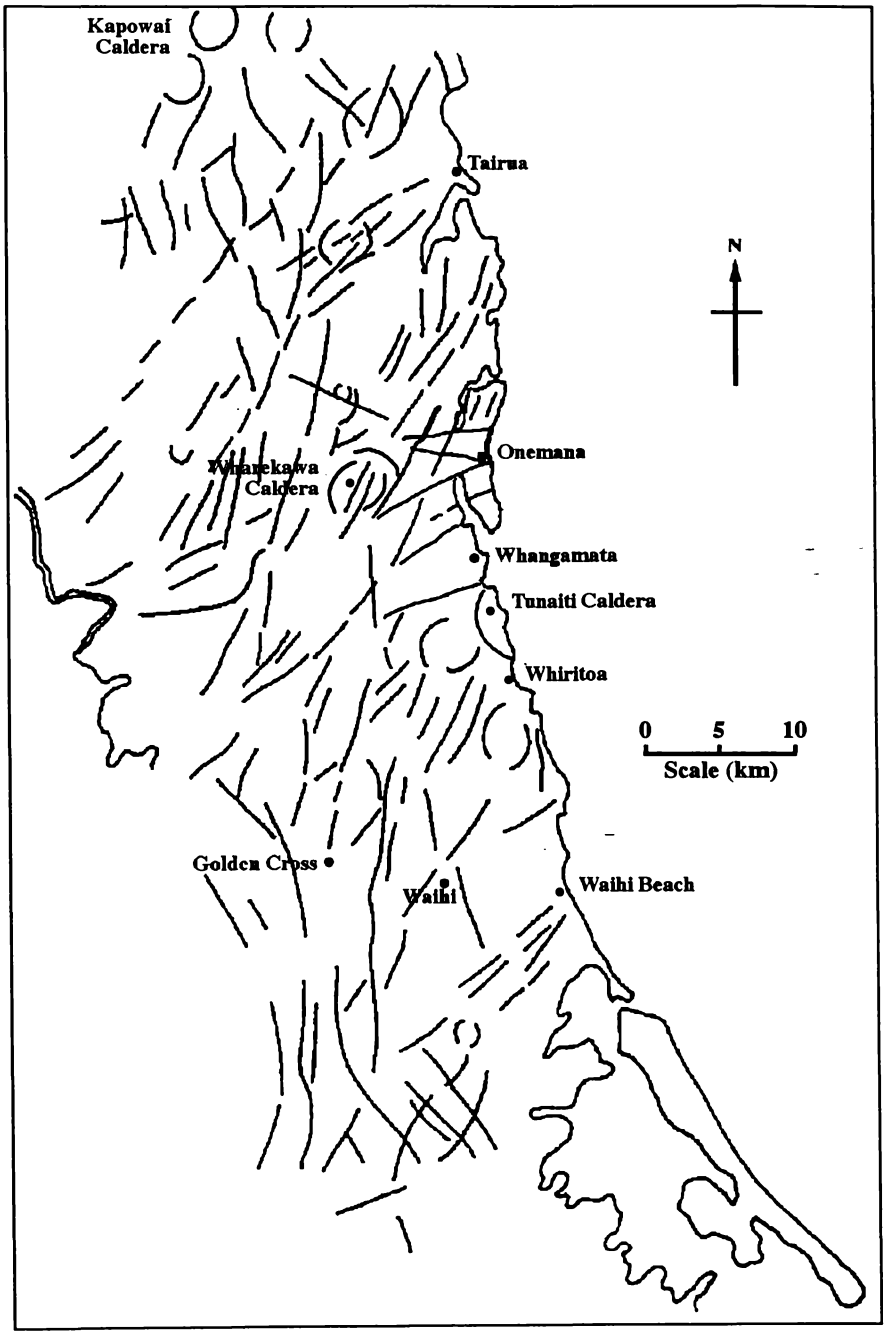

Figure 3.2. Lineations interpreted from SAR imagery (adapted from Belliss et al. 1994).

Clarke et al. (1990). The N-striking faults are separated into two separate groups: unmineralised, and mineralised faults in the Eastern Fault Zone between the NE-striking Pokohino and Whitipirorua faults.

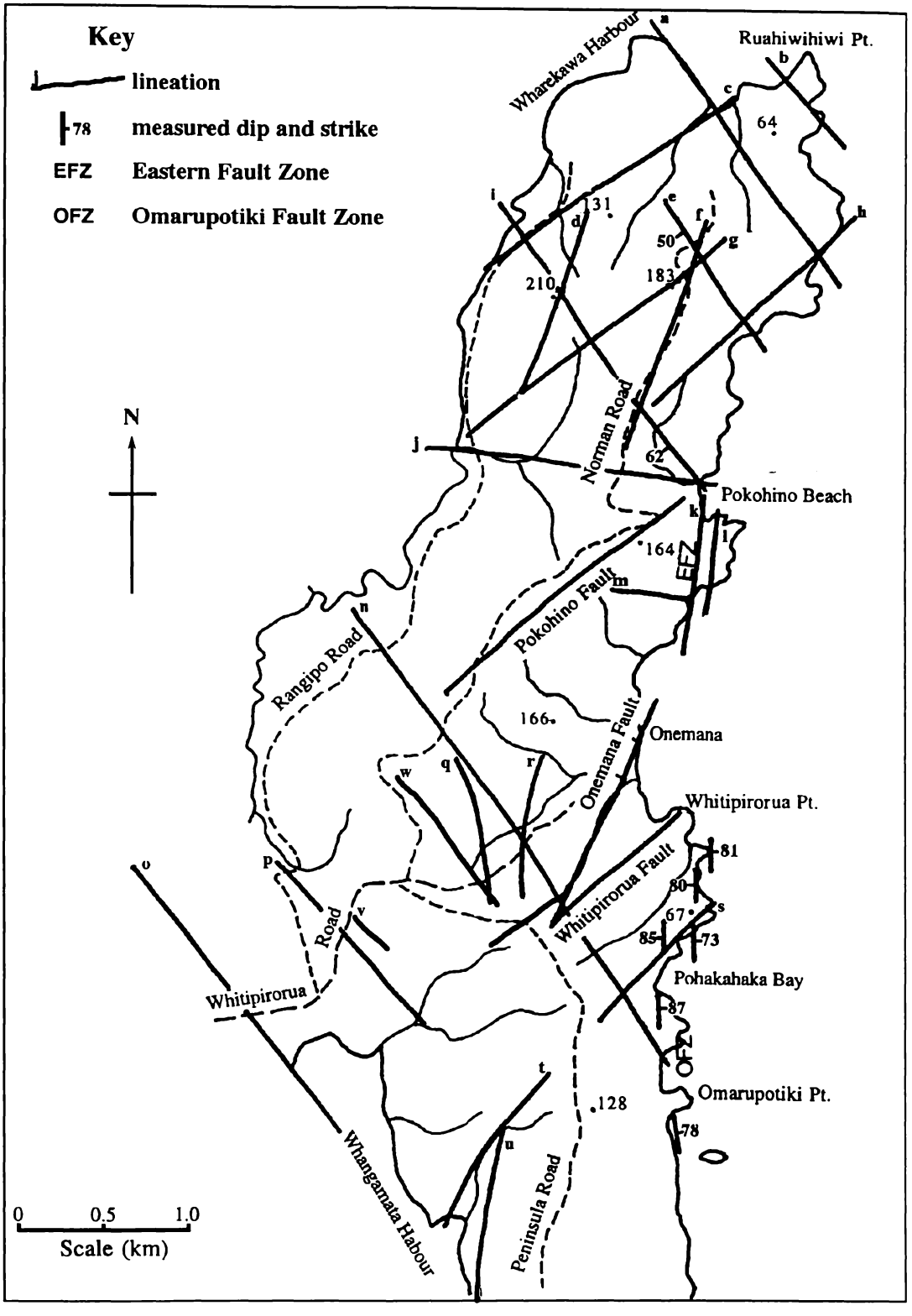

Figure 3.3. Structure of the Onemana area based on aerial photos and SAR lineations, geophysical anomalies and observed faults.

The faults are thought to be generated by more than one stress regime. The structure of the area is thought to play a major role in the location of vents for the rhyolitic volcanism, and late stage hydrothermal activity.

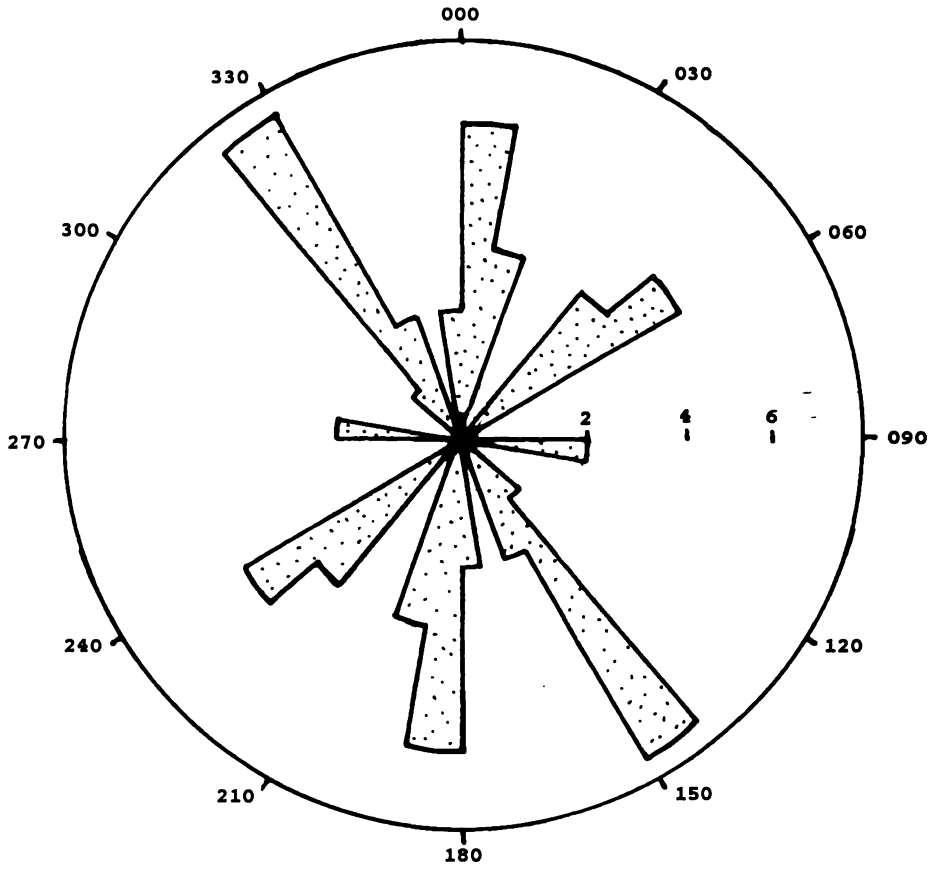

Figure 3.4. Rose diagram of fault patterns within the Onemana area, based on lineations represented in Fig. 3.3. Number of measurements = 28.

3.3.1 N-striking faulting

Unmineralised N-striking structures: Omarupotiki Fault Zone

Exposed in headlands from Whitipirorua Point to Omarupotiki Point are numerous N-striking faults. These faults collectively constitute the Omarupotiki Fault Zone (OFZ) which is up to 100m wide. These faults are not associated with any major photo lineaments, and there are no N-striking lineations to the west within the Pohakahaka Dome Complex. Faults are near vertical with dips dominantly to the east varying from 70°-90°. The strike on faults varies between 160°-180°.

Most faults are infilled with a fine grained, pale yellow clay, generally no more than 5cm wide. Faults exposed in the north side of Pohakahaka Bay show thick (up to 8m) shear zones infilled with clay and boulders (Fig. 3.5). The sheared wall rocks included in the crush zone are subrounded, clast supported, and up to 60cm in diameter.

N-striking structures identified from magnetic lineations are evident in the centre and in the west of the study area. These lineations are not represented at the surface, and are thought to represent basement fractures.

N-striking lineations within the alteration corridor labelled in Figure 3.3 as (q), (r) and the Onemana Fault have only been identified as photo lineations. No mineralisation appears to correspond to these structures, and although q and r occur near Breccia Knob they are not associated with any resistivity anomalies.

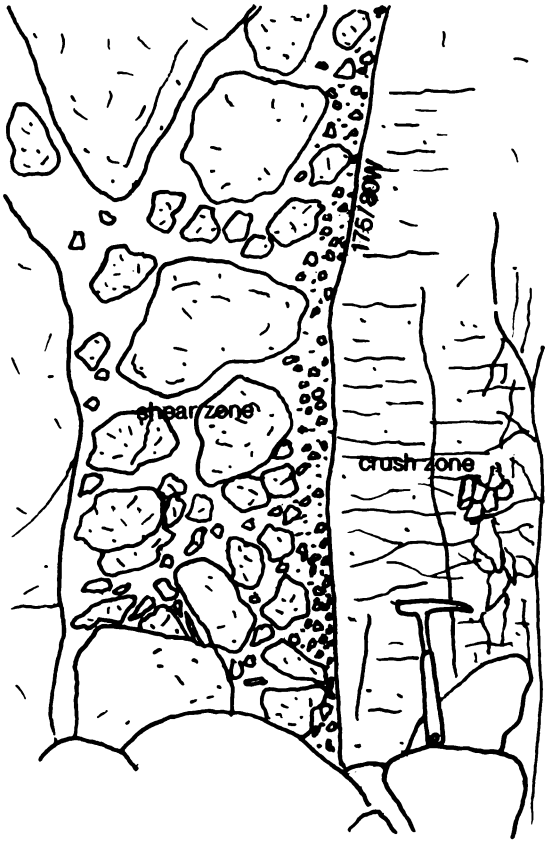

Figure 3.5. N-striking fault in the Pohakahaka Bay area (T12 662449), showing 0.5m wide shear zone with boulders of pyroxene rhyolite and clay gouge (looking north). Hammer is 33cm long.

Mineralised N-striking structures: Eastern Fault Zone

The Eastern Fault Zone (EFZ) in the Pokohino Beach area is a 150m wide zone containing N-striking veins, vein stockworks, and faults with associated intense silicification and brecciation. The EFZ is thought to be an extension of the unmineralised OFZ.

Structures measured in the OFZ and EFZ are displayed in Figure 3.6. Both Zones are dominated by steeply dipping N-trending structures. Faults in the EFZ are dominated by strike trends between 000° and 040°, but also overlaps with fault trends of the OFZ between 330° and 020°. Variation between the zones may be expected as movement within the EFZ has probably been rejuvenated, and may have been subjected to different stress regimes. This may explain the NNE-NE structures evident within the zone.

From aerial photos and outcrops the zone is delineated by two N-striking lineations (k, l). Vein stockworks appear to be closely associated with the locations and alignment of the lineations, and are best developed along lineation (k). The lack of large persistent veins is probably due to the nature of the rhyolites and shallow level of the exposure of the mineralised system. Work done by Brathwaite et al. (1994) on nearby epithermal gold deposits (Wharekirauponga, Neavesville, Ohui) showed rhyolite hosted veining to be characterised by thin discontinuous veining, though thick, continuous veining is evident in rhyolite at Golden Hills. Veining is complex within the EFZ with vein stockworks complicated by hydrofracturing and brecciation. Veining typically shows pinch and swell structures, and the dip and strike along a vein varies. Veins are typically steep with dips ranging from 60°-90°E and strikes varying between 330°-030°. Small veins (<5mm) occur on the periphery of more complex stockwork zones. These veins appear to be associated with a single phase of deposition. Complex veining ranges from 10mm to 1.5 m wide. These veins commonly have uneven undulating boundaries, include dilatant breccia of silicified rhyolite, and are braided with some braids acting as links to other veins. The veins comsists of multiphase chalcedonic quartz with minor grey sulphide-bearing quartz and limonitic bands. Veins are typically vuggy with infills of drusy quartz.

Post-mineralisation movement along the N-striking structures is evident in the Pokohino Beach area (T12 664471), where unaltered highly deformed fluvial sediments are juxtaposed against highly altered rhyolite lavas (Fig 3.7).

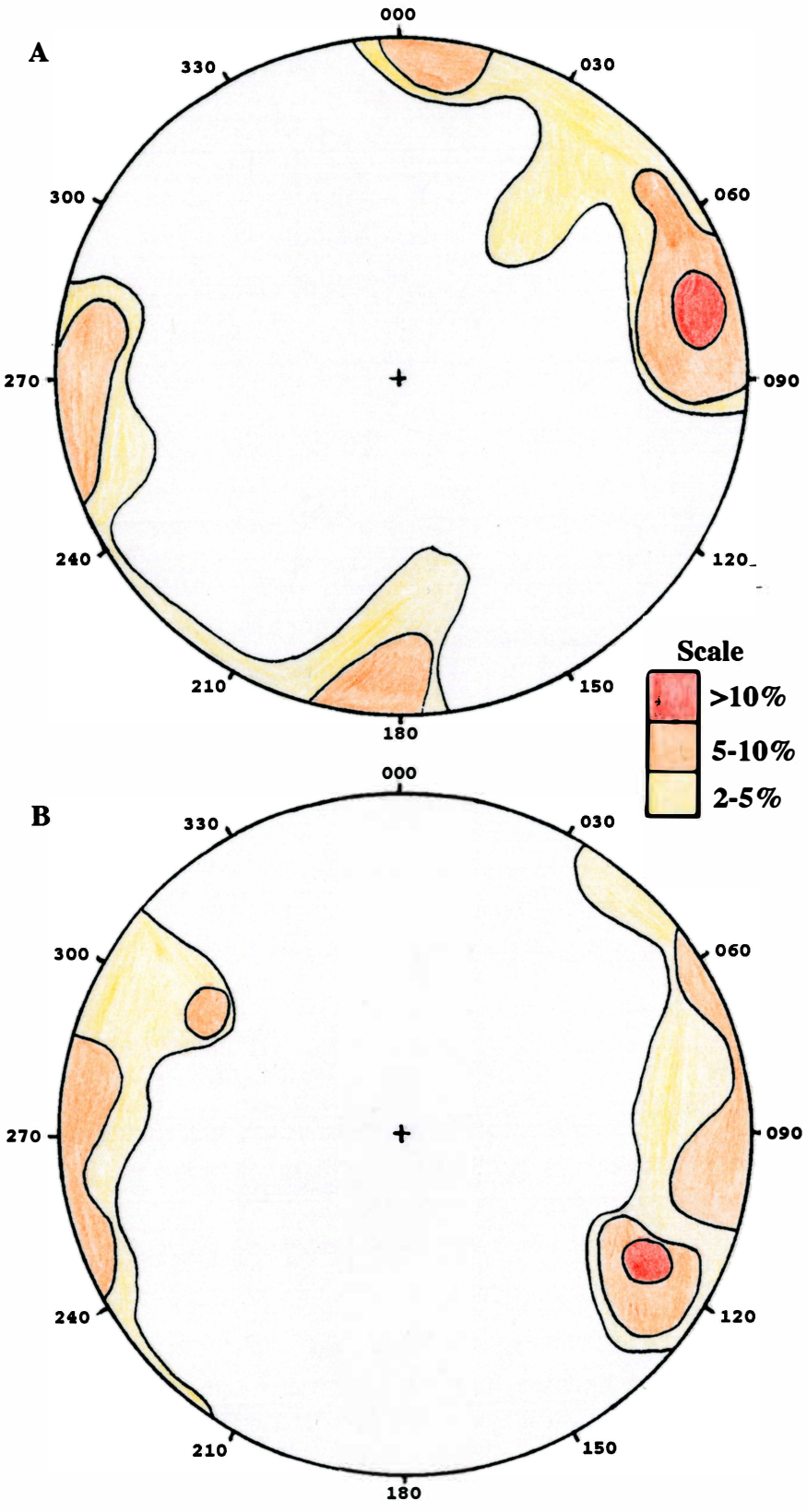

Figure 3.6. Contoured stereonet analyses of fault trends measured from line surveys in A) the OFZ (T12 663450; no. of measurements 59), and EFZ (T12 662467; no. of measurements 54).

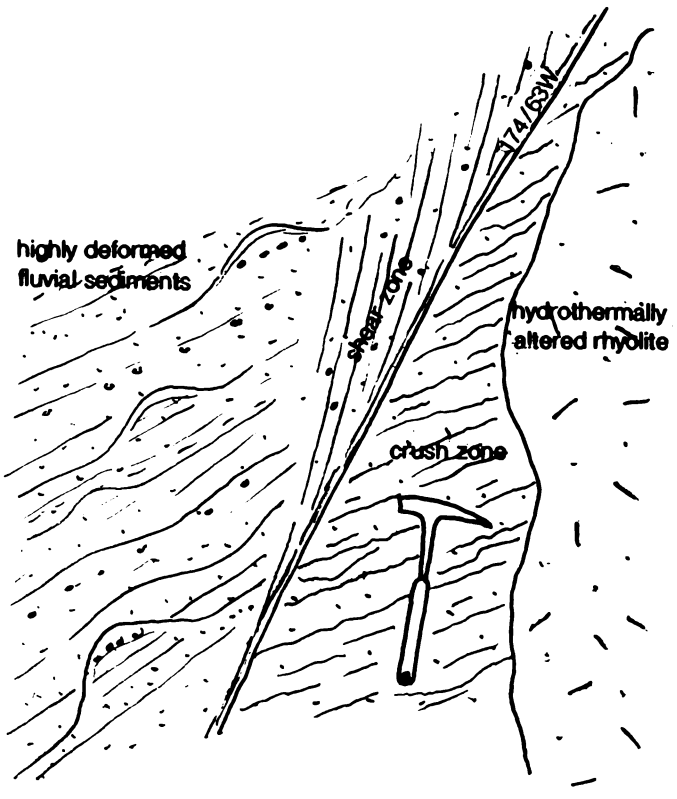

Figure 3.7. Unaltered fluvial sediments faulted against a highly altered rhyolite lava flow, within the EFZ (T12 664470). Hammer is 33cm long.

3.3.2 NE-striking structures

Continuous NE trending lineations are most notable across the northern half of the peninsula. Evidence for the NE-striking structures was best shown by photo interpretation, aerial magnetics, and SAR imagery. Few major NE structures were observed in outcrop.

The Whitipirorua Fault appears as a well defined photo lineament striking 040°, extending from Whitipirorua Point to Peninsula Road, and corresponds to the southern edge of the alteration zone (Fig. 2.27, 3.3). A major structure 8km long can be identified from SAR imagery in the vicinity of the Whitipirorua Fault, but this strikes at 055°. No exposure of the fault was found within the Onemana area. Drilling to the north of the fault around Breccia Knob revealed rhyolite lavas below lake sediments at approximately 50masl. The maximum height of rhyolites on the southern side of the fault is 90-100masl, suggesting a minimum downward displacement of 40-50m on the northern side of the fault.

This downward displacement to the north has produced a graben or half graben structure between the Whitipirorua Fault and Pokohino Fault.

The Pokohino Fault is evident only in aerial photos, where it extends for 2.5km across the Pokohino Dome Complex. The fault may extend further SW to The Knob, although evidence for the fault is weak due to the subdued topography. The morphology of the Pokohino Dome Complex indicates that it is elongated in a NE direction, and lava flows appear to have been erupted from a number of vents aligned along a NE trend.

NE-striking structures within the Wharekawa Dome Complex (c, g, h) have all been identified as photo lineations, with SAR imagery also identifying (c) and (g). From SAR imagery lineation (c) extends 6km inland.

NE-striking structures within the Pohakahaka Dome Complex (s, t) have been identified from aerial photos and SAR imagery, although they appear to be continuous in the SAR image. Where lineation (s) intersects the coastline a similar striking fault was observed in outcrop, 040/80 NW.

3.3.3 NW-striking faults

A NW-striking shear zone (160/50 SW) is exposed in a forestry road cutting (T12 665492) in the northern end of the study area, and is thought to be associated with a NW trending photo lineament (e). The shear zone dips 50° to the southwest and is up to 25cm wide. Mylonitic structures are evident in the shear zone (Fig. 3.8). Another fault measured in coastal section (155/62 SW), north of Pokohino Beach may correspond to lineation (i).

Two NW-striking structures have been identified from resistivity data within the NE trending structural corridor (v, w). These lineations coincide with high levels of alteration, and localised brecciation. Lineation (v) appears to coincide closely with a distinctive photolineament, (p).

From the aerial magnetic survey two major NW-striking structures have been identified (Vidanovich 1991). Lineation (i) corresponds to a magnetic lineation, and a similar striking lineation is evident at the southern end of the alteration corridor (o). Lineation o notably bounds the NE-trending altered zone to the south, and the northern end is similarly bounded by (i): however, as data coverage ends at the coast, it is uncertain whether (i) truncates the NE-trending alteration zone (Vidanovich 1991).

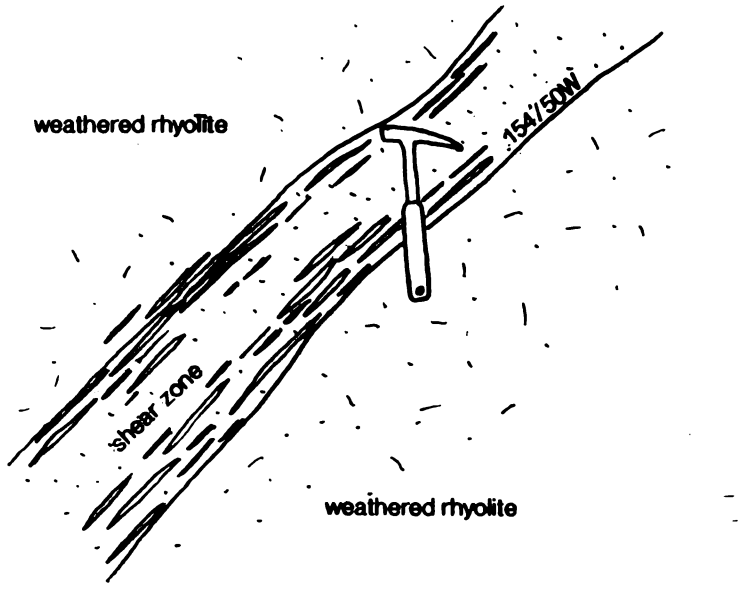

Figure 3.8. NW-striking shear zone exposed in a forestry road cutting (T12 665492) showing mylonite structures. Hammer is 33cm long.

3.3.4 E-W striking faults

E-W striking faulting appears to be a minor fault trend in the Onemana area. Some E-W structures are evident within the NE trending alteration corridor, but show little evidence for fluid movement. Lineation (m) is evident in aerial photos as a short lineament approximately 500m long, though does not appear to coincide with any major E-W striking structure in coastal section. E-W striking structures measured in coastal section between Onemana and Pokohino Beach strike between 070° and 100°, and dip between 62° and 78° N.

An E-W striking photo lineament (j) appears to cross cut the peninsula between the Pokohino and Wharekawa dome complexes. From SAR imagery it appears this structure may continue up to 7km inland. From coastal exposures it appears that the fault has juxtaposed the rhyolite lavas of the Pokohino Dome Complex against the Wharekawa Pyroclastics.

3.4 Associated volcanism

The N-striking fault zone within the Pohakahaka Dome Complex is thought to be related to the inferred vent positions of the pyroxene rhyolite flows exposed

in coastal exposures. Orientation of flow banding on the exposed lava flows suggest there are up to three vents that are probably aligned in a north-south direction within or adjacent to the fault zone.

Eruption of the biotite rhyolites of the Pokohino and Wharekawa dome complexes is thought to be related to the NE-striking faulting. Flow morphology and direction of flow banding suggest that eruptives of the Pokohino Dome Complex correspond to a major NE-striking linear structure. Two NE-striking structures are evident in the Wharekawa Dome Complex, but there is little conclusive evidence to suggest that there are any vents located along these structures.

The eruption of the Glassy Rhyolite and associated pyroclastics may be controlled by the E-W striking photo lineament between the Pokohino and Wharekawa dome complexes. Outcrops appear to coincide with the position of the E-W striking structure. The upstanding dome shaped outcrop (T12 659478) is distinctly elongated in an E-W direction (Fig 2.24). Aerial magnetic data also shows the Glassy Rhyolite to be an elongated magnetic low.

3.5 Development of faults

The eruption of the pyroxene rhyolites along the N-striking structures in the Pohakahaka Dome Complex suggests a different stress regime existed prior to the development of the NE structures and the eruption of the biotite rhyolites.

Several theories are suggested for the development of the NE-trending structures. Either the NE-trending structures could be splay faults or secondary strike-slip faults associated with the KOST, or form fault boundaries to a large rotated block or a series of rotated blocks (Fig. 3.9), or represent a regional change in the direction of extension.

If the NE-striking structures at Onemana are related to the KOST, then dextral-transcurrent movement along the NE-striking structures would be expected. There is no evidence for dextral movement along the NE-striking structures, but evidence from Sibson's (1987) jog model suggests sinistral-transcurrent movement. It is possible, however, for movement along a fault to change in response to changes in the stress regime.

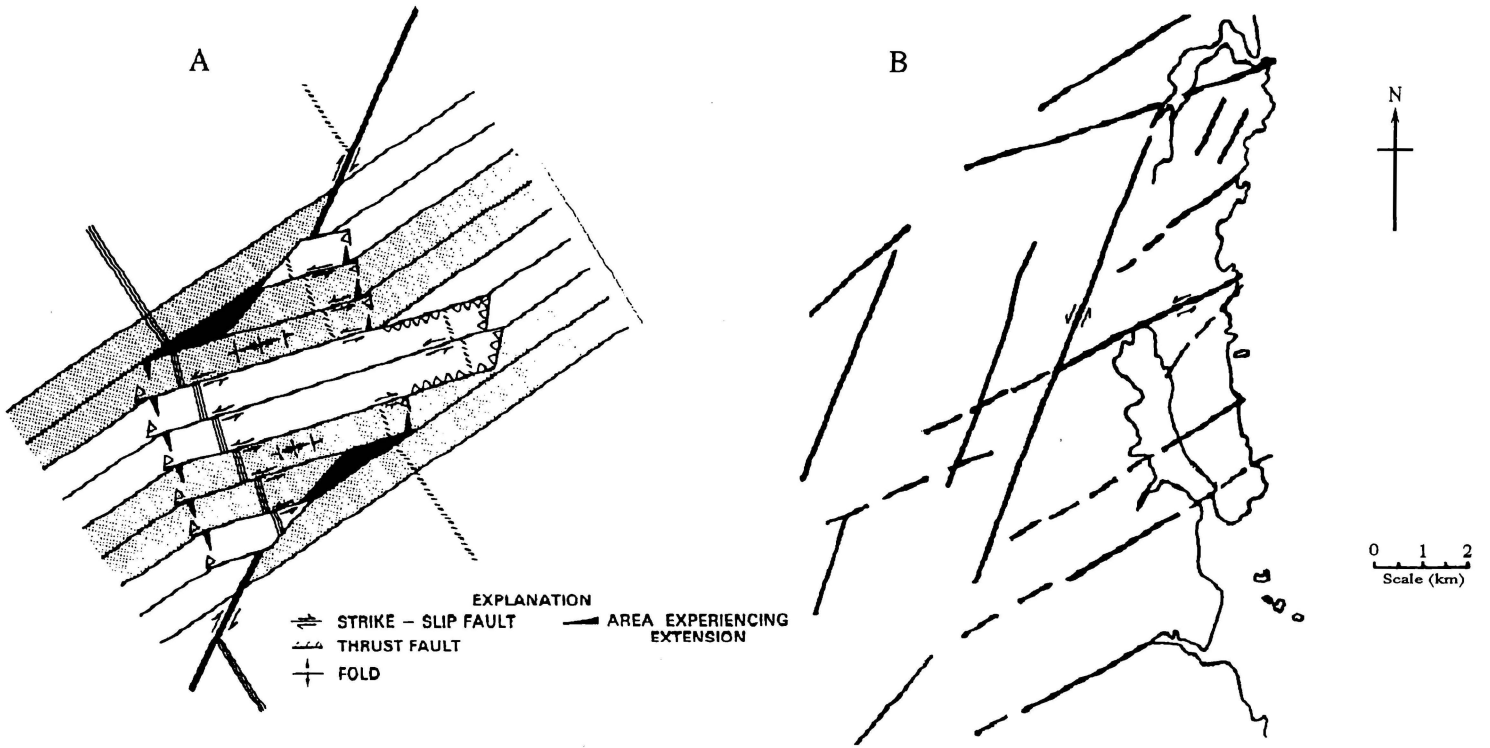

Figure 3.9. A) geometric model illustrating the development of structure in a surface rupture in the Imperial Valley, California (adapted by Biddle and Christie-Blick 1985, from Terres and Sylvester 1981). B) NNE - NE structural patterns determined from SAR imagery in the Onemana/Whangamata area.

Block rotation may explain the suspected sinistral movement along the NE-striking structures. Figure 3.9a shows a geometric model developed by Terres and Sylvester (1981), based on a small example where left stepping en echelon sinistral shears formed when blocks of soil rotated up to 70° in response to dextral-transcurrent movement along a fracture. Sengör et al. (1985) described a larger example, where a 70km long block was rotated 80° along the North Anatolian Fault, Turkey. From SAR imagery the Whitipirorua Fault appears to be a continuous lineation, and is not offset by NNE-striking lineations (Fig. 3.9b). Dextral movement along the NNE-trending KOST may have resulted in large scale block rotation resulting in NE-trending faults with sinistral movement.

The occurrence of mineralised structures confined between two NE-striking boundary faults (Whitipirorua and Pokohino faults) is similar to the dilatational jog model applied to Waihi (Wellman 1954; Sibson 1987), where the lode system developed due to dextral transcurrent movement along the N-striking en echelon boundary faults (Sibson 1987). To apply the model to the NE-trending alteration corridor, movement along the NE-striking boundary faults would have to be sinistral to cause extension along the N-striking structures. Similar non-mineralised structures have also been described in granodiorites of the central Sierra Nevada, California (Segall and Pollard 1983; Martel et al. 1988), and as jointing within arches in the Arches National Park, Utah (Cruikshank and Aydin 1994).

Typically the driving faults of the dilatational jog are unmineralised, which appears to be evident at Onemana. Block rotation within the dilatational jog may complicate the jog model by causing zones of extension and compression. This may be the case for the EFZ where mineralisation in response to extension is evident in the EFZ in the Pokohino Beach area, but little evidence for mineralisation exists to the south within the NE-trending alteration zone. This could be inferred as dilation in the north due to normal faulting, and compression in the south as a result of thrust faulting.

Structures within the dilatational jog appear to vary in their direction of strike from N to NW. This appears to be common in other fault jogs (e.g. Segall and Pollard 1983; Sibson 1987, 1989; Martel et al. 1988), with some secondary faulting nearly perpendicular to the master fault (Segall and Pollard 1983). The occurrence of high angles between the N-striking cross faults and NE-striking boundary faults may be explained by block rotation. Nur et al. (1986) and Ron

et al. (1986) suggested sinistral strike-slip movement accompanied by extension between boundary faults would cause counterclockwise rotation of internal blocks, along with dextral slip on cross faults (Fig. 3.10). This would then produce a high angle between the two sets of faults. Another possible cause for the variation in the direction of strike on the cross faults, is that their strike may be controlled by pre-existing fractures within the underlying rhyolites. This may explain the occurrence of N-striking mineralised structures within the EFZ, where movement along the NE-striking faults rejuvenated strike-slip movement along the older N-striking structures (EFZ) between the Whitipirorua and Pokohino faults and not the OFZ.

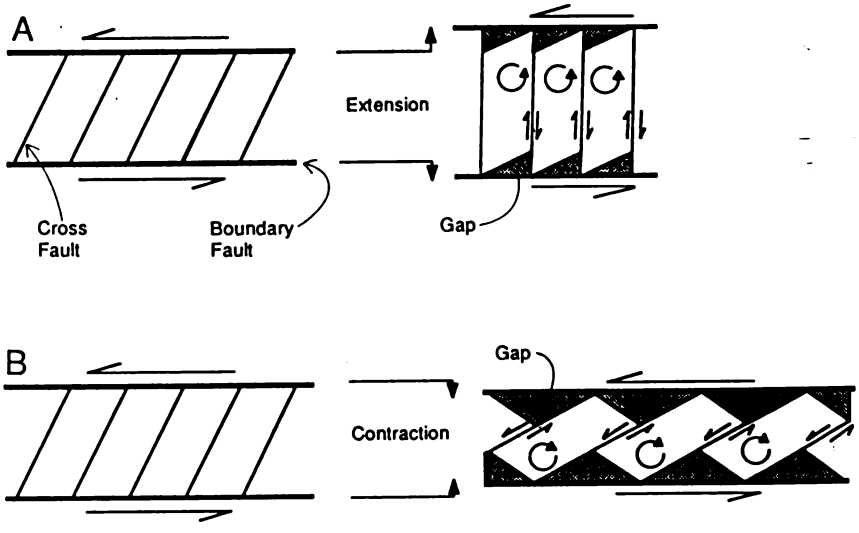

Figure 3.10. (A) counterclockwise rotation of blocks between cross faults as boundary faults move sinistrally. Dextral movement occurs on cross faults, and extension occurs across the zone. (B) clockwise rotation of blocks between cross faults and contraction across the fault zone as the cross faults slip sinistrally (after Martel et al. 1988).

3.6 Brecciation associated with faulting

Areas of brecciation occur in a number of localities within the NE-striking alteration corridor. The only breccia observed within a fault occurs along a N-striking fault in the Pokohino Beach area (T12 664471) (Fig. 3.11). Based on Sibson's (1989) classification of fault breccias, it appears the breccia is the result of attrition along a major shear zone prior to mineralisation and dilation.

Where hydrothermal brecciation has occurred as a result of dilation, the breccia shows jigsaw textures, and boiling textures may also be evident. Rapid slip transfer may cause local brecciation by hydraulic implosion of wall rock into a cavity space, followed by subsequent fluid inflow (Sibson 1986). Associated with this drop in pressure, boiling can occur. Historic strike-slip rupturing along the Cerro Prieto Fault, Southern California, appears to have triggered

major boiling episodes, and hydrothermal eruptions within the geothermal field (Sibson 1987). Areas of hydrothermal brecciation, inferred vents for hydrothermal eruptions, and associated boiling textures appear to coincide with NW-striking resistivity anomalies.

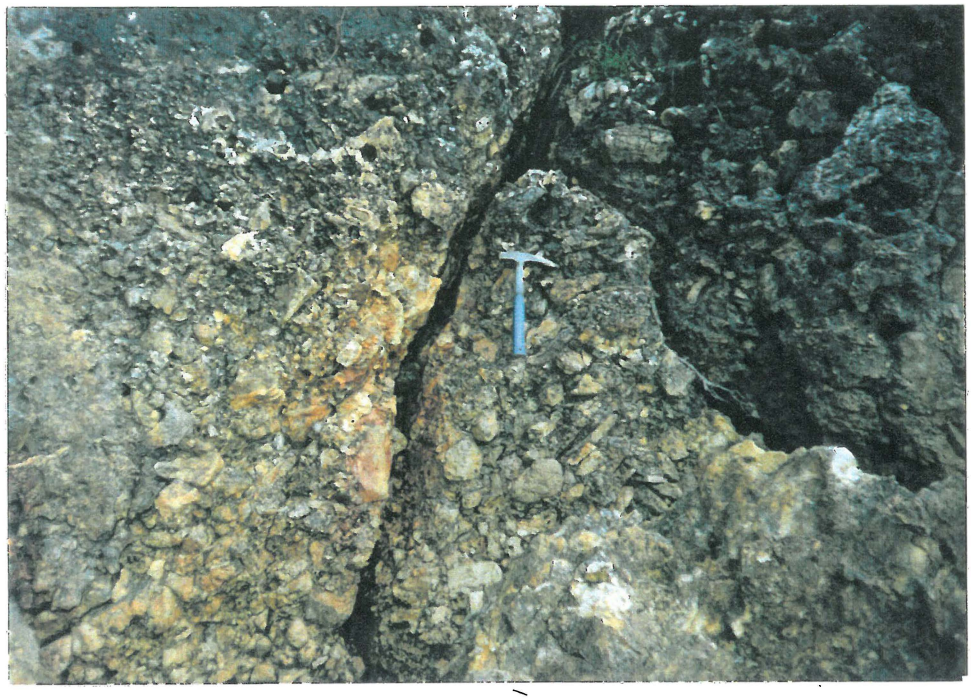

Figure 3.11. Silicified fault breccia along a N-striking structure within the EFZ (T12 664471). Fracture in centre is striking E-W and dipping to the north.

3.7 Timing of faulting

It is evident that the structures in the Onemana region have played a major role in localising the rhyolitic volcanism and late stage hydrothermal activity. Stress regimes are complex, and it is beyond the scope of this study to analyse them, but it appears probable that more than one stress regime has affected the area in time and space. Using the relationship of volcanism and mineralisation with faulting it is possible to develop a probable order of faulting (Fig 3.12).

It is assumed the N-striking faulting associated with the eruption of the pyroxene rhyolites are the oldest structures evident in the area. These N-striking faults are thought to be cut by the NE-striking Whitipirorua Fault. Contrasting models are illustrated by Martel et al. (1988) for the development of a simple fault zone regarding the age of the fractures within the fault zone to those of the zone boundaries (Fig 3.13). The development of N-striking structures may be related to Peng and Johnson's (1972) model (Fig. 3.13a),

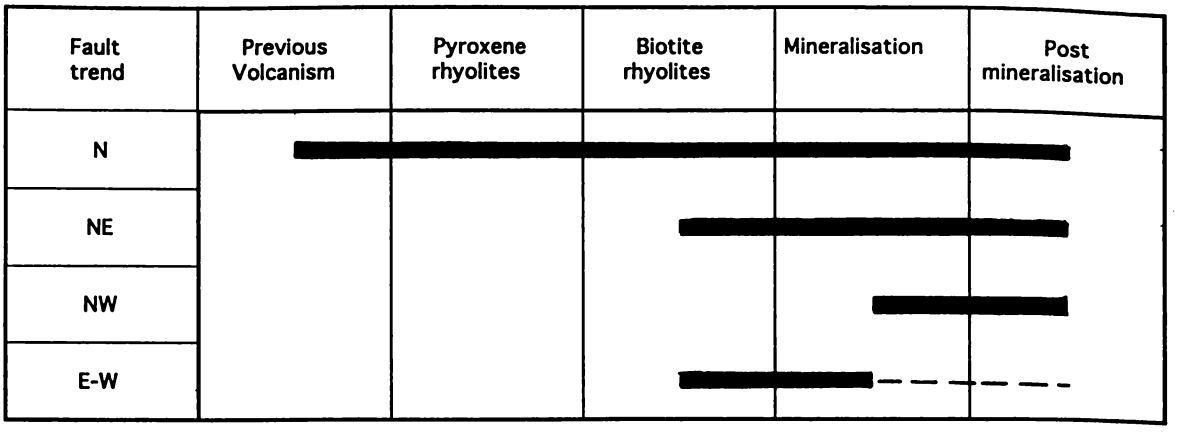

Figure 3.12. Suggested relative age of faulting compared with volcanism and mineralisation in the Onemana area.

where the newly active NE-striking faults rejuvenated movement on the N-striking faults within the EFZ, providing zones for mineralisation. The NW-striking structures evident from resistivity anomalies may have developed in response to strike-slip shear on the Whitipirorua and Pokohino faults, as in Figure 3.13b, but were further complicated by dilatational movement of blocks between these faults within the NE-trending alteration corridor (Fig. 3.10).

It is evident from exposures that movement occurred along N-striking faults within the NE-trending alteration corridor (EFZ) after the mineralisation phase. Therefore it is assumed that this movement was initiated by movement along at least one of the NE-striking boundary faults.

Placing a time constraint on the development of the E-W striking structures is difficult, but it is possible that these structures are associated with the youngest phase of rhyolite volcanism in the Onemana area. Evidence from aerial magnetics suggest that the NW striking structures (i) and (o) are post-mineralisation.

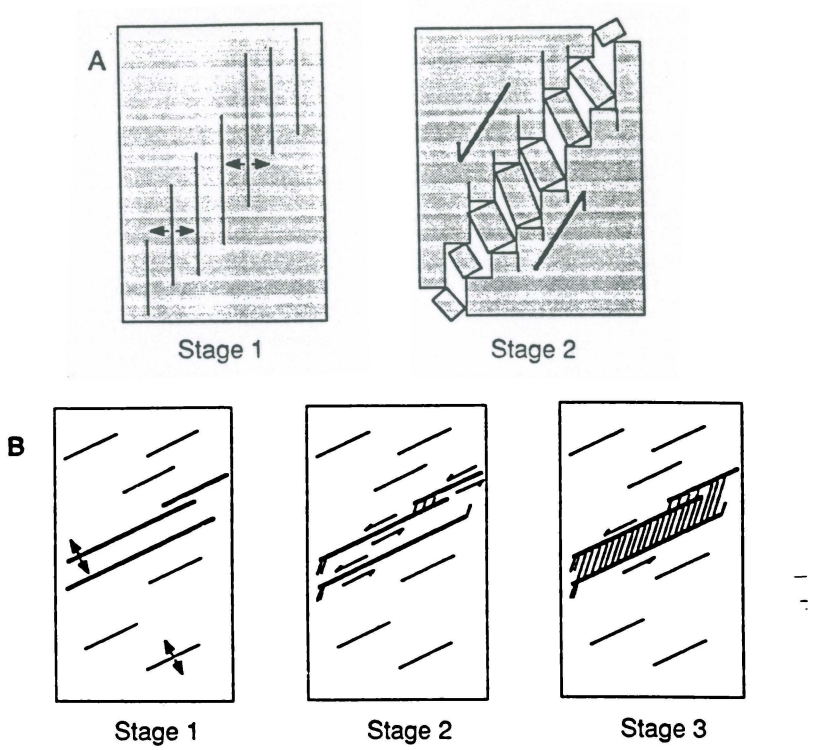

Figure 3.13. Comparison of the development of a laboratory shear fracture zone (A) produced by Peng and Johnson (1972) and (B) development of simple fault zones by Martel et al. (1988). (A) a zone of en echelon fractures forms (stage 1) before the zone boundaries form (stage 2). (B) faulting sequence begins with initial extension fractures (stage 1), progresses to slip along faults (stage 2), and evolves to the development of simple fault zones with boundary faults (stage 3). The internal fractures are younger than the fault zone boundaries and do not extent across the boundaries (after Martel et al. 1988).

Chapter Four
Petrography and Mineralogy

4.1 Introduction

The volcanics of the Onemana area are dominated by porphyritic rhyolitic domes and flows. The rhyolites have been subdivided into two groups based on their mineral assemblage: pyroxene rhyolites and biotite rhyolites. The biotite rhyolites are subdivided further on the basis of variation in the mineral assemblage and texture. Other units in the area include several multilithological pyroclastic deposits associated with the biotite rhyolites, hydrothermal eruption deposits, and lake sediments, and a two-pyroxene andesite lava.

Approximately 140 thin sections were used to determine the petrographic characteristics of the units. Modal analyses of representative unaltered samples are shown in Table 4.1. Modal analyses were performed on a SWIFT automatic point counter based on 400 counts per sample.

This chapter discusses the mineral chemistry of fresh, unaltered phenocrysts from twelve samples representing the volcanic units from the Onemana area. Polished thin sections were analysed using the JEOL electron microprobe with LINK ZAF - 4/FLS software at the Department of Geology, University of Auckland. Minerals analysed were feldspars, biotites, pyroxenes and Fe-Ti oxides. Other unknown minerals were probed to help identification, and are not included here. Full analytical results are presented in Appendix II.

4.2 Pyroxene rhyolites

The pyroxene rhyolite domes and flows consist of all the eruptives derived from the Pohakahaka Dome Complex. All samples have been weathered to some degree, which made the identification of the pyroxene type impossible, due to replacement by clays. Modal analyses show that the mineral assemblage is variable, but is generally, plagioclase - quartz - relict

Table 4.1. Selected modal analyses for volcanic rocks in the Onemana area: tr = trace, 1 = zircon, 2 = vughs infilled with tridymite, 3 = chlorite, 4 = wood fragments, 5 = apatite.

Lavas/ Domes Sample	Qtz	Plag	Bio	Hyp	Aug	Pyx	Opq	Other	GM
Pohakahaka Dome Complex									
W941261	3.00	6.00				1.25	0.25	3.50[2]	86.00
W941267	4.50	14.00				2.25	0.75	tr[1,5]	78.50
W941289	0.75	7.25				1.00	tr	tr[1]	91.00
W941305	1.50	12.75				2.25	0.50		83.00
W941309	1.50	7.25				1.50	tr		89.75
W941322	2.75	15.00				1.50	0.50	tr[1,5]	80.25
Pokohino Dome Complex									
W941335	3.25	12.25	1.00				tr		83.50
W941345	4.00	12.75	tr				tr		83.25
W941348	1.75	2.75	0.50				tr		95.00
W941368	4.25	6.25	0.25				tr		89.25
Wharekawa Dome Complex									
W941264	4.00	8.00	0.75				tr		87.25
W941266	1.25	3.25	0.75				0.25		94.50
W941340	3.75	3.75	tr				tr	6.25[2]	86.25
W941341	1.25	9.00	0.50				tr	tr[2]	89.25
W941344	2.75	12.25	0.25				tr		84.75
W941397	4.50	5.75	0.25				tr		89.50
Eastern Flows									
W941263	0.75	5.25					tr		94.00
W941396	1.00	12.50	2.25	0.50			0.75	tr[1]	83.00
W941395	2.00	6.25	tr				tr		91.75
Glassy Dome Rhyolite									
W941279	3.50	5.50	0.75				tr	tr[5]	90.25
W941337	3.50	7.25	0.75				tr		88.50
Rangipo Andesite									
W941284		12.75		2.25	2.00		0.25		82.75
W941347		12.25		3.50	1.25		1.00		82.00

Table 4.1. Continued.

Pyroclastics/Breccia Sample	Qtz	Plag	Bio	Opq	Crystal	Lithics	Pumice	Other	Matrix
Wharekawa Pyroclastics									
W941274	3.25	2.75	tr	tr	6.00	42.00	0.75		51.25
Glassy Dome Pyroclastics									
W941285	0.75	5.25	0.50	tr	6.50	46.50	17.75	tr[5]	29.25
W941349	1.25	2.75	0.50	tr	4.50	58.75	5.25	tr[3]	31.50
W941332	2.00	3.00	tr	tr	5.00	69.75	3.75		21.50
Wharekawa Ignimbrite									
W941352	1.00	3.00	tr		4.00	39.25	28.25		28.50
Onemana Breccia									
W941281	0.75				0.75	43.00			56.25
W941302	11.25				11.25	30.75		tr[4]	58.00
W941358	2.75				2.75	22.75			74.50

pyroxene Fe-Ti oxides ± zircon ± apatite. Groundmass textures are dominantly spherulitic to poikilitic.

4.2.1 Phenocrysts

Plagioclase

Plagioclase (An_{25-33}) is the dominant phenocryst in the pyroxene rhyolites, with a range from 6 to 15 modal %. Plagioclase phenocrysts are typically anhedral to subhedral. Some anhedral examples are evident in the freshest samples (sample W941322) where they occur up to 5.0mm long (Fig. 4.1a). Normal and reverse zoning is common and oscillatory zoning was observed in samples W941267 and W941322. Both simple and polysynthetic twinning is evident in most plagioclase.

The compositional range of the plagioclase plots them within the oligoclase and andesine fields (Fig. 4.2a). The range of compositions for plagioclase in the pyroxene rhyolites occurs well within the range of plagioclase compositions from other Minden Rhyolites, e.g. Hot Water Beach Rhyolite (An_{25-38}) and Whenuakite Rhyolite lavas (An_{15-50}) (Adams 1992), rhyolite lavas from Tunaiti (An_{23-50}) (Fulton 1988), and Cooks Beach and Hahei Dome lavas (Rogers 1994).

Quartz

Quartz is common in the pyroxene rhyolites, and varies in abundance from 0.75 and 4.5 modal %. Quartz occurs up to 2.5mm in diameter, and is typically anhedral, embayed, and exhibits resorbed outer margins.

Figure 4.1 (over page). A) zoned plagioclase within a spherulitic pyroxene rhyolite. Sample W941320, X20 magnification, plane-polarised light. B) radiating crystallites within pyroxene rhyolite. Sample W941267, X400 magnification, plane-polarised light. C) well developed spherulitic textures within Eastern Flow biotite rhyolite. Note plagioclase phenocryst in centre of spherulite. Sample W941263, X20 magnification, plane-polarised light. D) lithic-rich ignimbrite from Glassy Dome Pyroclastics. Note chlorite in top right corner. Sample W941390, X20 magnification, plane-polarised light. E) Glassy Dome Rhyolite showing well developed perlitic fractures and subhedral to euhedral plagioclase and biotite. Sample W941278, X20 magnification, plane-polarised light. F) Rangipo Andesite showing felted and granular groundmass and phenocrysts of plagioclase and augite. Sample W941284, X20 magnification, cross-polarised light.

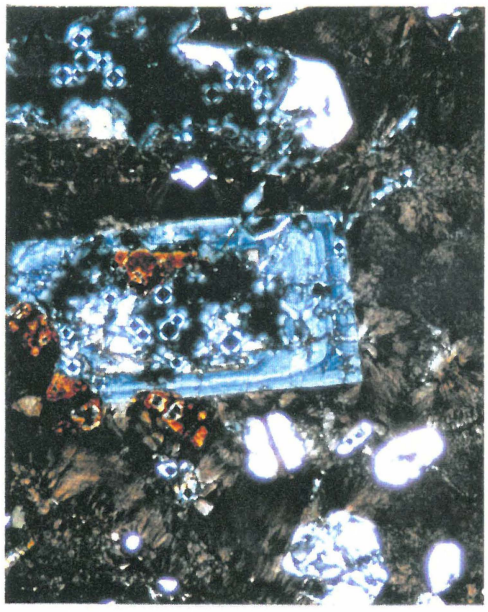

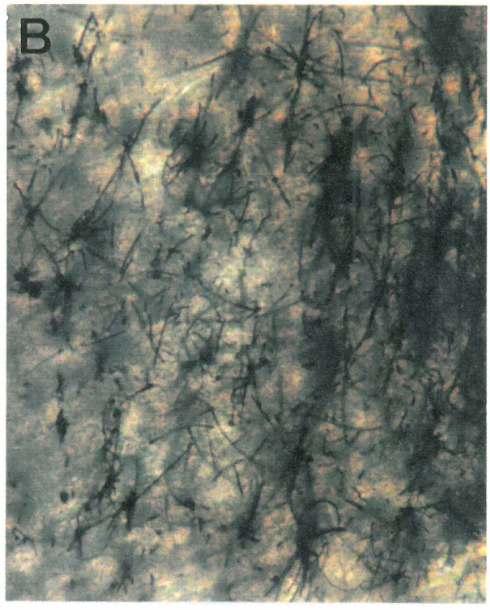
B

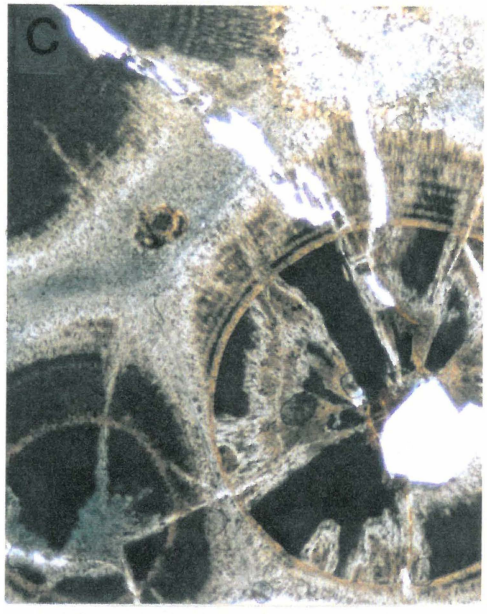
C

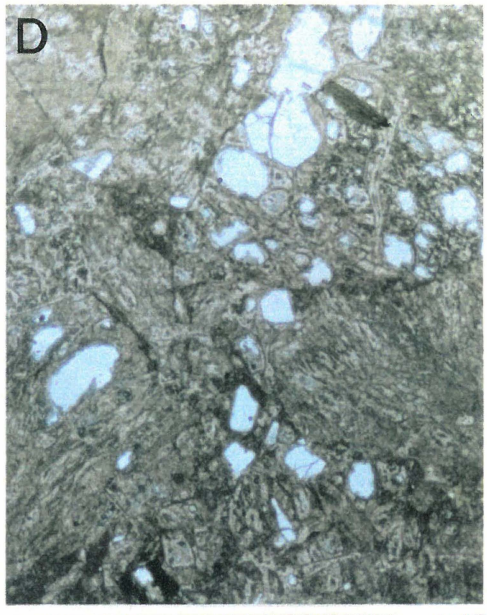
D

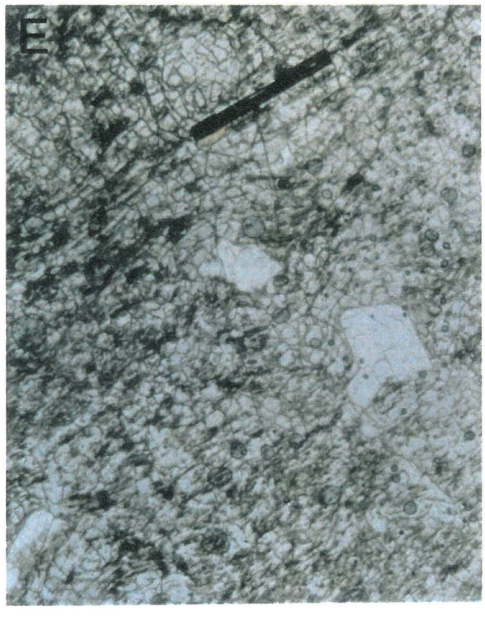
E

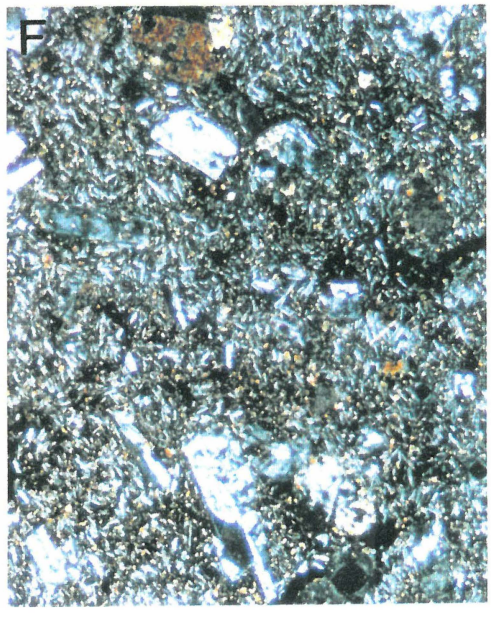
F

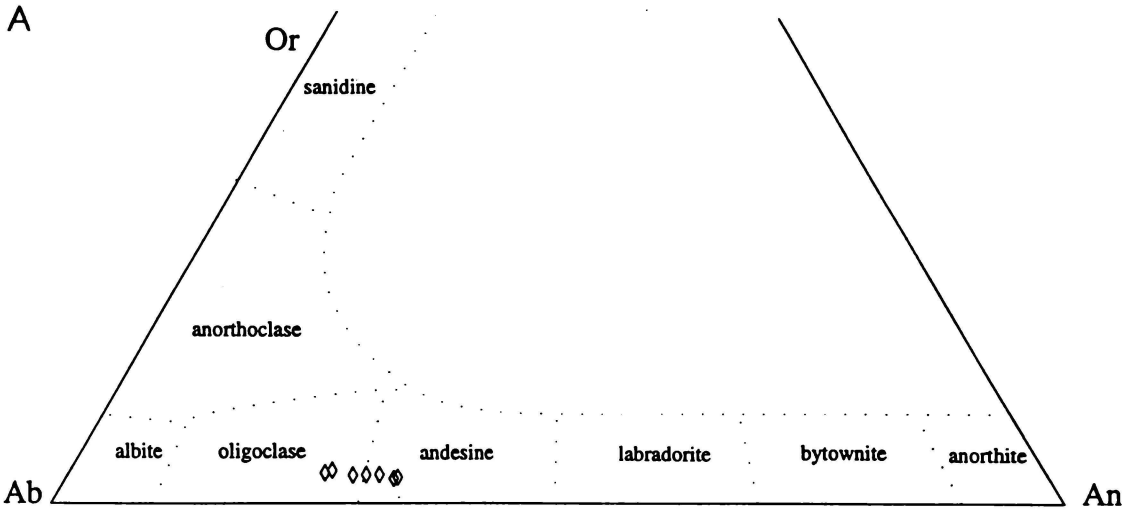

Pyroxene rhyolite

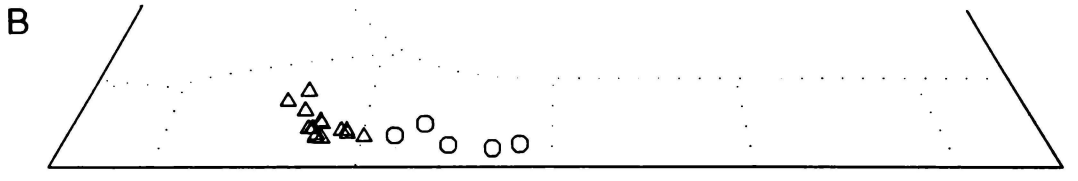

Biotite rhyolites: Pokohino Dome Complex (△), Wharekawa Dome Complex (○)

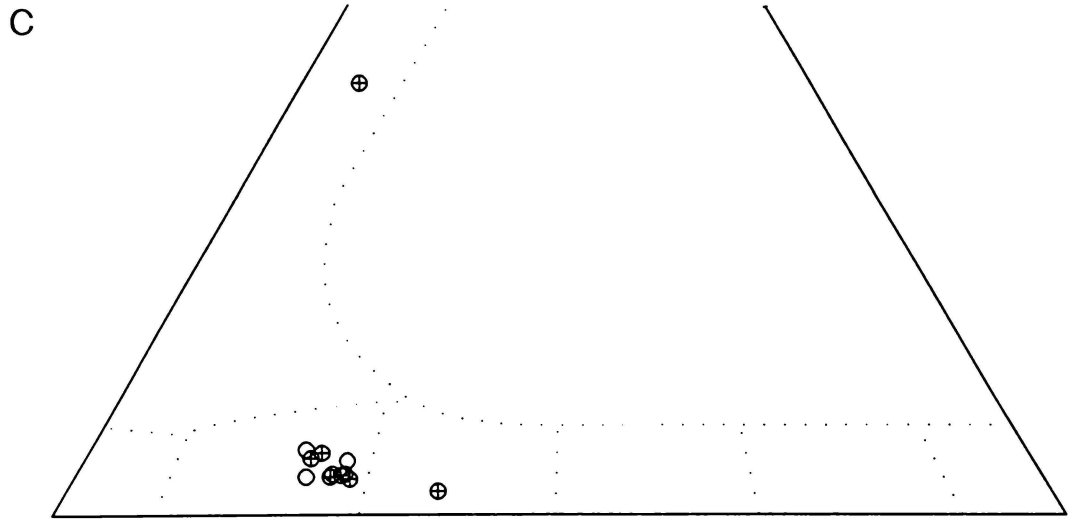

Glassy Dome eruptives: rhyolite (⊕), and pyroclastics (○)

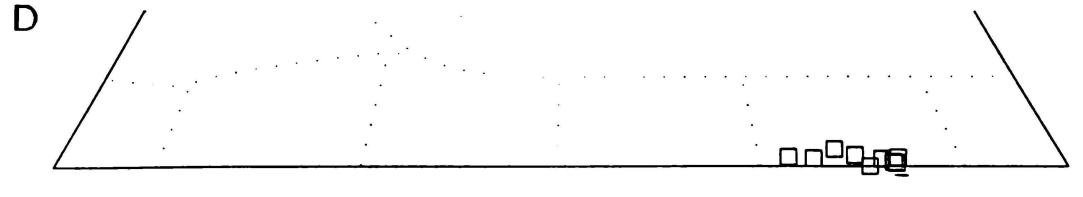

Rangipo Andesite

Figure 4.2. An-Ab-Or ternary classification diagrams for selected plagioclase feldspars in the volcanic rocks of the Onemana area.

Relict pyroxenes

All pyroxenes seen in thin section have been completely altered to illite and Fe oxides, and therefore could not be probed. Relict pyroxene is typically subhedral, with some still showing well developed prismatic cross-sections. Pyroxene abundances are fairly constant, with an average of 2 modal %, and occur up to 1mm in length. Pyroxenes commonly form glomeroporphyritic clusters.

Fe-Ti oxides

Fe-Ti oxide abundance is generally very low (<1 modal %) in the pyroxene rhyolites, but appear to be more abundant than in the biotite rhyolites. Fe-Ti oxides are subhedral to euhedral, up to 0.5mm across, and are dominated by titanomagnetite with minor ilmenite. Some magnetite crystals contain ilmenite exsolution lamellae. Fe-Ti oxides also commonly occur as inclusions within and closely associated with pyroxene.

Accessory minerals

Rare small (<0.1mm) euhedral zircon crystals occur associated with pyroxene phenocrysts (samples W941267 and W941376), and in the groundmass.

Rod-like crystals of apatite up to 0.05mm form inclusions within plagioclase phenocrysts in samples W941267 and W941322.

4.2.2 Groundmass

Groundmass textures are varied from spherulitic to flow banded. Groundmass constitutes 80-90 modal %. Most spherulites show sheaf or circular textures, with less common axiolitic textures. Experiments by Lofgren (1970; 1971a,b) suggest that circular spherulites form at about 400°C. The above devitrification textures are superimposed on existing groundmass features. Some samples are assumed to have originally been vitrophyric, but the glassy textures have been obscured by devitrification textures. Well developed perlitic textures are still evident in samples W941267 and W941373.

Crystallites are also common in most samples, with crystallites occurring as radiating clusters up to 0.2mm in diameter (Fig. 4.1b). Weakly developed flow banding is evident in most samples, but samples W941308 and W941309 show well developed flow banding around phenocrysts. Samples

W941261, W941308 and W941309 show amygdaloidal textures, where vesicles are infilled by quartz pseudomorphs (tridymite ?). Limonite staining from weathering is evident in most samples.

4.3 Biotite rhyolites

The biotite rhyolites constitute the most extensive rock type in the Onemana area. Most of the biotite rhyolites have been erupted from vents within the Pokohino and Wharekawa dome complexes, except the Eastern Flows. The biotite rhyolites are typically pink, flow banded, and spherulitic. Much of the primary textures have been overprinted due to hydrothermal alteration in the southern and eastern parts of the Pokohino Dome Complex. The primary mineral assemblage for the biotite rhyolites is plagioclase - quartz - biotite - Fe-Ti oxides ± zircon.

4.3.1 Phenocrysts

Plagioclase

Plagioclase (An_{19-45}) varies from 2 to 13 modal %, is typically subhedral to anhedral, and up to 2mm in length. Some large euhedral crystals up to 6mm occur in sample W941347. Simple and polysynthetic twinning is common, and zoning occurs, but to a lesser degree than was observed in the pyroxene rhyolites. Most phenocrysts are extensively fractured and stained by limonite. In well developed spherulitic samples plagioclase forms the nuclei for the growth of spherulites. Plagioclase is completely replaced in hydrothermally altered samples.

Results from microprobe analysis shows that the composition range of plagioclase in the Pokohino (An_{19-29}) and Wharekawa (An_{32-45}) dome complexes are notably distinct (Fig. 4.2b).

Quartz

Quartz occurs commonly as anhedral phenocrysts up to 2.5mm in diameter, although, euhedral quartz crystals occur in sample W941365. Quartz abundance ranges from 1.75-4.5 modal %, which is similar to the abundances in the pyroxene rhyolites. Some phenocrysts show well developed fractures that are limonite stained. Resorption, shown by embayed textures, is common.

Biotite

Biotite occurs as subhedral elongated phenocrysts up to 2mm in length. Some euhedral forms are evident, but occur only as small phenocrysts. Biotite is commonly weathered/altered to illite and Fe oxides especially along cleavage planes. Biotite abundances are generally low (<1 modal %), but an anomalously high abundance was found in sample W941396 (2.2 modal %).

The biotite appears to have a similar chemistry in all rhyolite lavas (including the Glassy Dome Rhyolite), as shown by the Al - Mg - Fe+Mn ternary diagram (Fig. 4.3). The biotites from the Onemana area have distinctly low Al contents, which sets them apart from biotites within the Whiritoa/Whangamata rhyolites (Fulton 1988), and TVZ rhyolites (Ewart 1979). The plotted field for the biotites analysed overlap with the range of compositions obtained by Adams (1992) for Hot Water Beach (HWB) rhyolites.

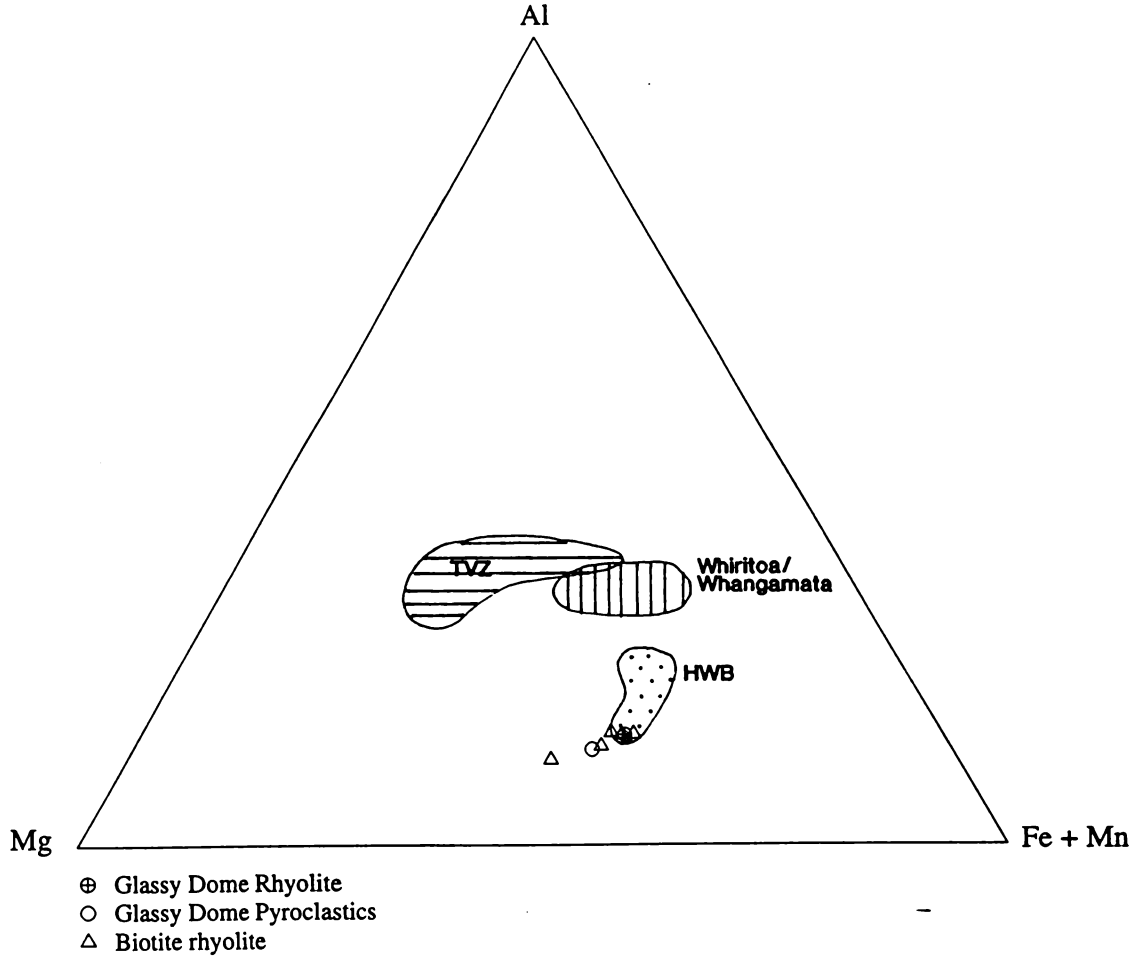

Figure 4.3. Al - Mg - Fe+Mn ternary diagram showing the distribution of biotite for selected rocks from Onemana, and their comparisons with biotites from TVZ (Ewart 1979), Whiritoa/Whangamata (Fulton 1988), and Hot Water Beach rhyolites (Adams 1992).

Studies by Abdel-Rahman (1994) demonstrates that biotite compositions depend largely upon the nature of magmas from which they crystallised. Biotites from rhyolites in the Onemana area plot closely to those analysed by Abdel-Rahman (1994) from rocks derived from alkaline magmas.

Fe-Ti oxides

Titanomagnetite and ilmenite (<0.2mm) occur only as trace amounts, though abundances of 0.75 modal % was found in sample W941396. Ilmenite is generally more abundant than titanomagnetite. Fe-Ti oxides are commonly euhedral with hexagonal shapes. Fe-Ti oxides have a close association with biotite.

Accessory mineral: zircon

A single zircon crystal was observed in sample W941348, associated with a biotite phenocryst. Zircon forms distinct euhedral prisms up to 0.2mm long.

4.3.2 Groundmass

The groundmass textures of the biotite rhyolites are dominated by spherulitic and flow banded textures, with rare granophyric and trachytic textures (sample W941265). Spherulites occur up to 6mm in diameter and typically show sheaf and circular textures with rare axiolitic and bowtie structures. Sample W941263 from the Eastern Flows shows well developed circular spherulitic textures up to 9mm in diameter (Fig. 4.1c). Perlitic fractures are commonly associated with samples that have well developed spherulitic textures.

Flow banding is evident in most samples, but is best developed in areas already identified as flows. Flows from the Pokohino Dome Complex show well developed thin planar flow banding (<0.5mm wide), elongated phenocrysts and vesicles. Flow pk6 is distinctly vesicular with samples W941298, 299 and 300 showing abundant elongated vesicles (20-40%). Samples from the Ridge Dome Flow show well developed flow structures, overturned folds, and wavy flow banding.

Crystallites are evident in most samples. They occur commonly as radiating structures, but are elongated in well developed flows. Most samples from

the Main Dome and some from the Pokohino Dome Complex have amygdaloidal textures with vesicles infilled by tridymite.

Autoclastic breccias (samples W941363 to W941365) are silicified, monolithologic, with subangular to angular clasts of spherulitic biotite rhyolite, matrix supported with 40% lithics, and poorly sorted.

The hyaloclastic breccias are clast dominated (>80%) with brown subrounded devitrified, spherulitic clasts surrounded by a fine grained matrix. Large (6mm) circular spherulites occur dispersed throughout the rock with secondary sheaf-like spherulites occurring on their outer margins. Well developed perlitic fractures with limonite staining is also evident.

4.3.3 Wharekawa Pyroclastics

The Wharekawa Pyroclastics are a group of pyroclastic breccias and flows with minor ash and lapilli fall deposits erupted from the Peak Dome in the Wharekawa Dome Complex. There is considerable variation in the physical characteristics of the Wharekawa Pyroclastics, but the mineral assemblage is consistent, plagioclase - quartz - biotite ± Fe-Ti oxides.

Unit 1 is weakly to partially welded, poorly sorted, crystal and lithic-rich, with a fine grained glassy matrix. Crystals consist of broken anhedral plagioclase (0.1-0.5mm), anhedral to subhedral quartz (0.1-0.8mm), biotite, (<0.4mm) and opaques (<0.2mm). Lithics in thin section are dominated by angular spherulitic rhyolite (50%) up to 1mm in diameter. More variability is shown in the larger lithics (0.1-2.5m). Four lithic types have been identified:

1) brown, well developed spherulitic rhyolite with phenocrysts of plagioclase, quartz, biotite, and Fe-Ti oxides

2) brown, devitrified rhyolite with resorbed plagioclase and quartz

3) slightly silicified spherulitic biotite rhyolite with euhedral quartz and elongated vesicles

4) hydrothermally altered porphyritic andesite with numerous plagioclase, relict pyroxenes (altered to illite), and Fe-Ti oxides

Small pumice (<0.5mm) with fiamme structures also occur in low abundances (<1%).

Unit 2 is partially welded, coarse grained, moderately sorted, crystal and lithic-rich, with a fine grained vitrophyric groundmass. Crystal abundances are similar to those described above for unit 1. Crystal abundance is approximately 5%. Lithics are dominated by subrounded spherulitic rhyolite (0.1-6.0mm), and minor subrounded to rounded devitrified rhyolite (0.1-0.4mm). Rare small, vesicular, subrounded pumice are also evident (<0.02mm).

Unit 3 is partially to densely welded, poorly sorted, coarse grained, matrix supported with a vitrophyric matrix. Lithic types are similar to those seen in unit 1 with subrounded spherulitic rhyolite (0.1-0.8mm) the dominant lithic type.

Unit 4 is partially welded, moderately sorted, coarse grained, dominated by subround pumice up to 10mm in diameter (40%), and has a vitrophyric matrix. Lithic abundances are lower than the underlying units (5-10%). Subrounded glassy biotite rhyolite with perlitic fractures is the dominant lithic type. Minor spherulitic and devitrified rhyolite lithics are also evident. Euhedral plagioclase, anhedral quartz, and subhedral biotite occur as crystals in the pumice. Contorted fiamme structures are evident in most pumice.

4.4 Glassy Dome Rhyolite and associated pyroclastics

Glassy Dome Pyroclastics

The Glassy Dome Pyroclastics are moderately to poorly sorted, matrix to clast supported, typically lithic-rich (45-65 modal %), and have abundant pumice (up to 18 modal %). The matrix is fine grained devitrified glass with a crystal content varying between 5 to 7 modal %. Crystals are dominated by anhedral to subhedral broken plagioclase and quartz up to 1.5mm, and minor biotite up to 0.4mm long. Some euhedral quartz is evident in sample W941285. Mineral chemistry of plagioclase and biotite in the Glassy Dome Pyroclastics is similar to those in the Glassy Dome Rhyolite and biotite rhyolites (Fig. 4.2c, 4.3).

The lithics are dominated by porphyritic glassy rhyolite with well developed perlitic fractures. Glassy rhyolite lithics are subangular to subrounded and up to 1.5mm in diameter. Subhedral to euhedral phenocrysts include

numerous plagioclase up to 1.8mm long, with rare apatite inclusions, quartz up to 2mm in diameter, biotite up to 0.8mm long and rare Fe-Ti oxides. Rare subrounded dacite (?) lithics up to 1.2mm diameter also occur which are porphyritic with relict phenocrysts of hornblende, biotite, and minor plagioclase in a fine grained pilotaxitic groundmass. Altered porphyritic andesite is rare and contains relict pseudomorphs after plagioclase and pyroxene phenocrysts, in a fine grained glassy groundmass with small opaques and feldspar laths.

Dark grey to brown fibrous pumice with euhedral phenocrysts of plagioclase (An_{21-27}), quartz and biotite occur up to 20mm in diameter. Most pumice show fiamme structures which are distorted around crystals. Biotite is commonly aligned along its longest axis parallel with the direction of flow. Rare zircon inclusions occur in biotite in sample W941391.

The green ignimbrite is densely welded, with lithics (up to 10mm), fibrous pumice (up to 8mm), and crystals (up to 0.4mm) in a devitrified glassy matrix. Lithic types are the same as those described above. The mineral assemblage includes minor amounts of chlorite (up to 0.5mm) (Fig. 6.1d). Some biotite has been replaced by chlorite.

Glassy Dome Rhyolite

The Glassy Dome Rhyolite has a similar mineral assemblage to the other biotite rhyolites; plagioclase - quartz - biotite ± sanidine ± Fe-Ti oxides ± apatite. All phenocryst types are well developed showing subhedral to euhedral shapes. Plagioclase (An_{22-37}) is the most abundant (6.5 modal %) and largest phenocryst (up to 4mm long). One sanidine phenocryst was identified by microprobe (Fig. 4.2c). Rare apatite inclusions occur within some plagioclase. Apatite crystals are rod-like and are up to 0.05mm long. Quartz phenocrysts (3.5 modal %) up to 2.5mm in diameter are intensely embayed with resorbed margins. Fresh unaltered biotite up to 1mm long occurs in low abundances (0.75 modal %) (Fig. 4.1e), and small (<0.2mm) cubic Fe-Ti oxides occur in trace amounts. Composition of biotites is similar to those in the biotite rhyolites.

A slightly devitrified glassy groundmass dominates the sample (90 modal %). Extensive well developed perlitic fractures occur and some small scale flow structures are evident in sample W941278 (Fig. 4.1e). Sample W941279 shows limited development of spherulitic textures.

4.5 Wharekawa Ignimbrite

The Wharekawa Ignimbrite is a massive, partially welded, lithic-rich (30-40%) ignimbrite. The lithics are subangular to subrounded, and include the following types:

1) light brown, vesicular, spherulitic biotite rhyolites up to 10mm in diameter

2) black, vesicular, flow banded obsidian up to 5mm, with perlitic fractures, and phenocrysts of plagioclase and biotite

3) grey hornblende - biotite dacite (?) up to 8mm diameter, with well formed plagioclase phenocrysts and glomerophenocrysts, relict hornblende and biotite, with rare quartz, in a fine grained glassy groundmass

4) dark grey pyroxene andesite up to 6mm, with fresh phenocrysts of plagioclase, augite, and hypersthene

5) brown, crystal-rich rhyolite, with large well developed plagioclase, hornblende, quartz and biotite, in a devitrified spherulitic groundmass with perlitic fractures

Numerous (10%) subrounded, vesicular, dark grey pumice are also evident up to 10mm in diameter.

The crystal-rich matrix is dominated by broken plagioclase up to 2mm long, and quartz up to 2.5mm in diameter, with minor biotite and hornblende up to 0.5mm long, and rare opaques. The crystals occur in a fine grained devitrified glassy groundmass.

4.6 Rangipo Andesite

The Rangipo Andesite is an intersertal glomeroporphyritic two-pyroxene andesite. The mineral assemblage for the andesite is plagioclase hypersthene - augite - Fe-Ti oxides.

Plagioclase (An_{75-83}) is the dominant phenocryst (12 modal %) and occurs up to 2mm long. It is commonly subhedral and occasionally resorbed. Plagioclase phenocrysts from the Rangipo Andesite are very calcic, and range in composition from An_{75} to An_{83} plotting within the bytownite field (Fig. 4.2d). One example of normal zoning was seen, with a decrease from the core (An_{83}) to the rim (An_{75}). These compositions tend to be

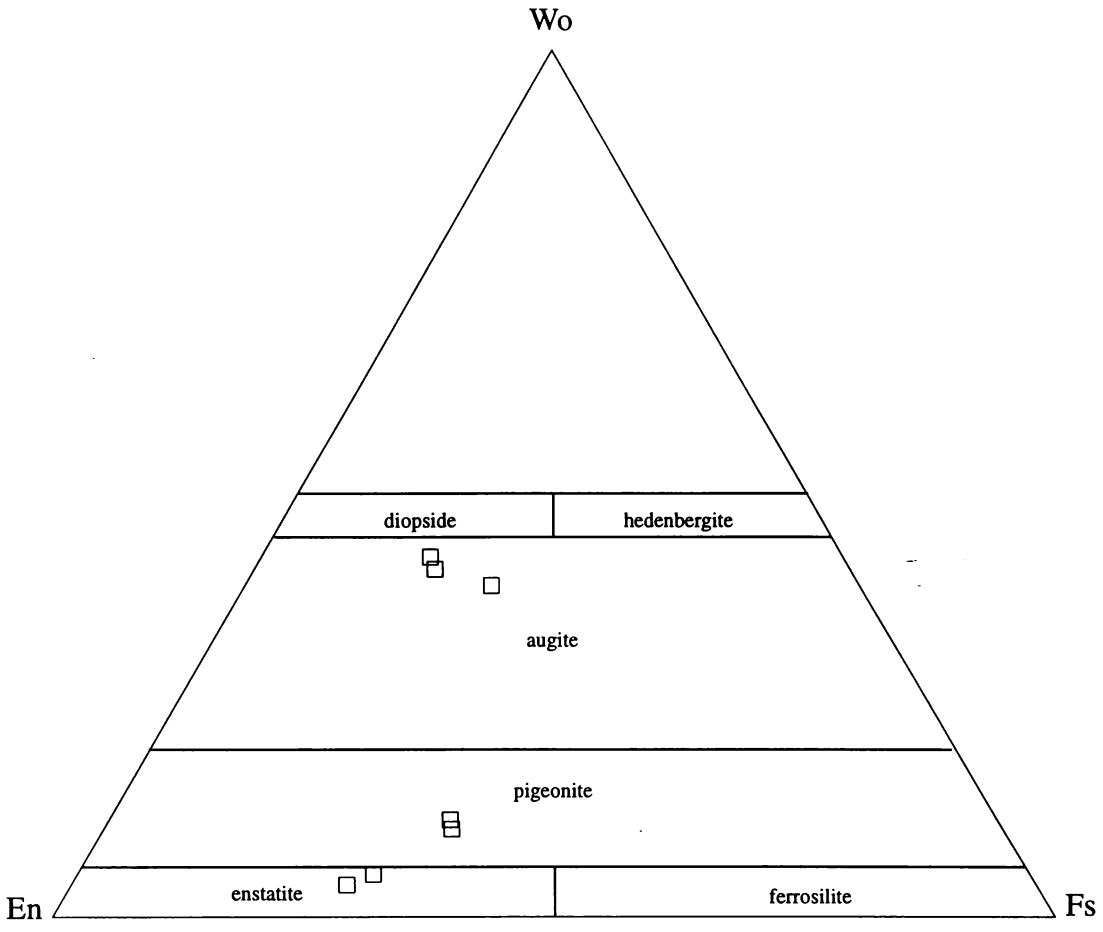

Figure 4.4. Wo - Fs - En ternary diagram for selected pyroxene from the Rangipo Andesite. Classification based on

higher than those obtained by Adams (1992) from the Tapuaetahi Andesite (An_{53-76}), but occur within the range determined by Fulton (1988) from a basaltic andesite (An_{63-85}), and Hunt (1988) from andesites in the Whiritoa Hill area (An_{44-91}).

Hypersthene (3 modal %) occurs as anhedral phenocrysts up to 1mm long. Augite has a lower abundance than hypersthene (1.25-2.0 modal %), and is generally anhedral and up to 1mm in length. Microprobe analysis of the pyroxenes showed orthopyroxene composition ranges between Wo_{4-11}, Fs_{27-35}, and En_{55-70}, which plots within the enstatite and pigeonite fields, while the clinopyroxenes have a limited range within the augite field between Wo_{38-42}, Fs_{16-24}, and En_{37-41} (Fig. 4.4). Granular Fe-Ti oxides up to 0.4mm in diameter are common (1 modal %), and is closely associated with augite.

Glomeroporphyritic clots occur which are up to 2.5mm in diameter and are composed of plagioclase, with lesser amounts of hypersthene and augite.

The groundmass is typically intersertal and textures vary between felted and pilotaxitic. The groundmass is composed of varying amounts of plagioclase laths, granular pyroxenes and opaques, set in glass (Fig. 4.1f).

The mineral assemblage of the Rangipo Andesite is comparable to the Taurahuehue Andesite and Taurauikau Andesite of the Coromandel group as defined by Skinner (1986; 1993), and Adams et al. (1994). Other two-pyroxene andesites are the Jubilee Andesite in the Lower Waitekauri Valley (Haworth 1993), the Tapuaetahi Andesite near Whenuakite (Adams 1992), and an unnamed andesite in the Whiritoa Hill area (Hunt 1991).

4.7 Lake sediments

The lake sediments are dominated by fine grained sand and silt derived from the erosion of nearby rhyolites. Much of the sediment has been weakly to intensely silicified. The sediments are generally moderately to well sorted. The sand-sized fraction is generally low (1-5%), with the sediments dominated by fine grained quartz and silts and muds. XRD analyses suggest the mud-sized fraction is dominated by hydrothermally derived kaolinite. The sand-sized fraction is made up of a variety of fragments:

1) anhedral, broken quartz up to 1mm in diameter

2) subrounded, dark brown, highly altered porphyritic rhyolite up to 1.5mm in diameter, some with altered plagioclase phenocrysts evident

3) rare, subrounded spherulitic rhyolite, up to 0.8mm

4) rare wood fragments up to 0.5mm long in sample 100

5) rare, small (<0.2mm long) anhedral plagioclase

6) rare, subhedral to euhedral, cubic opaques up to 0.3mm diameter

Petrographic analysis by Coote (1994) also identified relict biotite as part of the crystal framework and within rhyolite clasts. Other clast types identified from drill core chips by Coote (1994) include, flow banded vesicular rhyolite, and a porphyritic clast with textures characteristic of an intrusive rock.

Samples (W941306, 310, 356) appear to be vesicular, where vesicles have been infilled by hydrothermally derived quartz. Flow structures are evident in sample W941306, which is thought to be due to remobilisation of sediments by rising hydrothermal fluids. This occurred prior to the sediments being silicified. These structures coincide with high concentrations of fine disseminated pyrite.

4.8 Onemana Breccia

The Onemana Breccia has been weakly hydrothermally altered to intensely silicified. The breccia ranges from poorly sorted near source, to moderately sorted further from source. The deposit is typically massive, dominantly matrix supported, lithic-rich, with a variable crystal content. Lithic abundances around Breccia Knob range between 30 to 45 modal %, but decrease to 22 modal % at 1km from source (sample W941356). The deposit contains a variety of lithics that have been derived from the vent area:

1) light brown subrounded clasts of fine grained silicified sediments

2) subrounded to subangular rhyolite up to 5mm, includes remnant pyroxenes and plagioclase, groundmass replaced by quartz and adularia

3) subangular, silicified rhyolite up to 10mm

4) subangular, layered sinter up to 8mm

5) rare vein quartz

Lake sediment clasts are the most abundant clast types varying between 15 to 42 modal %. Rhyolite lithic abundance varies between 1 to 8 modal %. Broken anhedral quartz crystals are common thoughout the deposit with a maximum abundance of 11 modal % near Breccia Knob (sample W941302).

The matrix is fine grained and dominated by mud and silt sized fragments, fine grained quartz and rare pyrite. Hydrothermal alteration has altered the original deposit. Vughs have been infilled with anhedral interlocking secondary quartz and kaolinite clays. Around The Knob and in samples W941358, 359, and 360 pyrite is disseminated.

Chapter Five

Petrochemistry

5.1 Introduction

Thirty five new major and trace element analyses were determined for volcanic rocks in the Onemana area. Major and trace element analyses were determined by X-ray fluorescence (XRF) at the Analytical Facility, Victoria University, Wellington.

Unaltered and altered samples were analysed, with distinctive aims in mind. This chapter will discuss the petrochemistry of the unaltered samples, and determine if there is a genetic relationship between the rocks of the study area. Harker plots are used for major and trace elements, and comparisons will be made with other rhyolitic centres in the CVZ and TVZ. Table 5.1 shows normalised major and trace element data for nineteen unaltered samples from the Onemana area.

5.2 Classification

Classification of the volcanic rocks in the Onemana area are based on the classification scheme of K_2O wt% versus SiO_2 wt% (Peccerillo and Taylor 1976) (Fig. 5.1). Ewart (1982) adapted the Peccerillo and Taylor (1976) classification to include a distinction between high-K, medium-K and low-K rhyolites. The volcanic rocks in the Onemana area are dominated by rhyolites (75-78 wt% SiO_2), with most being classified as high-K rhyolites (3.07-4.89 wt% K_2O) based on Ewart's (1982) classification. The rhyolites show a close grouping in composition and have high total alkalies.

The pyroxene rhyolites are the only rocks that plot in the medium-K rhyolite field with K_2O values between 3.0 to 3.7 wt%. The range of K_2O is large for a given SiO_2 content. All the biotite rhyolites plot within the high-K rhyolite field with a K_2O content between 3.7 and 4.5 wt%. The Glassy Dome Rhyolites and pyroclastics show a larger abundance of K_2O content (4.0 - 4.9 wt%), but no significant difference in SiO_2 compared with the biotite rhyolites.

Table 5.1. Major (wt%) and trace element abundances (ppm) of selected volcanic rocks in the Onemana area

	Pyroxene Rhyolites				Biotite rhyolites						
W no.	941261	941267	941321	941322	941335	941348	941368	941264	941266	941284	941341
Location	663/456	663/432	662/449	662/447	650/463	648/469	666/474	659/492	663/432	660/482	665/494
SiO2	77.06	75.70	76.52	75.27	77.99	77.47	78.03	76.92	78.07	77 19	77.47
TiO2	0.15	0.25	0.25	0.23	0.08	0.08	0.09	0.17	0.09	0.07	0.08
Al2O3	13.17	13.62	14.51	13.07	14.71	12.91	14.22	13.60	14.05	13.60	14.26
Fe2O3†	0.33	0.45	0.50	0.51	0.22	0.24	0.12	0.29	0.28	0.24	0.22
FeO†	1.20	1.63	1.82	1.83	0.78	0.85	0.42	1.06	1.01	0.88	0.80
MnO	0.02	0.06	0.03	0.02	0.01	0.01	0.01	0.01	0.02	0.01	0.01
MgO	0.10	0.13	0.23	0.25	0.07	0.07	0.08	0.22	0.05	0.06	0.07
CaO	0.56	1.11	0.37	1.27	0.26	0.65	0.40	0.95	0.30	0.34	0.31
Na2O	3.71	3.94	2.45	4.34	1.86	3.47	2.31	3.00	2.20	3.07	2.60
K2O	3.67	3.07	3.28	3.15	4.01	4.25	4.29	3.75	3.92	4.52	4.17
P2O5	0.02	0.02	0.03	0.05	0.01	0.01	0.02	0.02	0.01	0.02	0.01
Fe2O3*	1.63	2.22	2.40	2.50	1.04	1.16	0.57	1.43	1.37	1.19	1.09
LOI*	1.96	1.56	4.96	1.71	3.57	1.54	3.36	2.38	2.72	1.97	2.60
Total*	99.97	99.51	100.23	100.13	99.98	100.16	100.02	99.67	100.14	99.86	100.17
Ba	733	719	606	744	571	730	607	757	556	704	627
Rb	118	103	110	110	153	144	163	138	149	168	156
Sr	34	74	36	94	23	43	29	76	19	21	19
Th	12	11	11	10	17	15	16	13	14	14	16
U	3	3	3	3	4	4	4	4	2	5	3
Pb	15	17	13	20	22	21	23	20	18	21	20
Zr	163	181	200	177	101	97	105	133	97	93	102
As	7	8	8	6	14	8	14	4	10	11	8
Nb	7	5	7	5	6	6	6	5	10	7	7
La	23	31	45	98	11	20	14	26	11	18	15
Ce	46	50	36	56	22	39	29	45	25	31	34
Y	32	39	58	167	21	26	21	20	19	22	26
Sc	6	7	6	7	5	5	4	4	7	6	7
V	5	9	8	8	2	2	2	12	2	3	2
Cr	1	1	2	2	2	1	1	2	1	1	1
Ni	3	2	5	9	3	2	2	3	3	1	3
Cu	4	4	5	5	3	3	1	3	2	1	3
Zn	35	50	46	75	22	27	17	36	40	21	37
Ga	15	16	18	15	16	14	17	15	19	16	17
Zr/Th	13.58	16.45	18.18	17.70	5.90	6.40	6.56	10.20	6.90	6.64	6.38

* Original values † Recalculated assuming $Fe_2O_3/(Fe_2O_3 + FeO)=0.2$

Table 5.1. Continued

	Glassy Dome Pyroclastics		Glassy Dome Rhyolite			Rangipo Andesite		
W no.	941338	941391	941278	941279	941337	941284	941346	941347
Location	659/476	648/473	659/477	659/479	660/475	643/466	643/465	645/464
SiO2	78.80	77.91	77.87	77.64	77.78	56.35	57.34	57.02
TiO2	0.08	0.08	0.08	0.09	0.08	1.17	1.22	1.18
Al2O3	12.89	13.32	12.75	13.06	12.85	17.56	17.57	17.89
Fe2O3†	0.26	0.24	0.28	0.25	0.22	1.87	1.77	1.61
FeO†	0.94	0.86	1.02	0.91	0.79	6.72	6.36	5.78
MnO	0.01	0.02	0.03	0.02	0.02	0.14	0.15	0.17
MgO	0.59	0.16	0.14	0.32	0.13	3.69	3.16	3.59
CaO	1.47	0.84	0.91	1.13	1.11	7.63	7.20	7.80
Na2O	0.87	1.66	2.31	2.18	2.20	3.30	3.44	3.37
K2O	4.08	4.89	4.61	4.40	4.82	1.40	1.61	1.41
P2O5	0.01	0.01	0.01	0.01	0.01	0.17	0.19	0.18
Fe2O3*	1.17	1.11	1.31	1.15	1.01	9.14	8.70	7.90
LOI*	10.38	7.34	7.29	1.29	7.99	0.95	0.88	1.14
Total*	100.17	100.16	100.09	100.17	100.22	99.58	100.11	100.19
Ba	678	838	738	761	415	302	342	397
Rb	127	198	217	183	225	41	53	39
Sr	384	87	127	108	38	298	295	307
Th	14	13	12	13	13	5	5	4
U	2	3	2	4	3	2	1	1
Pb	5	18	17	14	18	8	9	8
Zr	83	87	88	90	87	146	155	149
As	1	6	7	6	7	2	2	2
Nb	4	3	4	4	5	3	3	5
La	31	20	22	30	25	31	14	13
Ce	52	39	44	50	47	35	37	37
Y	17	21	22	28	24	71	31	28
Sc	5	4	3	4	5	28	29	32
V	3	2	2	2	3	252	247	259
Cr	1	0	1	2	1	30	11	31
Ni	2	3	2	3	4	7	4	6
Cu	3	1	3	3	2	18	14	18
Zn	51	34	36	35	33	86	84	86
Ga	13	13	14	15	14	20	19	21
Zr/Th	5.93	6.69	7.33	6.92	6.69	29.20	31.00	37.25

* Original values † Recalculated assuming $Fe_2O_3/(Fe_2O_3 + FeO)=0.2$

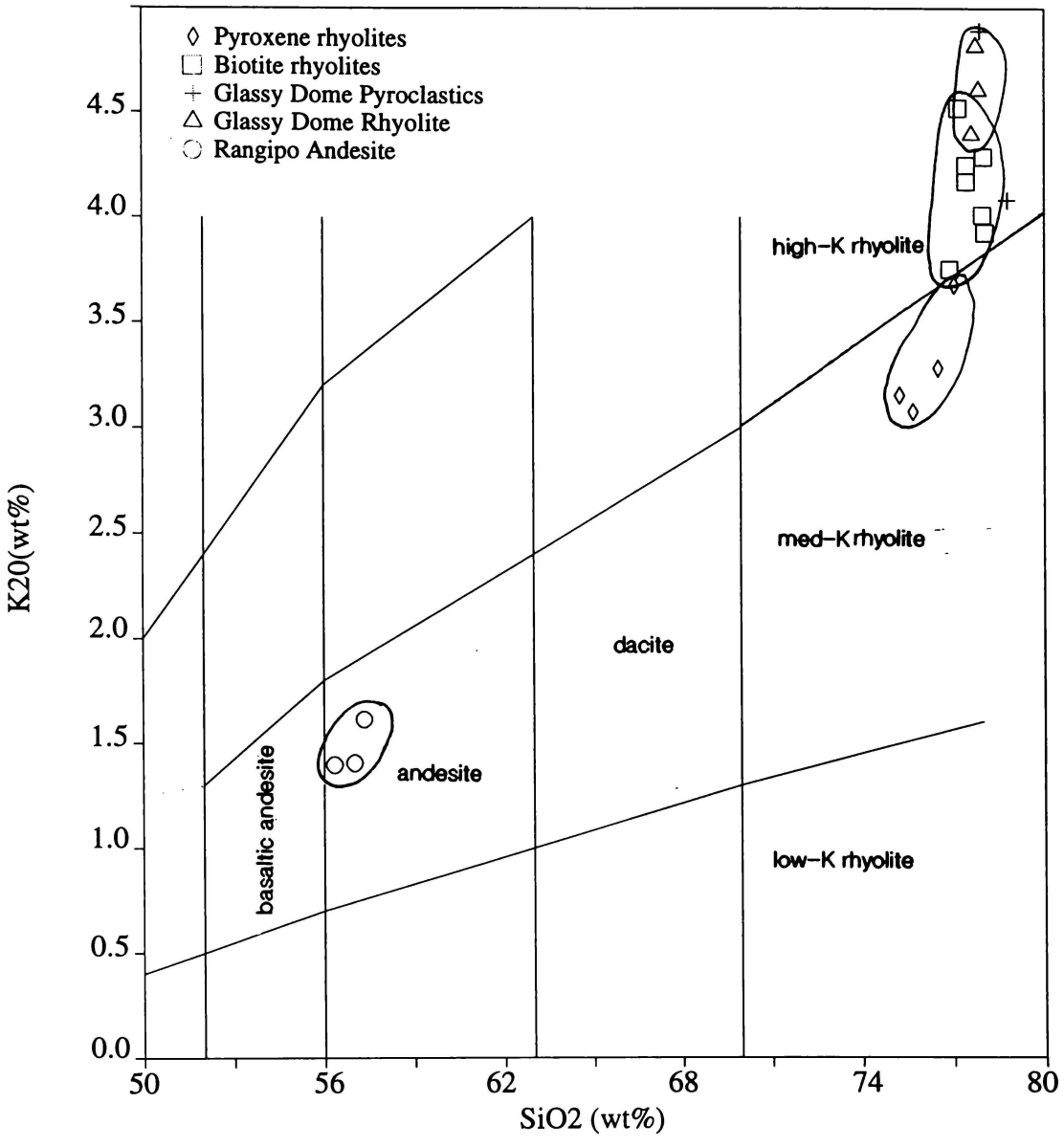

Figure 5.1. K_2O versus SiO_2 for selected volcanic rocks from the Onemana area. Classification scheme after Peccerillo and Taylor (1976) and Ewart (1982).

The Rangipo Andesite plots within the andesite field close to the basaltic andesite boundary. The K_2O content is fairly constant at 1.5 wt% with a SiO_2 range of 56 to 58 wt%. This range is comparable to andesites from the Waiwawa Subgroup and Kuaotunu Subgroup of the Coromandel Group (Skinner 1993; Adams et al. 1994) and the Jubilee Andesite (Haworth 1993).

The AFM diagram (Fig. 5.2) differentiates between tholeiitic and calc-alkaline volcanic rocks on the basis of Fe enrichment in tholeiitic suites during magma differentiation. All eruptives from the Onemana area plot below the calc-alkaline boundary. The Rangipo Andesite plots as the most mafic sample, with a large compositional gap between the andesites and the rhyolites.

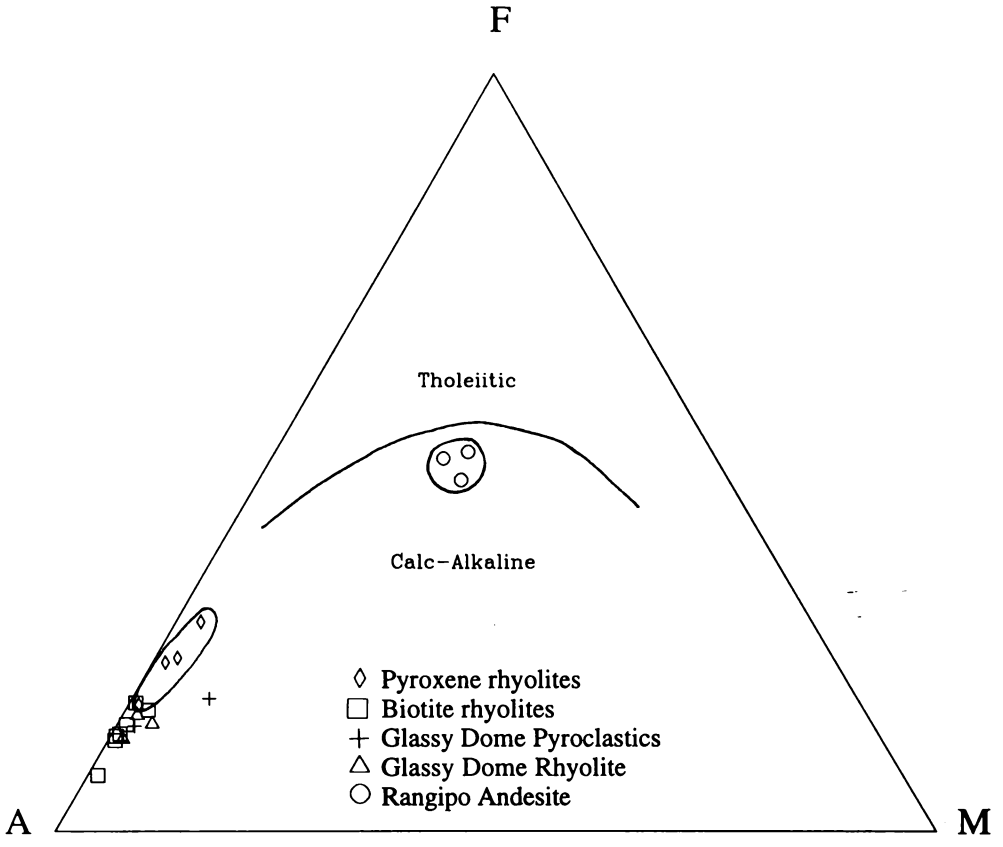

Figure 5.2. AFM diagram of the volcanic rocks from the Onemana area. A=Na_2O+K_2O, F=Fe_2O_3+FeO, M=MgO. The calc-alkaline - tholeiitic boundary is after Wilson (1989).

Using Le Maitre's (1982) classification of sodic and potassic volcanic rocks (Fig. 5.3), it is evident that the biotite rhyolites and Glassy Dome Rhyolites plot within the potassic field, with the andesites plotting well within the sodic field. The pyroxene rhyolites are dominantly sodic, but overlay both fields.

5.3 Major and trace element trends

5.3.1 Major element trends

Major element trends are best displayed in variation diagrams (Harker diagrams), where the weight percent of an oxide is plotted against the weight percent of SiO_2. Coherent trends on Harker diagrams are generally considered to represent the course of chemical evolution (Wilson 1989).

Harker diagrams for TiO_2, FeO, MgO, CaO, Na_2O and K_2O versus SiO_2 are shown in Figure 5.4a-f. Only K_2O shows an increase with increasing SiO_2, while the other oxides show decreases. Trends evident within the rhyolites do not appear to be related to the andesites, which is best shown in the Na_2O plot

(Fig. 5.4e). MgO and CaO do not show any significant trends within the rhyolites. There appears to be a near vertical linear trend between the pyroxene rhyolites and the biotite rhyolites in the TiO_2, FeO, Na_2O, and K_2O plots, due to the wide range of oxides over a small SiO_2 contents. The Glassy Dome Rhyolites show a wider range in major element content and plot within the biotite rhyolite range for TiO_2, FeO, and Na_2O abundances.

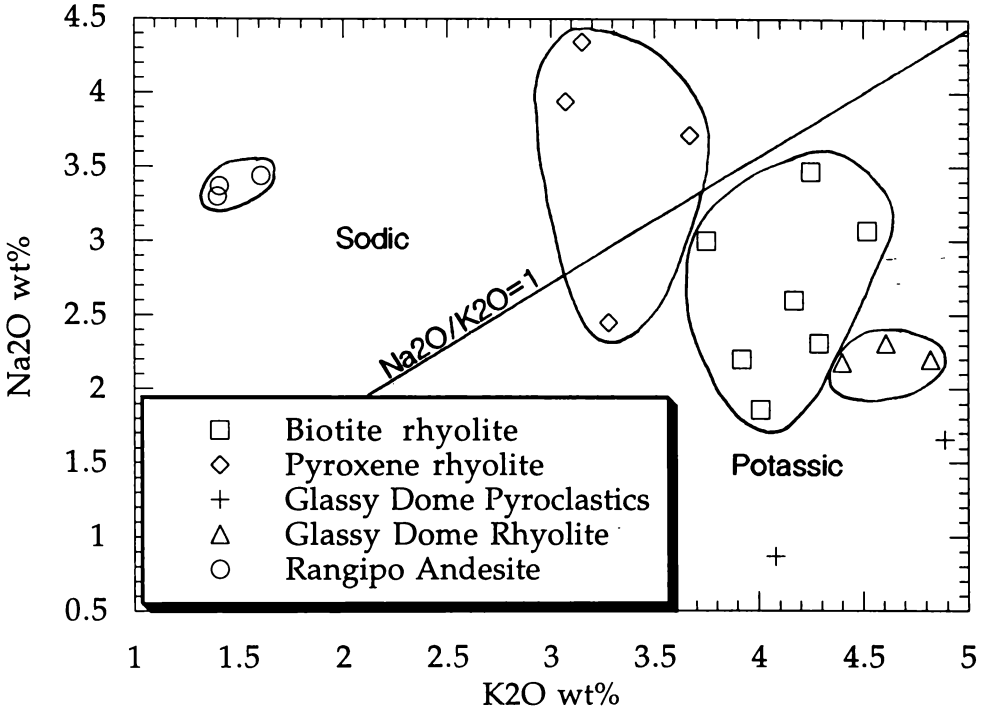

Figure 5.3. Na_2O versus K_2O for selected volcanic rocks from Onemana. The $Na_2O/K_2O=1$ boundary divides sodic and potassic rhyolites (after Le Maitre 1982).

5.3.2 Trace elements

Trace element versus SiO_2 plots

Harker diagrams can be plotted for trace elements (Fig. 5.5a-j) and be interpreted in a similar way. The plots were generally similar to those of the major elements with the rhyolites having distinct compositions from the Rangipo Andesite as would be expected. Only Th and Rb show increasing trends with increasing SiO_2 contents while the other trace elements (Zr, La, Ce, Zn, Y, Cu) show decreases. Generally the Glassy Dome Rhyolite plots within the biotite rhyolite field except in the Rb vs. SiO_2 plot (Fig. 5.5c).

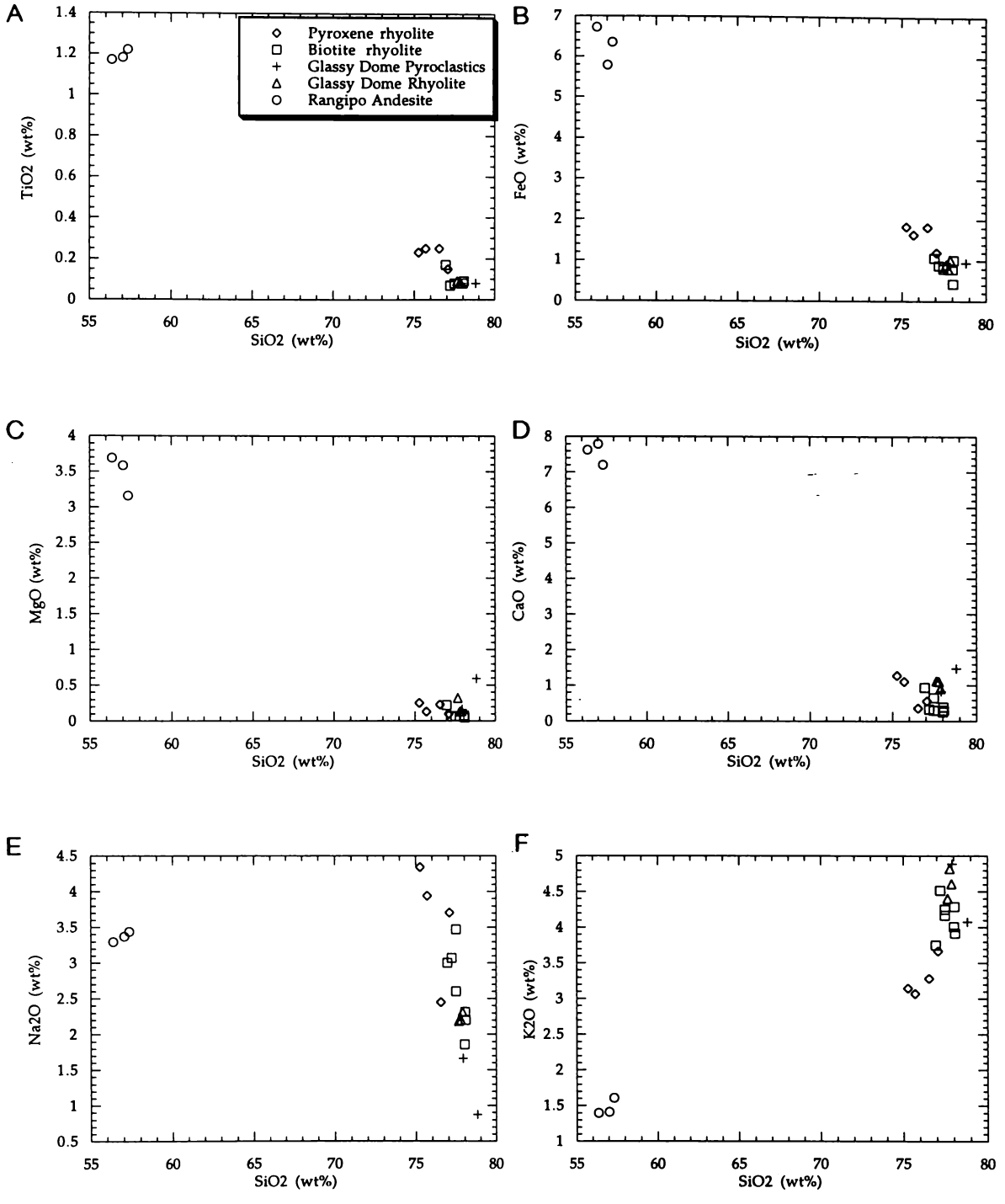

Figure 5.4. Harker diagrams for selected volcanic rocks from Onemana, showing weight percent of major element oxides plotted against SiO_2 (wt%). Weight percent has been normalised to 100% volatile-free.

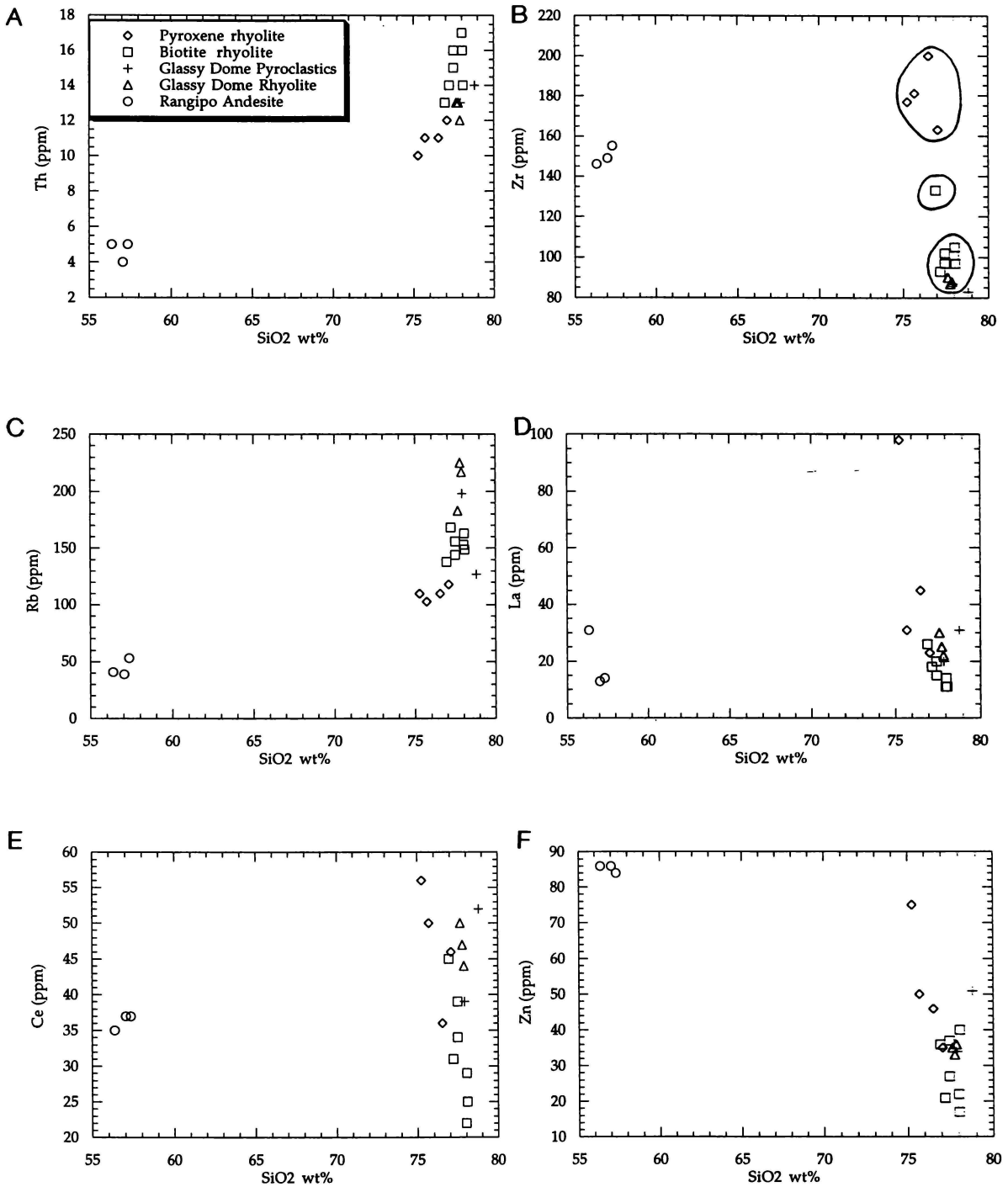

Figure 5.5. Harker diagrams for selected volcanic rocks from Onemana, showing trace elements plotted against SiO_2 (wt%).

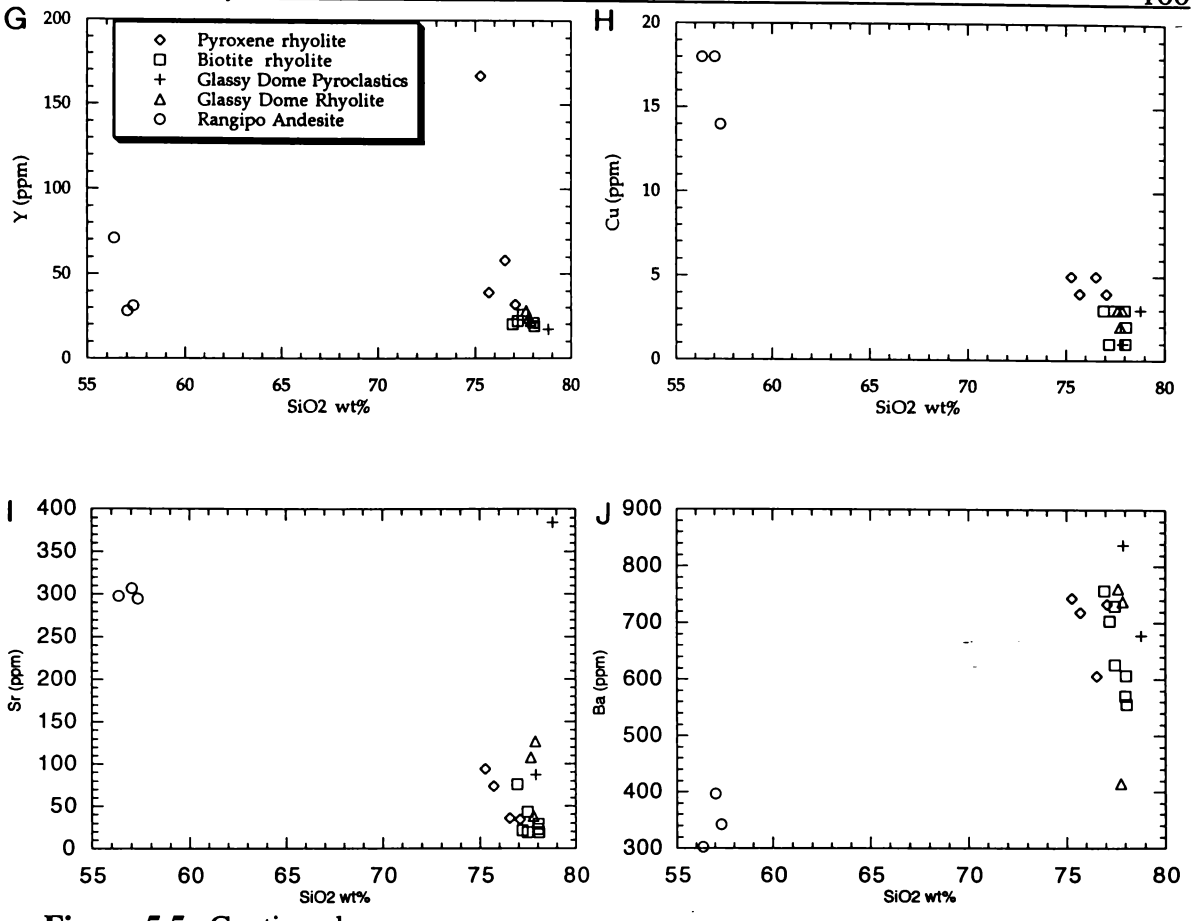

Figure 5.5. Continued.

The Zr vs. SiO2 plot shows that the Zr abundances are distinctive for the pyroxene and biotite rhyolites, with the pyroxene rhyolites having high Zr (163-200 ppm)and the biotite rhyolites having low Zr (33-105 ppm), except for sample W941264 which has a discete intermediate value (133 ppm).

Anomalous REE and Y contentsare evident in some pyroxene rhyolites (W941321, W941322) and Rangipo Andesite (W941284) samples. Anomalous REE and Y values were found in fresh Kiwitahi Volcanics by Dunbar (1991) and rhyolites in the Hikuai area (McGunnigle 1995). These abundances were thought to be caused by fine scale alteration not detectable by petrographic techniques (Dunbar 1991).

Element versus element plots

Incompatible element versus incompatible element plots should show linear relationships if they are genetically related, i.e. genetically related rocks should have similar incompatible element ratios. Examples for these types of plots are shown in Figure 5.6a-d. Incompatible elements are termed by Wilson (1989) as elements which are incompatible with respect to normal mantle minerals and

are termed large-ion lithophile (LIL), e.g. K, Rb, Sr, Ba, Zr, Th, and light REE. Few of these elements can be termed truly incompatible in the rhyolitic rocks of the Onemana area, due to incompatible elements being compatible with some mineral phases present, e.g. Sr in plagioclase and K, Rb, and Ba in biotite, and Zr in zircon.

Incompatible elements Sr and Ba (Figs. 5.5i,j)are commonly used for such element versus element plots, but for these rocks they show a wide scatter and possibly controlled by the fractionation of plagioclase and sanidine. Sr behaves as an incompatible element until plagioclase becomes a crystallising phase (Mason and Moore 1982), and similarly for Ba and Rb in biotite. The abundance of Zr may be controlled by the crystallisation of zircon, which occurs in minor abundances within the pyroxene rhyolites. Th is thought to be the most incompatible element for the volcanic rocks in the Onemana area.

The La versus Ce plot (Fig. 5.6a) shows a distinctive positive linear trend between the biotite rhyolites and the Glassy Dome Rhyolite. The Rangipo Andesite and pyroxene rhyolites, however, are not always consistent with this trend. Variations in Ce may result from Ce substituting Sr in intermediate to acidic liquids (Cox et al. 1979). Ce may also vary due to increasing weathering. The plot suggests that the biotite rhyolites and Glassy Dome Rhyolites were sourced from magmas with similar La/Ce ratios (~0.5), but this trend is thought to be typical for most volcanic rocks. Outlying points are caused by anomalous La abundances

The Rb vs. Th diagram (Fig. 5.6b) shows similar Rb/Th ratios for the Rangipo Andesite, pyroxene rhyolites and biotite rhyolites, but distinct ratios for the Glassy Dome Rhyolites.

The Zr vs. Th plot (Fig. 5.6c) shows a high degree of scatter, but each rock type can be enclosed in distinct fields, suggesting each rock type was sourced from areas with different Zr/Th ratios. The biotite rhyolite sample W941264 plots distinctly away from the other biotite rhyolites. This is also evident in the Zr vs. Ce plot (Fig. 5.6d). This suggests the Ridge Dome lava flow has a different magma source from the other biotite rhyolites.

The Zr vs. Ce plot (Fig. 5.6d) shows that each rock type can be enclosed in distinct fields, although there is a higher degree of scatter within each field compared with the Zr vs. Th plot due to anomalous Ce values (see above).

On the basis of Zr abundances, the rhyolites can be divided into two types:

Type 1a Biotite rhyolites: contain biotite phenocrysts and have high K, Rb, and Th contents and low Zr (83-105 ppm). The Glassy Dome Rhyolite falls into this group.

Type 1b Biotite rhyolite (sample W941264): contains biotite phenocrysts, but has anomalously high Ba, Rb, Zn, REE, and Zr (133 ppm).

Type 2 Pyroxene rhyolites: contains pyroxene phenocrysts and have relatively low K, Rb, and Th contents, and high Zr (163-200 ppm).

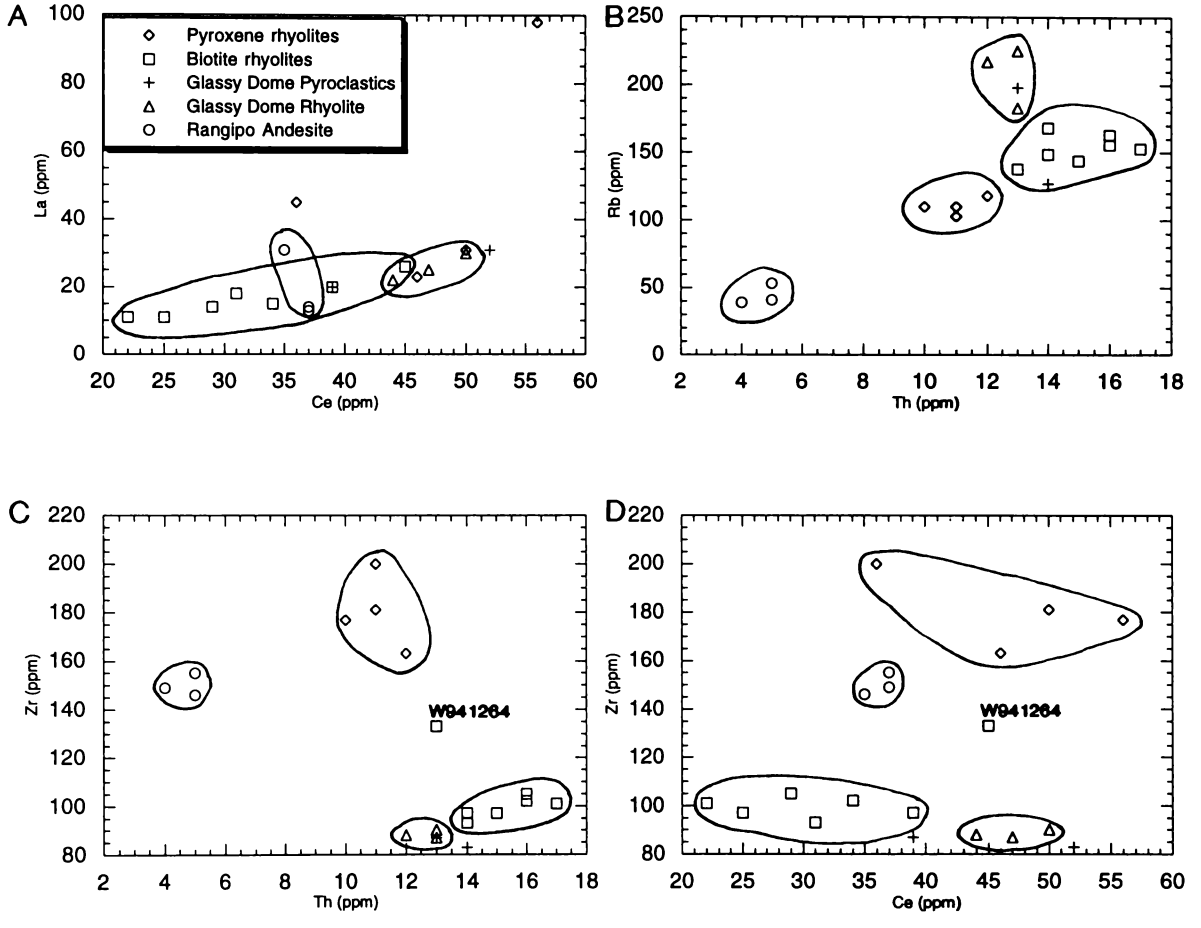

Figure 5.6. Incompatible element-element plots for selected rocks from Onemana.

Ratio versus element plots

Allegre and Minister (1978) describe a method based on magmatophile elements (M elements) and hypermagmatophile elements (H elements) to distinguish between fractional crystallisation and equilibrium partial melting, where the ratio of M/H was compared to M. Typical H elements are Ta, Th, Rb, La, and Ce, and M elements comprise the heavy REE, Sr and Hf. Figure 5.7 shows Rb/Zr vs. Rb. Based on Allegre and Minister's (1978) model, a horizontal relationship suggests fractional crystallisation, while a sloping trend

may indicate partial melting. Each rock type plots discretely away from each other and appear to show a sloping trends within each of the fields. This suggests that each rock type has developed by partial melting of separate magma bodies.

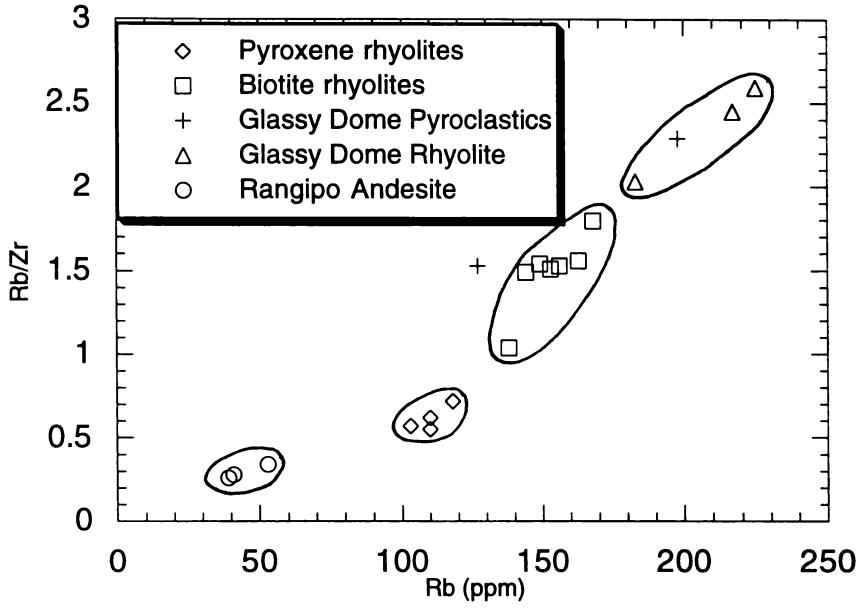

Figure 5.7. Rb/Zr versus Rb plot for selected volcanic rocks from Onemana.

If trace element ratios are not consistent throughout the rocks in the region then it is unlikely that the rocks are related. The plots of incompatible elements vs. incompatible elements and Rb/Zr vs. Rb plots suggest the rhyolites were formed by partial melting of different source regions of the continental crust producing rocks with discrete incompatible element ratios and Zr abundances.

5.4 Primitive mantle normalised spidergrams

A selection of spidergrams for volcanic rocks from the Onemana area are shown in Figure 5.8. Trace element data are normalised against primitive mantle values, e.g. those of Taylor and McLennan (1985). Most elements plotted are incompatible, though Sr is probably affected by the crystallisation of plagioclase, Ba and Rb by biotite, and Ti by titanomagnetite and ilmenite. Plots of average trace element abundances from each rock type at Onemana (note, anomalous values were omitted) are compared to other average plots from eastern Coromandel.

Trace element trends for the rhyolites (Fig. 5.8a,b,c) show that they are enriched in LIL elements and Y, and depleted in Nb, Sr, P, and Ti. Pyroxene rhyolites show little variation in the LIL elements, but show larger variations in La and Y, and some minor variations in Sr and P. Plots for the biotite rhyolite (Fig. 5.8b) and Glassy Dome Rhyolite (Fig. 5.8c) show similar trends, though the Glassy Dome Rhyolite has higher La, Ce, and Sr abundances. Both of these rhyolites appear to be slightly more enriched than the pyroxene rhyolites in LIL elements Ba, Rb, Th, K, and U, and depleted in La, Ce, P, Sr, Ti, and Y.

Comparisons with other eastern Coromandel rhyolites show that the trends for all the rhyolites are similar. The pyroxene rhyolite is slightly more enriched in P, Sr, Ti, and Y. The biotite rhyolites plot closely to the Staircase Rhyolite, which is 5km NW of Onemana (Trotter 1995). The Glassy Dome Rhyolite shows slightly depleted values in Nb, P and Ti.

The Rangipo Andesite shows enriched LIL elements and depleted Nb, P and Sr. The general trend shown by the trace elements in the Rangipo Andesite is similar to that shown by the rhyolites, except troughs at P and Ti are not as significant as in the rhyolites. Generally, abundances of Ba, Rb, Th, U and K are depleted and Sr, P and Ti are enriched in comparison to the rhyolites.

Comparison of the Rangipo Andesite with other eastern Coromandel andesites show that they all have a similar trace element trend, e.g. the McBeths Andesite (McGunnigle 1995) 6km to the NW.

5.5 Discussion

The calc-alkaline volcanic rocks of Onemana are dominated by high-K to medium-K rhyolites (75-78 wt% SiO_2) with minor andesite (56-58 wt% SiO_2). There is a large compositional gap between the andesite and rhyolites. The occurrence of high-K rhyolites, which are common in rifting environments north of the Whitipirorua Fault is consistent with structural data suggesting the northern Onemana Peninsula is dominated by rifting. The rhyolites that occur outside the rift (pyroxene rhyolites) are medium-K rhyolites.

Major and trace element variation diagrams do not show linear trends between the andesite and rhyolites, suggesting there is little evidence for relating the two groups of rocks. Trends evident between the two groups in trace element plots may be related to regional geochemical affinities. Linear trends are

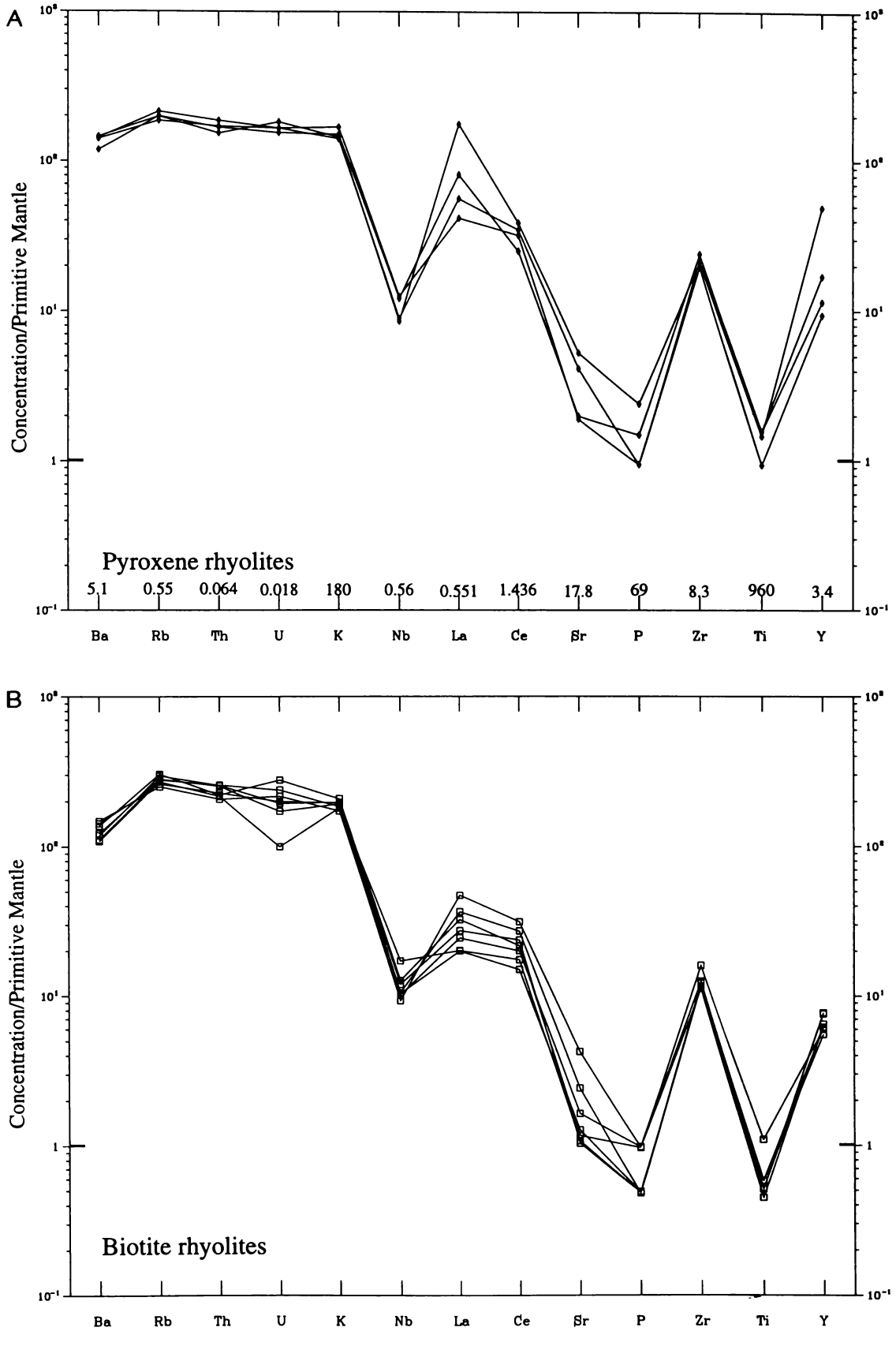

Figure 5.8. Primitive mantle normalised spidergrams (after Taylor and McLennan 1985) for representative volcanic rocks from the Onemana area (A-D). E) comparisons with other eastern Coromandel rhyolites from Fulton (1988), Adams (1992), Rogers (1994), and Trotter (1995). F) comparisons with other Coromandel Group andesites from Adams (1992), Haworth (1993), McGunnigle (1995).

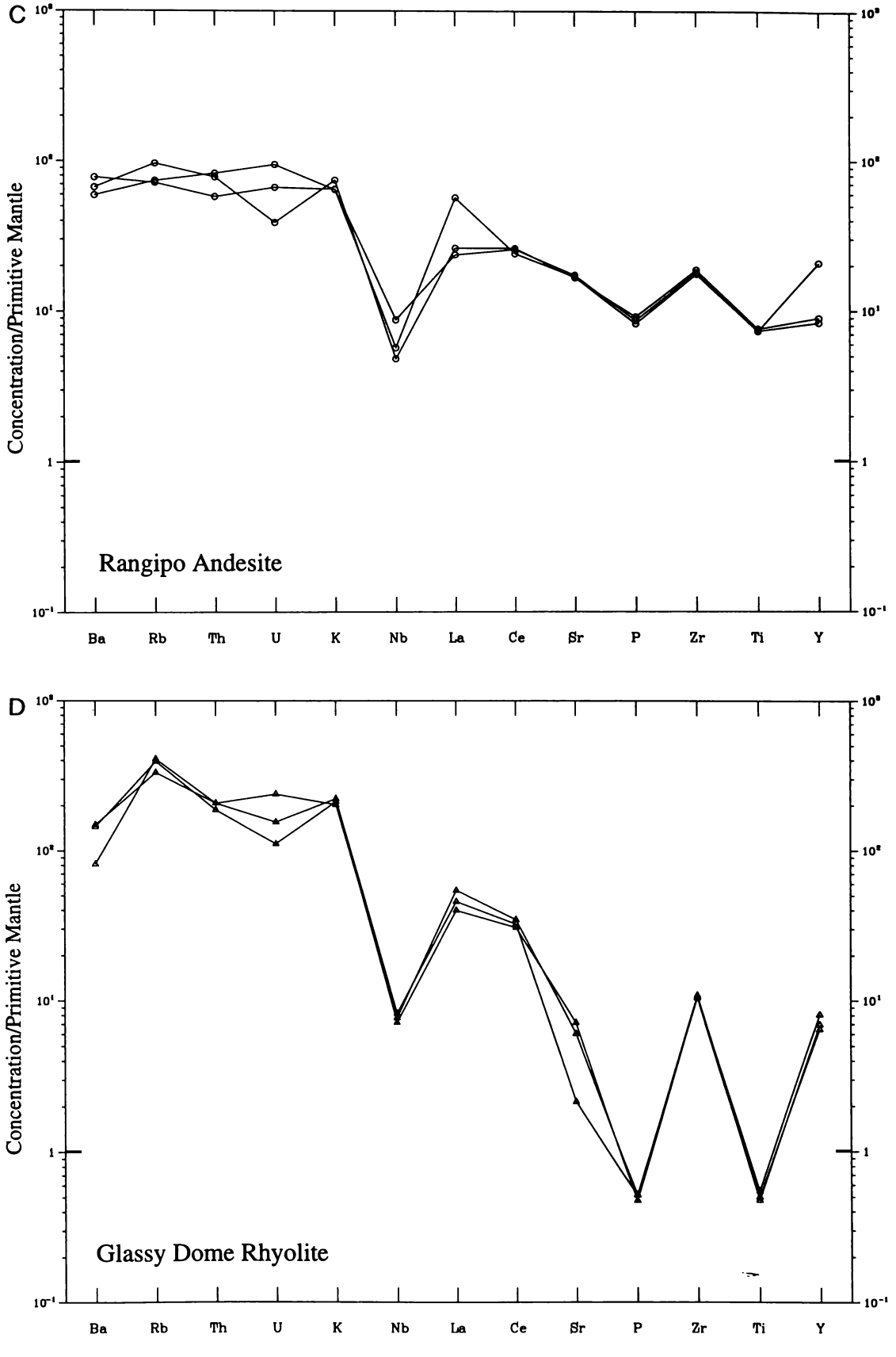

Figure 5.8. Continued.

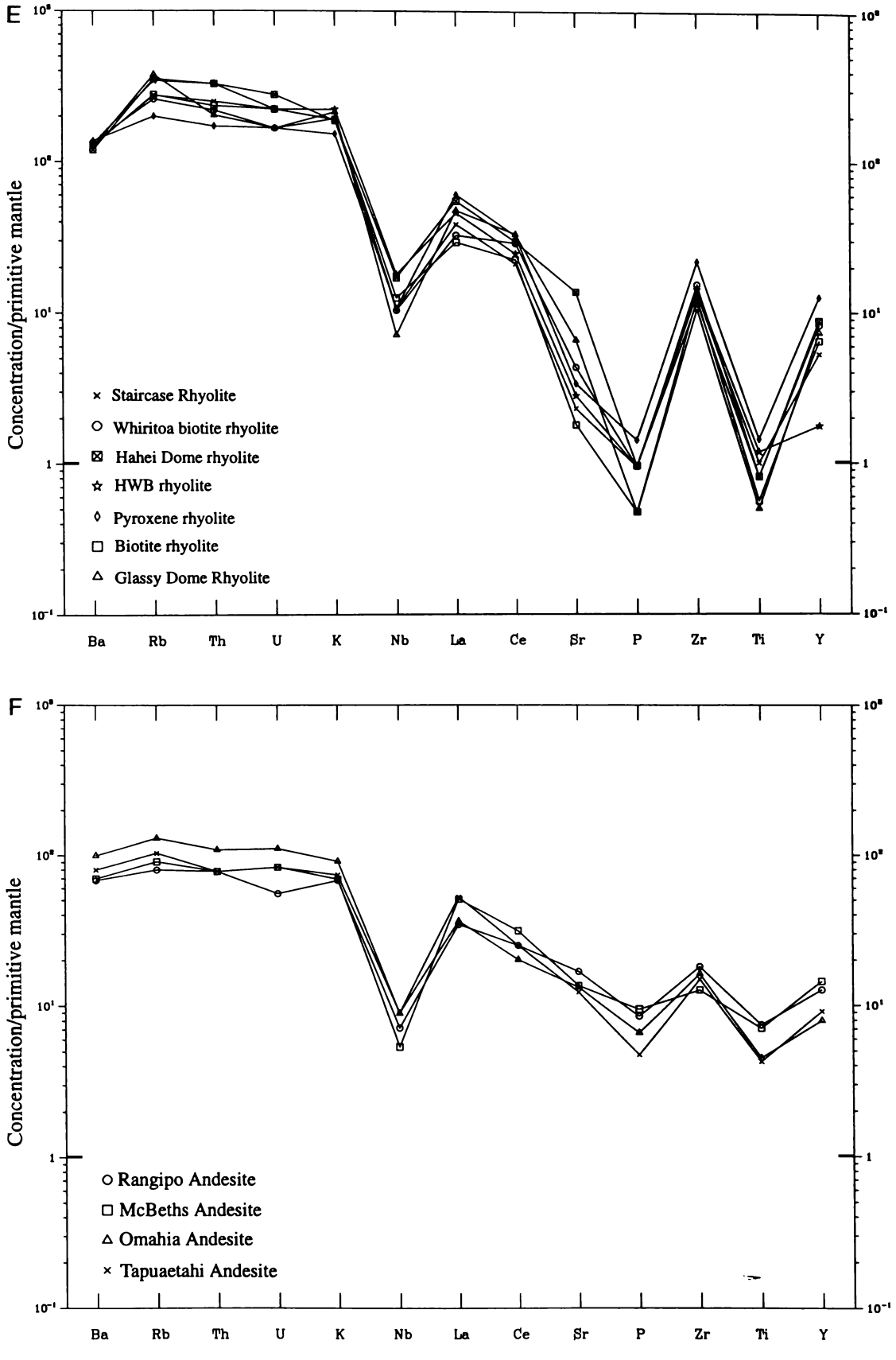

Figure 5.8. Continued.

evident within the rhyolites, which generally show trends from the pyroxene rhyolites through the biotite rhyolites to the Glassy Dome Rhyolites. These apparent trends are thought to have resulted from the limited SiO_2 range.

In rhyolitic rocks of this type it is difficult to select a truly incompatible trace element, but the most likely incompatible elements are Zr and Th, as these elements are thought to be least likely affected by crystallising minerals from the magma and weathering. Plots of Zr vs. Th (Fig. 5.6d) show that the pyroxene rhyolites have distinct Zr/Th ratios from the biotite rhyolites (and Rangipo Andesite), which indicates that these lavas have evolved independently, and have been derived from magma source regions within the continental crust with differing Zr/Th ratios. The pyroxene and biotite rhyolites appear to have been derived from different areas within the crust due to each rock type having distinct Zr contents. The eruption of the Ridge Dome lava (sample W941264) is thought to be associated with a different source magma to the other biotite rhyolites.

Primitive mantle normalised spidergrams show the rhyolites to be enriched in LIL elements and Y, and depleted in Nb, Sr, P, and Ti. This trend appears consistent with other eastern Coromandel rhyolites. The close proximity and similar geochemical signatures suggest the Staircase Rhyolite (Trotter 1995) is closely related to the biotite rhyolites in the Onemana area. An important point to note is that the Staircase Rhyolite is closely associated with a NE-trending structure, similar to the Pokohino Dome Complex.

Comparisons of the Rangipo Andesite with other eastern Coromandel andesites show that they all have similar signatures, though it appears the Rangipo Andesite is most closely related to the McBeths Andesite. The McBeths Andesite has been stratigraphically identified by McGunnigle (1995) as younger than the Minden Rhyolites in the Hikuai area.

Trace element abundances displayed by the spidergrams can be indicative of the type of environment the magma developed in. Comparisons with a range of tectonic settings determined by Thompson et al. (1984) shows that the rhyolites and andesites have trends similar to that of a volcanic arc setting. With the most persistent characteristic being the trough at Nb, which Wilson (1989) explains as the retention of Nb at the source during partial melting. These subduction related trends are not thought to be consistent with rhyolite volcanism on the eastern Coromandel Peninsula. Rogers (1994) attributed this trend to rhyolites in the Hahei area due to contamination by subductively

derived andesite. It is evident that andesite lavas occur below the rhyolites in the Pauanui area, 10km north of the study area to a depth greater than 1100m (Trotter 1995).

Comparisons of eastern Coromandel rhyolites with TVZ rhyolites (Fulton 1988; Adams 1992; Rogers 1994) show that trace element trends are similar, suggesting a similar mode of origin. The origin of the TVZ rhyolites has been discussed by several authors (Cole 1979; Reid 1983; Graham et al. 1992; Smith and Gamble 1993), with theories favouring the partial melting of the subvolcanic granulites and Mesozoic metasediments, though the melting of Mesozoic metasediments is disputed by Smith and Gamble (1993). Graham et al. (1992) also notes the partial melting process is most likely to occur in an extensional stress regime, e.g. TVZ. Two models of rhyolite petrogenesis is suggested for the TVZ rhyolites by Smith and Gamble (1993): partial melting of the continental crust, or fractional crystallisation of a basaltic magma. The former is suggested for the Onemana area rhyolites as there is little evidence for basalt or fractional derivatives. The continental crust under the Onemana are a is thought to include Jurassic sediments and andesite from previous arc volcanism. The inconsistencies in the continental crust means magma formed in different areas of the crust will have different trace element abundances.

In summary it appears that there is little evidence for a relationship between the Rangipo Andesite and rhyolites. The rhyolites can be divided into two groups high Zr (pyroxene rhyolites) and low Zr (biotite rhyolites, Glassy Dome Rhyolite). The biotite rhyolite sample W941264 is classed as a medium Zr rhyolite. The rhyolites are thought to be closely associated with partial melting of the continental crust in a rifting environment (Chapters Two and Three). Geochemical evidence suggests the Glassy Dome Rhyolite is closely associated with the biotite rhyolite and only varies from the biotite rhyolites in Rb plots. The paleotectonic setting for the eruption of the Onemana volcanic rocks is thought to be in a extensional setting within an older volcanic arc.

Chapter Six
Hydrothermal Alteration

6.1 Introduction

Hydrothermal alteration is a general term embracing the mineralogical, textural and chemical responses of rocks to a changing thermal and chemical environment in the presence of hot water, steam or gas (Henley and Ellis 1983). The primary mineralogy of the host rock is altered to a variety of alteration minerals, which form in response to changes in pressure, temperature and fluid composition.

Pervasive weak to intense alteration occurs within a NE-trending corridor bounded by the Whitipirorua and Pokohino Faults. Intense alteration is evident within the biotite rhyolite lavas of the Pokohino Dome Complex between Onemana and Pokohino Beach. Weak to intense alteration is evident throughout the lake sediments and Onemana Breccia. The biotite rhyolites are also intensely altered around The Knob. The porous nature of the rhyolites and lake sediments increases the water/rock ratio causing widespread alteration. Alteration between Onemana and Pokohino Beach is strongly controlled by N-striking faulting within the EFZ. Alteration within the lake sediments appears to be closely associated with NW-striking structures identified from resistivity anomalies.

The NE-trending alteration corridor shows up clearly as a broad weakly magnetic zone (Figs. 2.28, 3.2) between the reversely magnetic rhyolitic rocks of the Pokohino and Pohakahaka dome complexes. The alteration zone is clearly defined to the SE along the Whitipirorua Fault, but is less defined along its NW boundary (Pokohino Fault). Hydrothermal alteration results in the conversion of primary magnetite to pyrite and pyrrhotite (Henley and Hedenquist 1986), resulting in an altered area being defined by a broad magnetic low.

This chapter will investigate the nature of the surface alteration mineralogy and geochemical changes of the host rock as a result of increasing alteration. Changes in primary minerals through alteration, and identification of alteration types was done using thin section petrography and X-ray diffraction (XRD).

Selected samples were analysed using XRF to determine chemical changes within the host rock with increasing alteration (Table 6.1). Microprobe analyses were also done to identify unknown alteration minerals.

6.2 Alteration mineralogy

Primary minerals are altered to different secondary minerals depending on their susceptibility to alteration and type of conditions the mineral is being exposed to. Thus alteration mineralogy can be used to determine the type of environment of formation. Typically glass is the most susceptible, frequently altering first to opal, smectite, calcite or zeolites then to mixed layer clays (Henley and Ellis 1983). Steiner (1968) gives a decreasing order of mineral susceptibility as, olivine, magnetite, hypersthene, hornblende, biotite = plagioclase. Mineral susceptibility in the biotite rhyolites follows a similar trend with decreasing potential for alteration as Fe-Ti oxides > biotite > plagioclase > quartz.

Glass

The glassy groundmass of the rhyolites is the first to show signs of alteration. Where weakly altered glass is replaced by kaolinite, illite, smectite, and mixed layer clays with increased alteration. Replacement of glass by zeolites is evident within the Pokohino Beach area (sample W941314), where vughs up to 10cm long are infilled with white fibrous zeolites (Fig. 6.1a). XRD analysis of the zeolites identified thomsonite as the dominant zeolite. Where highly altered, fine grained anhedral interlocking quartz and K-feldspar replace the spherulitic glassy groundmass.

Figure 6.1. (over page). A) fibrous zeolites partially infilling a vugh in a previously altered quartz + K-feldspar type zone. Sample W941326, X20 magnification, plane-polarised light. B) biotite altered to illite within a quartz + K-feldspar type alteration zone. Sample W941328, X80 magnification, cross-polarised light. C) plagioclase core altered to K-feldspar within a quartz + K-feldspar type alteration zone. Sample W941315, X80 magnification, cross-polarised light. D) plagioclase partially replaced by epidote within an epidote type alteration zone. Sample W941269, X80 magnification, cross-polarised light. E) brecciated veinlet, with silicified rhyolite clasts in a matrix of fine grained quartz + K-feldspar followed by coarse grained quartz. Sample W941299, X20 magnification, cross-polarised light. F) fibrous pyrophyllite infilling vughs after coarse grained quartz. Sample W941296, X80 magnification, cross-polarised light.

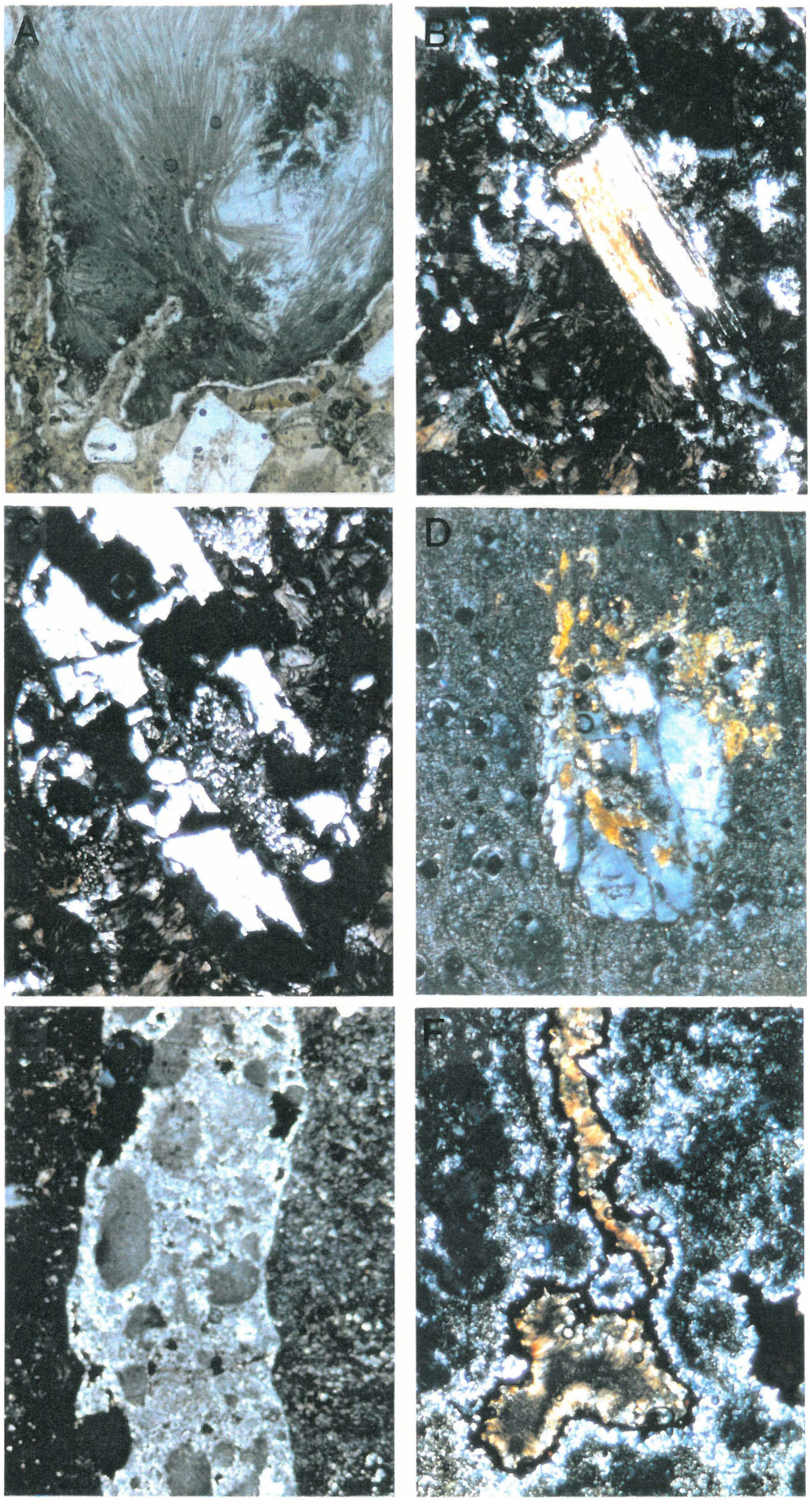
A
B
C
D
E
F

Fe-Ti oxides

Ilmenite is the dominant oxide in the biotite rhyolites, and hence minerals altered from ilmenite are Ti enriched leucoxene and sphene. These minerals commonly occur in the altered rhyolites in the vicinity of The Knob, and in the altered lake sediments and HEB. They are less common in the rhyolites exposed between Onemana and Pokohino Beach. Abundant fine pyrite and rare marcasite is disseminated throughout the moderately altered lake sediments and HEB. However the occurrence of the pyrite within the lake sediments and HEB may not be directly related to the alteration of the Fe-Ti oxides, but may be related to the abundance of carbonaceous material.

Biotite

Alteration of biotite begins in weak to moderate stages of alteration, with biotite being partially altered to Fe-Ti oxides. With increasing degrees of alteration biotite is altered to illite (Fig. 6.1b) and rarely to chlorite leaving only a skeletal relict of the original phenocryst. Quartz and K-feldspar completely replace biotite in areas of strong alteration.

Plagioclase

Plagioclase is the most abundant primary phenocryst in the biotite rhyolites, but its abundance is greatly reduced through increasing alteration. With moderate alteration, illite crystallises along cracks and cleavages in plagioclase phenocrysts. Some phenocrysts are distinctly more altered in the core (Fig. 6.1c), which may be due to the core being more calcic than the rim. Microprobe analyses of a plagioclase phenocryst in sample W941269, shows a normally zoned plagioclase with a core of An_{24} and a rim of An_{19}. Similar alteration of plagioclase was described by Conrad et al. (1992) at the Tayoltita Mine, Mexico, where alteration was concentrated in the more calcic core.

Epidote (identified through petrographic techniques) is a less common alteration mineral of plagioclase at Onemana, but is a major alteration mineral of plagioclase in samples W941269 and W941365 (Fig. 6.1d). In sample W941269 thin veins (0.1mm wide) of epidote are evident in thin section.

6.3 Alteration types

There are two main areas of alteration within the NE-trending corridor: within the biotite rhyolites between Onemana and Pokohino Beach; and with the biotite rhyolites, lake sediments and HEB west of the Onemana village. Each area has an alteration type that represents a different hydrothermal environment. Alteration types west of Onemana are characteristic of surface to near surface acidic alteration, while between Onemana and Pokohino Beach alteration assemblages are more related to deeper neutral to alkaline fluids. Based on these characteristics the alteration zones have been grouped into the following alteration types:

A) Alkaline alteration types
   1. weak clay
   2. zeolite
   3. epidote
   4. quartz + K-feldspar
   5. quartz silicification

B) Acidic alteration types
   1. kaolinite
   2. quartz + illite/smectite ± pyrophyllite
   3. opaline quartz silicification

Figures 6.2 and 6.3 shows the distribution of these alteration types. It is unknown how these two areas are linked as there is a lack of exposure between them. A probable scenario is that the alkaline type alteration exposed along the coast extends under the acid type alteration west of Onemana.

6.3.1 Alkaline alteration types

Weak clay type

The weak clay zone occurs as an alteration zone on the periphery of the other alteration types (except quartz silicification), and represents weak to moderate alteration (Fig. 6.2). It is dominant in exposed lavas along the Onemana Beach. The extent of this zone is unknown due to the lack of exposure inland, but it is thought it grades outward into argillic alteration or unaltered rock. The alteration assemblage within this zone is: quartz (tridymite) + montmorillonite ± kaolinite ± chlorite ± hematite. Quartz is the only primary phenocryst

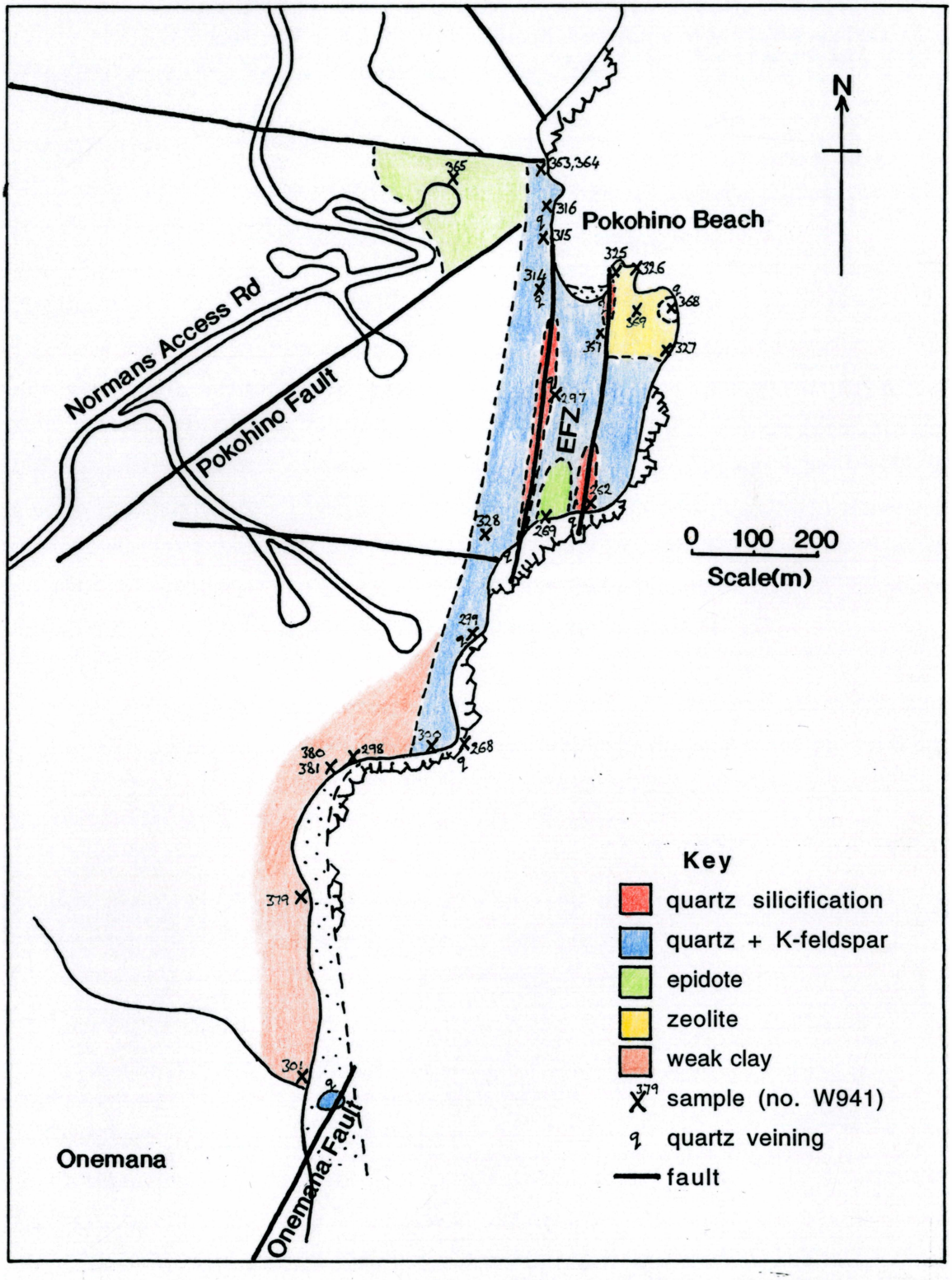

Figure 6.2. Surface distribution of alkaline alteration types within the biotite rhyolites between Onemana and Pokohino Beach.

remaining with biotite and plagioclase leached to clays. Vesicles and vughs have been infilled with anhedral, interlocking, fine grained quartz, clays, and hematite. Quartz veinlets up to 0.1mm wide are common. Brecciation zones up to 0.5mm wide are also evident along the veinlets. The spherulitic groundmass shows variable alteration to clays (10-60%).

The occurrence of K-feldspar in sample W941301 suggests in some areas the weak clay type alteration may have occurred as an overprinting phase, possibly as a deeper equivalent of the kaolinite type alteration.

Zeolite type

The zeolite zones forms a 100m wide zone adjacent to the eastern margin of the EFZ. The N-S extent of the zone is unknown, but is thought to be greater than 150m. XRD analyses of zeolites removed from vughs in sample W941326 shows thomsonite to be the main zeolite present. Wirsching (1981) obtained thomsonite by hydrothermal reaction of nepheline with 0.1 or 0.01N $CaCl_2$ solution at temperatures of 150-250°C. This compares with 225-245°C from Barrer and Denny (1961), and 200-275°C from Juan and Lo (1969).

Petrographic and XRD analyses show quartz and K-feldspar to be abundant within this zone. In thin section zeolites dominantly occur within vughs (Fig. 6.1a). Some vughs show an earlier deposition of quartz, which suggests that the development of the zeolites is a late stage feature.

Plagioclase is generally fresh throughout much of the zeolite zone, but with increasing alteration, clay followed by fine grained quartz and K-feldspar replaces plagioclase. Closer to the EFZ plagioclase is up to 80% replaced by fine grained K-feldspar.

Biotite is variably replaced by opaques and illite. Fe-Ti oxides show increased replacement by hematite ± leucoxene.

Veining up to 2cm wide is common throughout the zeolite zone, but the veining is typically thin, and appears to represent one phase of quartz deposition. Close to the EFZ, brecciation is evident along these veinlets with up to 50% of the original rock replaced by quartz, K-feldspar and zeolites (sample W941325).

The zeolite zone occurs adjacent to a highly silicified zone, and is thought to have overprinted earlier quartz + K-feldspar alteration. It is unknown whether the zeolite type varies through the zone. General trends in calcium zeolites from mordenite at temperatures of about 100°C, through laumonite from 150°C to wairakite at higher temperatures have been shown by Steiner (1968) and Gottardi and Galli (1985). Similar zonation was also seen at Katayama, Japan (Brown 1978).

Epidote type

Epidote type alteration represents moderate to high levels of alteration, with the alteration of plagioclase to epidote characteristic of this zone. Epidote was evident in only two samples; 300m NW of Pokohino Beach (W941365), and within the EFZ (W941269). The alteration assemblage of this zone is epidote + K-feldspar + quartz + illite ± kaolinite ± chlorite ± leucoxene. Most active geothermal systems in which measurements of present and paleotemperatures exceed 200-250°C contain epidote as a major hydrothermal mineral (Bird et al. 1984). Beaufort et al. (1992) showed epidote occurred at temperatures between 200-350°C in a fossil hydrothermal system at Saint Martin

Plagioclase is commonly altered to illite along cleavages and fractures. Fine grained euhedral epidote replaces up to 80% of the plagioclase (Fig. 6.1d). Plagioclase is also altered to K-feldspar, quartz and illite.

Epidote is commonly dispersed throughout the groundmass, and is also evident in discontinuous veinlets up to 0.1mm wide in sample W941269. The occurrence of kaolinite only in vesicles in sample W941269 suggests that it is a late stage feature.

Quartz + K-feldspar type

Quartz + K-feldspar type alteration grades from the lesser altered weak clay and epidote type alteration zones. The alteration assemblage in these zones is characterised by quartz + K-feldspar ± illite ± illite/smectite ± pyrite ± hematite. This zone is the dominant alteration type in coastal bluffs which extend from north of the Onemana Beach to 200m north of Pokohino Beach. An area of quartz + K-feldspar type alteration is also evident to the east of the EFZ. This area appears to be strongly related to two photolineaments that form the boundaries for the EFZ. This zone clearly terminates to the north against an E-W striking structure.

Much of the original rock has been replaced by a mosaic of euhedral interlocking quartz, though the original spherulitic texture is still evident. Most samples show more than two distinct phases of deposition with a crustiform quartz layer followed by microcrystalline quartz and K-feldspar. The quartz and K-feldspar deposition appears to be closely associated with brecciation (Fig. 6.1e). Work done by Drummond and Ohmoto (1985), and Hedenquist and Henley (1985) show that when pressure is released (ie. brecciation) the formation of K-feldspar is favoured.

The replacement of plagioclase within this zone is complete. Remnant plagioclase shows honeycombed structures of fine grained K-feldspar. Similar structures were seen by Henneberger and Browne (1988) where K-feldspar replaced the leached plagioclase along its rim, fractures, and cleavage, leaving the leached cavities. These cavities are sometimes infilled with quartz in more silicified samples.

There is little evidence of primary biotite in this zone. Where biotite was seen it was altered to illite and opaques, but with higher alteration it was altered to quartz. Fe-Ti oxides are commonly altered to hematite ± leucoxene and rarely pyrite.

Irregular veins of quartz ± pyrite ± hematite are common within this zone. XRD analyses indicate K-feldspar is present in many of the veins, though this was not seen in thin section.

Quartz silicification type

Intense quartz silicification occurs within the quartz + K-feldspar type alteration. Quartz silicification is well developed in zones that coincide with strong N-striking photolineaments that delineate the EFZ. This zone coincides with areas of high frequency of chaotic veining and stockwork development. The host rock is highly brecciated, which suggests quartz deposition was caused by periodic hydrothermal fracturing followed by the influx of cooler fluids. Multiple phases of quartz deposition and brecciation have reworked previous breccias and veins.

Fine grained quartz has replaced over 90% of the groundmass, though some primary textures are still evident (spherulites). Pyrite is disseminated

throughout the silicified rock. K-feldspar was identified as a minor phase by XRD analyses.

6.3.2 Acidic alteration types

Kaolinite type

A pervasive kaolinite + quartz ± illite ± pyrite ± leucoxene ± sphene alteration assemblage occurs west of the Onemana village and is hosted by biotite rhyolites, lake sediments, and HEB. This type of alteration is characteristic of shallow zones of acid-sulphate steam condensate, in which H_2S separated from a deeper chloride water has oxidised to H_2SO_4 (Henley and Hedenquist 1986; Henneberger and Browne 1988).

Kaolinite identified through XRD analyses is thought to be a late stage alteration product, as kaolinite forms at low temperatures and appears to overprint higher temperature alteration assemblages. Studies by Browne (1978) on surface kaolinite in active geothermal fields, showed kaolinite did not persist above 60°C.

Kaolinite alteration is most intense around silicified zones and along NW trending structures. The pervasiveness of the alteration in the area may reflect extensive lateral flow through some of the lake sediments. In areas of intense kaolinite alteration disseminated pyrite and patches of illite are common.

Coote (1994) shows this zone grades into a deeper zone of mixed layer clays and then into quartz + K-feldspar ± pyrite alteration assemblages below Breccia Knob.

Quartz + illite/smectite ± pyrophyllite type

Isolated zones of quartz + illite/smectite ± kaolinite ± illite ± pyrophyllite ± leucoxene ± sphene occur along NW trends from Breccia Knob, and in isolated zones south of The Knob, and SW of Breccia Knob (Fig. 6.3). Illite/smectite was identified through XRD techniques. The occurrence of stratified illite/smectite suggests a temperature of 150-230°C (Henley and Ellis 1983). The high temperatures near the top of the hydrothermal system may be explained by overpressuring prior to hydrothermal brecciation.

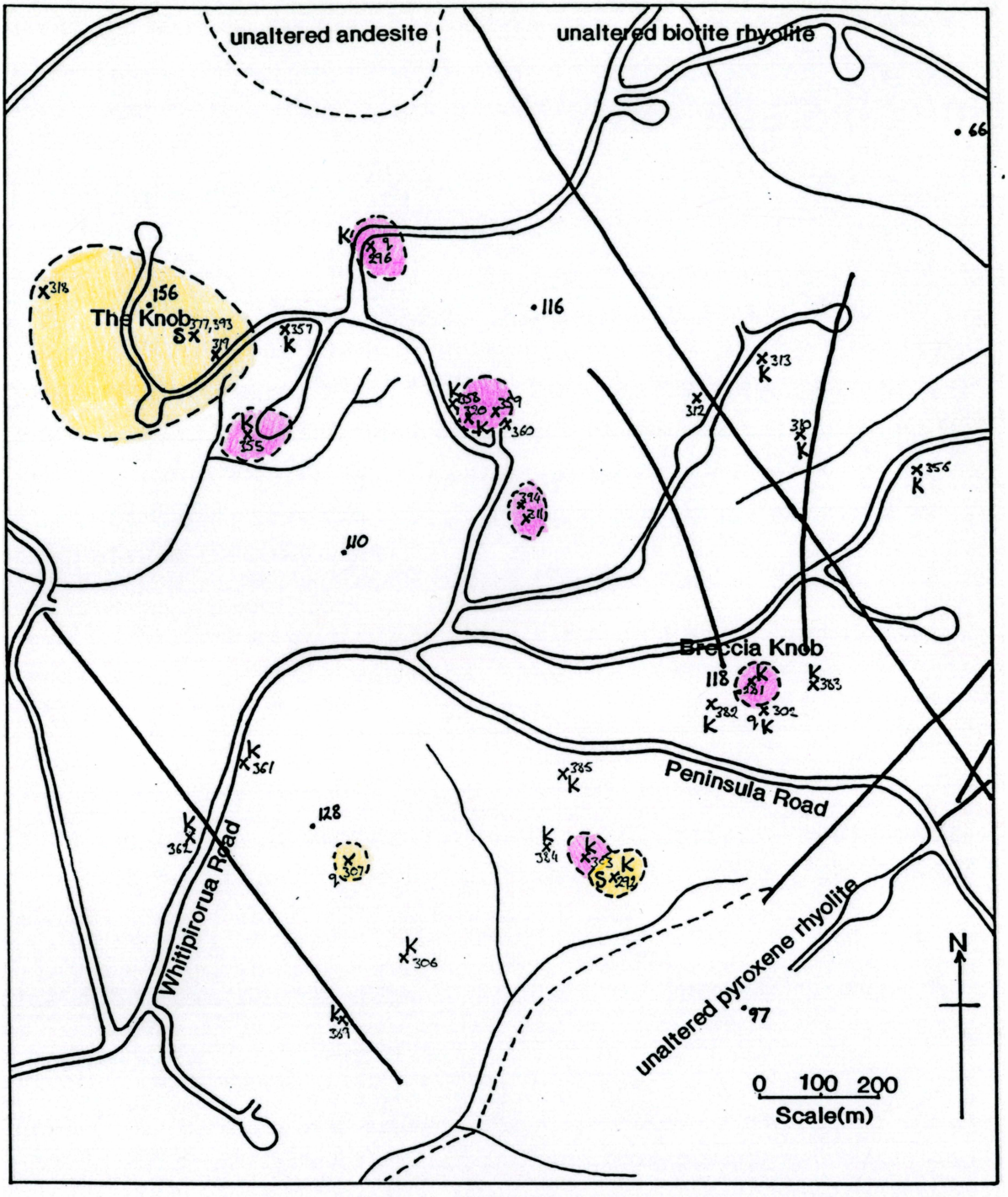

Figure 6.3. Surface distribution of acidic alteration types west of Onemana.

Pyrophyllite was identified by petrographic methods in two samples (W941296, W941320) within the HEB and biotite rhyolite. In sample W941296 fibrous pyrophyllite was evident within vughs of a biotite rhyolite (Fig. 6.1f). One quartz vein was seen in the area sample W941296 was taken.

Quartz + opaline silicification type

Quartz + opaline silicification outcrops in areas around The Knob, Breccia Knob, on a ridge 1km south of the The Knob, and in a valley 400m SW of Breccia Knob (Fig. 6.3). Sinters are evident near the top of The Knob and in the valley SW of the Breccia Knob. The sinters show purple and white layers, and where hosted by lake sediments appear to have incorporated the sediments which have then been silicified. Brecciation is evident in the sinter outcrop SW of Breccia Knob, where blocks of sinter up to 0.5m in diameter have been recemented in a silicified matrix.

Boiling structures are evident at Breccia Knob and on the NW trending ridge, where bladed quartz after calcite has formed in vughs of the silicified lake sediment and HEB.

Kaolinite alteration has overprinted silicification at Breccia Knob and the sinter deposit to the SW. Silicification at The Knob and along the NW trending ridge remain barren of kaolinite suggesting these deposits post-date the kaolinite alteration.

6.4 Alteration geochemistry

Suites of unaltered to highly altered biotite rhyolites were analysed to determine chemical changes caused by the passage of hydrothermal fluids through the rocks (Table 6.1). Major and trace elements were analysed using XRF (see Chapter five). Variations in the geochemistry of geothermal systems and epithermal deposits has been discussed by Henley and Ellis (1983), Drummond and Ohmoto (1985), Silberman and Berger (1985) and Hayba et al. (1985). Clarke et al. (1990) has attempted to show variation in host rock geochemistry at various gold deposits in the Coromandel Peninsula. Henneberger and Browne (1988) also discuss geochemical variation of host rocks at Ohakuri, in the Taupo Volcanic Zone. Comparing fresh and hydrothermally altered rhyolite rocks in the Wairakei system, Steiner (1977) showed a characteristic loss of Na and Ca, and gain of K and Si through the alteration zone.

Table 6.1. Major (wt%) and trace element abundences (ppm) of selected altered biotite rhyolite samples within the NE-trending alteration corridor, Onemana.

Alteration type	Unaltered	Alkaline Alteration types: Weak clay		Zeolite			Epidote	Quartz + K-feldspar					Q si.	Acidic Alteration types: Ill/sm	Opaline quartz si.	
W no.	941368	941301	941298	941325	941326	941327	941269	941299	941300	941328	941314	941315	941262	941296	941318	941319
Location	666/474	660/461	661/466	665/474	665/474	666/473	664/470	663/469	662/467	663/471	664/474	664/475	664/470	644/460	639/460	642/458
SiO2	78.03	82.06	80.49	76.45	74.49	75.60	73.01	80.83	80.87	73.67	84.53	78.24	91.53	85.01	86.74	99.02
TiO2	0.09	0.07	0.07	0.07	0.08	0.08	0.09	0.06	0.08	0.10	0.06	0.07	0.08	0.07	0.06	0.07
Al2O3	14.22	10.18	11.25	12.02	14.27	14.24	14.21	9.92	10.35	17.20	10.05	12.92	4.73	8.45	8.06	0.62
Fe2O3†	0.12	0.05	0.13	0.42	0.22	0.15	0.05	0.16	0.01	0.21	0.15	0.11	0.06	0.07	0.07	0.01
FeO†	0.42	0.18	0.46	1.51	0.80	0.54	0.18	0.57	0.04	0.76	0.56	0.38	0.21	0.25	0.24	0.04
MnO	0.01	0.00	0.00	0.00	0.00	0.00	0.00	0.00	0.00	0.00	0.00	0.00	0.00	0.00	0.00	0.00
MgO	0.08	0.07	0.31	0.23	0.10	0.35	0.08	0.19	0.07	0.11	0.04	0.09	0.00	0.04	0.01	0.01
CaO	0.40	0.18	0.12	0.22	0.34	0.37	0.16	0.11	0.09	0.12	0.08	0.37	0.08	0.06	0.17	0.07
Na2O	2.31	1.45	1.92	1.68	2.22	3.01	0.47	1.11	1.10	1.14	0.59	2.45	0.08	0.22	0.95	0.09
K2O	4.29	5.74	5.25	7.38	7.45	5.64	11.72	7.02	7.38	6.64	3.91	5.34	3.21	5.80	3.69	0.06
P2O5	0.02	0.02	0.01	0.03	0.02	0.02	0.03	0.02	0.02	0.03	0.02	0.02	0.01	0.02	0.01	0.01
Fe2O3*	0.57	0.25	0.61	2.03	1.08	0.71	0.25	0.78	0.05	1.01	0.75	0.51	0.29	0.35	0.33	0.05
LOI*	3.36	1.43	3.48	2.92	2.56	5.20	1.29	1.31	0.84	3.96	3.19	2.40	1.98	1.36	1.63	0.83
Total*	100.02	100.19	99.83	99.96	100.21	100.05	100.17	100.15	100.01	100.14	100.03	99.56	99.46	100.25	99.85	100.08
Ba	607	613	622	883	1009	668	93	771	716	559	380	682	511	359	516	104
Rb	163	256	224	337	325	223	176	325	314	309	192	220	166	375	173	9
Sr	29	19	15	38	36	32	13	20	13	16	12	32	14	22	18	7
Th	16	12	12	13	15	16	17	11	13	16	10	16	4	10	8	7
U	4	4	3	2	3	4	3	2	4	4	3	4	1	1	2	2
Pb	23	14	12	24	21	19	4	12	12	19	12	21	5	7	10	1
Zr	105	89	97	87	101	101	105	73	94	115	71	98	40	82	66	83
Nb	6	6	5	4	5	6	6	2	6	6	3	4	1	4	3	5
As	14	5	26	228	110	59	14	137	3	94	151	99	47	39	47	2
La	14	10	9	15	25	18	25	12	11	14	8	19	3	7	11	0
Ce	29	22	18	31	43	33	52	27	19	26	16	34	6	17	22	1
Y	21	15	21	21	30	22	31	17	18	21	10	24	1	3	10	4
Sc	4	2	4	5	5	5	2	2	1	6	1	4	2	4	3	0
V	2	3	4	4	4	3	3	3	3	5	4	3	7	4	3	3
Cr	1	0	0	13	1	2	1	2	0	2	4	2	2	1	1	0
Ni	2	3	4	7	5	3	4	3	4	4	3	3	1	4	2	0
Cu	1	2	2	4	3	4	3	3	2	3	4	3	2	3	1	0
Zn	17	3	8	18	16	14	2	8	1	8	5	8	2	2	3	0
Ga	17	11	15	15	15	16	17	10	9	19	11	15	3	8	10	8

* Original values † recalculated assuming $Fe_2O_3/(Fe_2O_3 + FeO) = 0.2$

The elevated contents of K, Ba, Au, As, Sb and depleted Na, Ca in wallrocks to veining in Hauraki gold deposits are typical for alteration associated with epithermal mineralisation (Silberman and Berger 1985; Clarke and Govett 1988; 1990). Rock geochemistry studies for epithermal gold deposits have shown that there is no consistent pattern in anomalous geochemical signatures or geochemical zonation for such systems (Clarke et al. 1990).

Few geochemical trends are evident with increasing alteration in the biotite rhyolites, but each type of alteration does have a distinct compositional range.

Major elements

Most oxides show wide fluctuations except TiO_2, MnO, and P_2O_5 which are consistently low. The SiO_2 content shows slight increases in the quartz + K-feldspar zone and then into the silicified zone, but shows decreases in the zeolite and epidote zones. This suggests the hydrothermal reactions within the zeolite and epidote zone involves silica leaching.

The Al_2O_3 content in rocks from the zeolite and epidote zones shows little change from the unaltered rocks, but shows large decreases in highly silicified zones. The corresponding decrease in K_2O with Al_2O_3 within the silicified zone supports the petrographic and XRD evidence for the removal of K-feldspar.

MgO only shows minor increases in the zeolite type alteration, but is removed in highly silicified rocks. Both CaO and Na_2O show decreases with increasing alteration. This decrease is reflected petrographically with the removal of plagioclase.

K_2O shows an increase with increasing alteration to quartz + K-feldspar type alteration but then decreases in highly silicified zones. Sample W941269 shows high K_2O values (11.72 wt%) within the epidote zone.

Trace elements

Ba, Rb and As appear to be the most mobile elements within the hydrothermally altered biotite rhyolites. The elements Zr, Ga, and REE (La, Ce, Y) appear to be immobile in most alteration types, although increases in La and Ce occur in the epidote zone. The abundance and variation of Sc, V, Cr, Ni, and

Cu is too small to determine if these elements are immobile, because analytical error may exceed the elements' variation.

Generally Rb follows a similar trend as K_2O with increasing alteration. This suggests that Rb substitutes for K in K-feldspars. Sr is generally consistent, but increases in the zeolite zone. This may be due to Sr substituting for Ca in the zeolites. Silicified rocks appear to be depleted in Sr and Rb (especially in samples from near The Knob; W941318, W941319) compared to adjacent K-feldspar type alteration. Rb is notably lower in the K_2O-rich epidote zone.

Ba shows large increases in the zeolite zone, but is constant within the quartz + K-feldspar zone. The epidote zone shows a depleted Ba content. Henneberger and Browne (1988) suggest Ba was incorporated into zeolites and K-feldspar in similar amounts in altered rocks at Ohakuri, but here only the zeolite zone shows enrichment. Ba is also depleted with increased silicification.

Base metals Zn and Pb are depleted with increasing alteration.

As is also evident in highly variable amounts. The occurrence of As in geothermal systems and epithermal deposits is closely associated with the occurrence of Au and Ag (Henley and Ellis 1983; Silberman and Berger 1985; Henley and Hedenquist 1986; Clarke et al. 1990).

Figure 6.4 shows the distribution of As within the altered biotite rhyolites. As abundances in the unaltered biotite rhyolites vary between 4 and 14ppm. Highest abundances of As were seen to occur within the quartz + K-feldspar zone, with higher concentration with increasing alteration. Anomalously low values were recorded in sample W941300 (3ppm). It is unclear why the As concentration is so low in this sample, but similar values were obtained from sample W941301 in the weak clay zone (5ppm). The high concentrations within the zeolite zone is thought to have resulted from the previous quartz + K-feldspar type alteration. As concentrations appear to decrease with increased silicification. Low concentrations were also evident within the epidote type alteration.

High As concentrations are not concentrated in the main upflow zones, but appear to form a halo around these zones within the quartz + K-feldspar type alteration. It is thought that as with K-feldspar, As deposition is strongly related to boiling from the loss of pressure.

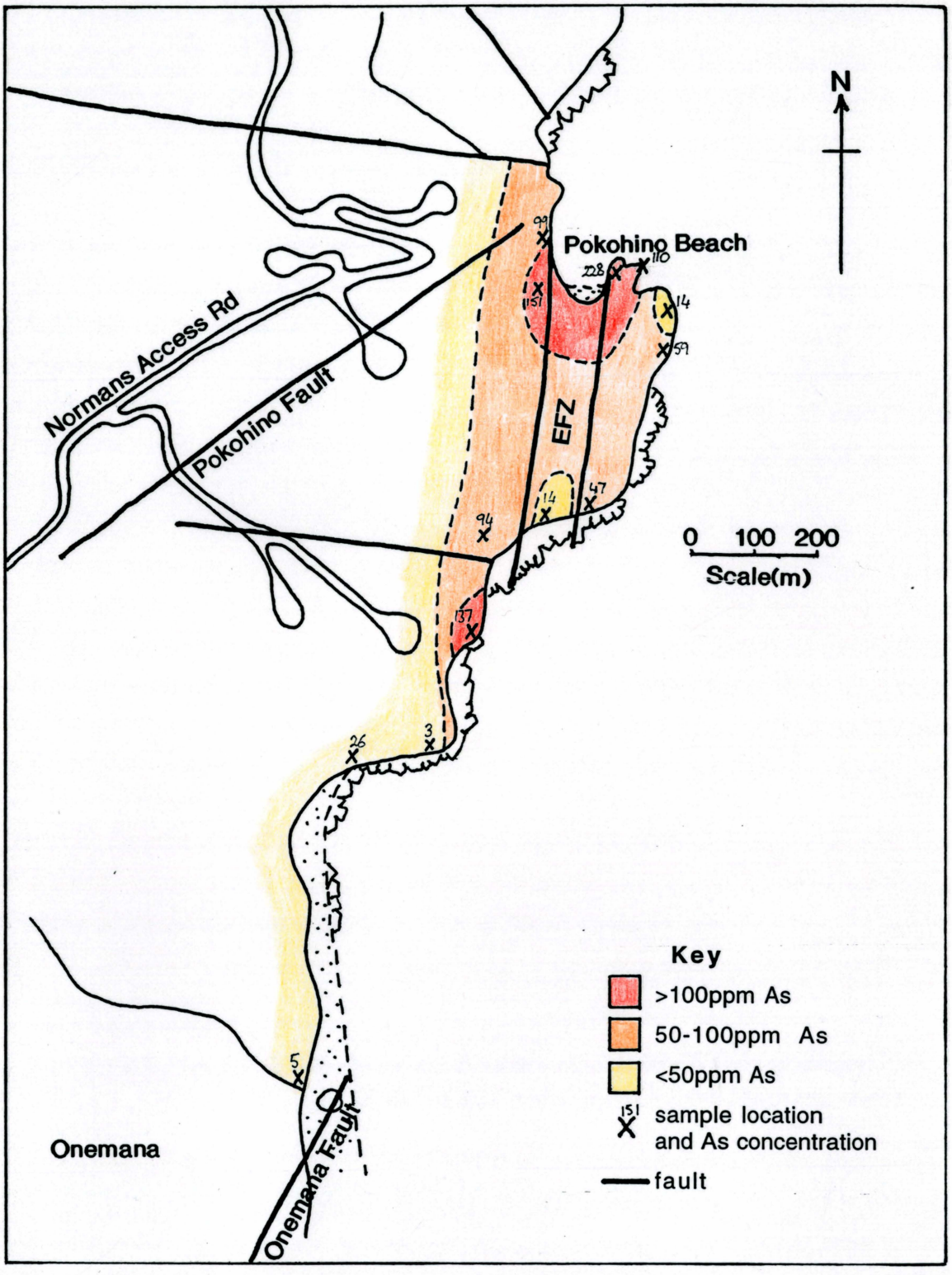

Figure 6.4. Surface distribution of As within altered biotite rhyolites between Onemana and Pokohino Beach.

6.5 Stages of activity

The evolution of the hydrothermal system at Onemana can be divided into three main phases (Fig. 6.5): early alteration by alkaline-chloride fluids, then widespread alteration by acid-sulphate fluids, then final hot spring activity.

Initial alkaline-chloride fluids

Initial geothermal activity involved alkaline-chloride fluids rising up active N and NW-striking fractures, producing zones of quartz + K-feldspar and quartz silicification type alteration. The alteration mineralogy suggests the temperature of the alkaline fluid was in excess of 230°C. Alternating sealing and brecciation through hydrothermal fracturing, resulted in zones of stockworks and breccias with peripheral veining in the main upflow zones. The zeolite zone is thought to have formed by the reaction of cooler fluids with hot alkaline-chloride fluids. Zoning may have occurred through this fluid interface zone as in other geothermal systems (e.g. Wairakei), but only thomsonite was identified suggesting moderate to high temperatures (150-250°C). The occurrence of epidote type alteration is indicative of propylitic alteration which typically grades from the quartz + K-feldspar zone and into argillic assemblages (not seen). The occurrence of this zone between the two main upflow zones suggest there is little linkage between the two.

Local sealing of main fluid conduits and hydrothermal fracturing triggered by a seismic event may have triggered the hydrothermal eruption sourced from Breccia Knob (see Chapter Three). It is difficult to determine the type of near-surface alteration that was occurring prior to the eruption, but large blocks of sinter are evident within the HEB.

Acid-sulphate fluids

The second stage of activity is dominated by widespread kaolinite alteration. Any evidence for this type of alteration between Onemana and Pokohino Beach has been removed by erosion. The alteration by acid-sulphate fluids appears to have concentrated along NW trending structures evident from resistivity work.

Typical of other active and fossil hydrothermal systems (Waiotapu, Hedenquist, 1986; Golden Cross, de Ronde and Blattner, 1988; Ohakuri, Henneberger and Browne, 1988) is that the acid-sulphate fluid is derived from

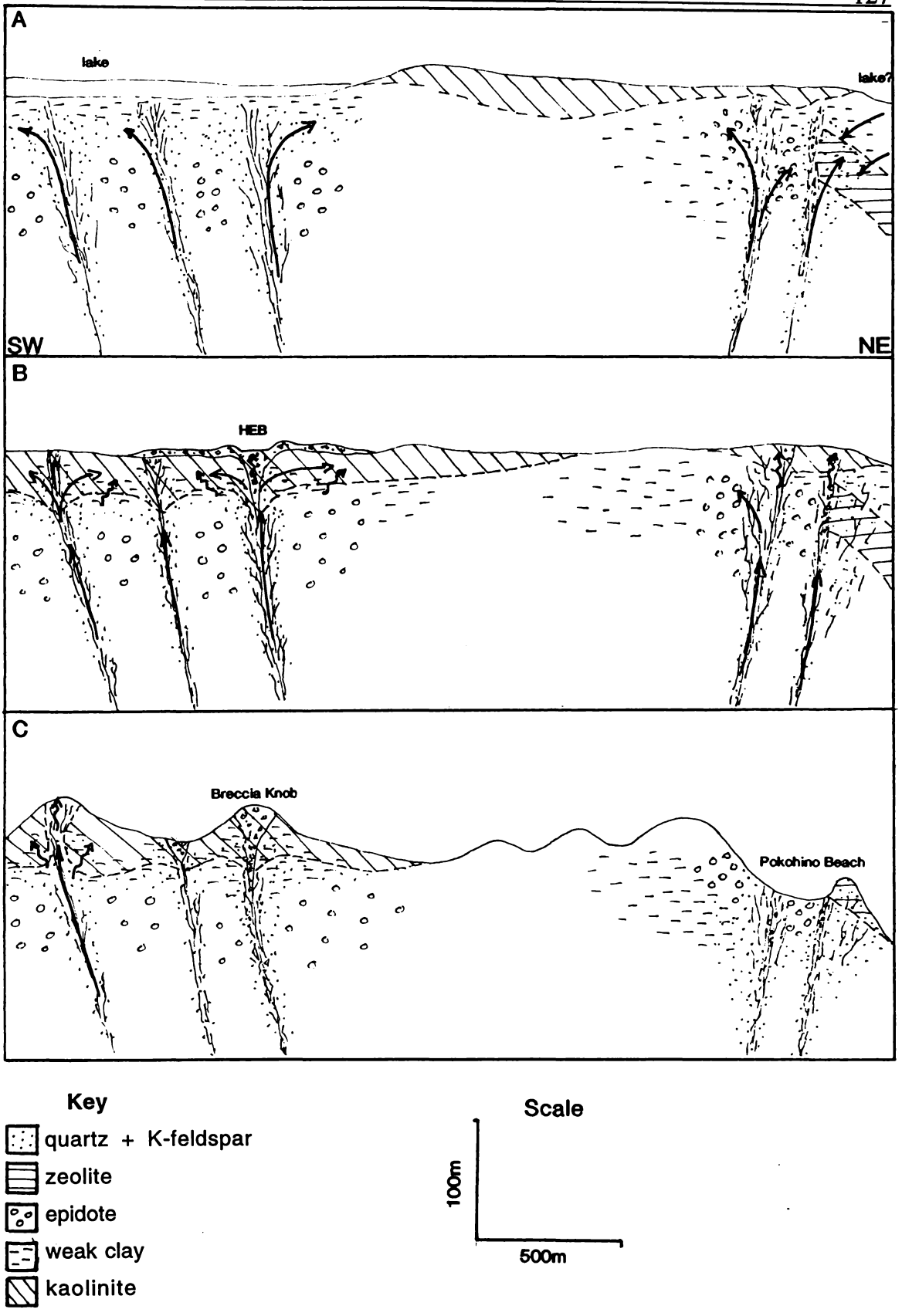

Figure 6.5. Simplified SW-NE cross section through the Onemana hydrothermal system during successive stages of activity: A) initial alteration by alkaline fluids; B) overprinting by acidic kaolinite alteration; C) late stage hot spring activity, and the approximate present day erosion surface.

the boiling of deep alkaline-chloride fluids, and percolates down permeable channels to depth.

The cause of change in the dominant fluid in the hydrothermal system at Onemana is unknown. A suggestion may be related to the hydrothermal eruption from Breccia Knob, where the eruption site produced a major release valve for an overpressurised system, causing boiling and H_2S gas loss, allowing acid sulphate waters to form. XRD analyses of samples from drilling around Breccia Knob and on the NW-trending ridge identify kaolinite up to 60m below the present day surface.

Final hot spring activity

Hot spring activity continued at The Knob and along the NW-trending ridge after acid-alteration ceased forming sinters and silicifying host rocks. These two zones do not appear to be structurally linked, and it is assumed they are not structurally linked to Breccia Knob. Local brecciation is evident within these areas, and boiling structures are evident on the NW-trending ridge. No other alteration zones appear to be associated with this final stage of activity.

6.6 Discussion

The evolution of the hydrothermal system shows characteristics that are similar to other fossil and active geothermal systems in the Coromandel Peninsula and TVZ, e.g. Wairakei, Steiner (1977); Waiotapu, Hedenquist (1986); Ohakuri, Henneberger and Browne (1986); Golden Cross, de Ronde and Blattner (1988); Wharekirauponga, Rabone et al. (1989).

The style of alteration is comparable with other epithermal deposits within the Karangahake-Ohui Structural Trend, which show an inner quartz + K-feldspar zone which grades out into argillic and propylitic alteration assemblages, e.g. Wharekirauponga, Golden Cross, Maratoto, Karangahake, Waitekauri (Brathwaite et al. 1989).

Distinctive of the hydrothermal system at Onemana is the occurrence of epidote and zeolites, and the absence of calcite, which suggests the hydrothermal system had a low CO_2 content. This is similar to Wairakei where epidote and wairakite are common but are replaced by calcite at Broadlands due to a higher CO_2 content (Henley and Hedenquist 1986).

The source of the hydrothermal fluids appears to be strongly related to N-striking structures within the EFZ, and NW-trending resistivity anomalies west of Onemana. These zones are denoted by increased intensity of alteration. The structures exposed between Onemana and Pokohino Beach represent a deeper part of the hydrothermal system than that exposed to the west of Onemana. Quartz + K-feldspar alteration assemblages that are common in coastal cliffs were also found below Breccia Knob starting at 60masl approximately (Coote 1994). The occurrence of quartz + K-feldspar is at a similar height in coastal exposures, which may suggest at least 60m has been eroded off the system in the Pokohino Beach area. The amount of material eroded off the altered area to the west of Onemana is not thought to be large as numerous surface/near surface features are still preserved in the area.

The change in dominant fluid chemistry may be related to the eruption of the HEB. Common with hydrothermal eruptions in extensional settings is a reduction in fluid pressures which is restored by inward percolating fluids (Sibson 1989). This eruption may have caused a local drop in the water table and boiling allowed acid-sulphate waters to form. The vent system formed by a hydrothermal eruption establishes chemical environments conducive to precious metal mineralisation long after the eruption has ceased (Hedenquist and Henley 1986). This was shown by Hedenquist and Henley (1986) at the Champagne Pool, Waiotapu.

The close association of lake environments with geothermal areas is common in the TVZ, e.g. Waiotapu, Rotokawa. From thin section it is evident some of these sediments were unconsolidated when the hydrothermal system developed within them. The occurrence of widespread alteration suggests the lake(s) had reduced in size or disappeared to allow the local water table to drop.

Chapter Seven
Volcanic and Hydrothermal Setting

7.1 Introduction

This chapter presents a general overview of the style of volcanic and hydrothermal activity by bringing together the ideas and evidence previously discussed. Also this chapter will discuss the evidence for the applicability of a caldera model to the Onemana area, and compare the style of volcanic and geothermal activity with other rhyolite centres in the Coromandel and TVZ.

7.2 Overview

Initial rhyolitic activity

The pyroxene rhyolites of the Pohakahaka Dome Complex appears to be the oldest unit outcropping within the study area. Vent locations of the pyroxene rhyolite lavas are thought to have been controlled by N-trending structures, with vents possibly aligned along or near the present coastline south of Onemana. The pyroxene rhyolites are dominated by domes and lavas with minor autoclastic breccias. The thickness of individual flows is not known, but the rhyolite pile is greater than 128m thick. The pyroxene rhyolites are truncated to the north by the NE-trending Whitipirorua Fault. Although no detailed mapping has been done to the south of the study area, the area is dominated by rhyolite domes and flows, possibly as a southern extension of the Pohakahaka Dome Complex.

Biotite rhyolites: rifting related volcanism?

The northern half of the Onemana Peninsula is dominated by biotite rhyolites which appear to have erupted from two main dome complexes: the Pokohino and Wharekawa dome complexes. The only difference between the lavas of these eruption centres is the variation in the chemistry of plagioclase (Pokohino, An_{19-29}; Wharekawa, An_{32-45}).

The occurrence of the Wharekawa Pyroclastics below the biotite rhyolites of Peak Dome, suggest that the eruptions of the Peak Dome lavas were preceded by a phase of explosive volcanism. Evidence of this phase was not seen elsewhere for the other biotite rhyolite domes and flows.

The vent locations of the biotite rhyolites appears to be controlled by NNE to NE-trending structures in the NNE-trending KOST. This structural zone has been described as a rift structure by Merchant et al. (1988), and Rabone (1991). Geochemical analysis of the biotite rhyolites classify them as high-K rhyolites, which are common in rift settings. Analysis of the Staircase Rhyolite 5km NW of Onemana (Trotter 1995) shows a close trace element signature to the biotite rhyolites. The Staircase Rhyolite also appears to be controlled by a NE-trending structure. Although the biotite rhyolites are chemically and mineralogically similar, it is evident from trace element abundances that the biotite rhyolites were erupted from more than one magma body.

Evidence for vent locations east of the present day coastline is shown by the biotite rhyolite lavas which have flowed to the NW and lapped onto the Wharekawa Dome Complex. Near Ruahiwihiwi Point these lavas have flowed into a body of water (possibly a lake) where the lavas brecciated to form a hyaloclastite. Lake sediments are also evident west of the Onemana village. The lake was thought to have formed due to downthrow on the northern side of the Whitipirorua Fault.

The eruption of the Glassy Dome Rhyolite and associated pyroclastics between the Pokohino and Wharekawa dome complexes appears to be the latest phase of rhyolite volcanism erupted within the study area. Chemically and mineralogically it is similar to the biotite rhyolites, but varies from the biotite rhyolites in Rb abundances. The location of the Glassy Dome Rhyolite appears to coincide with an E-W trending structure. Much of the Glassy Dome Pyroclastics consists of avalanch breccia which has originated from the collapse of domes similar to the present Glassy Dome Rhyolite.

Late stage volcanism

The Wharekawa Ignimbrite laps onto the Wharekawa Dome Complex in the north of the study area. The occurrence of lithics and minerals not found within the study area, suggests the Wharekawa Ignimbrite was erupted from a vent outside the study area.

The Rangipo Andesite has intruded through the biotite rhyolites of the Wharekawa Dome Complex in the west of the study area. Chemically and mineralogically it is similar to other Coromandel Group andesites, but appears to have similar trace element abundances as the McBeths Andesite (McGunnigle 1995) which outcrops 6 km to the NW This suggests the Rangipo Andesite may be associated with the magma body that fed the McBeths Andesite. Correlation between these two units provides important stratigraphic evidence that the andesites are younger than the regions rhyolites.

Late stage geothermal activity

Widespread hydrothermal alteration and quartz veining occurs in a 1.5km wide NE-trending zone between the Pokohino and Whitipirorua faults. NW and N-striking structures between these structures appear to control the zones of alteration. It is thought sinistral movement along NE-striking faults (Whitipirorua and Pokohino faults) produced these extensional crossfaults, which provides zones for fluid upflow. The structural controls evident here is thought to be similar to those described at Waihi (Wellman 1954; Sibson 1987).

The main upflow zones are typified by a central quartz silicification zone, surrounded by a broad quartz + K-feldspar zone which grades out into epidote and weak clay type alteration. High levels of the hydrothermal system exposed west of Onemana are typified by pervasive kaolinite alteration with small areas of quartz + illite/smectite ± pyrophyllite and opaline quartz silicification.

The alteration mineralogy and zoning is typical of other deposits on the eastern Coromandel (e.g. Wharekirauponga, Golden Cross, Maratoto, Karangahake, Waitekauri) associated with rhyolitic volcanism, and similar to many deposits in the TVZ (e.g. Ohakuri). The preservation of surface/near surface features of the hydrothermal system at Onemana makes it possible to make comparisons with active hydrothermal systems in the TVZ, e.g. Rotokawa and Waiotapu.

A possible heat source for the hydrothermal system at Onemana is difficult to determine and may not be exposed in surface outcrops. Heat sources for geothermal systems hosted by silicic volcanics are typically provided by deep (5km) intrusive bodies (Henley and Ellis 1983; Henley and Hedenquist 1986). Unaltered andesite lava occurs less than 200m from the nearest alteration. If a hydrothermal system was focused around the Rangipo Andesite, mineralisation and hydrothermal alteration would be characteristic of high sulphidation epithermal deposits. However alteration at Onemana is typical of

a low sulphidation system, which is common in caldera settings in the TVZ. As discussed in Chapter Five the rhyolite volcanism of the area is derived from discrete rising magma bodies. It is possible one of these magma bodies supplied the heat source. Ore deposition usually occurs at least 1 Ma later than the emplacement of the host rock (Heald et al. 1987).

7.3 Applicability of the caldera model

Caldera facies and formation

Calderas are common collapse features within volcanic areas dominated by silicic volcanism. Calderas have been recognised or inferred based on the identification of a number of common facies (Cas and Wright 1987; Briggs and Fulton 1990):

1) thick intracaldera ignimbrites and co-ignimbrite breccias, and thin outflow sheets with a radial distribution

2) late-stage rhyolite domes and flows which lie within or at the margins of the caldera

3) moat deposits that lie between the intracaldera rhyolite lavas and the caldera wall

4) negative gravity anomalies

5) hydrothermal activity and epithermal activity may occur both inside and outside the caldera margins

6) semi-circular structures observed by remote sensing

Recently active rhyolite calderas can be recognised using the identification of rhyolite dome complexes within ring structures and associated negative gravity anomalies (Rogan 1982; Wilson et al. 1984; Briggs and Fulton 1990). However, older calderas may show topographical inversion. This is suggested by Briggs and Fulton (1990) for some Coromandel examples, e.g. Tunaiti Caldera.

Caldera forming eruptions begin when pressure within the volatile-rich cap of the magma chamber can no longer be contained (Wohletz and Heiken 1992). Initial activity results in regional tumescence and the development of ring fractures. The eruption of the volatile-rich magma results in the caldera collapse and deposition of thick intracaldera ignimbrites and thinner outflow sheets. Late-stage volcanism occurs as intracaldera rhyolite domes and ring fracture volcanism. Sedimentation in lacustrine environments is common

between the rhyolite domes and caldera walls. Hydrothermal systems develop within the caldera deposits and floor rocks along extensional faults that cross ring faults (Lipman 1984; Henley and Hedenquist 1986).

Figure 7.1 shows Briggs and Fulton's (1990) interpretation of a possible sequence of events in the development of the Tunaiti Caldera, south of Onemana.

Onemana caldera?

Initial observation of the Onemana Peninsula shows it to be an elongated peninsula dominated by rhyolite domes and lavas. The peninsula has a distinct semi-circular shape, which also extends through offshore islands to the south (Fig. 7.2). If the peninsula is part of a much more extensive ring fault the size of the caldera may have been in excess of 15km in diameter, making it one of the largest calderas in the Coromandel. A significant and unknown amount of coastal erosion has occurred to the east. Flow orientation in coastal exposures suggest rhyolite lavas in the northeast of the study area were erupted offshore. The western boundary of the peninsula is steep, and many bluffs are apparent, although it only appears to be fault bounded in the south. Lineations that may coincide with potential ring fractures are not easily seen. Ring structures associated with caldera collapse may have been destroyed by NW and NE-trending faults, and also may have been covered by resurgent volcanism.

A weak negative gravity anomaly (0 to -10mgal) exists over the southern half of the Onemana Peninsula with a focus at the southern tip. The gravity anomaly is not as intense as other calderas in the CVZ: Wharekawa (-20mgal), Kapowai (-10mgal), Waihi (-20mgal). Negative gravity anomalies can suggest thick caldera infill. Well defined negative gravity anomalies occur over most TVZ calderas (Wilson et al. 1984). Briggs and Fulton (1990) suggest topographic inversion and possible resurgence may reduce the value of using gravity anomaly maps to recognise calderas in the Coromandel.

Within the study area there is a distinct lack of thick and continuous ignimbrites. Pyroclastic material evident within the area has resulted from the growth and destruction of nearby domes. The occurrence of andesite lithics within the deposits suggest the rhyolites in the north of the study intruded through and flowed over older andesites. The existence of a precaldera andesite volcano below the Reporoa Caldera is suggested by Nairn et al. (1994) due to the occurence of andesite lithics within proximal lag breccias.

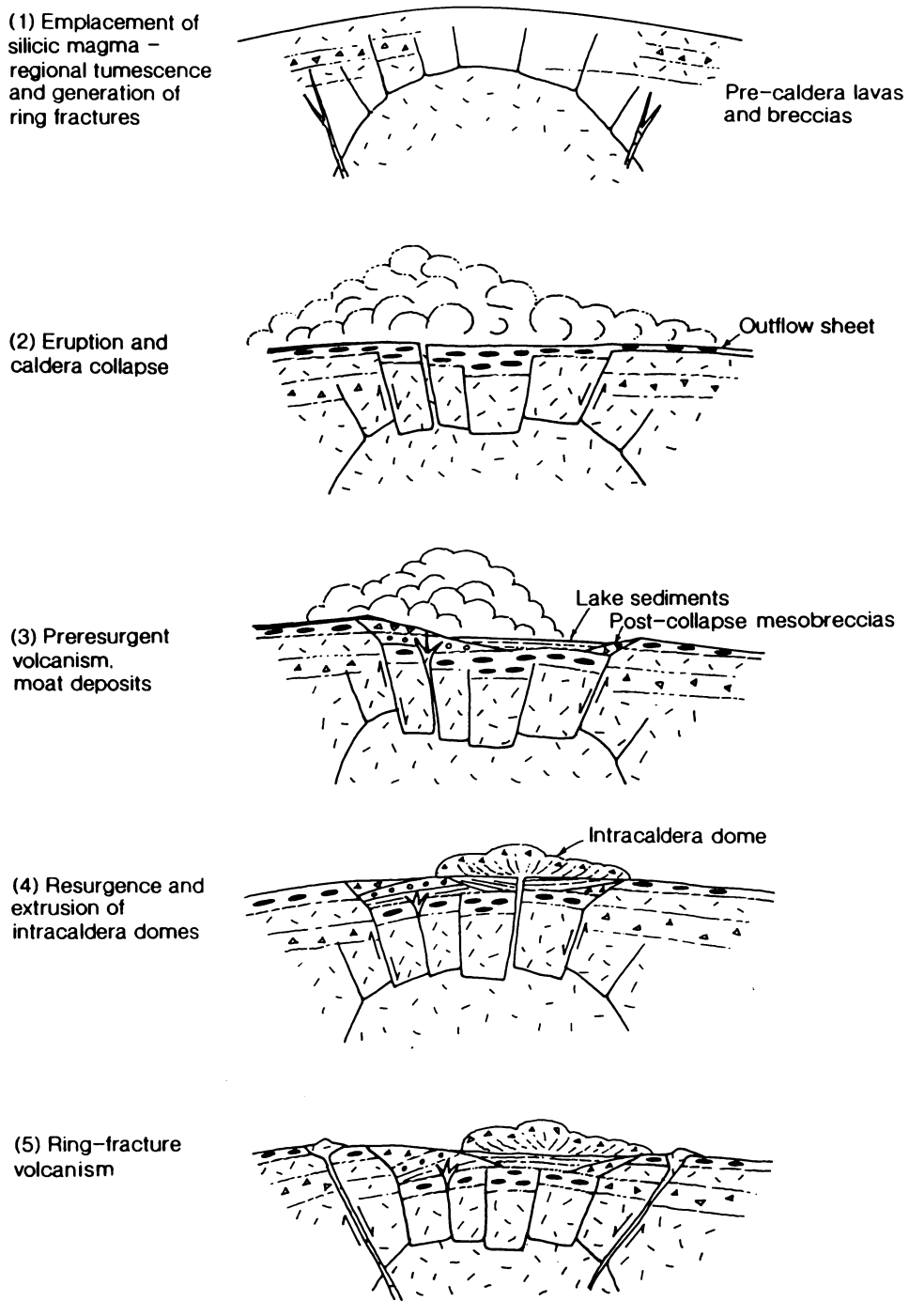

Figure 7.1. Schematic diagrams showing the possible sequence of events in the development of the Tunaiti Caldera (after Briggs and Fulton 1990).

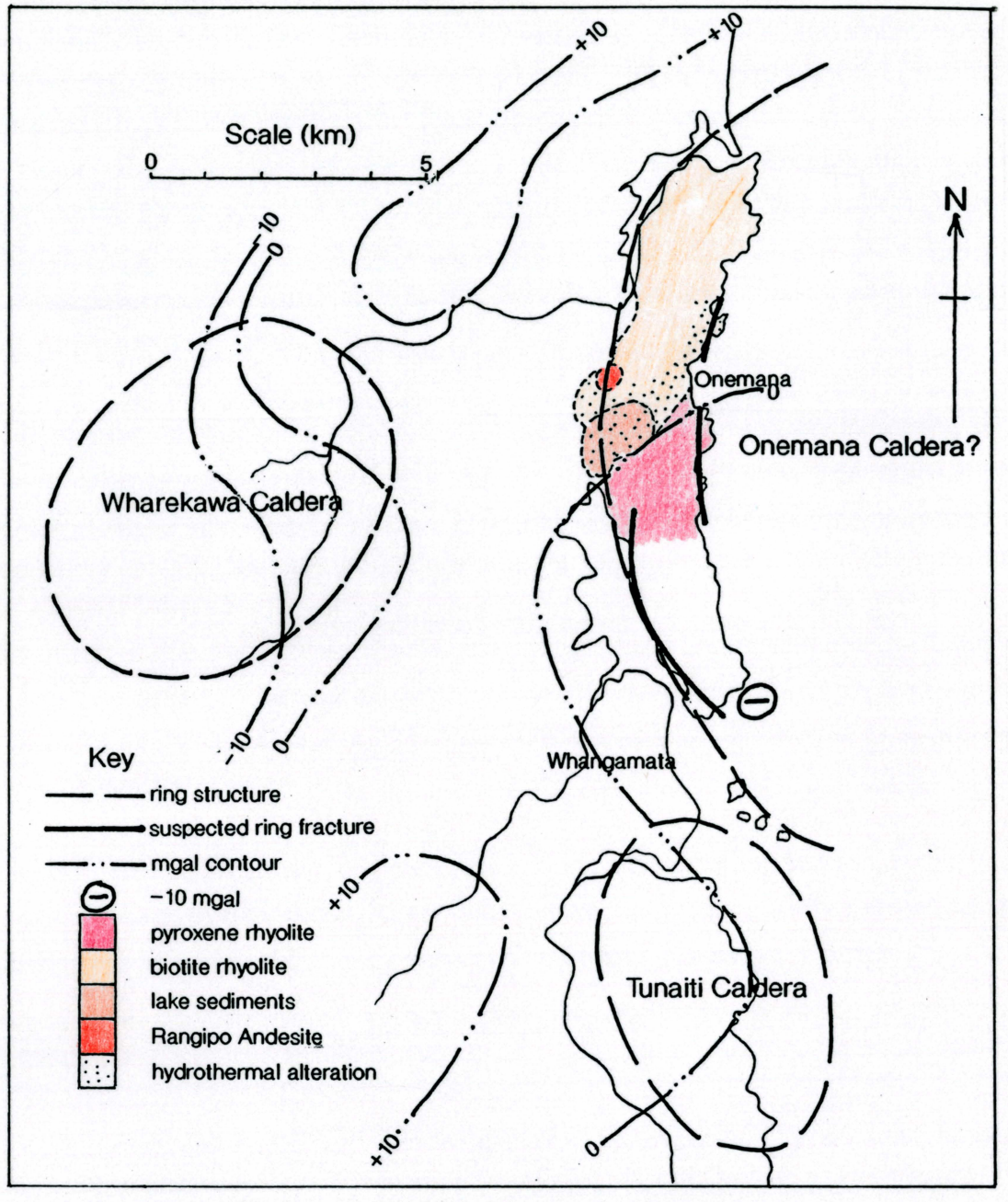

Figure 7.2. Inferred ring structures and gravity anomalies in the Onemana and surrounding areas.

The eruption of the rhyolites at Onemana may be associated with resurgent volcanism on or near the main ring fracture zone. There are two main types of rhyolites in the study area which vary in mineralogy, chemistry and structural controls. A possible scenario for the eruption of these rhyolites may be that the pyroxene rhyolites erupted along ring faults (N-S striking structures?), and the eruption of the biotite rhyolites along NE-trending structures, resulting from a NE-trending extensional zone coinciding with the ring fractures. This is a common occurrence with intracaldera rhyolite domes in TVZ volcanic centres, e.g. Maroa and Okataina (Wilson et al. 1984).

The occurrence of lakes is common in most rhyolite volcanic centres in the TVZ. Thick lake sediments occur between the Pohakahaka and Pokohino dome complexes. The occurrence of the lake sediments appears to be controlled by the down-faulting of the northern side of the Whitipirorua Fault. The existence of another water body adjacent the Wharekawa Dome Complex is evident in the north of the study area where a rhyolite lava has flowed into water forming a hyaloclastite. The occurrence of accretionary lapilli in unit 1 of the Wharekawa Pyroclastics suggests a close relationship between the eruption and the availability of water.

The hydrothermal system at Onemana is hosted by lake sediments and rhyolite lavas. Its occurrence in a graben/half graben coinciding with a possible ring fault is common in other TVZ centres (Henley and Hedenquist 1986).

Comparisons to TVZ centres

Volcanism in the central TVZ is dominantly rhyolitic which has been erupted from eight main caldera volcanoes, Rotorua, Okataina, Kapenga, Mangakino, Maroa, Reporoa, Whakamaru and Taupo. The activity span of these eruption centres is limited (150-600ka), although they have complex caldera collapse histories (Wilson et al. 1984). The age range for the Coromandel calderas is poorly constrained, but it is likely that they would have had a similar activity span as the TVZ calderas.

Collapse structures in the TVZ are generally larger (20-50 km diameter) than the calderas in the Coromandel (<10 km diameter). The smaller TVZ calderas (Rotorua) are associated with a single vent and are short lived. At Taupo, Maroa and Okataina, deep seated NE-trending basement lineaments have controlled vent positions both within and beyond the caldera margin (Wilson et

al. 1984; Cole 1989). NE-trending structures at Onemana appear to control the vent locations of the biotite rhyolite lavas from the Pokohino Dome Complex. The basement fracture zones associated with the NE-trending Haroharo and Tarawera linear vent zones at Okataina form the two fundamental structures which have controlled location and activity of the Okataina Volcanic Centre (Cole 1989).

The ratio of erupted material to intruded material is lower at centres where lava extrusions are the dominant erupted material (Okataina, Maroa), which may be the case for the Onemana area.

Lakes and lacustrine deposits are common within calderas in the TVZ. They either occur as large bodies of water in collapse structures, i.e. form caldera lakes (Taupo, Rotorua), or small lakes formed from damming of drainage systems by lava flows and caldera walls (Okataina).

Many of the geothermal systems in the TVZ are located near identified ring structures (e.g. Wairakei, Broadlands, Waiotapu, Waimangu) while others are located along major graben-forming faults that cut across ring structures (e.g. Waikite, Te Kopia, Orakeikorako) (Henley and Hedenquist 1986). Structural interpretation of the Onemana area (Chapter Three) suggests that the hydrothermal system is located within a graben/half graben structure, which may coincide with a possible ring structure.

7.4 Summary

Volcanic activity at Onemana is dominated by two phases of rhyolitic volcanism. The oldest phase of volcanism in the area is the eruption of the pyroxene rhyolites along N-S trending structures. These structures have a similar strike as the peninsula, but may represent possible ring fractures. The pyroxene rhyolites are truncated by the NE-trending Whitipirorua Fault. This fault forms a graben/half graben structure which has been infilled with thick lake sediments, which overlie biotite rhyolites to the north. Vents for the biotite rhyolite lavas appear to be controlled by NE-trending structures.

Increasingly, areas of rhyolite volcanism in the eastern Coromandel are being identified or inferred as calderas, Kapowai and Wharekawa (Skinner 1986), Tunaiti (Briggs and Fulton 1990), Whenuakite (Adams 1992), and Waitekauri (Haworth 1993). Onemana has many features typical of a caldera, but lacks extensive ignimbrite deposits, and has been extensively eroded to the east

inhibiting the delineation of a circular feature. It is also possible the area consists of a number of calderas, which may overlap each other.

The potential size of the caldera in the Onemana area is large by Coromandel standards. Its large size may be related to its proximity to an area dominated by rifting, which may favour the accumulation of larger volumes of magma near the surface (Wilson 1989; Briggs and Fulton 1990). Briggs and Fulton (1990) suggest that calderas in the eastern Coromandel may be controlled by NE-trending structures. These NE-trending structures also control the location of the hydrothermal system, which developed as the rhyolitic volcanism waned. The location of the hydrothermal system may be related to the intersection of NE-trending structures with ring fractures of a caldera. The hydrothermal system at Onemana, which is hosted by lake sediments and biotite rhyolite lavas, is characteristic of other hydrothermal systems found in extensional settings at caldera margins in the TVZ.

In comparison to TVZ calderas the Onemana Caldera is of a similar size to Rotorua, and includes many features seen in the TVZ calderas. A possible equivalent of the Onemana area in the TVZ may be the Okataina volcanic centre. Evidence for a caldera in the Onemana area is conflicting. Several features suggest the possibility of a caldera:

- topographical expression
- weak negative gravity anomaly
- occurrence of lake sediments
- semi-circular structures
- late stage rhyolite domes and flows
- hydrothermal activity

The lack of known ignimbrites sourced from the Onemana area and significant erosion makes it difficult to positively identify the area as a caldera. It is suggested that the volcanism and hydrothermal activity in the study area may represent two separate phases of rhyolite activity and geothermal activity that occurred along a ring fault of a caldera.

Chapter Eight
Summary and Conclusions

Introduction

The study area is located on the northern half of the Onemana Peninsula on the eastern Coromandel Peninsula. Eastern Coromandel is dominated by late Cenozoic rhyolitic volcanism of the Whitianga Group. Some of this rhyolitic volcanism has been associated with caldera formation. The study area comprises of rhyolite domes and lava flows, with minor andesitic lavas, pyroclastics and lake sediments. In the central region of the study area, rhyolite lavas and lake sediments host a fossil hydrothermal system. Erosion of this system in some areas is slight and some surface features are still preserved, including hydrothermal eruption breccias and sinters.

Lithological units

The Onemana area is dominated by three rhyolite dome complexes: Pohakahaka, Pokohino, and Wharekawa dome complexes:

The Pohakahaka Dome Complex in the south of the study area consists of pyroxene rhyolite domes, lavas and minor autoclastic breccias. The pyroxene rhyolites are typically pinkish-brown, flow banded, spherulitic and porphyritic. Flow directions of lavas in coastal sections suggest a series of vents aligned along the present day coastline. Autoclastic breccias appear to be closely associated with a possible vent structure at the southern headland of Pohakahaka Bay. The autoclastic breccias are thought to have formed by shearing and the induced movement of water through these zones. The mineral assemblage of these lavas is plagioclase (An_{25-33}) > quartz > relict pyroxene > Fe-Ti Oxides ± zircon ± apatite.

The Pokohino Dome Complex is a 3.5km long 1.5km wide belt of biotite rhyolite domes, flows and minor autoclastic breccias, stretching from The Knob to Pokohino Beach. Biotite rhyolite from the Pokohino Dome Complex are pink, flow banded, spherulitic with phenocrysts of plagioclase, quartz and biotite. Original textures and mineralogy has been altered in the

east along the coastline and around The Knob by hydrothermal alteration. Lava flows on the eastern side appear to have flowed in a SE direction from a NE-trending ridge. Aerial photo interpretation suggests these lavas were erupted as coulées. The mineral assemblage of the biotite rhyolites is plagioclase (An_{19-25}) > quartz > biotite > Fe-Ti oxides ± zircon. The biotites have distinctly low Al contents which is typical of biotites derived from alkaline magmas (Abdel-Rahman 1994).

The biotite rhyolites of the Wharekawa Dome Complex consist of domes, lavas and vent intrusives. Three domes have been identified within the dome complex: Ridge Dome, Main Dome and Peak Dome. The biotite rhyolites of the Wharekawa Dome Complex are similar to those of the Pokohino Dome Complex, except the composition of plagioclase is distinctive (An_{32-45}). Pyroclastic and associated epiclastic material (Wharekawa Pyroclastics) exposed in coastal sections north of Pokohino Beach suggests that the eruption of the Peak Dome lavas were preceded by an explosive phase.

The Eastern Flows are a series of lavas that have flowed from the east and lapped onto the rhyolites of the Wharekawa Dome Complex. In the north of the study area it is evident that the lavas have flowed into a subaqueous environment (lake?) and have become brecciated forming a hyaloclastite. Identification of hyaloclastite facies associated with a bifurcating flow was made in the Ruahiwihiwi Beach area. The brecciated rhyolite is intensely spherulitic with some spherulites up to 30cm diameter.

The Glassy Dome Pyroclastics are a sequence of pyroclastic falls and flow deposits, and avalanche breccia associated with the alternating growth and destruction of the Glassy Dome Rhyolite. The deposition of layers of ash and lapilli, surges, and ignimbrites preceded dome growth. A thick block-and-ash deposit resulted from the collapse of a rhyolite dome or lava. It is thought that the present Glassy Dome Rhyolite is the last in a series of domes that formed and were subsequently destroyed. The rhyolite is a green/grey glassy porphyritic biotite rhyolite with well developed perlitic fractures. The mineral assemblage is plagioclase (An_{22-37}) > quartz > biotite ± sanidine ± apatite.

In the north of the study area the Wharekawa Ignimbrite laps onto the rhyolites of the Wharekawa Dome complex. The ignimbrite is a pinkish-grey, partially welded, lithic-rich, massive unit. The inclusion of many

lithic clasts foreign to the study area and the inclusion of hornblende in the matrix suggests the ignimbrite was erupted outside the study area.

The Rangipo Andesite is thought to be the eroded remnents of a volcanic plug which erupted through the biotite rhyolites on the margin of the Pokohino Dome Complex. The andesite is dark grey with phenocrysts of calcic plagioclase (An_{75-83}), hypersthene and augite in a fine grained intersertal groundmass of feldspar laths. Geochemistry suggests that the Rangipo Andesite is closely associated with the McBeths Andesite, which outcrops 6km to the NW.

Lake sediments outcrop over an area of $2km^2$ between the Pohakahaka and Pokohino dome complexes. The sediments are dominated by sand and silt sized fragments derived from the surrounding rhyolites. The lake resulted from the down-faulting of the northern side of the Whitipirorua Fault producing a graben/half graben. The lake sediments are overlain by a multilithological hydrothermal eruption breccia. The eruption is thought to have been erupted from Breccia Knob where the deposit is thickest (>15m) (Robson and Stevens 1991). Hydrothermal eruptions are thought to occur due to over-pressurisation of the geothermal environment.

Structure

The structural regime of the Onemana Peninsula is dominated by NW, N, and NE striking faulting, with minor E-W striking faults. The Onemana area occurs within the NNE-trending KOST, which appears to be an extensional rift-type feature with dextral movement (Merchant et al. 1988; Rabone 1989). The KOST is thought to be the principal controlling structure in the area. Dextral movement along the KOST may have resulted in large scale block rotation resulting in the NE-trending faults with sinistral movement.

The structure has played an important role in controlling the volcanism and hydrothermal activity of the area. N-striking structures are thought to control the location of vents for the pyroxene rhyolites, while NE-striking structures appear to control the location of vents for the biotite rhyolites. This is most distinctive in the Pokohino Dome Complex. The location of the Glassy Dome Rhyolite may have been controlled by E-W striking faulting. NW and N striking mineralised structures are confined between the NE-striking Whitipirorua and Pokohino faults. Sinistral and

extensional movement along these two faults could have produced extensional cross-faults where upwelling geothermal fluids were confined, similar to the Waihi model (Wellman 1954; Sibson 1987). Block rotation within the dilatational jog may explain the variation in fault trends for mineralised structures.

Petrochemistry

The volcanic rocks of Onemana are dominated by medium-K to high-K rhyolites (75-78 wt% SiO_2) and minor andesite (56-58 wt% SiO_2). No diagnostic trends were evident in major and trace element contents, and the rocks generally show tightly grouped compositions. The rhyolites can be divided into two groups: high Zr (pyroxene rhyolites), and low Zr (biotite rhyolites, Glassy Dome Rhyolite). The biotite rhyolite sample W941264 (Ridge Dome lava) is classed as a medium Zr rhyolite. Plots of Zr vs. Th show that all the volcanic rocks have distinct Zr/Th ratios, which indicates that these lavas have evolved independently, and have been derived from magma source regions within the continental crust with differing Zr/Th ratios

Primitive mantle normalised spidergrams show the volcanic rocks to be enriched in LIL elements and Y, and depleted in Nb, Sr, P, and Ti. Trace element abundances from the volcanic rocks from Onemana are consistent with other eastern Coromandel volcanics. There is close correlation between the biotite rhyolites and the Staircase Rhyolites 5km NW of Onemana (Trotter 1995), and between the Rangipo Andesite and the McBeths Andesite 6km NW of Onemana (McGunnigle 1995). Trace element trends at Onemana are also similar to those seen TVZ eruptives.

The origin of the rhyolites at Onemana is most likely related to partial melting of the contenential crust, in an extensional setting within an older volcanic arc.

Hydrothermal Alteration

Pervasive weak to intense alteration occurs within a NE-trending corridor bounded by the Whitipirorua and Pokohino faults. This zone has been identified as a broad weakly magnetic zone (Vidanovich 1991).

There are two main areas of alteration within the NE-trending corridor: in the biotite rhyolites between Onemana and Pokohino Beach; and with the biotite rhyolites, lake sediments and HEB west of the Onemana village. Alteration types west of Onemana are characteristic of surface to near surface acidic alteration, while between Onemana and Pokohino Beach alteration assemblages are more related to deeper neutral to alkaline fluids. Alkaline alteration consists of an inner core of quartz silicification, surrounded by quartz + K-feldspar alteration, which grades out into epidote and weak clay alteration assemblages. Zeolites also occur as an overprinting alteration assemblage. Acid alteration consists of pervasive kaolinite alteration, with small areas of quartz + illite/smectite ± pyrophyllite alteration and opaline quartz silicification.

Suites of unaltered to highly altered biotite rhyolites were analysed to determine any chemical changes caused by the passage of hydrothermal fluids through them. Generally with increased alteration there was an increase in SiO_2, K_2O, Rb, As, and a decrease in CaO, Na_2O, Zn, and Pb. The occurrence of As appears to be associated with areas of brecciation from boiling, and in areas dominated by quartz + K-feldspar type alteration.

The formation of the hydrothermal system at Onemana involved initial alkaline-chloride fluids rising up N and NW-striking fractures, producing alkaline-type alteration suites. The eruption of the Onemana Breccia is thought to have occurred towards the end of this stage. The second stage of activity is dominated by widespread kaolinite alteration from acid-sulphate fluids. Hot spring activity continued after this stage forming sinters. The evolution of the hydrothermal system and style of alteration is similar to other fossil and active hydrothermal systems within the KOST and TVZ.

Volcanic and Hydrothermal Setting

The Onemana area shows many volcanic and hydrothermal features typical of caldera settings on the eastern Coromandel and TVZ. The distinctive semi-circular shape of the Onemana Peninsula suggests a possible caldera in excess of 15km diameter, making it one of the largest calderas in the Coromandel. A weak negative gravity anomaly exists over the southern half of the peninsula, suggesting a thick low density caldera infill. However, within the study area there is a distinct lack of thick and continuous pyroclastic deposits.

The eruption of the rhyolites at Onemana may be associated with late stage volcanism on or near the main ring fracture zones, with vent locations of the pyroxene rhyolites occurring along possible ring faults. It is thought the eruption of the biotite rhyolites and hydrothermal activity is related to a NE-trending extensional zone coinciding with the ring fractures. The occurrence of lake sediments and a hyaloclastite suggests lakes were a common feature around the rhyolite dome complexes. The hydrothermal system hosted by lake sediments and biotite rhyolites is similar to other hydrothermal systems near caldera ring faults in the TVZ.

A possible modern day equivalent of the Onemana area may be the Okataina volcanic centre. Evidence for a caldera in the study area is conflicting, although it is possible that the volcanism and hydrothermal activity at Onemana occurred on or near a ring fault of a caldera.

Further Research

Identification of the ages of different phases of volcanism and hydrothermal alteration is needed to gain an age range of activity in the Onemana area and help determine which phase of volcanism is responsible for the hydrothermal activity. Further structural analysis is needed to better understand the structural controls on the NW and N-striking mineralised faults. Further field mapping west of Onemana may identify possible outflow sheets resulting from the collapse of a caldera.

References

Abdel-Rahman, A-F. M. 1994: Nature of biotites from alkaline, calc-alkaline, and peraluminous magmas. *Journal of Petrology*, 35: 525-542.

Adams, J. C. 1992: *A facies approach to the geology of the Hot Water Beach - Whenuakite Region, Coromandel Volcanic Zone.* Unpublished MSc thesis, lodged in the library, University of Waikato, Hamilton.

Adams, C. J., Graham, I. J., Seward, D., and Skinner, D. N. B. 1994: Geochronological and geochemical evolution of late Cenozoic volcanism in the Coromandel Peninsula, New Zealand. *New Zealand Journal of Geology and Geophysics*, 37: 359-379.

Allegre, C. J., and Minister, J. F. 1978: Quantitative models of trace element behaviour in magmatic processes. *Earth and Planetary Science Letters*, 38: 1-25.

Barker, R. 1994: Recent exploration in the Hauraki Goldfield, Coromandel Peninsula. New Zealand Mining, 13: 9-15.

Barrer, R. M., and Denny, P. J. 1961: Hydrothermal chemistry of the silicates. Part X. A partial study of the field CaO-Al_2O_3-SiO_2-H_2O. *Journal of Chemistry Society* (London), 1956: 983-1000.

Bell, J. M., and Fraser, C. 1912: The geology of the Waihi-Tairua Subdivision, Hauraki Division. *NZ Geological Survey Bulletin* , 15.

Belliss, S., E., and Christie, A., B. 1994: Processing of Japan Earth Resources-1 Synthetic Aperture Radar data to aid geological mapping in the central Coromandel Peninsula. *AusIMM NZ Conference 1994:* 33-49.

Beaufort, D., Patrier, P., Meunier, A., and Ottaviani, M. M. 1992: Chemical variations in assemblages including epidote and/or chlorite in the fossil hydrothermal system of Saint Martin (Lesser Antilles). *Journal of Volcanology and Geothermal Research*, 51: 95-114.

Bird, D. K., Shiffman, P., Elders, W. A., Williams and McDowell, S. D. 1984: Calc-silicate mineralisation of active geothermal systems, *Economic Geology*, 79: 671-695.

Bonnichsen, B., and Kauffman, D. F 1987: Physical features of rhyolite lava flows in the Snake River Plain volcanic province, southwestern Idaho. In, Fink, J. H. (ed.) The emplacement of silicic domes and lava flows. *The Geological Society of America, Special Paper 212:* 119-145.

Brathwaite, R. L., Christie, A. B., and Skinner, D. N. B. 1989: The Hauraki Goldfield - regional setting, mineralisation and recent exploration. In, Kear, D. (ed.), *Mineral Deposits of New Zealand. The AusIMM, Monograph 13:* 45-56.

Brathwaite, B., Swain, A., and Christie, T. 1994: Patterns of quartz veining in rhyolitic and andesitic host rocks at the Wharekirauponga, Neavesville and Ohui epithermal gold deposits, Hauraki Goldfield. *AusIMM NZ Conference 1994:* 175-188.

Briggs, R. M., and Fulton, B. W. J. 1990: Volcanism, structure, and petrology of the Whiritoa-Whangamata coastal section, Coromandel Volcanic Zone, New Zealand: facies model evidence for the Tunaiti Caldera. *New Zealand Journal of Geology and Geophysics* 33: 623-633.

Brooker, M. R., Houghton, B. F., Wilson, C. J. N., and Gamble, J. A. 1993: Pyroclastic phases of a rhyolitic dome-building eruption: Puketarata tuff ring, Taupo Volcanic Zone, New Zealand. *Bulletin Volcanology,* 55: 395-406.

Brown, P. R. L. 1978: Hydrothermal alteration in active geothermal fields. *Annual Review of Earth and Planetary Sciences,* 6: 229-250.

Cas, R. 1978: Silicic lavas in Paleozoic flyschlike deposits in New South Wales, Australia: behaviour of deep subaqueous silicic flows. *Geological Society of America Bulletin,* 89: 1708-1714.

Cas, R. A. F., and Wright, J. V. 1987: *Volcanic successions, modern and ancient.* Allen & Unwin, London.

Christie, A. B., and Brathwaite, R. L. 1986: Epithermal gold-silver and porphyry copper deposits of the Hauraki Goldfield - a review. In, Henley, R. W., and Roberts, P. J. (eds.), *Guide to active epithermal (geothermal) systems and precious metal deposits of New Zealand. Monograph Series on Mineral Deposits* No.26, Gebruder Borntraegger, Berlin: 129-145.

Christie, A. B., Belliss, S. E., and Brathwaite, R. L. 1994: Use of remote sensing data to aid geological mapping of the Waihi 1;50 000 scale map sheet, Coromandel region. *AusIMM NZ Conference 1994:* 51-65.

Christie-Blick, N., and Biddle, K. T. 1985: Deformation and basin formation along strike-slip faults. In, Biddle, K. T., and Christie-Blick, N. (eds.), Strike-Slip Deformation, Basin Formation, and Sedimentation. *The Society of Economic, Palaeontology and Mineralogy,* Special Publication No. 37: 1-36.

Clarke, D. S., Sporli, K. B., Smith, I. E. M., Locke, C. A., Kobe, H. W., Black, P. M., and Ballance, P. F. 1990: The geological setting of gold deposits in the Coromandel Volcanic Zone, New Zealand. *Pacific Rim '90 Congress, Australian Institute of Mining and Metallurgy:* 1-14.

Clarke, D. S., and Govett, G. J. S. 1988: Rock geochemistry in the exploration for Southwest Pacific epithermal gold deposits (abs.). *Bicentennial Gold 88 Extended Poster Programme,* Geological Society of Australia Abstracts, No.23: 369.

Clarke, D. S., and Govett, G. J. S. 1990: Southwest Pacific epithermal gold: a rock geochemistry perspective. In: J. W. Hedenquist, N. C. White, and G. Siddeley, (eds.), *Epithermal Gold Mineralisation of the Circum-Pacific: Geology, Geochemistry, Origin and Exploration*. Journal of Geochemical Exploration.

Cole, J. W. 1979: Structure, petrology, and genesis of Cenozoic volcanism, Taupo Volcanic Zone, New Zealand. *New Zealand Journal of Geology and Geophysics*, 22: 631-657.

Conrad, M. E., Petersen, U., and O'Neil, J. R. 1992: Evolution of an Au-Ag producing hydrothermal system: the Tayoltita Mine, Durango, Mexico. *Economic Geology*, 87: 1451-1474.

Coote, A. 1994: A petrological study of drillcore from ONRC1, ONRC2, ONRC3, ONRC4, ONRC5, ONRC6, Onemana, Coromandel. *Unpublished report for Heritage Mining Ltd.*

Cruikshank, K. M., and Atilla, A. 1994: Role of fracture localisation in arch formation, Arches National Park, Utah. *Geological Society of America Bulletin*, 106: 879-891.

Cunningham, C. G., McNamee, J., Vásquez, J. P., and Erickson, G. E. 1991: A model of volcanic dome-hosted precious metal deposits in Bolivia. *Economic Geology*, 86: 415-421.

Dadd, K. A. 1992: Structures within large volume rhyolite lava flows of the Devonian Comerong Volcanics, southwestern Australia, and the Pleistocene Ngongotaha lava dome, New Zealand. *Journal of Volcanology Geothermal Research*, 54: 33-51.

Deer, W. A., Howie, R. A., and Zussman, J. 1992: An introduction to the rock forming minerals, second edition. *Longman Scientific and Technical*, London.

de Ronde, C. E. J., and Blattner, P. 1988: Hydrothermal alteration, stable isotopes, and fluid inclusions of the Golden Cross epithermal gold-silver deposit, Waihi, New Zealand. *Economic Geology*, 80: 126-147.

Downey, J. F. 1935: Gold mines of the Hauraki District, New Zealand. *Government Printer*, Wellington.

Drummond, S. E., and Ohmoto, H. 1985: Chemical evolution and mineral deposition in boiling hydrothermal systems. *Economic Geology*, 80: 126-147.

Dunbar, H. M. 1991: *Petrology and geochemistry of the southern Kiwitahi volcanics*. Unpublished MSc thesis, lodged in the library, University of Waikato, Hamilton.

Ewart, A. 1979: A review of the mineralogy and chemistry of tertiary to recent dacitic, latitic, rhyolitic and related salic volcanic rocks. In Barker, F. (ed.) *Trondhjemites, Dacites and Related Rocks.* Elsevier Scientific Publishing Company, Amsterdam.

Ewart, A. 1982: The mineralogy and petrology of Tertiary-Recent orogenic volcanic rocks: with special reference to the andesitic-basaltic compositional range. In: Thorpe, R. S. (ed.), *Andesites: orogenic andesites and related rocks.* Wiley: 26-87.

Fink, J. 1983: Structure and emplacement of a rhyolite obsidian flow: Little Glass Mountain, Medicine Lake Highland, northern California. *Geological Society of America Bulletin,* 94: 326-380.

Fink, J., and Manley, C. R. 1987: Origin of pumiceous and glassy textures in rhyolite domes and flows. In, Fink, J. H. (ed.) The emplacement of silicic domes and lava flows. *The Geological Society of America, Special Paper* 212: 77-88.

Fink, J., and Malin, M. C., and Anderson, S. W. 1990: Intrusive and extrusive growth of the Mount St. Helens lava dome. *Nature,* 348: 435-437.

Fisher, R. V., and Heiken, G. 1982: Mt. Pelée, Martinique: May 8 and 20, 1902, pyroclastic flows and surges. *Journal of Volcanology and Geothermal Research,* 13: 339-372.

Fraser, C. 1910: The geology of the Thames Subdivision, Hauraki, Auckland. *NZ Geological Survey Bulletin* , 10.

Fraser, C., and Adams, J. H. 1907: The geology of the Coromandel Subdivision, Hauraki, Auckland. *NZ Geological Survey Bulletin* , 4.

Fulton, B. W. J. 1988: *The volcanic geology of the Whiritoa-Whangamata area.* Unpublished MSc thesis, lodged in the library, University of Waikato, Hamilton.

Gadsby. M. R., SpÖrli, K. B., and Clarke, D. S. 1990: Structural elements in epithermal gold deposits of the Coromandel Peninsula, New Zealand. *The AusIMM NZ Conference 1990:* 145-152.

Gottardi, G., and Galli, E. 1985: Natural zeolites. Springer-Verlag, Berlin.

Graham, I. J., Gulson, B. L., Hedenquist, J. W., and Mizon, K. 1992: Petrogenesis of Late Cenozoic volcanic rocks from the Taupo Volcanic Zone, New Zealand. *Geochimica et Cosmochimica Acta,* 56: 2797-2820.

Haworth, A. V. 1993: *The volcanic geology and hydrothermal alteration of the Lower Waitekauri Valley, Waihi, New Zealand.* Unpublished MSc thesis, lodged in the library, University of Waikato, Hamilton.

Hayba, D. O., Bethke, P. M., Heald, P., and Foley, N. F. 1985: Geologic, mineralogic and geochemical characteristics of volcanic-hosted epithermal precious-metal deposits. *Reviews in Economic Geology*, 2: 129-167.

Heald, P., Foley, N. K., and Hayba, D. O. 1987: Comparative anatomy of volcanic hosted epithermal deposits: acid-sulphate and adularia-sericite types. *Economic Geology*, 82: 1-26.

Hedenquist, J. W. 1986: Geothermal systems in the Taupo Volcanic Zone: their characteristics and relation to volcanism and mineralisation. *Royal Society of New Zealand Bulletin*, 23: 134-168.

Hedenquist, J. W., and Henley, R. W. 1985: Hydrothermal eruptions in the Waiotapu Geothermal System, New Zealand: their origin, associated breccias and relation to precious mineral mineralisation. *Economic Geology*, 80: 1640-1668.

Henley, R. W., and Allis, A. J. 1983: Geothermal systems, ancient and modern: a geochemical review. *Earth Science Reviews*, 19: 1-50.

Henley, R. W., and Hedenquist, J. W. 1986: Introduction to the geochemistry of active and fossil geothermal systems. In, Henley, R. W., Hedenquist, J. W., and Roberts, P. J. (Eds.), *Guide to the active epithermal (geothermal) systems and precious metal deposits of New Zealand, Monograph Series on Mineral Deposits* 26: 1-22.

Heiken, G., and Wohletz, K. 1987: Tephra deposits associated with silicic domes and lava flows. In, Fink, J. H. (ed.) The emplacement of silicic domes and lava flows. *The Geological Society of America*, Special Paper 212: 55-76.

Henneberger, R. C., and Browne, P. R. L. 1988: Hydrothermal alteration and evolution of the Ohakuri hydrothermal system, Taupo Volcanic Zone, New Zealand. *Journal of Volcanology and Geothermal Research*, 34: 211-231.

Hildreth, W. 1983: The compositionally zoned eruption of 1912 in the Valley of Ten Thousand Smokes, Katmai National Park, Alaska. *Journal of Volcanology Geothermal Research*, 18: 1-56.

Hildreth, W. 1987: New Perspective's of the eruption of 1912 in the Valley of Ten Thousand Smokes, Katmai National Park, Alaska. *Bulletin Volcanology*, 49: 680-693.

Hochstein, M. P., and Nixon, I. M. 1979: Geophysical study of the Hauraki Depression, North Island, New Zealand. *New Zealand Journal of Geology and Geophysics*, 22: 1-19.

Hochstein, M. P., and Rogan, A. M. 1980: Taupo Volcanic Zone; geophysical features and structures. In: Hochstein, M. P., and Hunt, T. M. (eds.) Guide to geophysics of the volcanic and geothermal areas of the North

Island, New Zealand: 37-43. *The Royal Society of NZ, Miscellaneous Series*, No. 3, Wellington, New Zealand.

Hochstein, M. P., Tearney, K., Rawson, S., Davey, F. J., Davidge, S., Henrys, S., and Backshall, D. 1986: Structure of the Hauraki Rift (New Zealand). *Royal Society of New Zealand*, 24: 333-348.

Hodder, A. P. W. 1984: Late Cenozoic rift development and intra-plate volcanism in northern New Zealand inferred from geochemical discrimination diagrams. *Technophysics*, 101: 293-318.

Jones, J. G. 1970: Intraglacial volcanoes of the Laugarvatn region, Southwest Iceland, II. *The Journal of Geology*, 78: 127-140.

Jones, J. G., and Nelson, P. H. H. 1970: The flow of basalt lava from air into water it's structural expression and stratigraphic significance. *Geological Magazine.*

Juan, V. C., and Lo, H. J. 1969: Phase relations in the system $NaAlSi_3O_8$-$CaAl_2Si_2O_8$-H_2O at low temperatures and pressures. *Proceeding of the Geological Society China (Formosa)*, 12: 21-29.

Kano, K., Takeuchi, K., Yamamoto, T., and Hoshizumi, H. 1991: Subaqueous rhyolite block lavas in the Miocene Ushikiri Formation, Shimane Peninsula, SW Japan. *Journal of Volcanology and Geothermal Research*, 46: 241-254.

Kokelaar, P. 1986: Magma-water interactions in subaqueous and emergent basaltic volcanism. *Bulletin of Volcanology*, 48: 275-291.

Krupp, R. E., and Seward, T. M. 1987: The Rotokawa geothermal system, New Zealand. An active epithermal gold depositing environment. *Economic Geology*, 82: 1109-1129.

Le Maitre, R. W. 1989: *A classification of igneous rocks and glossary of terms*. Blackwell, Oxford.

Link, M. H., Roberts, M. T., and Newton, M. S. 1985: Walker Lake Basin, Nevada: an example of Late Tertiary (?) to Recent sedimentation in a basin adjacent to an active strike-slip fault. In, Biddle, K. T., and Christie-Blick, N. (eds.), *Strike-Slip Deformation, Basin Formation, and Sedimentation. Soc. Econ. Paleontol. Mineralog., Special Publication* , 37: 1-36.

Lipman, P. W. 1984: The roots of ash flow calderas in western North America: windows into the tops of granitic batholiths. *Journal of Geophysical Research*, 89: 8801-8841.

Lloyd, E. F. 1972: Geology and hot springs of Orakeikorako. *New Zealand Geological Survey Bulletin*, 85.

Lofgren, G. 1970: Experimental devitrification rate of rhyolitic glass. *Bulletin of the Geological Society of America*, 81: 553-560.

Lofgren, G. 1971a: Experimentally produced devitrification textures in natural rhyolite glass. *Bulletin of the Geological Society of America*, 82: 111-124.

Lofgren, G. 1971b: Spherulitic textures in glassy and crystalline rocks. *Journal of Geophysical Research*, 76: 5635- 5648.

McGunnigle, N. K. 1995: *Volcanic geology of the Hikuai region, eastern Coromandel.* Unpublished MSc thesis, lodged in the library, University of Waikato, Hamilton.

Mc Phie, J., Doyle, M., and Allen, R. 1993: *Volcanic Textures, a guide to the interpretation of textures in volcanic rocks.* Centre for Ore Deposits and Exploration Studies, University of Tasmania.

Mason, B., and Moore, C. B. 1982: *Principles of geochemistry.* John Wiley & Sons, New York.

Marini, L., Principe, C., Chiodini, G., Cioni, R., Fytikas, M., and Marinelli, G. 1993: Hydrothermal eruptions of Nisyros (Dodecanese, Greece). *Journal of Volcanology and Geothermal Research*, 56: 71-94.

Martell, S. J., Pollard, D. D., and Segall, P. 1988: Development of simple strike-slip fault zones, Mount Abbot quadrangle, Sierra Nevada, California. *Geological Society of America Bulletin*, 100: 1451-1465.

Mellors, R. A., Waitt, R. B., Swanson, D. A. 1988: Generation of pyroclastic flows and surges by hot-rock avalanches from the dome of Mount St. Helens volcano. *Bulletin of Volcanology*, 50: 14-25.

Merchant, R. J., Corbett, G. J., and Smith, M. J. 1988: The Ohui prospect, prospecting licence 31-874, Coromandel Peninsula, NZ status report. *Unpublished report for Austpac Gold Exploration (NZ) Ltd.*

Miller, T. P. 1994: Dome growth and destruction during the 1989-1990 eruption of Redoubt Volcano. *Journal of Volcanology and Geothermal Research*, 62: 197-212.

Moore, J. G., Phillips, R. L., Grigg, R. W., Peterson, R. W., and Swanson, D. A. 1973: Flow of lava into sea, 1969-1971, Kilauea Volcano, Hawaii. *Geological Society of America Bulletin*, 84: 537-546.

Nairn, I. A. 1989: Geology of Mount Tarawera, sheet V16AC. *NZ Geological Survey*, DSIR.

Nairn, I. A., and Wiradiradja, S. 1980: Late Quaternary hydrothermal explosion breccias at Kawerau Geothermal Field, New Zealand. *Bulletin of Volcanique*, 43: 1-13.

Nairn, I. A., Wood, C. P., and Bailey, R. A. 1994: The Reporoa Caldera, Taupo Volcanic Zone: source of the Kaingaroa Ignimbrites. *Bulletin of Volcanology*, 56: 529-537.

Nakada, S., and Kobayashi, T. 1991: Lava dome and pyroclastic flows of the 1991 eruption at Unzen volcano. *Bulletin of the Volcanological Society Japan*, 36, in press.

Nelson, S. A. 1981: The possible role of thermal feedback in the eruption of silicic magmas. *Journal of Volcanology and Geothermal Research*, 11: 127-137.

Nelson, C. E., and Giles, D. L. 1985: Hydrothermal eruption mechanisms and hot spring gold deposits. *Economic Geology*, 80: 1633-1639.

Nur, A., Ron, H., and Scotti, O. 1986: Fault mechanisms and the kematics of block rotations. *Geology*, 14: 746-749.

O'Leary, G. P. 1978: A geophysical study of the Whitianga Graben. BSc. Hons. thesis, University of Auckland.

Peccerillo, A., and Taylor, S. R. 1976: Geochemistry of Eocene calc-alkaline from the Kastamonu area, Northern Turkey. *Contributions to Mineralogy and Petrology*, 58: 63-81.

Peng, S., and Johnson, A. M. 1972: Crack growth and faulting in cylindrical specimens of Chelmsford granite. *International Journal Rock Mechanics, Mining Science, and Geomechanical Abstracts*, 9: 37-86.

Pichler, H. 1965: Acid hyaloclastics. *Bulletin Volcanology*, 28: 293-310.

Rabone, S. D. C., Moore, D. H., and Barker, R. G. 1989: Geology of the Wharekirauponga epithermal gold deposit, Coromandel region. In: Kear, D. (ed.) *Mineral Deposits of New Zealand.* AusIMM, monograph 13: 93-97.

Rabone, S. D. C. 1991: Residual total force magnetic anomaly map, Coromandel region, 1:100 000. *NZ Geological Survey Report* , M183.

Reid, F. 1983: Origin of the rhyolitic rocks of the Taupo Volcanic Zone, New Zealand. *Journal of Volcanology and Geothermal Research*, 15: 315-338.

Richards, J. R., Cooper, J. A., and Black, P. M. 1966: Potassium argon age on plutonic intrusives on Cape Collvile Peninsula and Cuvier Island, New Zealand. *Nature*, 211: 725-726.

Robson, R. N., and Stevens, M. R. 1991: An occurrence of hydrothermal eruption breccia, Onemana, Coromandel Peninsula, New Zealand. *Proceedings of the 25th Annual Conference 1991*, New Zealand Branch of the AusIMM: 211-221.

Rogers, J. 1994: *Rhyolite volcanics of the Cooks Beach/Hahei region, eastern Coromandel Peninsula.* Unpublished MSc thesis, lodged in the library, University of Waikato, Hamilton.

Ron, H., Aydin, A., and Nur, A. 1986: Strike-slip faulting and block rotation in the Lake Mead fault zone. *Geology* , 14: 1020-1023.

Sato, H., Fujii, T., and Nakada, S. 1992: Crumbling of dacite dome lava and generations of pyroclastic flows at Unzen volcano. *Nature* 360: 664-666.

Scofield, J. C. 1967: Sheet 3 Auckland (1st Ed.). *Geological Map of New Zealand 1:250 000.* DSIR, Wellington.

Scott, B. J., and Cody, A. D. 1982: The 20 June 1981 hydrothermal explosion at Tauhara Geothermal Field, Taupo. *Dept. of Scientific and Industrial Research,* New Zealand.

Segall, P., and Pollard, D. D. 1983: Nucleation and growth of strike-slip faults in granite. *Journal of Geophysical Research,* 88: 555-568.

Sengör, A. M. C., Burke, K., and Dewey, J. F. 1985: Strike-slip faulting and related basin formation in zones of tectonic escape, Turkey as a case study. In: Biddle, K.T., and Christie-Blick, N. (eds.) Strike-slip deformation, basin formation, and sedimentation. *Society of Economic Palaeontology, Mineralogy,* Special Publication 37: 227-264.

Seward, D., and Moore, P. R. 1987: New fission track ages for some Minden Rhyolites (Whitianga Group), eastern Coromandel Peninsula. *New Zealand Geological Survey Record* , 20: 105-109.

Sibson, R. H. 1986: Brecciation processes in fault zones. *Pure and Applied Geophysics* 316: 248-251.

Sibson, R. H. 1987: Earthquake rupturing as a mineralising agent in hydrothermal systems. *Geology* 15: 701-704.

Sibson, R. H. 1989: *Structure and mechanism of fault zones in relation to fault-hosted mineralisation.* Australian Mineral Foundation.

Sigvaldason, G. E. 1992: Recent hydrothermal explosion craters in an old hyaloclastite flow, central Iceland. *Journal of Volcanology and Geothermal Research,* 54: 53-63.

Silberman, M. L., and Berger, B. R. 1985: Relationship of trace-element patterns to alteration and morphology in epithermal precious-metal deposits. In, Barnes, H. L. (ed.): Geochemistry of hydrothermal ore deposits (2nd ed.), John Wiley and Sons, New York: 203-232.

Skinner, D. N. B. 1986: Neogene Volcanism of the Hauraki Volcanic Region, in: Late Cenozoic volcanism in New Zealand, I. E. M. Smith (ed.). *The Royal Society of New Zealand, Bulletin.* 23: 21-47.

Skinner, D. N. B. 1993: The geology of Coromandel Harbour area (sheets S11 east: T11 west). Geological map of New Zealand 1:50 000. *Institute of Geological and Nuclear Sciences Ltd. map 4.* Lower Hutt, New Zealand.

Smith, I. E. M., and Gamble, J. A. 1993: Northland and Taupo Zone volcanism, North Island, New Zealand. Australian Geological Survey Organisation.

Steiner, A. 1968: Clay minerals in hydrothermally altered rock at Wairakei, New Zealand. *Clays Clay Minerals,* 16: 193-213.

Steiner, A. 1977: The Wairakei geothermal area, North Island, *New Zealand. New Zealand Geological Survey Bulletin,* 90.

Stevenson, R. J., Briggs, R. M., and Hodder, A. P. W. 1992: Emplacement of a low-viscosity, fountain-fed pantelleritic lava flow. *Journal of Volcanology and Geothermal Research,* 57: 39-56.

Swanson, D. A., Dzurisin, D., Holcomb, R. T., Iwatsubo, E. Y., Chadwick, W. W., Csasdevall, T. J., Ewart, J. W., and Heliker, C. C. 1987: Growth of the lava dome at Mount St. Helens, Washington (USA), 1981-1986. In, Fink, J. H. (ed.) *The emplacement of silicic domes and lava flows. The Geological Society of America, Special Paper* , 212: 1-16.

Taylor, S. R. and McLennan, S. M. 1985: *The continental crust: its composition and evolution.* Blackwell, Oxford.

Terres, R., and Sylvester, A. G. 1981: Kinematic analysis of rotated fractures and blocks in simple shear. *Seismological Society of American Bulletin,* 71: 1593-1605.

Thompson, B. N. 1966: Geology of the Coromandel Region. *NZ Geological Survey Report* 14.

Thompson, R. N., Morrison, M. A., Hendry, G. L., and Parry, S. J. 1984: An assessment of the relative roles of a crust and mantle in magma genesis: an elemental approach. *Philosophical Transactions of the Royal Society of London,* A310: 549-590.

Trotter, W. M., 1995: *Volcanic geology of the Pauanui-Opoutere Beach region, Coromandel Volcanic Zone.* Unpublished MSc thesis, lodged in the library, University of Waikato, Hamilton.

Vidanovich, P. P. 1991: An aeromagnetic survey over an extinct geothermal system, Onemana, Coromandel Peninsula , New Zealand. *Proceedings of the 25th Annual Conference 1991,* New Zealand Branch of the AusIMM: 222-224.

Walcott, R. I. 1984: Reconstruction of the New Zealand region for the Neogene. *Palaeogeography, Palaeoclimatology, Palaeoecology,* 48: 217-231.

Wellman, H. W. 1954: Stress pattern controlling lode formation and faulting at Waihi Mine, and notes on the stress patterns in the northwestern part of the North Island of New Zealand. *NZ Journal of Science and Technology*, 36B: 201-206.

Westrich, H. R., Stockman, H. W., Eichelberger, J. C. 1988: Degassing of a rhyolite magma during ascent and emplacement. *Journal of Geophysical Research*, 93: 6503-6511.

Wilson, M. 1989: *Igneous petrogenesis: a global tectonic approach.* Chapman & Hall, London.

Wilson, C. J. N., Rogan, A. M., Smith, I. E. M., Northey, D. J., Nairn, I. N., and Houghton, B. F. 1984: Caldera volcanoes of the Taupo Volcanic Zone, New Zealand. *Journal of Geophysical Research*, 89: 8463-8484.

Wirsching, U. 1981: Experiments on the hydrothermal formation of calcium zeolites. *Clays Clay Minerals*, 29: 171-183.

Wohletz, K., and Heiken, G. 1992: *Volcanology and geothermal energy.* Oxford, University of California Press.

Yamagishi, H., and Dimroth, E. 1985: A comparison of Miocene and Arcean rhyolite hyaloclastics: evidence for a hot fluid rhyolite lava. *Journal of Volcanology and Geothermal Research*, 23: 337-356.

Appendix I

Sample Data

W No. = University of Waikato Earth Science Department sample number, prefix W941

Location = NZMS 260 T12

Biotite rhyolites:
PDC = Pokohino Dome Complex
WDC = Wharekawa Dome Complex
EF = Eastern Flows

Analysis:
XRF = x-ray fluorescence
XRD = x-ray diffraction
MP = microprobe
PS = polished section

W No.	Location	Lithology	Analysis
261	663/456	pyroxene rhyolite	XRF
262	664/470	biotite rhyolite-PDC	XRF, XRD
263	670/492	biotite rhyolite-EF	PS
264	659/492	biotite rhyolite-WDC	XRF, PS
265	658/492	biotite rhyolite-WDC	MP, PS
266	653/483	biotite rhyolite-WDC	XRF
267	663/432	pyroxene rhyolite	XRF, MP, PS
268	663/471	quartz vein	
269	664/470	biotite rhyolite-PDC	XRF, XRD, MP, PS
270	664/477	Wharekawa Pyroclastics-lithic	
271	664/477	Wharekawa Pyroclastics-lithic	
272	664/477	Wharekawa Pyroclastics-lithic	
273	664/477	Wharekawa Pyroclastics-lithic	
274	664/477	Wharekawa Pyroclastics	
275	664/477	Wharekawa Pyroclastics	
276	664/477	Wharekawa Pyroclastics	
277	664/477	Wharekawa Pyroclastics	
278	659/477	Glassy Dome Rhyolite	XRF
279	659/479	Glassy Dome Rhyolite	XRF, MP, PS
280	660/482	biotite rhyolite-WDC	XRF
281	651/453	Onemana Breccia	XRD
282	651/453	Onemana Breccia-sinter lithic	
283	651/453	Onemana Breccia	XRD
284	643/466	Rangipo Andesite	XRF, MP, PS
285	647/474	Glassy Dome Pyroclastics	
286	649/475	Glassy Dome Pyroclastics	
287	652/491	biotite rhyolite-WDC	
288	655/494	biotite rhyolite-WDC	
289	663/457	pyroxene rhyolite	PS
290	664/455	pyroxene rhyolite	XRD
291	664/451	pyroxene rhyolite	
292	649/450	lake sediment	XRD

W No.	Location	Lithology	Analysis
293	650/465	biotite rhyolite-PDC	
294	651/474	biotite rhyolite-PDC	XRD
295	644/460	biotite rhyolite-PDC	
296	664/472	biotite rhyolite-PDC	XRF, XRD, MP, PS
297	661/466	biotite rhyolite-PDC	XRD, PS
298	661/466	biotite rhyolite-PDC	XRF, XRD
299	663/469	biotite rhyolite-PDC	XRF, XRD
300	662/467	biotite rhyolite-PDC	XRF, XRD
301	660/461	biotite rhyolite-PDC	XRF, XRD
302	651/452	Onemana Breccia	XRD
303	648/450	Onemana Breccia	XRD
304	652/448	pyroxene rhyolite	
305	652/448	pyroxene rhyolite	
306	646/448	lake sediments	XRD
307	645/450	lake sediments	XRD
308	664/454	pyroxene rhyolite	
309	663/453	pyroxene rhyolite	
310	653/457	lake sediments	XRD
311	647/456	Onemana Breccia	XRD
312	650/458	Onemana Breccia	XRD
313	651/459	lake sediment	XRD
314	664/474	biotite rhyolite-PDC	XRF, XRD
315	664/475	biotite rhyolite-PDC	XRF, XRD
316	664/475	biotite rhyolite-PDC	XRD
317	664/475	quartz vein	
318	639/460	biotite rhyolite-PDC	XRF, XRD
319	642/458	biotite rhyolite-PCD	XRF, XRD
320	646/457	Onemana Breccia	XRD
321	662/449	pyroxene rhyolite	XRF
322	662/447	pyroxene rhyolite	XRF, MP, PS
323	661/442	pyroxene rhyolite	
324	656/442	pyroxene rhyolite	
325	665/474	biotite rhyolite-PDC	XRF, XRD
326	665/474	biotite rhyolite-PDC	XRF, XRD, MP, PS
327	666/473	biotite rhyolite-PDC	XRF, XRD
328	663/471	biotite rhyolite-PDC	XRF, XRD
329	665/492	biotite rhyolite-WDC	
330	660/487	biotite rhyolite-WDC	
331	660/487	biotite rhyolite-WDC	
332	659/477	Glassy Dome Pyroclastics	MP
333	652/471	biotite rhyolite-WDC	XRF
334	650/464	biotite rhyolite-PDC	
335	650/463	biotite rhyolite-PDC	XRF, PS
336	651/467	biotite rhyolite-PDC	
337	661/475	Glassy Dome Rhyolite	XRF
338	660/476	Glassy Dome Pyroclastics	XRF
339	659/476	Glassy Dome Pyroclastics	
340	661/484	biotite rhyolite-WDC	PS
341	665/494	biotite rhyolite-WDC	XRF
342	665/491	biotite rhyolite-WDC	
343	655/485	biotite rhyolite-WDC	
344	654/485	biotite rhyolite-WDC	
345	654/470	biotite rhyolite-PDC	PS
346	643/465	Rangipo Andesite	XRF
347	645/464	Rangipo Andesite	XRF, PS

W No.	Location	Lithology	Analysis
348	648/469	biotite rhyolite-PDC	MP, PS
349	647/472	Glassy Dome Pyroclastics	
350	651/488	biotite rhyolite-WDC	
351	659/498	Wharekawa Ignimbrite	
352	660/497	Wharekawa Ignimbrite	
353	663/451	pyroxene rhyolite	
354	659/496	biotite rhyolite-WDC	
355	643/457	biotite rhyolite-PDC	XRD
356	654/461	lake sediments	XRD
357	643/459	biotite rhyolite-PDC	XRD
358	646/458	Onemana Breccia	XRD
359	647/457	Onemana Breccia	XRD, PS
360	647/457	Onemana Breccia	XRD
361	643/452	lake sediments	XRD
362	642/450	lake sediments	XRD
363	664/476	biotite rhyolite-PDC	XRD
364	664/476	biotite rhyolite-PDC	
365	662/476	biotite rhyolite-PDC	XRD, PS
366	664/471	biotite rhyolite-PDC	XRD
367	664/471	biotite rhyolite-PDC	XRD
368	666/474	biotite rhyolite-PDC	XRF, XRD, MP, PS
369	665/474	biotite rhyolite-PDC	XRD
370	664/490	biotite rhyolite-WDC	
371	663/489	biotite rhyolite-WDC	
372	660/476	Glassy Dome Pyroclastics	PS
373	655/447	pyroxene rhyolite	
374	649/440	pyroxene rhyolite	
375	657/446	pyroxene rhyolite	
376	657/447	pyroxene rhyolite	MP, PS
377	642/459	biotite rhyolite-PDC	
378	660/465	biotite rhyolite-PDC	
379	660/465	biotite rhyolite-PDC	
380	661/467	biotite rhyolite-PDC	XRD
381	661/467	biotite rhyolite-PDC	XRD
382	652/453	Onemana Breccia	XRD
383	648/450	Onemana Breccia	XRD
384	648/451	Onemana Breccia	XRD
385	648/452	Onemana Breccia	XRD
386	656/496	Wharekawa Ignimbrite	
387	649/474	Glassy Dome Pyroclastics	
388	643/466	Rangipo Andesite	
389	648/456	lake sediments	XRD
390	647/471	Glassy Dome Pyroclastics	XRD, PS
391	648/473	Glassy Dome Pyroclastics	XRF, MP, PS
392	657/496	Wharekawa Ignimbrite	PS
393	642/459	biotite rhyolite-PDC	
394	645/447	lake sediments	
395	671/502	biotite rhyolites-EF	PS
396	667/500	biotite rhyolites-WDC	PS
397	670/497	biotite rhyolites-EF	PS

Appendix II

Microprobe Analyses

Key:
C=core
R = Rim
cpx = clinopyroxene
opx = orthopyroxene
mt = titanomagnetite
il = ilmenite

Table II.1: Plagioclase analyses

Sample	Pyroxene rhyolite 267		322						Biotite rhyolite 269	
							C	R	C	R
SiO2	60.93	59.13	60.78	60.34	61.96	60.25	61.11	61.86	62.55	63.36
TiO2	0.10	0.01	0.00	0.04	0.00	0.02	0.10	0.03	0.00	0.00
Al2O3	23.74	22.36	25.10	25.11	24.17	25.10	25.04	24.54	23.59	22.62
FeO	0.19	0.21	0.35	0.27	0.23	0.36	0.24	0.26	0.24	0.30
MnO	0.00	0.00	0.03	0.00	0.13	0.00	0.08	0.00	0.00	0.00
MtO	0.00	0.00	0.00	0.00	0.04	0.00	0.00	0.01	0.00	0.00
CaO	5.93	4.98	6.50	6.46	5.21	6.58	6.36	5.89	5.02	4.09
Na2O	7.52	7.54	7.51	7.17	8.16	7.18	7.57	7.97	8.10	8.26
K2O	0.55	0.61	0.40	0.47	0.60	0.50	0.57	0.56	0.92	1.31
Cl	0.01	0.06	0.04	0.02	0.05	0.05	0.06	0.03	0.00	0.01
Cr2O3	0.00	0.01	0.05	0.08	0.00	0.00	0.00	0.10	0.02	0.02
NiO	0.00	0.00	0.00	0.00	0.00	0.00	0.13	0.16	0.00	0.00
P2O5	0.00	0.00	0.00	0.00	0.00	0.00	0.00	0.00	0.00	0.00
SO3	0.05	0.03	0.06	0.04	0.07	0.02	0.00	0.10	0.04	0.02
Total	98.67	94.62	100.64	99.56	100.10	99.96	100.65	100.82	100.18	99.94
An	29.37	25.74	31.60	32.31	25.18	32.63	30.67	28.08	24.17	19.86
Ab	67.39	70.51	66.08	64.89	71.37	64.42	66.06	68.75	70.56	72.57
Or	3.24	3.75	2.32	2.80	3.45	2.95	3.27	3.18	5.27	7.57

Table II.1: Continued

Sample	269		368							326
				C	R			C	R	C
SiO2	62.44	61.67	59.35	61.04	58.41	61.14	61.66	62.79	61.33	62.30
TiO2	0.08	0.08	0.05	0.02	0.02	0.02	0.01	0.11	0.00	0.04
Al2O3	23.85	23.51	24.08	23.59	22.35	24.12	23.62	23.39	20.86	23.76
FeO	0.15	0.14	0.16	0.07	0.13	0.00	0.20	0.13	0.12	0.15
MnO	0.00	0.06	0.03	0.00	0.00	0.00	0.14	0.02	0.00	0.01
MtO	0.00	0.00	0.00	0.00	0.00	0.00	0.00	0.00	0.08	0.00
CaO	5.19	5.09	5.69	5.21	4.67	5.32	5.11	4.78	3.46	4.85
Na2O	8.15	7.50	7.21	8.18	7.56	7.40	8.29	7.93	6.25	8.10
K2O	0.78	1.16	0.57	0.58	0.59	0.69	0.59	0.73	1.18	0.76
Cl	0.00	0.05	0.09	0.05	0.04	0.03	0.00	0.00	0.05	0.00
Cr2O3	0.09	0.00	0.00	0.00	0.00	0.17	0.00	0.09	0.00	0.12
NiO	0.00	0.12	0.00	0.00	0.00	0.15	0.00	0.00	0.06	0.00
P2O5	0.00	0.00	0.00	0.00	0.00	0.00	0.00	0.00	0.05	0.00
SO3	0.00	0.04	0.00	0.03	0.00	0.01	0.02	0.03	0.00	0.11
Total	100.41	98.93	96.89	98.60	93.58	98.66	99.26	99.62	93.09	99.77
An	24.87	25.40	29.31	25.17	24.51	27.24	24.55	23.90	21.39	23.76
Ab	70.68	67.71	67.20	71.50	71.80	68.56	72.07	71.75	69.92	71.81
Or	4.45	6.89	3.50	3.34	3.69	4.21	3.38	4.35	8.69	4.43

Table II.1: Continued

Sample	326 R			348		265				
SiO2	61.34	59.80	58.71	61.33	61.23	57.81	58.27	57.80	58.20	56.71
TiO2	0.04	0.00	0.00	0.00	0.00	0.04	0.00	0.02	0.00	0.03
Al2O3	22.58	25.05	24.39	24.58	24.48	25.72	26.25	26.93	24.51	26.86
FeO	0.19	0.14	0.00	0.17	0.25	0.45	0.28	0.12	0.37	0.47
MnO	0.00	0.03	0.04	0.00	0.01	0.00	0.10	0.00	0.00	0.00
MtO	0.06	0.01	0.00	0.00	0.00	0.02	0.00	0.00	0.00	0.02
CaO	4.27	5.39	4.66	5.45	4.73	6.75	7.77	8.57	6.21	8.98
Na2O	7.63	7.70	7.45	7.52	8.07	6.51	6.68	6.09	6.81	5.69
K2O	1.05	0.71	0.80	0.64	0.75	0.81	0.43	0.36	0.59	0.44
Cl	0.07	0.05	0.11	0.05	0.00	0.01	0.02	0.00	0.05	0.00
Cr2O3	0.00	0.00	0.00	0.01	0.00	0.04	0.01	0.00	0.00	0.00
NiO	0.00	0.00	0.13	0.00	0.00	0.02	0.06	0.05	0.16	0.00
P205	0.00	0.00	0.00	0.00	0.00	0.00	0.00	0.00	0.00	0.00
SO3	0.06	0.08	0.03	0.00	0.08	0.00	0.00	0.00	0.06	0.02
Total	96.86	98.65	95.99	99.53	99.26	98.05	99.39	99.74	96.68	99.15
An	22.09	26.72	24.41	27.50	23.39	34.62	38.14	42.81	32.28	45.35
Ab	71.44	69.09	70.61	68.66	72.20	60.43	59.34	55.05	64.06	52.00
Or	6.47	4.19	4.99	3.84	4.41	4.95	2.51	2.14	3.65	2.65

Table II.1: Continued

Sample	Glassy Dome Pyroclastics 332 C	R		391 C	R	Glassy Dome Rhyolite 279			C	R
SiO2	62.93	61.83	63.09	61.72	60.70	72.24	61.11	62.00	62.13	62.72
TiO2	0.01	0.11	0.08	0.09	0.00	0.17	0.05	0.07	0.09	0.16
Al2O3	22.37	19.46	23.42	23.62	23.91	12.41	24.58	24.05	23.87	22.58
FeO	0.20	0.47	0.09	0.19	0.17	0.98	0.15	0.14	0.12	0.00
MnO	0.05	0.04	0.08	0.01	0.00	0.06	0.08	0.00	0.00	0.08
MtO	0.00	0.03	0.00	0.00	0.00	0.10	0.00	0.00	0.00	0.16
CaO	4.20	3.29	4.56	5.40	5.02	0.66	5.60	4.35	5.30	4.46
Na2O	7.76	6.25	8.04	7.76	7.71	2.91	7.81	7.70	7.77	7.49
K2O	1.22	2.01	0.72	0.79	0.77	4.86	0.70	1.05	0.76	1.14
Cl	0.05	0.06	0.02	0.01	0.02	0.09	0.01	0.03	0.02	0.00
Cr2O3	0.00	0.12	0.00	0.00	0.05	0.00	0.03	0.11	0.03	0.00
NiO	0.00	0.00	0.00	0.03	0.24	0.00	0.00	0.00	0.27	0.00
P205	0.00	0.00	0.00	0.00	0.00	0.00	0.00	0.00	0.00	0.00
SO3	0.00	0.12	-0.07	0.07	0.04	0.00	0.00	0.01	0.00	0.00
Total	98.48	93.30	99.83	99.30	98.11	94.06	99.80	99.16	99.82	98.38
An	21.32	19.36	22.84	26.49	25.24	5.63	27.23	22.27	26.15	23.02
Ab	71.30	66.56	72.87	68.89	70.15	44.96	68.72	71.33	69.38	69.97
Or	7.38	14.08	4.29	4.61	4.61	49.40	4.05	6.40	4.47	7.01

Table II.1: Continued

Sample	279		sanidine	Rangipo Andesite 284 C	R				C	R
SiO2	61.02	58.89	72.14	47.34	48.48	46.72	48.96	47.01	49.24	47.98
TiO2	0.08	0.01	0.10	0.04	0.04	0.14	0.11	0.00	0.13	0.07
Al2O3	24.11	26.13	12.98	33.33	31.18	32.70	30.73	32.28	30.76	30.69
FeO	0.14	0.28	1.07	0.56	1.30	0.78	1.25	1.10	1.58	1.54
MnO	0.00	0.00	0.00	0.03	0.00	0.06	0.10	0.00	0.00	0.00
MtO	0.00	0.00	0.08	0.03	0.33	0.10	0.09	0.25	0.27	0.30
CaO	5.10	7.40	0.69	16.59	14.91	16.37	13.75	15.70	14.99	14.97
Na2O	7.90	6.77	2.78	1.80	2.67	1.94	2.80	2.05	2.35	2.10
K2O	0.73	0.45	4.79	0.06	0.15	0.14	0.17	0.00	0.32	0.20
Cl	0.00	0.01	0.11	0.00	0.09	0.02	0.04	0.03	0.03	0.01
Cr2O3	0.00	0.00	0.02	0.06	0.00	0.00	0.04	0.08	0.07	0.00
NiO	0.00	0.12	0.02	0.05	0.06	0.06	0.05	0.00	0.01	0.02
P205	0.00	0.00	0.00	0.00	0.00	0.00	0.00	0.05	0.08	0.00
SO3	0.00	0.00	0.00	0.00	0.13	0.11	0.01	0.06	0.08	0.04
Total	98.86	99.64	94.44	99.62	99.02	98.65	97.67	98.14	99.24	97.49
An	25.17	36.66	6.04	83.29	74.85	81.66	72.29	80.89	76.39	78.75
Ab	70.54	60.69	44.04	16.35	24.26	17.51	26.64	19.11	21.67	19.99
Or	4.29	2.65	49.92	0.36	0.90	0.83	1.06	0.00	1.94	1.25

Table II.1: Continued

Sample	284	
	C	R
SiO2	47.37	46.27
TiO2	0.06	0.05
Al2O3	33.01	34.26
FeO	0.62	1.07
MnO	0.08	0.05
MtO	0.01	0.05
CaO	16.50	16.18
Na2O	1.82	1.71
K2O	0.08	0.16
Cl	0.04	0.00
Cr2O3	0.01	0.00
NiO	0.08	0.00
P205	0.00	0.00
SO3	0.03	0.08
Total	99.32	99.65
An	82.96	83.12
Ab	16.56	15.90
Or	0.48	0.98

Table II.2: Biotite analyses

	Biotite rhyolite						Glassy Dome Pyroclastics			
Sample	368			348			332			391
SiO2	36.74	38.69	50.78	35.40	41.21	34.92	44.63	39.17	41.13	32.83
TiO2	4.88	4.15	2.30	4.95	3.86	4.78	2.42	4.16	3.25	4.21
Al2O3	14.27	16.74	17.32	13.65	13.40	13.37	14.85	14.21	13.90	13.41
FeO	28.55	24.49	13.69	30.62	25.01	28.16	18.51	25.70	22.70	25.29
MnO	0.23	0.19	0.01	0.28	0.35	0.24	0.25	0.10	0.09	0.11
MtO	4.42	3.20	1.95	4.43	3.42	4.14	2.55	3.42	3.15	3.93
CaO	0.08	0.04	0.06	0.02	0.16	0.09	0.25	0.24	0.27	0.13
Na2O	0.61	0.46	0.92	0.64	0.86	0.58	0.16	0.24	0.00	0.57
K2O	8.17	6.83	5.37	8.33	6.97	7.88	6.96	7.30	7.26	7.24
Cl	0.35	0.35	0.29	0.34	0.31	0.38	0.21	0.32	0.21	0.35
Cr2O3	0.07	0.06	0.00	0.00	0.00	0.01	0.02	0.00	0.00	0.00
NiO	0.06	0.00	0.00	0.22	0.00	0.14	0.11	0.00	0.01	0.00
P205	0.00	0.01	0.04	0.00	0.00	90.00	0.00	0.00	0.18	0.00
SO3	0.00	0.02	0.00	0.00	0.08	0.01	0.15	0.00	0.05	0.00
Total	97.98	94.90	92.62	98.35	95.40	94.21	90.38	94.52	91.87	87.83

Table II.2: Continued

Sample	391			Glassy Dome Rhyolite 279		
SiO2	61.05	33.10	34.25	35.33	36.61	41.61
TiO2	0.69	4.12	3.49	5.34	4.64	3.17
Al2O3	11.69	14.04	16.46	13.88	13.75	13.83
FeO	3.99	25.64	22.25	29.76	29.14	22.84
MnO	0.00	0.22	0.12	0.30	0.29	0.22
MtO	0.57	3.45	2.88	4.34	4.20	3.28
CaO	1.62	0.07	0.22	0.20	0.13	0.28
Na2O	1.01	0.59	0.44	0.63	0.53	0.59
K2O	3.95	7.32	6.29	8.27	8.36	7.40
Cl	0.05	0.35	0.38	0.37	0.30	0.29
Cr2O3	0.00	0.07	0.00	0.01	0.03	0.00
NiO	0.00	0.05	0.01	0.00	0.05	0.00
P205	0.00	0.00	0.00	0.00	0.00	0.00
SO3	0.00	0.01	0.15	0.07	0.05	0.03
Total	84.57	88.60	86.22	98.39	97.52	93.30

Table II.3: Pyroxene analyses

Sample	Rangipo Andesite 284						
	opx	cpx	opx	cpx	opx	opx	cpx
SiO2	54.29	49.34	53.04	51.41	52.04	53.34	48.3
TiO2	0.32	0.87	0.62	0.67	0.46	0.45	1.37
Al2O3	3.16	6.53	3.06	6.06	5.86	3.15	5.02
FeO	18.35	9.64	20.75	10.22	19.42	17.55	14.65
MnO	0.40	0.31	0.66	0.36	0.36	0.33	0.45
MtO	23.09	13.38	18.61	13.34	17.66	24.91	12.38
CaO	2.40	18.68	4.75	17.89	5.02	1.85	17.84
Na2O	0.35	0.33	0.26	0.67	0.15	0.00	0.28
K2O	0.11	0.04	0.17	0.15	0.16	0.01	0.00
Cl	0.03	0.08	0.02	0.03	0.01	0.02	0.00
Cr2O3	0.01	0.01	0.00	0.08	0.08	0.03	0.00
NiO	0.00	0.00	0.00	0.00	0.04	0.00	0.00
P205	0.00	0.00	0.02	0.00	0.01	0.00	0.00
SO3	0.02	0.00	0.02	0.02	0.02	0.01	0.05
Total	102.00	98.74	101.66	100.76	100.98	101.58	100.02
Wo	4.91	41.68	10.14	40.27	11.22	3.69	38.37
Fs	29.33	16.79	34.58	17.96	33.88	27.29	24.59
En	65.74	41.51	55.26	41.76	54.88	69	37.02

Table II.4: Fe-Ti oxides analyses

Sample	Pyroxene rhyolite 267					322				376
	mt	mt	mt	mt	mt	mt	mt	il	mt	mt
SiO2	5.38	2.64	6.92	6.23	13.21	4.60	4.80	5.59	6.68	11.51
TiO2	11.46	13.19	34.05	33.14	12.24	12.98	12.33	43.71	16.92	14.24
Al2O3	1.97	1.71	0.96	1.20	3.13	2.63	4.24	2.68	4.61	8.61
FeO	73.70	75.82	54.57	52.63	66.77	74.21	73.31	44.26	65.08	53.35
MnO	0.83	0.37	0.88	1.10	0.83	0.49	0.22	0.58	0.32	0.42
MtO	0.50	0.33	2.20	2.54	0.55	0.26	0.21	0.51	0.35	0.57
CaO	0.00	0.05	0.09	0.17	0.17	0.93	0.28	0.12	0.55	0.08
Na2O	0.64	0.36	0.15	0.55	0.55	0.45	0.31	0.57	1.38	0.11
K2O	0.21	0.10	0.38	0.24	0.52	0.27	0.22	0.29	0.20	0.13
Cl	0.08	0.20	0.00	0.06	0.07	0.00	0.08	0.11	0.39	0.06
Cr2O3	0.03	0.06	0.01	0.00	0.00	0.00	0.14	0.00	0.07	0.03
NiO	0.09	0.04	0.00	0.07	0.06	0.12	0.02	0.20	0.03	0.00
P205	0.08	0.05	0.31	0.27	0.00	0.71	1.29	0.25	0.00	0.17
SO3	0.00	0.01	0.36	0.05	0.00	0.00	0.00	0.00	0.01	0.06
Total	94.69	93.93	99.95	97.81	97.99	96.81	96.45	98.19	96.47	88.70

Table II.4: Continued

Sample	376			Biotite rhyolite 265				348		
	mt	mt	mt	il	il	il	il	mt	mt	il
SiO2	4.94	6.43	6.13	5.15	5.15	7.12	5.26	9.85	5.64	20.25
TiO2	10.12	11.98	19.54	45.35	45.35	44.48	44.86	13.00	16.36	35.02
Al2O3	3.04	5.06	4.90	3.25	3.25	3.26	3.38	4.70	4.77	3.30
FeO	73.30	58.54	60.83	42.35	42.35	37.36	42.28	63.23	62.78	33.21
MnO	0.44	0.48	0.53	3.32	3.32	6.48	2.81	0.33	0.17	2.50
MtO	0.28	0.61	0.83	0.91	0.91	0.95	0.98	0.00	0.14	0.00
CaO	0.09	0.06	0.00	0.02	0.02	0.08	0.05	0.08	0.03	0.17
Na2O	0.38	0.26	0.37	0.40	0.40	0.48	0.41	0.55	1.23	0.85
K2O	0.04	0.05	0.00	0.17	0.17	0.22	0.22	0.42	0.19	0.83
Cl	0.06	0.09	0.00	0.03	0.03	0.04	0.00	0.04	0.04	0.03
Cr2O3	0.11	0.14	0.06	0.10	0.10	0.02	0.06	0.02	0.04	0.00
NiO	0.00	0.06	0.14	0.09	0.09	0.00	0.16	0.00	0.08	0.02
P205	0.00	0.00	0.00	0.00	0.00	0.08	0.00	0.03	0.11	3.10
SO3	0.04	0.09	0.00	0.09	0.09	0.07	0.00	0.00	0.07	0.00
Total	91.84	83.09	92.76	100.51	100.51	100.35	99.79	92.08	90.97	99.23

Table II.4: Continued

Sample	348	Glassy Dome Rhyolite 279		
	il	il	il	il
SiO2	14.96	4.67	4.54	4.54
TiO2	40.26	47.26	47.62	47.62
Al2O3	2.91	2.55	2.70	2.70
FeO	36.89	42.97	43.97	43.97
MnO	3.07	1.64	1.64	1.64
MtO	0.14	0.45	0.37	0.37
CaO	0.07	0.10	0.03	0.03
Na2O	0.98	0.26	0.15	0.15
K2O	0.66	0.23	0.19	0.19
Cl	0.05	0.00	0.00	0.00
Cr2O3	0.00	0.06	0.03	0.03
NiO	0.21	0.21	0.03	0.03
P205	1.43	0.00	0.00	0.00
SO3	0.00	0.00	0.00	0.00
Total	101.16	99.76	101.03	101.03